MANCHESTER 1824

The University of Manchester

Rejection and Critical Flux of Calcium Sulphate in a Ceramic Titanium Dioxide Nanofiltration Membrane

A thesis submitted to the University of Manchester for the degree of

Doctor of Philosophy
(Environmental and Sustainable Technology)

In the Faculty of Engineering and Physical Sciences

2013

AMER NAJI AHMED AL-NA'EMI

School of Chemical Engineering and Analytical Science

List of Contents

Total word account = 64493

List of Figures

List of Tables

Nomenclature & Abbreviations

The following lists define the Roman and Greek letters in addition to the abbreviations used throughout this thesis.

Roman letters

a	Activity of uncharged solute (mol. m^{-3}).
a_i	Activity of ion i .
a_i^m	Activity of ion i inside membrane pores.
A	Filtration surface area.
A_k	Membrane porosity (dimensionless).
A_m	Area of the membrane.
B	Salt permeability constant.
c	Uncharged solute concentration within pore (mol. m^{-3}).
c_i	Concentration of ion i in salt solution (mol. m^{-3}).
c_i^b	Concentration of ion i at external bulk solution.
c_i^m	Concentration of ion i in membrane (mol. m^{-3}).
$c_{i,avg.}$	Average concentration of ion i inside membrane pores.
$c_{i,(x=0)}$	Concentration of ion i at feed-membrane interface.
$c_{i,(x=\Delta x)}$	Concentration of ion i at feed-permeate interface.
c_1	Concentration of ion at feed side (mol. m^3).
c_2	Concentration of ion at the permeate side (mol. m^3).
C^{feed}	Concentration of solute in feeds (mol. m^{-3}).
$C^{permeate}$	Concentration of solute in permeates (mol. m^{-3}).
C_i^{feed}	Concentration of ion i in the bulk (mol. m^{-3}).
$C_i^{permeate}$	Concentration of ion i in permeates (mol. m^{-3}).
$C_{i,bulk}$	Bulk concentration of ion i.
$C_{i,new}^{perm}$	New estimated permeate concentration of ion i.
$C_{i,old}^{perm}$	Old assumed permeate concentration of ion i.
C_{water}	Water concentration in permeate.

C^+	Cations (counterions) in the internal electrical field of double layer.
C^-	Anions (co-ions) in the internal electrical field of double layer.
$C_\circ$	Electrolyte concentration at the bulk.
dc_i^m/dx	The concentration gradient of component *i*.
$d\psi^m/dx$	The axial potential gradient inside pores.
D	Diffusivity of water in membrane.
D_i	Effective diffusion coefficient of component i in membrane.
$D_{i,p}$	Hindered diffusivity of ion i $(\mathrm{m}^2.\mathrm{s}^{-1})$.
$D_{i,\infty}$	Molecular diffusion coefficient of ion i at infinite dilution$(\mathrm{m}^2.\mathrm{s}^{-1})$.
D_p	Uncharged solute pore diffusion coefficient $(\mathrm{m}^2.\mathrm{s}^{-1})$
D_S	Diffusivity coefficient of salt.
e	Elementary charge $(1.6022 \times 10^{-19}\ \mathrm{C})$.
f	Firmly bound ions on the matrix.
F	Faraday constant $(9.64867 \times 10^4\ \mathrm{C/mol})$.
g	Gravity factor.
h	Step size.
i_{V-H}	Vant-Hoff factor (dimensionless).
I	Ionic strength.
J_c	Solute flux towards the membrane due to convection.
J_{cp}	Solute flux through the membrane.
J_{cw}	Pure water flux after cleaning.
J_{fw}	Pure water flux after fouling.
J_F	Filtrate flux (permeate flow rate).
J_i	Flux of ion i $(\mathrm{mol.\,m^{-2}.\,s^{-1}})$.
$J_{i_{mass}}$	Mass flux of component i through membrane.
J_{iw}	Pure water flux before fouling.
J_J	Salt flux through the membrane.
J_s	Uncharged solute flux $(\mathrm{mol.\,m^{-2}.\,s^{-1}})$.
J_V	Permeate volume flux$(\mathrm{m^3.\,m^{-2}.\,s^{-1}})$.
J_w	Water flux through the membrane
k	Bulk conductivity of circulating electrolyte $(\mathrm{S.\,m^{-1}})$.

K	Adjustable step size value.
k_B	Boltzmann constant (1.3806×10^{-23} J/K).
K	Darcy law permeability of medium.
K^{-1}	Debye length (thickness of the diffuse double layer).
K_c	Uncharged solute hindered factor for convection (dimensionless).
$K_{i,c}$	Hindered coefficient for convection (dimensionless).
$K_{i,d}$	Hindered coefficient for diffusion (dimensionless).
K_S	Salt partition coefficient.
K_{SP}	Thermodynamic solubility product.
l	Thickness of the membrane.
L	Constant describe the physical characteristics of membrane.
L_e	Effective average path length in the porous medium.
L_P	Permeability (specific flux) of membrane.
$L_{P_{initial}}$	Initial permeability.
L_s	Shortest distance measured along the direction of flow.
M	Solute molar concentration.
n	Number of particles produced during dissociation.
N_A	Avogadro number (6.022×10^{-23}/mol).
N_{steps}	Number of steps.
P	Applied pressure increment (Pa).
Pe_*	Modified Peclet number (DSPM model).
Pe^*	Modified Peclet number (uncharged solute hydrodynamic model).
P_F	Pressure at inlets feed channel.
P_{in}	Module inlet pressure.
P_{out}	Module outlet pressure.
P_{perm}	Permeate side pressure.
P_R	Retentate pressure at the end of channel.
P_{TMP}	Trans-membrane pressure.
Q_F	Flow rate through the membrane.
r_i	Stokes' radius of ion i (m).
r_p	Effective membrane pore radius(m).

R	Salt rejection.
R_g	Universal gas constant.
R_i	Rejection of ion (i).
$ratio_i$	Ratio between new and old permeates concentration of ion i.
$relax$	Under relaxation factor.
S	Solubility of water in membrane.
S_m	Super saturation ratio at membrane surface.
t	Process time.
T	Absolute temperature(K).
v	Mass average velocity of the fluid through the membrane.
V	Solute velocity $(\mathrm{m.\,s^{-1}})$.
$V_{app.}$	Apparent volume.
V_F	Volume of filtrate.
V_p	Pore volume.
V_s	Partial molar volume for uncharged solute $(\mathrm{m^3.\,mol^{-1}})$.
V_w	Molar volume of water.
x	Distance normal to membrane(m).
X	Membrane charge density $(\mathrm{mol.\,m^3})$.
X^m	Effective membrane charge density$(\mathrm{mol.\,m^3})$.
Y	Dimensionless group for uncharged solute.
z	Electrolyte valence.
z_i	Valance of ion i (dimensionless).

Greek letters

α	Degree of dissociation.
$\gamma_{i,pore}$	Activity coefficient of ion i in the pore side of the interface.
$\gamma_{i,sol}$	Activity coefficient of ion i in the solution side of the interface.
ΔE_{stre}:	Measured electrical (streaming) potential(V).
ΔP	Pressure gradient (the ratio of pressure charge with respect to position).
Δx	Effective thickness of the membrane active layer (m).
Δx_e	Equivalent thickness of the membrane active layer (m).
$\Delta\pi$	Osmotic pressure (bar).
$\Delta\rho_i$	Mass density gradient component i.
$\Delta\psi_{Don}$	Donnan potential (V).
ε	Porosity.
ε_r	Relative permittivity of water (78.54 at 25 ℃).
$\varepsilon_\circ$	Permittivity of free space (8.854×10^{-12} C. m^{-1}. V^{-1}).
ϵ	Chemical potential of uncharged solute.
ζ	Zeta potential(V).
λ_i	Ratio of stocks radius of ion i to the effective pore radius.
η	Dynamic viscosity of the solution(Pa. s).
μ	Fluid viscosity.
π	Standard dimensionless constant (3.141).
ρ	Solution density.
σ	Surface charge density (C. m^2).
σ^d	Net charge density at any point in the double layer.
σ^s	Electrical charge on membrane surface (C. m^2).
τ	Tortuosity.
ϕ	Parameter refers to the characteristic of membrane–electrolyte.
$\emptyset_i$	Steric partitioning coefficient of ion i (dimensionless).
φ	Membrane potential.
ψ^m	Electrical potential of the membrane(V).
$\Psi_{(x)}$	Electrical potential at (x) direction.
$\Psi_\circ$	Initial electrical potential.

Abbreviations

NF	Nanofiltration.
RO	Reverse Osmosis.
UF	Ultrafiltration.
MF	Microfiltration.
GS	Gas separation.
PV	Prevaporation.
CFF	Cross-flow filtration.
DEF	Dead-end filtration.
MWCO	Molecular weight cut off.
EDL	Electrical double layer.
H-S	Helmoholtz-Smoluchowski equation.
TMS	Theorell, Meyer, and Sievers model.
i. e. p	Iso-electric point.
ENP	Extended Nernst-Planck equation.
EF	Electro-filtration.
FRR	Flux recovery ratio.
CP	Concentration polarisation.
CF	Critical flux.
PWF	Pure water flow rate.
SP	Streaming potential.
NOM	Natural organic matters.
DSPM	Donnan steric pore partitioning model.
SEM	Scanning electron microscopy.
EDAX	Energy dispersive X-ray spectroscopy.
IC	Ion chromatography.
ICP-AES	Inductively coupled plasma atomic emission spectroscopy.
SHP	Steric hindered pore model.
KSM	Kedem-Spiegler model.

ABSTRACT

This thesis describes the rejection efficiency and the fouling behaviour of calcium sulphate solutes in a 1 nm tubular ceramic titanium dioxide nanofiltration membrane. Calcium sulphate is considered as one of the greatest scaling potential inorganic salts that responsible for membrane fouling which represents a main challenge in the expansion of membrane processes for desalination of brackish and saline water.

The surface charge type and magnitude for the composite amphoteric TiO_2 membrane were characterised using streaming potential measurements. Electrokinetic membrane experiments were conducted in a background electrolyte comprising 0.01 M (NaCl). The zeta potential was estimated from the measured streaming potential using the Helmoholtz-Smoluchowski equation and the surface charge density was subsequently calculated using the Gouy-Chapman and Graham equations. The experimental results showed that the membrane was negatively charged at neutral pH and its iso-electrical point (i. e. p) was at pH of 4.0.

The rejection behaviour of calcium sulphate at three different initial concentrations (0.001, 0.005 and 0.01 M) were investigated compared to other naturally occurring minerals ($NaCl, Na_2SO_4, CaCl_2$) in single salt solutions. The rejection experiments were conducted at five different applied trans-membrane pressures ranged from 1.0 to 5.0 bars. Salt retention measurements showed that the rejection sequence was R ($CaSO_4$) > R (Na_2SO_4) > R ($CaCl_2$) > R (NaCl). This rejection sequence behaviour showed an inverse relationship with the diffusion coefficients of the four salts. The salt with the lowest diffusion coefficient ($CaSO_4$) showed the highest rejection (43.3%), whereas that with the highest diffusion coefficient showed the lowest rejection. The rejection of calcium sulphate solution at saturation concentration was also conducted after a suspension solution of 0.015 M ($CaSO_4$) was prepared and filtered. The ionic analysis for calcium sulphate permeates indicated that, for the negatively charged TiO_2 membrane, the rejection for bivalent anion (SO_4^{2-}) was higher than that of the bivalent cation (Ca^{2+}).

The critical flux (CF) experiments were carried out at six trans-membrane pressure ranged from 1.0 to 6.0 bars to identify the form and the onset of calcium sulphate fouling (as gypsum) using different concentrations below saturation concentration (0.001, 0.005, 0.01 M) and at saturation concentration. Two different flux-pressure techniques have been applied and compared to determine the critical flux values; these are: step by step technique and standard stepping technique. The obtained critical flux results from both measuring techniques (for all the four sessions) confirmed that the critical flux was reached and exceeded. The present work indicated that the resulting critical flux values from both measuring procedures were decreased as the ionic strengths of the calcium sulphate solutes were increased.

A mathematical model has been proposed to identify the key parameters that affect the transport performance inside the TiO_2 nanofiltration membrane. The original Donnan steric pore model (DSPM) was used to simulate the rejection of 0.01 M sodium chloride as a reference solution. The membrane effective pore radius was estimated using two different transport models, both of these models depend on the permeation test of uncharged solute (glucose). The Donnan potential was determined based on the membrane effective fixed charge density which was determined by supposing that the membrane surface charge was uniformly distributed in the void volume of cylindrical pores. The theoretical rejection of NaCl solute for the present DSPM model was found to be in agreement with the experimental data.

Declaration

No portion of the work referred to in this thesis has been submitted in support of an application for another degree or qualification of this or any other University or other institute of learning.

Amer Naji Ahmed Al-Na'emi
July 2013

Intellectual property statement

i. The author of this thesis (including any appendices and/or schedules to this dissertation) owns certain copyright or related rights in it (the "Copyright") and s/he has given The University of Manchester certain rights to use such Copyright, including for administrative purposes.

ii. Copies of this thesis, either in full or in extracts and whether in hard or electronic copy, may be made only in accordance with the Copyright, Designs and Patents Act 1988 (as amended) and regulations issued under it or, where appropriate, in accordance with licensing agreements which the University has entered into. This page must form part of any such copies made.

iii. The ownership of certain Copyright, patents, designs, trademarks and other intellectual property (the "Intellectual Property") and any reproductions of copyright works in the thesis, for example graphs and tables ("Reproductions"), which may be described in this thesis, may not be owned by the author and may be owned by third parties. Such Intellectual Property and Reproductions cannot and must not be made available for use without the prior written permission of the owner(s) of the relevant Intellectual Property and/or Reproductions.

iv. Further information on the conditions under which disclosure, publication and commercialisation of this thesis, the Copyright and any Intellectual Property and/or Reproductions described in it may take place is available in the University IP Policy (see http://www.campus.manchester.ac.uk/medialibrary/policies.intelctuall-property.pdf.), in any relevant Thesis restriction declarations deposited in the University Library, The University Library's regulations (see http://www.manchester.ac.uk/library/aboutus/regulations) and in The University's Guidance for the Presentation of Thesis.

Dedication

To

My beloved wife Dr. Khulood Al-Jareh for her big inspiration

My lovely children Yossur and Yasser

My home….Iraq

Acknowledgements

First of all, thanks to Allah the Beneficent, the Merciful, for his blessing and assistance in accomplishing this work.

I would like to express my great appreciation and gratitude to my supervisor **Dr. Alastair D. Martin** for his invaluable instructive guidance, support and useful suggestions during the period of my PhD study.

I wish to thank my internal assessors Dr. Ted Roberts and Dr. Flor Siperstein for their helpful advices.

Special thank must go to Mr. John Riley the technician in the school of Chemical Engineering and Analytical Science for helping me to setup my experimental rig.

Many thanks are also goes to the all workshop technicians staff at the School of Chemical Engineering and Analytical Science especially Mr. Brian Hancock for technical support and manufacturing the parts for my experimental work.

I wish to express my deep gratitude to Dr. Rasha Amer Hajarat for her kind help especially in the modelling part of this study.

I would like to thank Mr. Alastair Bewsher and Mr. Paul Lythgoe from the Analytical Geochemistry Unit at the School of Earth, Atmospheric and Environmental Science (University of Manchester) for conducting the analytical analyses for the samples.

Special thanks and gratitude goes to the Iraqi Ministry of Higher Education and Scientific Research for sponsoring the present work.

Last but not least, my sincere thanks go to my mother for her kindness and prayer and to my wonderful family especially my dear wife Dr. Khulood Al-Jareh for her love, patience and constant encouragement. Also, I would like to thank all my dear friends and colleagues for their continuing assistance…

CHAPTER 1

INTRODUCTION

1.1 Overview

Applications of nanofiltration (NF) membrane are increasing rapidly in many areas and desalination of brackish and saline water is one of these applications. Among the main techniques used for desalination, the pressure driven membranes have an important position. The classical reverse osmosis (RO) was known as a typical process for desalination; however, (relying on the final use) the NF membrane can be counted as a competing separation technique since the performance and the cost of the membrane are often superior when any filtration process has been chosen [1], [2].

The increase of salt-affected areas and water insufficiency considered as a major problems in many parts of the world and especially in arid and semi-arid regions such as the Middle East. Saline soil can be defined as the soil containing sufficient soluble salts which adversely affect the growth of most crop plants [3]. The lack of a natural fresh water supply for domestic and agricultural purposes together with the increase of saline water resources will continue to exacerbate the water shortage problems in many areas of the world. Based on this, integrated sustainable solutions are needed.

Desalination processes (which refer to water treatment techniques that remove salts from saline water) are capable of providing the solution. The membrane can be considered as the heart of the desalination system where the cost of the membrane unit is about 20−25 percent of total capital cost. As a result, any continuous long term effective membrane process should involve the reduction of membrane fouling [4].

Compared to other types of membranes, the nanofiltration membranes represent the most recently developed membrane process for liquid phase separation [5], [6]. These membranes offer an attractive approach to meeting multiple water quality objectives, such as removal of organic, inorganic and microbial contaminants; furthermore, removal of hardness at high productivity with less operation costs, which allow NF membranes to be one of the favourable alternatives in water treatment applications.

NF replaces RO in many implementations due to its unique characteristics such as lower energy consumption together with higher flux rate which make NF attractive for inorganic ion's separation processes such as water softening and wastewater recycling [7]. These properties allow ions to be separated by a combination of size and the electrokinetic effects of ultrafiltration (UF) and ion's diffusion mechanisms of RO.

The NF membranes have been vastly improved in the area of water flux, salts rejection performance (a measure of how a membrane element rejects the passage of dissolved ions) and the ability to maintain high performance levels at substantially low operating pressure. These specifications help to overcome several operational problems that are associated with conventional membrane filtration techniques.

Despite its tremendous potential in water treatment, certain limitations prohibit membrane processes from becoming a large scale continuous operation. One of the major limitations arises from membrane fouling (or scale formation) caused by inorganic salts due to the accumulation of scales on the membrane surface. A decline in membrane performance over a period of time resulting from this fouling leads to reduction in water permeate flux across the membrane [8].

Scale formation on the membrane surface is a serious problem that could lead to reduce permeates flux, increase feed pressure, decrease product quality and ultimately shortens the membrane life.

Consequently, membrane fouling greatly increases the operation costs by increasing: energy consumption, system down time, necessary membrane area, construction, labour and material cost for backwashing and cleaning processes.

Membranes fouling represent the "worst enemy" of the membrane filtration process applications. Fouling can reduce the water flux through the membrane by as much as 90 percent [9]. The term "mineral scale" is used to differentiate fouling due to inorganic salt deposits from other types of fouling (organic and biofouling).

Calcium sulphate ($CaSO_4$) considers as one of the most scaling prevalent salts together with calcium carbonate ($CaCO_3$). Both of these salts are responsible for fouling in NF membranes [4], [7].

The most common form of calcium sulphate scales that precipitates at room temperature is gypsum ($CaSO_4.2H_2O$) [9], [10]. The solubility of Gypsum (at 30 ℃) is about 50 times more than that of $CaCO_3$ [2]. Reduction of fouling is thus becoming a key issue in optimising the separation process.

1.2 Problem statement and applications of the research

Soil salinity in nature is normally a mixture of different salt species, where chloride and sulphate salts often dominate [11]. Salinisation is a process that leads to an excessive increase of water soluble salts in soil. Salts are composed of positively charged ions (cations) and negatively charged ions (anions). They can be dissolved in water as soluble salts or be present as suspended solids.

The naturally occurring sodium chloride (halite) and sodium sulphate (thenardiat) represent the most predominant salts composition in saline soils. Salts dissolve and move around with water and as a result of natural evaporation process, the salts are left behind.

Salinisation is the most common land degradation process, greatly reducing soil quality and vegetation cover, and particularly occurs in arid and semi-arid areas; where precipitation is too low to maintain a regular percolation through the soil. Under such climate conditions, soluble salts are accumulated in the soil, influencing soil proportions due to the destruction of the soil structure.

Soil salinisation can be divided to primary and secondary processes, the primary salinisation includes aggregation of salts due to the high salt content of parent material or in ground water, and secondary salinisation which is caused by human intrusion, such as unsuitable irrigation practice (with salt rich irrigation water and (or) insufficient drainage) [12].

Salt affected soils may prevent seeds germination, delay plant growth and diminish crop yield or cause irrigation difficulties. It is very difficult to reclaim the saline soils by using any fertilizer, conditioner or chemical adjustment, only leaching can remove salts from a plant's root zone [13].

The amount of water needed for the leaching process is linked to the elementary salt concentration in soil, the ultimate salt level required and the characteristics of irrigation water.

The soluble salt usually appears as white crusts on the soil surface, due to the capillarity and osmotic pressure; the water transfers to the soil surface, lowering soil fertility and productivity.

The remediation of salt-affected soils involves the reclamation and improvement of saline soil by using leaching processes in order to flush out salts from the upper soil surface in a process commonly called "broaching" (or leaching) [14].

Nowadays, many countries suffer from the problem of salt-affected soil; the present research suggests Iraq as an example. In this country the climate is very arid and hot with an average temperature of 30 ℃; in summer the peak temperature is over 50 ℃ with an average annual rainfall of (100−200 mm) [15]. The agriculture in Iraq is mainly limited by the availability of suitable irrigation water.

Now, Iraq is facing serious problems of salinity, drought, and desertification. Historically, Iraq possessed a rich agricultural land where the region between the two rivers Tigris and Euphrates was fertile enough to support the world's first major civilization. Currently, the flow of these two rivers is highly regulated and controlled by a series of dams and reservoir construction projects. As a result, the water available to Iraq reduced to less than 40% [15].

The river's salinity increased gradually over the last three decades. As a consequence, thousands of hectares of agricultural lands are affected by the scarcity of water resources and salinity of soil. The Iraqi ministry of agriculture stated that about 75% of entire land surface in the middle and southern parts of Iraq is salt-affected [16].

Based on this, it can be concluded that Iraq is actually suffering from two main problems, the first one is associated with the salinity of soil, and the second is the lack of fresh water resources.

According to the nature of Iraqi soils, the gypsiferous soil covers 25% of the total area of Iraq (forming about 9 million hectares) [16].

This type of soil usually contains sufficient gypsum to influence the soil's physical and chemical conditions. According to Pessarakli [17]; gypsum (or dihydrate calcium sulphate) represents one of the main important sources among the salts that usually affect soils.

The existence of naturally occurring gypsum in soils acts as a source of calcium and sulphate during the leaching process. Pessarakli [17] states that for arid regions, the naturally occurring dihydrate calcium chloride salt $CaCl_2.2H_2O$ (also called Sinjarite as an indication of the place where it was first discovered in a city called Sinjar, west of Mosul in Iraq [18]) normally exists together with calcium sulphate.

The soluble gypsum salt represents one of the greatest scaling potential species in the nanofiltration membrane process. This may add another problem in the remediation of saline gypsiferous soils. This problem is not only exclusive for Iraq but also to all other countries that has same arid weather and soil structures.

The conventional method that could be used for the cleaning up of the salt-affected soils often include the addition of water to flush out salts from the upper soil surface (plant root zone) in a process called leaching or soil washing. This method is not considered as a treatment procedure, as in fact this method represents a movement of salts from one place to another, with high operation costs and huge amounts of fresh water being contaminated.

Recently, there has been a growing interest by some environmental research companies to develop a new technique using RO membranes for soil remediation wastewater cleanup as an application of desalination technology, for instance, the Canadian CANDESAL® International Corporation (CIC) [19] has conducted much research and successfully demonstrated an advanced approach to the design and operation of a reverse osmosis (RO) system as a possible remediation action to treat the salt-contaminated leachate that resulted from the rehabilitation of salt-affected areas (see Figure 1.1).

The unique specifications of new generation ceramic NF membranes such as operating at a remarkably low pressure with excellent water flux production compared to RO membranes and reasonably high levels of salts rejection have led to intensive efforts to develop NF desalination technology to conserve progressively diminishing water resources in drought-prone zones and especially in arid regions.

As a new possible implementation of ceramic NF membranes, the present work suggests the adoption of a closed-loop (source area in-situ remediation) desalination and water purification system as a potential remediation approach for the salt-affected soils. In this system, the saline water is stored after the soil washing process (sufficient quantities of water is needed), and then pumped to NF modules where the desalinated water can be recycled for re-use and concentrated brine collected for disposal (can be reused in many industrial processes such as tanning or textile industries) . The treated saline water can possibly be reused again as irrigation water for agricultural activities.

The main purpose of such systems is to decrease the quantity of saline leachate that must be treated as a waste water, and to produce comparatively large quantities of clean water at an environmentally permissible level to allow its reuse (depending on needed applications) or return it back to the environment [19].

This methodology can be considered as a good prospective water management practice because it reduces (or eliminates) the contamination of fresh water sources. Additional water treatment procedures might be required, such as a conventional coagulation-sedimentation method or adding UF membranes before entering the NF module.

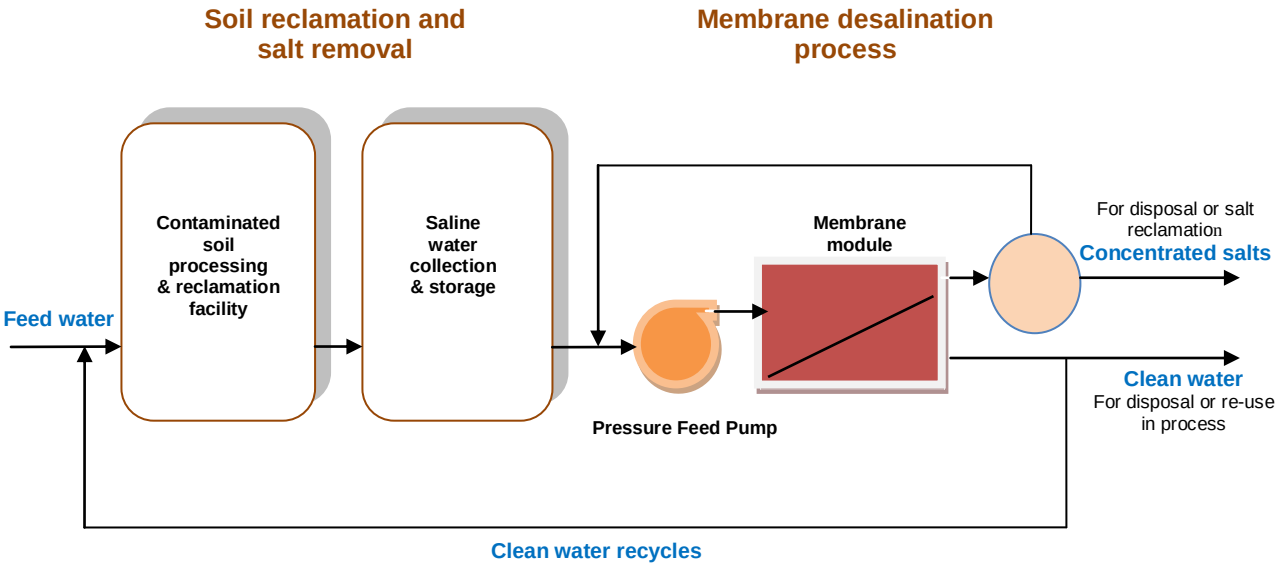

Figure 1.1: Schematic of salt-affected soils remediation process using leaching and desalination methodology [19].

The presence of calcium sulphate in such types of desalination technology could reduce the efficiency for the suggested membrane treatment methodology. High levels of calcium and sulphate in agricultural drainage water can possibly precipitate on the membrane surface as their concentrations increase. In other words, the existence of $CaSO_4$ in the salt-contaminated leachate can be considered as the main obstacle for the development of such an application.

In addition to the rejection performance and fouling of calcium sulphate, the rejection performance of other predominant salts that typically accumulate in soils such as $NaCl$, Na_2SO_4 and $CaCl_2$ (as mentioned in this section) will be investigated and compared. This research represents only the beginning of further extensive researches in this field.

The main applications for the present work include the desalination of saline inland water such as surface or ground water, agricultural drainage water, and moderate salinity leaching system water.

1.3 Objectives of the research

The project will investigate the main parameters that affect the rejection and fouling by calcium sulphate at tubular ceramic TiO_2 NF membrane with a pore size diameter of 1 nm.

The main goals of the present PhD study can be divided based on the following sections:

1.3.1 Zeta potential, surface charge density, Donnan potential:

In order to characterise the sign and magnitude of the TiO_2 membrane surface charge, the research will:

- Investigate the membrane charge by measuring the electrokinetic zeta potential to determine the iso-electric point for the membrane from the streaming potential method using the Helmholtz-Smoluchowski equation.

- Estimate the Donnan potential values based on the measured zeta potential values that are related to the membrane surface and effective fixed charge density which can be obtained from the Gouy-Chapmann and Graham equations.

1.3.2 Rejection of calcium sulphate:

In order to determine the rejection efficiency of $CaSO_4$ as a single salt compared to other predominant salts that typically accumulate in saline soils, the research will:

- Investigate the separation behaviour of calcium sulphate at three different initial concentrations (0.001, 0.005 and 0.01 M) at five different trans-membrane pressures in the range from 1.0 to 5.0 bar compared to the rejection performance of other naturally occurring minerals (NaCl, Na_2SO_4 and $CaCl_2$) in single salt solutions at the same concentrations and operating conditions.

- Investigate the rejection performance of a calcium sulphate solution at saturation concentration and compare it with the rejection of calcium sulphate solutions below saturation concentration.

1.3.3 Critical flux of calcium sulphate:

In order to study the fouling potential and the critical flux CF (an important parameter for characterising the fouling process) of calcium sulphate for the ceramic TiO_2 membrane, the research will:

- Describe the forms and fouling behaviour of calcium sulphate at different molar concentrations below saturation concentration (0.001, 0.005, 0.01 M) and at saturation concentration.

- Estimate the critical flux values of $CaSO_4$ by using two different flux-pressure techniques at six stepped heights covering an applied trans-membrane pressure range from 1.0−6.0 bar.

1.3.4 Assessing the transport in TiO_2 membrane:

In order to predict the mechanisms and parameters that affect and govern the transport in a NF membrane, the research will:

- Determine the effective pore radius of the membrane using two different models based on transport equations of solutes inside the membrane's pores, the Hagen-Poiseuille equation and permeation test of glucose (as an uncharged solute).

- Apply a mathematical model based on the original DSPM model to simulate the rejection of 0.01 M sodium chloride as a reference solution using FORTRAN program codes in order to compare the theoretical rejection (R %) with the experimental results.

1.4 Justification of the research

The present research has been considered as an addition to a series of other related previous studies conducted in the School of Chemical Engineering and Analytical Science (CEAS) - University of Manchester in the field of membrane separation processes.

Regarding the latest PhD work that was conducted at (CEAS) entitled "desalination nanofiltration membrane brackish water" by Hajarat [20]; the present work identified four points worthy of further discussion:

- The determination of the membrane zeta potential was done by using a micro-electrophoresis method. This procedure requires destroying the membrane and allows determining the zeta potential of a membrane sample after grinding, but the newly formed surface will differ considerably from the membrane surface especially when using a composite NF membrane structure where the outer metal oxide at the active skin layer differs from that in the inside supporting layers.

  The present work suggests measuring the membrane zeta potential by using a streaming potential technique which is an in situ method so there is no need to destroy the membrane.

  It is the first time that the zeta potential was estimated by using this method for tubular ceramic nanofiltration membrane at CEAS.

- The second point is related to a lack of knowledge regarding the estimation of the Donnan potential values (which represents a very important parameter especially in the transport models that are used to predict the performance in NF membranes since all the available partitioning models depend on this value); Hajarat [20] work didn't show how to determine this potential.

  The Donnan potential value changes according to the type of filtration process, membrane type, membrane pore radius, pH, and electrolyte ionic strength; so, based on these facts there is no standard value of Donnan potential that everybody can get directly from the scientific references.

  The present work suggests a procedure to determine the values of the Donnan potential based on the measured zeta potential values.

- The third point identified from Hajarat's work [20] is related to the operating pressure in the NF membrane process for the salts rejection experiments which was conducted at applied pressure ranging from $0.1-2.0$ bars; this range is probably suitable for a microfiltration membrane MF ($0.1-1.0$ bar) or ultrafiltration membrane UF ($0.1-2.0$ bar) but not for the pressure driven nanofiltration membrane in which the minimum typical operating pressure ranges from $3-5$ bars [21], [22], [23], [24].

  The present PhD work suggests increasing the applied operating pressure up to the typical values by designing and installing a completely new membrane filtration rig in order to study the effects of pressure increment on salts rejection.

  The present work designed and constructed a new vertical module to house the ceramic TiO_2 membrane inside it, made from Perspex and PVC capable of tolerating high pressure (up to 8 bars) in order to reduce (or eliminate) the accumulation of salts inside it instead of the corrosive aluminium module that Hajarat [20] used.

  Also, as a result of high pressure, the present work used a durable and flexible epoxy resin as a sealing material to prevent any possible leakage between the membrane and the module in order to force the solutes to pass inside the membrane, whereas Hajarat [20] used an O-ring as the only sealing material.

- The fourth point is related to the estimation of the membrane effective mean pore radius (r_p) which is a governing parameter that the main components of the extended Nernst-Planck equation depends on, such as ionic hindered coefficient factors for diffusion and convection, hindered diffusivity, and membrane steric partitioning coefficients. The previous work done by Hajarat [20] assumed that the mean pore radius is equal to the pore diameter (1 nm).

  The present work suggests determining the effective pore radius for the present TiO_2 membrane using two different models, the Hagen-Poiseuille equation and permeation test of uncharged solute (glucose).

In addition to the above four points, Hajarat study didn't perform any critical flux experiment to demonstrate the fouling behaviour of salts inside the ceramic TiO_2 membrane.

The soluble calcium sulphate salt represents one of the greatest scaling potential species in the nanofiltration membrane process, thus; the presence of this inorganic salt in any desalination process could lead to negative consequences on the efficiency of the membrane filtration process, such as: reduction of permeate flux with time, increment in feed pressure in addition to the shortening of membrane life as a result of fouling. These limitations prevent the technology of membrane desalination from becoming an important continuous operation and in the mean time economically and technically applicable.

Thus, extensive researches should be done in this area in order to reduce (or eliminate) the possible effects of fouling, starting from identifying the foulant and studying its behaviour, reaching to the adoption of a suitable fouling control strategy.

Within this domain, the CF concept is considered as a significant tool for quantifying the amount of fouling; however the theoretical prediction of critical flux of a certain solute based on its physio-chemical properties only still cannot be achieved as the theory dealing with surface interaction cannot be applied. Thus, the experimental measurements of the CF appear to be essential since this tool can lead to choose specific operation conditions in order to get better control in membrane fouling.

The mechanical, chemical, and thermal constancy of the new ceramic NF membrane generations in addition to other unique specifications such as the noticeably low operating pressures, excellent water flux production (compared to RO membranes) and reasonably high salts rejection levels have encouraged the researchers to use this type of filtration technology in many new applications, and the treatment of saline water resulting from the remediation of salt-affected soils is one of these new applications.

In the mean time, the rejection efficiencies of different salts in the ceramic NF membranes still require to be studied comprehensively and the potential mechanisms that govern the transport inside the nanofiltration membranes such as the Donnan exclusion mechanism and the sieving mechanism should be taken in consideration for each case separately in a way that can lead to develop the performances of these membranes.

Up to now there is no existing to any study which has attempted to make the link between the rejection and fouling of calcium sulphate at the same time using a tubular ceramic TiO_2 NF membrane which represents the main objectives of this research.

1.5 Structure of thesis

The structure of the present thesis consists of six Chapters outlined below:

- *Chapter 1* gives a short overview of the problem and the possible applications of the research. The objectives and justification of this work are presented.
- *Chapter 2* reviews the background literature that is related to the present work, focussing on the classification, flow operation modes, structure, manufacture, and amphoteric behaviour of ceramic NF membranes filtration processes. Relevant theories that the present study depends on such as electrical double-layer theory, Gouy-Chapman theory, critical flux theory, and mass transport in NF membrane are outlined.
- *Chapter 3* shows the specifications of the module and the TiO_2 membrane placed inside it. Detailed descriptions of the experimental materials and membrane filtration rig apparatus are presented in this chapter. The methodology of three different bench scale experiments used to evaluate the membrane zeta potential, salts rejection, and critical flux are explained. The re-generation procedure for the TiO_2 membrane is also described.
- *Chapter 4* focuses on the experimental results of electrokientic, rejection, and critical flux measurements in the present TiO_2 membrane. The membrane iso-electric point from the streaming potential method is also estimated. The solutes rejections (R %) of sodium sulphate, sodium chloride, calcium chloride, and calcium sulphate are evaluated and compared. The critical flux of calcium sulphate below and at saturated concentration using two different techniques is studied. Comprehensive discussion including comparison with previous researches for each experimental result is presented.
- *Chapter 5* provides a mathematical model based on the original DSPM model to identify the key parameters that affect the transport performance inside the present ceramic TiO_2 NF membrane using a reference solution of sodium chloride. The theoretical and experimental rejection results for the solute are compared and discussed.
- *Chapter 6* shows the conclusions of the present thesis and suggested future work, limitations and recommendations for process improvement are included.

CHAPTER 2

LITRATURE REVIEW

2.1 Membrane filtration processes

2.1.1 Definitions

It is hard to make a perfect definition of a membrane because such a definition depends mainly on the material and membrane structure besides its function and use. Mulder [21] defined a membrane as a "selective semi-permeable barrier between two phases that restricts the transport of particulate, colloidal, and / or dissolved chemical species other than solvent or water in a specific manner".

A membrane can be utilized to get potable water from ground, surface, and wastewater containing traces of dissolved pollutants. A membrane can be "thin" or "thick"; their structure can be "porous" or "non-porous", "homogeneous" or "heterogeneous". Furthermore, membranes can be constructed from neutral or electrically charged materials.

Membrane separation technologies are usually cheaper, quicker, and more effective than the conventional separation techniques such as evaporation or distillation. The process occurs in a continuous mode and can be joined with other separation processes with low energy consumption. However, it has some obstacles such as fouling which can lead to shortening a membrane's life or reducing selectivity.

Winston [22] defined the membrane filtration process as a "selective (or controlled) transfer of one species (in preference to other species) from one bulk phase to another bulk phase separated by a membrane". In membrane processes, the hydrostatic pressure, concentration difference, and electrical potential in the feed and permeate streams represent the most significant factors that create the driving force for the separation. The transfer of one species across a membrane requires one or more driving forces and the permeation rate through the membrane is normally proportional to these driving forces. The membrane separates the feed into two streams, they are the permeate stream and retentate (or concentrate) stream. Figure (2.1) shows a schematic representation of a membrane separation process.

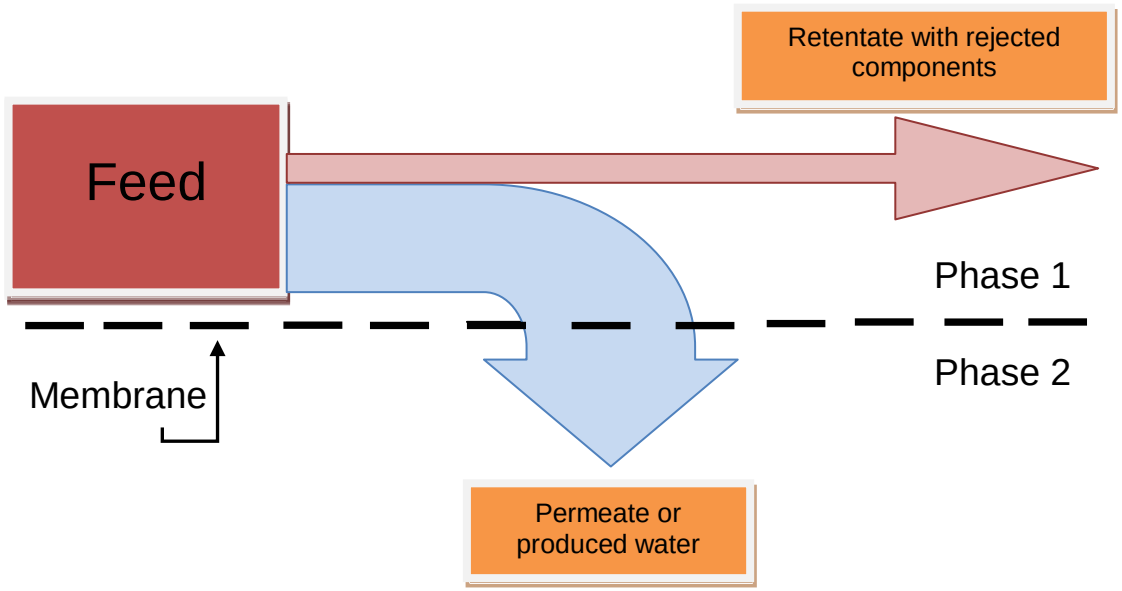

Figure 2.1: Schematic illustration of membrane separation process.

2.1.2 Classifications of membrane technology

Transport of selected species through the membrane is achieved by applying a driving force (pressure, concentration, temperature, or voltage) across the membrane. This transport can be affected either by a certain mechanism or by the physical properties of the membrane which might give a wide range of membrane classifications.

In terms of driving force and based on pore size and practice, membrane processes can be classified according to pressure driven processes into four distinguished filtration processes as follow [21], [25], [26]:

- Microfiltration (MF): primarily used to separate particles and bacteria from another smaller solute, pore size (0.05−2.0 μm) and operating pressure below 2.0 bar.
- Ultrafiltration (UF): usually used to separate colloids like proteins from smaller molecules like sugars and salts, pore size (0.05 μm −2.0 nm) and operating pressure between 1 and 10 bar.
- Nanofiltration (NF): normally used to achieve a separation of sugars, organic molecules, multivalent salts and monovalent salts from water, pore size (0.5−2.0 nm) and operating pressure between 5.0 and 20 bar.
- Reverse osmosis (RO) or hyperfiltration: this technique is mainly used to remove dissolved salts from water, with pore size less than 1 nm and operating pressures from 10−100 bar.

Besides, it is possible for a membrane to be classified according to the material of construction into synthetic and natural membranes; synthetic membranes are subdivided into organic membranes (polymer or liquid) and inorganic membranes (ceramic, metal, zeolite, etc...). In contrast, natural membranes (the first generation of membranes) are made of natural materials which can be subdivided into living membranes (cell membranes) and non-living membranes (liposome or vesicle membranes).

Membranes can be classified according to pore size into two main groups, one being porous and the other is nonporous. The porous membranes can be subdivided as follows [21], [27]:

- Macro-pores > 50 nm
- Meso-pores 2 nm < pore size < 50 nm
- Micro-pores < 2 nm

While nonporous membranes normally refer to gas separation (GS) or prevaporation (PV) processes (both of these techniques are also classified as pressure driven processes).

Furthermore, membranes can also be classified due to their morphology into symmetric membranes (porous and nonporous) and asymmetric membranes. These membranes consist of either a dense top layer (skin or active layer) supported by a porous sub layer or a composite type in which the top layer and sub layers originate from different materials. The resistance to mass transfer is determined to a large extent by the thin top layer [28].

2.1.3 Flow operation modes

In membrane filtration processes, two different types of operation modes can be identified, these are: dead-end filtration (DEF) mode and cross-flow filtration (CFF) mode. In the dead end mode all of the fluid to be filtered passes into the membrane and particles larger than the pore size are hooked up at the membrane surface. This causes a "filter cake" as the retained particles start to build up.

Whereas in the cross-flow filtration mode the medium to be filtrated flows through the open channels of the membrane carrier, which results in particles being retained in the channel's flow if their sizes exceed the radius of the membrane's pores, building up the concentrate [21].

The permeate flows by cross-flow through the pores, while the retentate flows of cross-flow filtration could remove the retained media and thereby reduce fouling, in other words; in dead-end filtration mode no flow is recycled and the only flow inside the membrane is the feed flow, whereas, in CFF mode the flow is recycled.

Figure (2.2) shows the differences in the dead-end and cross flow filtration modes in terms of changes in flux and cake thickness with time.

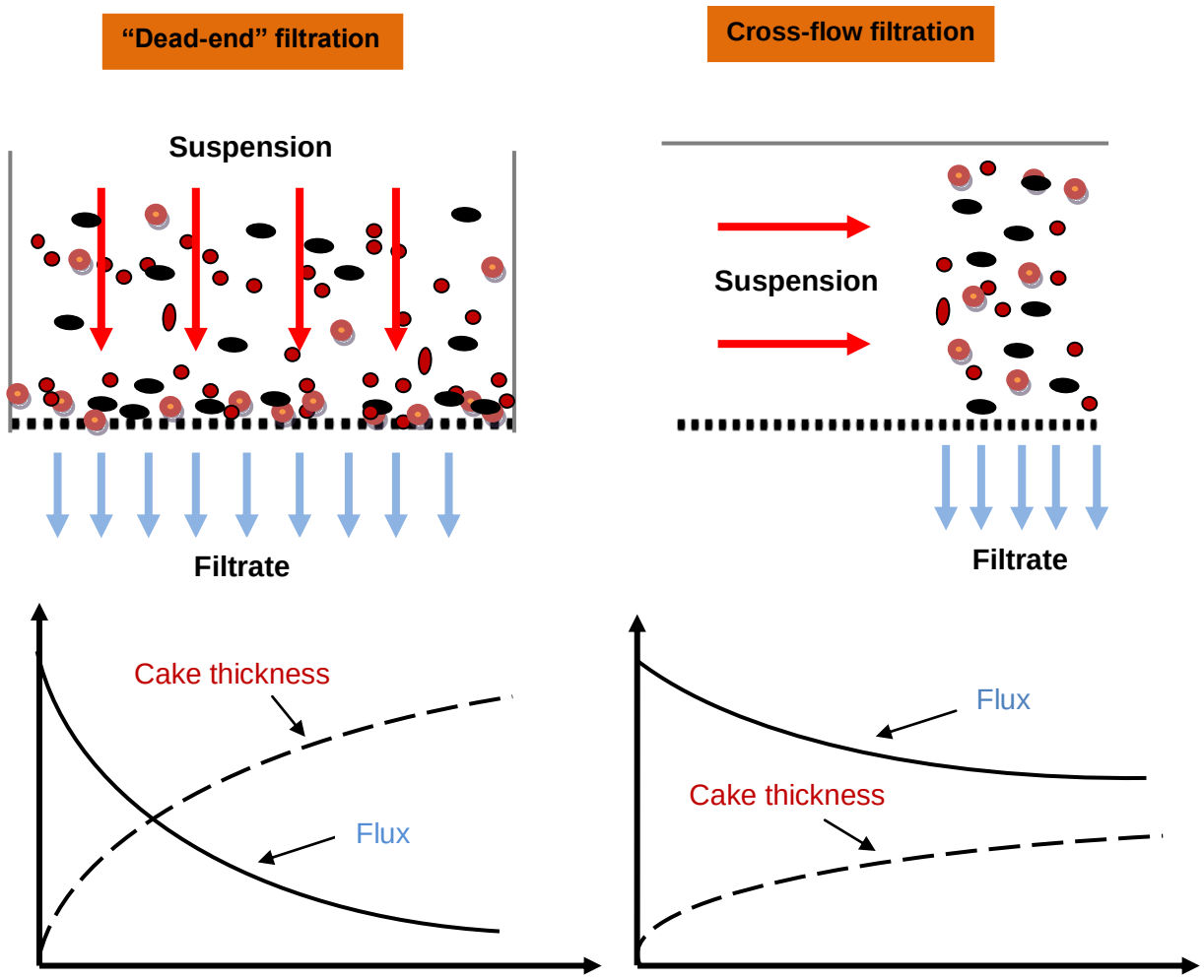

Figure 2.2: Schematic of dead-end and cross flow filtration mode [27].

2.1.4 Membrane filtration performance criteria

The performance of pressure driven membrane systems is usually monitored by several parameters. The main factors can be summarized as follows [21], [22]:

2.1.4.1Filtrate flux

The filtrate flux (J_F) or permeate flow rate represents one of the significant performance parameters. The filtrate flux is defined as instantaneous water flow rate (volume of permeate per unit time) through the membrane (Q_F) divided by the total filtration surface area (A). According to this, the filtrate flux is then expressed as follows:

$$J_F = \frac{Q_F}{A} \quad \textbf{(2.1)}$$

2.1.4.2 Membrane area

As shown in the previous section, the membrane area can be considered as a function of the process time. Based on this, reducing the membrane area required longer process time.

The membrane area can be defined as the unit surface area per module multiplied by the number of modules in use. The area of the membrane (A_m) can be estimated in terms of volume (V_F) and flux (J_F) of filtrate at certain process times as follows:

$$A_m = \frac{V_F}{J_F\, t} \quad \textbf{(2.2)}$$

2.1.4.3 Trans-membrane pressure

The trans-membrane pressure (P_{TMP}) is a measure of how much force it takes to push permeates through the membrane and is defined as the differential pressure across the membrane surface. The low P_{TMP} indicate clean water while high P_{TMP} indicate dirty or fouled membrane. This parameter represents the average pressure between the membrane module inlet pressure (P_{in}) and the membrane module outlet pressure (P_{out}), minus the permeate pressure side (P_{perm}), that is:

$$P_{TMP} = 0.5\,(P_{in} + P_{out}) - P_{perm} \quad \textbf{(2.3)}$$

2.1.4.4 Pressure drop

The pressure drop (ΔP) or hydraulic differential pressure occurs when the fluid passed through the membrane. The pressure drop can be defined as the loss of pressure between the inlets feed channel (P_F) and outlets retentate pressure (P_R) at the end of the channel.

The pressure drop represents the most important processing parameter to monitor because as the pressure drop (inside the membrane filtration system) remains constant, this indicates that there will be no change in system flow rate.

The pressure drop through the membrane is normally expressed as follows:

$$\Delta P = P_F - P_R \quad \textbf{(2.4)}$$

1.2.4.5 Membrane permeability

The permeability (L_P) or specific flux for the membrane is defined as the filtrate flux (J_F) divided by the trans-membrane pressure (P_{TMP}) which can be estimated as follows:

$$L_P = \frac{J_F}{P_{TMP}} \quad \textbf{(2.5)}$$

1.2.4.6 Osmotic pressure

Osmotic pressure of the feed represents a significant parameter in membrane separation processes. Osmotic pressure can be defined as the pressure of a solution against a semi permeable membrane to prevent water from flowing inward across the membrane. In other words, it is the pressure needed to cause a solvent (water) to leave the solution (brackish water, saline water, wastewater...etc) and break through the membrane.

For low concentration solutions, the Morse equation can be used to estimate the osmotic pressure (bar) as follows [29]:

$$\pi = i_{V-H} M R_g T \quad \textbf{(2.6)}$$

Here, i_{V-H} represents the dimensionless Vant-Hoff factor, M is the solute molar concentration, R_g is the universal gas constant ($0.08314\ \mathrm{L.bar.K^{-1}.mol^{-1}}$) and T is the absolute temperature. This formula gives the osmotic pressure on one side of the membrane, thus $\Delta\pi$ represents the difference between the pressures on the two membrane sides. For completed dissociated solutions in water such as sodium chloride or calcium sulphate, the Vant-Hoff factor can be determined as follow:

$$i_{V-H} = 1 + \alpha(n-1) \quad \textbf{(2.7)}$$

Here (α) represents the degree of dissociation and (n) is the number of particles produced during dissociation. So, for NaCl solution, then: α = 1 (100 % dissociation), n = 2 (since there are only two ions in the solution) and i_{V-H} = 2.

2.2 Ceramic membranes

2.2.1 Introduction

For many years, the implementations of commercialised membranes for liquid separation have been dominated by polymer membranes, but in the last decade the inorganic membranes have had their share of growth.

This increase can be attributed to the following main points (this holds particularly for ceramic membranes configuration) [27], [28], [30]:

- Mechanical, chemical, and thermal constancy.
- Possibility of back flushing and steam sterilization.
- High abrasion resistance.
- High flux.
- High durability.
- Bacterial resistance.
- Regeneration possibility.
- Dry storage after cleaning.

The early generations of ceramic membranes are intrinsically more expensive and complicated than polymer membranes. Then, the application of inorganic membranes were generally found in fields where polymer membranes can't or don't perform well. The cost of ceramic membranes vary in wide rang depending on the module type and pore size. In the recent years, the cost of the ceramic membranes showed a sharp decrease to reach almost the same prices as that of the organic membranes with well-known knowhow technologies.

Figure (2.3) shows a wide range of single-hole and multi-holes tubular support structures developed by Inopor ® Corporation [31].

Figure 2.3: Range of single-hole and multi-hole tubular support structures [31].

According to Burggraaf and Cot [28], the performance indicators of porous ceramic membrane systems such as permeation and separation efficiency factors depend mainly on:

- The micro-structural features of membranes, such as pore shape and size distribution, morphology, thickness and surface porosity.
- The architecture of the membrane and module.

Li [27] reported that the Alumina (Al_2O_3), Titania (TiO_2), Zirconia (ZrO_2), and Silica (SiO_2) represent the most commonly used materials for ceramic membranes (or a combination of these minerals oxides).

The configurations of most commercial ceramic membranes are disc and sheet which are usually assembled with a plate and frame module or tubular shape which are usually assembled with a tubular module.

Different types of geometries can be found in commercial ceramic membranes such as tubular single-hole geometry and monolith multichannel or honeycomb geometry which provides more separation area per unit volume of membrane element. The cylindrical shapes offer the best compromise between pressure resistances and cross-flow filtration mode [28].

Typical geometries of ceramic membranes are shown in Figure (2.4).

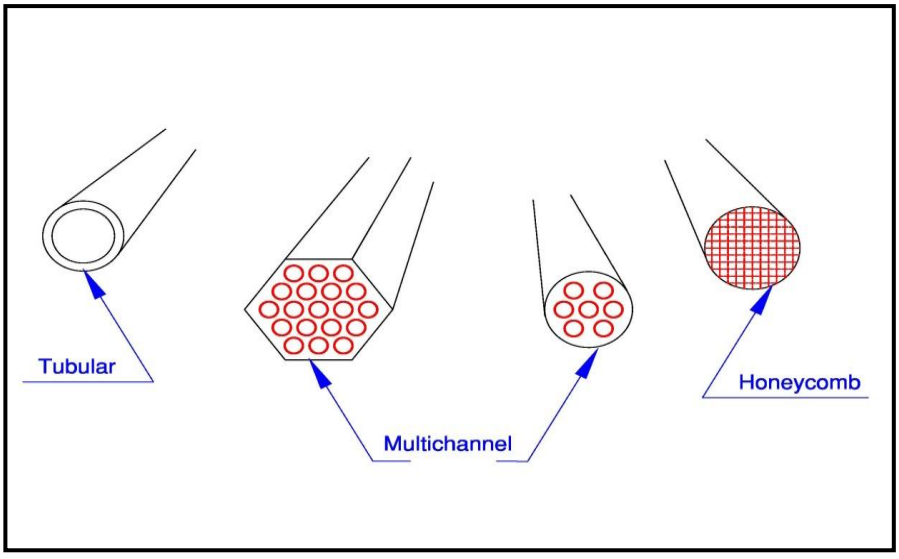

Figure 2.4: Geometries found in commercial ceramic membranes [28].

The higher flux of the ceramic membranes will decrease the required membrane area (for a given water flow) and the longer membrane life time may compensate the higher investment cost compared to the organic membranes.

2.2.2 Ceramic membrane structures

Ceramic membranes are usually described as composite (or asymmetrical) layered structures composed of 1 to 5 layers of one or more different ceramic materials.

These membranes normally consist of bottom macroporous mechanical support layer(s), intermediate mesoporous layers and a microporous active top layer where actual separation occurred [27].

A ceramic membrane may generally be classified as shown in Table (2.1):

Table 2.1: Classification of ceramic membrane structure [28].

Membrane	Structure	Pore diameter	Separation layer
Microfiltration	1 layer	5 μm	macroporous
	2 layers	0.25 μm	macroporous
	3 layers	0.1 μm	macroporous
Ultrafiltration	4 layers	3–5 nm	mesoporous
Nanofiltration / gas separation	4–5 layers	< 2 nm	microporous

As a general rule for the ceramic membrane's structure, the higher the membrane selectivity required, the more supported layers are needed.

Figure (2.5) shows an example for the pore characteristics of a four layer ceramic membrane. It can be seen from this figure that the intermediate layer(s) bridge the pore differences between the bottom supporting layer (layer 1) and top activated skin layer (layer 4).

Burggraaf and Cot [28] explains the basic concept behind such structures which is to minimise the overall hydraulic resistance of the permeate flow inside the membrane structure. This requires a defect-free small pore intermediate separation layer(s) and as thin as possible pore top layer. Such approach allows more flexible optimization of each layer. The support layer should offer a maximal mechanical strength and compression resistance, combined with minimal resistance to permeation while the top-layer should show the desired combination of solvent flux and solute rejection.

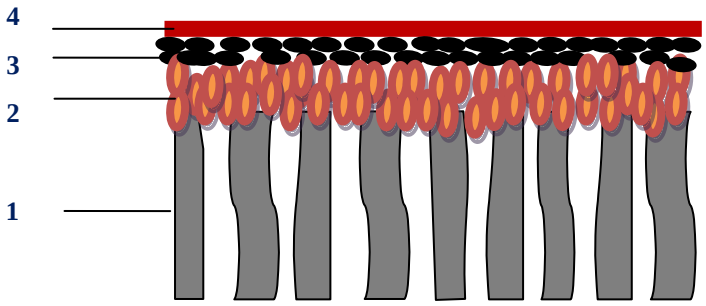

1: Porous support (1–15 µm)

2: Intermediate layer(s) (50–1000 nm)

3: Separation layer (3–50 nm)

4: Modified separation layer (< 2 nm)

4 + 3 + 2 + 1	**Nanofiltration membrane**
3 + 2 + 1	**Ultrafiltration membrane**
2 + 1	**Microfiltration membrane**

Figure 2.5: Schematic representation of an asymmetric (composite) ceramic membrane [1].

A schematic drawing of a four layers membrane support tube (inside-out operation mode) is shown in Figure (2.6). The enlarged part reveals the arrangements of the four layered structure of the ceramic membrane where the extruded support tube is layer one and the top active skin is layer four.

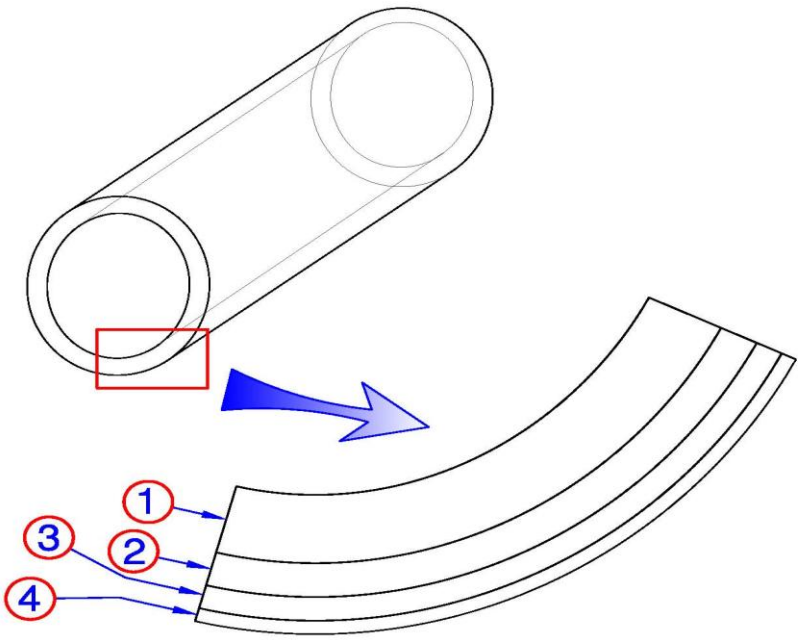

Figure 2.6: Schematic multilayer membrane support [28].

2.2.3 Manufacturing of metal oxide membranes

An inorganic membrane can be described as an asymmetric porous ceramic formed by a thin, selective layer supported on much thicker, highly permeable layers. Because the selective layer is quite thin; the membrane permeate fluxes are normally high. The support provides mechanical resistance to the medium.

Most common commercial ceramic membranes are usually made from oxide powders such as aluminum, zirconium, titanium or silica oxides (or a combination of them). For an aluminum membrane three different forms of alumina have been used to produce alumina membranes which are [32]:

- Alpha aluminum dioxide ($\alpha - Al_2O_3$)
- Gamma aluminum dioxide ($\gamma - Al_2O_3$)
- Theta aluminum dioxide ($\theta - Al_2O_3$)

Each of the above alumina membranes gives a different pore size, porosity, and surface area depending on the manufacturing process method.

Based on Li [27], the preparation of ceramic membranes generally consists of the following main steps:

- Formation of particles suspensions.
- Packing the particles into a membrane with a certain shape, e.g.; tube, flat...
- Membrane consolidation (at high temperatures).

Different shaping technical procedures are available to prepare symmetric or composite ceramic membranes such as slip casting, tape casting, extrusion and pressing, however, no matter what the selected process is; the final membrane product (including the support layers) can only be obtained from a firing step.

In addition to the above mentioned methods, there are two main procedures for the manufacturing of an inorganic ceramic membrane; these are: slip coating-sintering method and the sol-gel (solution-gelatinous) method [21], [33].

The slip coating-sintering method is normally used to produce membranes with a mean pore diameter down to about ($10-20$ nm), whereas the sol-gel method is used to produce membranes with a mean pore size range from less than (1 nm) to (10 nm) [28].

In the slip coating-sintering method, a porous support tube is made by pouring a dispersion of a fine-grain ceramic material and a binder into a mold and sintering at high temperature. Then, one surface of the tube is coated with a suspension of finer

particles in a binder solution of a cellulosic polymer or polyvinyl alcohol.

This mixture is called a slip suspension; it is then dried and sintered at high temperatures. The critical factors from using this technique are the viscosity of the suspension besides the coating speed and time.

Commonly several slip-coated layers are used in sequence, each formed layer being made from a suspension of gradually finer particles and led to an asymmetric structure.

The sol-gel process is one of the most appropriate methods for the preparation of functional oxide layers. In this technique the slip coating is taken to the colloidal level. The main advantage of using this technique is that the membrane pore size (especially for small pores) can be tightly controlled. Normally the substrate to be coated with sol-gel is a microporous ceramic tube produced by the slip coating-sintering technique.

The sol-gel composite ceramic membrane can be prepared by using two different routes; these are the colloidal (particulate) route or the polymer route. In the colloidal route, the metal salt is mixed with water to form a sol (which means nanoparticles dispersion) to be coated after that on membrane support layer(s) in the form of colloidal gel, whereas; in the polymer route, the mixture of metal-organic is mixed with organic solvent to form a sol to be coated after wards on a membrane support layer(s) in the form of a polymer gel. These solutions from the two routes are prepared by controlled hydrolysis of metal salts or metal alkoxide to hydroxides. However, it should be noted that the pore size of the membrane prepared using the polymer gel route resulted in a narrower pore size system than the colloidal route.

The drying and sintering steps determine the nature of the membrane. In order to avoid the cracking of the membrane coating; A careful drying treatment should be performed in an intermediate temperature range (80−350 ℃) which results in a material containing residual organics. A pure inorganic membrane is generally obtained in a final sintering step at (500−800 ℃) after organic groups and residual carbon has been burned out [21].

The reproducibility of the final product's properties is not easy to obtain and requires many precautions. The last step in the production process is the machining to obtain the final dimensions and surface quality.

The manufacturing steps of ceramic membranes using slip coating-sintering and sol-gel methods are shown schematically in Figure (2.7).

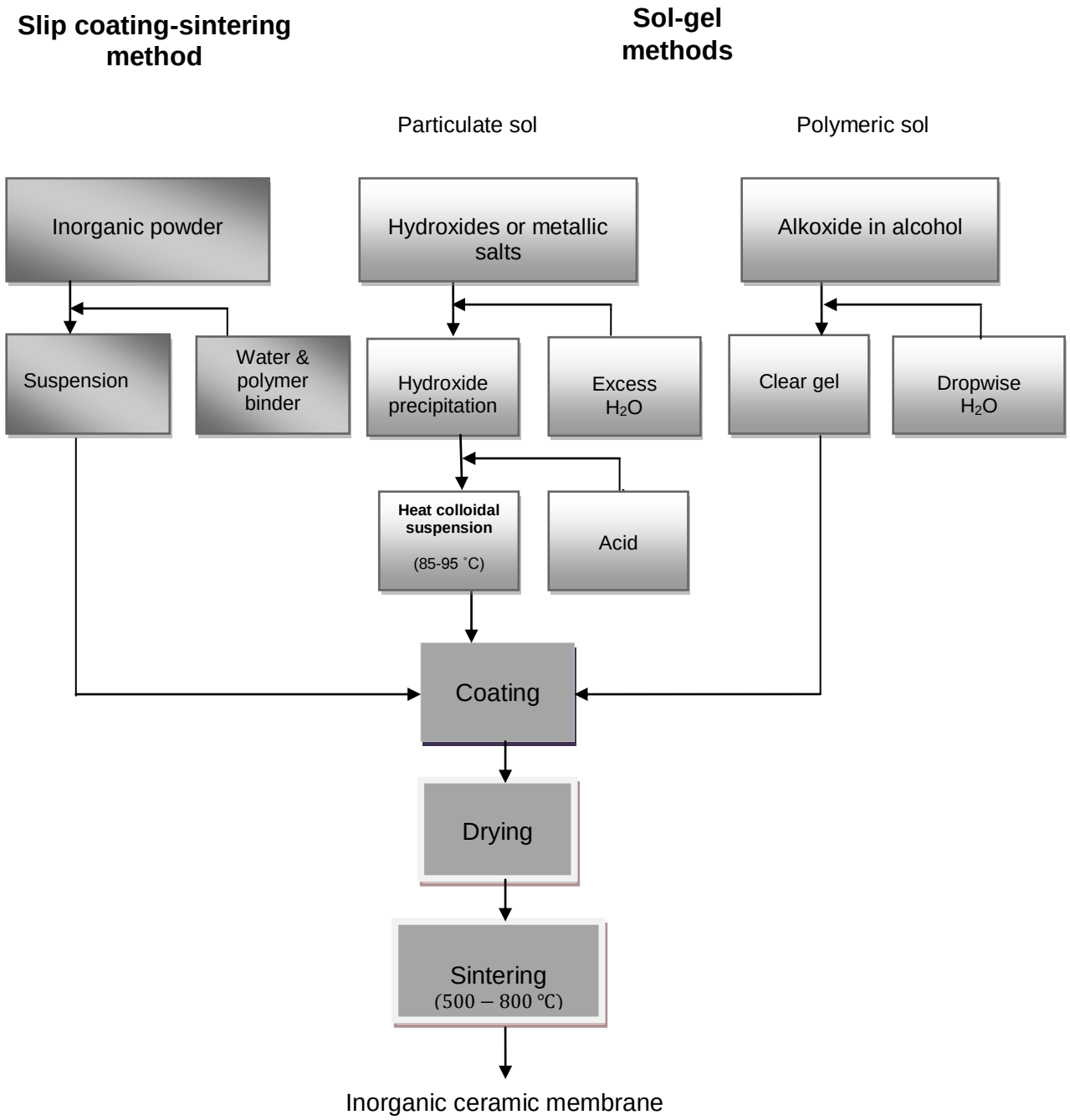

Figure 2.7: Schematic flow diagram for the manufacturing steps of ceramic membranes using slip coating-sintering and sol-gel processes [33].

The ceramic titanium dioxide NF membrane of the present work was selected as a result of the unique characterisation that this membrane shows, such as: good fouling resistance, high water flux, commercial availability, stability under extreme pH ranges and low fabrication cost because of their reduced sintering temperatures (for further details see section (3.2).

2.2.4 Amphoteric behaviour of ceramic membranes

Some membranes in the presence of water can have electrically charged surfaces. For ceramic membranes, the characteristics of the surface charge depend mainly on the chemical properties of the membrane and the chemistry of the solution.

As mentioned in the previous sections of this work, most mesoporous UF membranes and microporous NF ceramic membranes usually consist of minerals oxides.

When a mineral oxide is coming in contact with an aqueous medium it develops an electrical charge due to the amphoteric behaviour of surface sites to maintain the electroneutrality of the solution with reorganisation of ions at a solid-solution interface.

The mechanism of this amphoteric behaviour has been described by Moritz et al. [34]. In the presence of water, the surfaces of mineral oxide ceramic membranes are occupied by amphoteric MOH groups, these groups are able to be dissociated when the membrane surface comes in contact with polar liquid, such dissociation depends mainly on the pH of the solution.

This amphoteric behaviour can be expressed by the following two equations [34]:

1) $MOH + H^+ \rightarrow MOH_2^+ \leftrightarrow M^+ + H_2O$

2) $MOH + OH^- \rightarrow M(OH)_2^- \leftrightarrow MO^- + H_2O$

It can be seen that the first equation causes a positive charge whereas the second equation produces a negative charge on the solid surface

As a result for this behaviour, the characteristics of the membrane surface material with support structure such as pore size, thickness, porosity and zeta potential have an influence on the permeate flux, fouling tendencies and rejection properties of the solutes [35].

In some cases the amphoteric nature of the ceramic membranes can lead to preferential adsorption of a particular component and thus improves the retention [30].

Figure (2.8) explains the mechanism of charged surface formation as a result of amphoteric behaviour of metal oxides. It can be seen from this figure that the occurrence of a neutral and charged surface is due to the formation of metal aquo complexes at the oxide-solution interface [28].

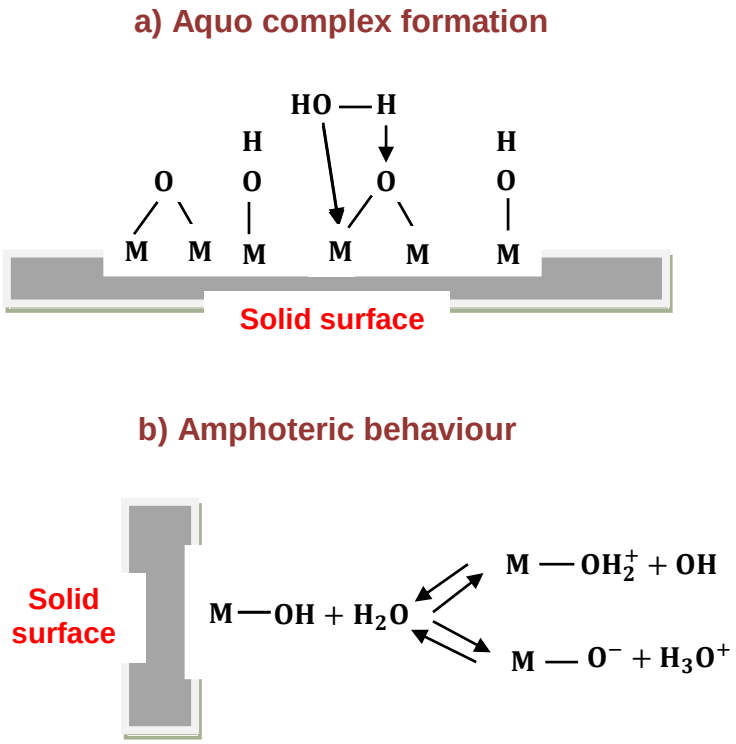

Figure 2.8: Mechanism of charged surface formation due to amphoteric behaviour of metal oxides [28].

2.3 Nanofiltration membrane

2.3.1 Introduction

The Nanofiltration (NF) membrane is considered as one of the pressure-driven membranes with features in between ultrafiltration and reverse osmosis membranes.

A nanofiltration membrane offers unique specifications such as a low working pressure, high permeate volume flux, high rejection of multivalent ion salts and organic molecules at low operation and maintenance costs. Because of these specifications, the applications of NF have been widely increased [2].

The era of NF membranes started in the early seventies when RO membranes with sensible water permeate volume flux which operated at comparatively low pressures were advanced. The RO membranes that worked at low pressure became recognized as NF membranes. By the second half of the eighties, NF became more common and a suggested definition for this membrane at that time was based on a molecular weight cut off value (MWCO) of 1000 g/mol [36].

This section reviews the general properties of NF membranes as well as the transport theory of NF membranes. Additionally, it provides a comparison between NF and RO membranes.

2.3.2 General properties of NF membranes

In general, nanofiltration membranes usually have the following distinct properties [37], [38]:

- The NF membrane pore size corresponds to a MWCO value of about 300–500 g/mol. Based on this; the separation of a certain component with this molecular weights ratio from higher molecular components can be accomplished. Membranes with a MWCO value of 1000 and above are treated as UF membranes.
- Based on their manufacturing materials, NF membranes can have either a slight positive or negative surface charge. The charge's interaction can play an important role when the separation of ions with different valences is needed especially when the dimensions of membrane's pore size are larger than the size of the ions.
- Nanofiltration membranes have a lower applied trans-membrane pressure and a higher flux than RO membranes.
- Nanofiltration membranes separation features lies between UF and RO membranes, thus; the efficiency of these membranes normally depend on a mixed mass transport mechanisms including the molecular sieving mechanism of UF membranes and the diffusion mechanism of RO membranes.
- A marked influence of the Donnan-effect in the case of an aqueous feed solution containing mixed electrolytes.

According to these properties, the most significant implementation areas for NF membranes can be shown as follows [36]:

- Segregation of ions with different valences.
- Segregation of low and high molecular weight components.

These basic properties and the possible applications of NF membranes can offer unique characteristics to perform the separation of salts or organics. The structure of a nanofiltration membrane which is represented by a bundle of charged capillaries with nanoscale pore radius can be added as a further evidence to establish the rejection of salts. Some similarities can be noted between the organic and the inorganic NF membrane's behaviour; however, specification exists with ceramic membranes due to the amphoteric properties of metal oxides in water media [2].

2.3.3 Transport theory of NF membranes

The growing development of NF membranes requires an understanding of the issues and the fundamental factors that affect the transport of both the solute and the solvent (usually water) in such membranes. According to Bird et al. [39] and Chaabane et al. [40] and by assuming that the transport is isothermal with no electrical effects, the basic theory that governs the transport of solutes in microporous media is often described as follows:

$$J_{i_{mass}} = -\rho_i \nu - D_i \Delta\rho_i \quad \textbf{2.8}$$

Here:

$J_{i_{mass}}$: Mass flux of component i through the membrane (mass per time per area).

ρ_i: Mass density of component i.

ν: Fluid mass average velocity through the membrane.

D_i: Effective diffusion coefficient of component i in membrane.

$\Delta\rho_i$: Mass density gradient

Bird et al. [39] showed that for pressure driven membrane processes where pore flow contributes mainly to flux, Darcy's law is usually used to evaluate the mass average velocity, as follows:

$$\nu = -\frac{K}{\mu}(\Delta P - \rho g) \quad \textbf{2.9}$$

K: Permeability of medium.

μ: Fluid viscosity.

ΔP: Pressure gradient with respect to position.

ρ: Solution density.

g: Gravity factor.

Sagle and Freeman [41] stated that by restricting the transport to only the x-direction (this would typically be the direction perpendicular to the membrane surface) and ignoring the effects of gravity, then substituting Equation (2.9) into Equation (2.8), gives:

$$J_{i_{mass,x}} = -\frac{\rho_i K}{\mu}\frac{dp}{dx} - D_i\frac{d\rho_i}{dx} \quad \textbf{2.10}$$

It can be seen from Equation (2.10) that the first term to the right corresponding to a convection term (typically represents the mass flux through membrane pores) and the second term to the Fickian diffusive flux through porous membranes.

Generally, the diffusion through the porous membranes is negligible when compared to the pressure-driven convection effects. Thus, the permeate volume flux can be considered as directly proportional to the applied pressure difference through the membrane. In other words, the applied pressure (or trans-membrane pressure) represents the only driving force that governs the transport of liquids inside porous membrane structures such as MF, UF and NF membranes [41].

The permeability (K) of a porous medium in the convection term of Equation (2.10) depends to a large extent on certain factors such as the porosity (ε) and the tortuosity (τ).

The porosity or fractional void space in the porous structure can be defined as the ratio of pore volume (V_p) to the apparent volume (V). The value of this fraction depends on the method used to determine the apparent volume (geometrical, fluid displacement) and on that used to assess pore volume. The porosity for MF, UF, and NF membranes are typically ranges from $0.3-0.7$ [41].

The tortuosity (τ) is considered as an indication to a direction that corresponds to a given macroscopic flow. It is defined as the effective average path length (actual length) in the porous medium (L_e) divided by the shortest linear distance (L_s) measured along the ends of the flow path. Based on this definition, it can be concluded that the value of tortuosity is always more than 1. However, cylindrical pores that perpendicular to the surface have tortuosity equal to unity [40].

The NF membrane represents a loss RO membrane thus; the transport of a molecule across the membrane is governed by diffusion mechanism. In this case, the second term in Equation (2.10) controls the flux across the membrane as well.

The diffusion mechanism of mass transport across microporous (NF and RO) membranes is typically characterized in terms of the "solution-diffusion model". In this model the salt and water dissolve first into the membrane material and then diffuse across the membrane [42], [43], [33].

According to the solution-diffusion model, the water flux through the membrane is given by the following expression [41], [44]:

$$J_w = L\,(\Delta p - \Delta \pi) \qquad \textbf{2.11}$$

In which

J_w : Water flux through the membrane.

Δp : Trans-membrane pressure drop.

$\Delta\pi$: Osmotic pressure difference.

L : Water permeability constant (depends on the physical specifications of the membrane).

Based on the theory of the solution diffusion model that is used to describe transport in nano porous films, (L) is given by [42], [33]:

$$L = \frac{DSV_w}{R_g T l} \quad \textbf{2.12}$$

Where:

D: Diffusion coefficient of water in the membrane.

S: Solubility of water in the membrane.

V_w: Molar volume of water in the external phase.

R_g: Universal gas constant.

T: Temperature.

l: Thickness of the membrane.

Similar to the water flux, the salt flux across a microporous membrane is described by the equation [33], [43]:

$$J_J = B\ (C^{feed} - C^{permeate}) \quad \textbf{2.13}$$

Here:

J_J: Salt flux through the membrane.

C^{feed}: Salt concentration in the feed solution.

$C^{permeate}$: Salt concentration in the permeate solution.

B: Salt permeability constant (depends on the physical characteristics of the membrane), is given by the following [33]:

$$B = \frac{D_S K_S}{l} \quad \textbf{2.14}$$

Where:

D_S: Diffusion coefficient of salt.

K_S: Salt partition coefficient.

Equation (2.13) shows that the salt flux is essentially independent of pressure. In other words, the salt flux depends mainly on salt concentration.

Instead of reporting salt flux values, the reduction of solute concentration during the membrane filtration process is usually represented in terms of a dimensionless solute rejection coefficient which basically measures the ability of the membrane to separate salt from the feed solution.

The percentage of salt rejection coefficient (R %) can be defined as follows [33]:

$$R = \left(1 - \frac{C^{permeate}}{C^{feed}}\right) \times 100\% \quad \textbf{2.15}$$

The salt concentration in the permeate phase can be related to the salt flux and water flux according to the following expression [2], [3]:

$$C^{permeate} = \frac{J_J}{J_w} \times C_{water} \quad \textbf{2.16}$$

C_{water}: Concentration of water in permeate phase.

By substituting the water flux equation (2.11) and the salt flux equation (2.13) in the permeate salt concentration equation (2.16) and rearranging the terms, the following membrane rejection term may be derived [45], [46]:

$$R = \left(\frac{\frac{L}{B}(\Delta P - \Delta\pi)}{1 + \frac{L}{B}(\Delta P - \Delta\pi)}\right) \times 100\% \quad \textbf{2.17}$$

Equation (2.17) illustrates the main factors that the salt rejection in microporous membrane mainly depends on, which are; the physical properties of the membrane (as a result of both water (L) and salt (B) permeability constants), the applied TMP difference in addition to the osmotic pressure difference.

2.3.4 Comparison between NF and RO membrane specifications

The main applications of NF membranes include the desalination of brackish water, removal of micro-pollutants, removal of organics, water softening, industrial waste water treatment (such as: pulp and paper, dairy, textile and pharmaceutical industries), and the treatments of surface and ground water. Whereas the main implementations of RO membranes include: the desalination of brackish and seawater, production of ultra pure water, and specific industrial waste water treatment.

Table (2.2) shows a summary of nanofiltration membrane specifications compared to reverse osmosis membranes [2], [5], [21], [27], [28]:

Table 2.2: Specifications of NF membranes compared to RO membranes.

	Specification	NF membranes	RO membranes
1.	Membrane	composite	asymmetric (composite)
2.	Active top layer	$\approx$ 1 µm	$\approx$ 1 µm
3.	Supported sublayer	$\approx$ 150 µm	$\approx$ 150 µm
4.	Pore size	< 2 nm	< 2 nm
5.	Driving force	pressure $(3 - 20$ bar$)$	pressure $(15 - 100$ bar$)$
6.	Flux range	$1.4 - 12$ $(\mathrm{l.m^{-2}.h^{-1}.bar^{-1}})$	$0.05 - 1.4$ $(\mathrm{l.m^{-2}.h^{-1}.bar^{-1}})$
7.	Separation principle	solution-diffusion model	solution-diffusion model
8.	Monovalent ions solute retention	$50 - 70\%$	$> 98\%$
9.	Bivalent ions solute retention	$> 90\%$	$> 99\%$
10.	Bacteria and virus retention	99.99%	99.99%
11.	Proteins retention	99.99%	99.99%
12.	Humic acid retention	99.99%	99.99%

It can be seen from Table (2.2) that NF and RO membranes are actually the same except that the network structure is more opened in NF membranes. As a result of this, the rejection of monovalent ions (such as Na^+ and Cl^-) becomes much lower, but the rejection of bivalent ions (such as Ca^+ and SO_4^-) remains very high [21].

Compared to ceramic NF membranes, conventional RO membranes have the following specifications [5], [21], [22], [27], [28]:

- High operation cost.
- High operating pressure.
- Low permeability (or permeate flux rate).
- Low chemical resistance.
- Low possibility of regeneration.
- Low abrasion resistance.
- High fouling tendency.
- Not applicable for dry storage after cleaning.
- Possibility of bacterial growth.
- Deformation under pressure.
- Not easy to clean.
- Low durability.
- Swelling problems.
- Modular construction not easy to scale up.
- More space requirements.
- Low thermal stability.
- Not applicable for steam sterilization and back flushing.
- Low structural stability.

However, the ceramic membranes still suffer from a few limitations, such as their brittle character which requires careful handling and the sealing problem due to the different thermal expansions of the ceramic membrane and module housing.

The unique characteristics of the newly developed commercial ceramic nanofiltration membranes encourages the researchers to try this type of membrane filtration process in many new applications in order to overcome several operational problems that are normally associated with conventional membrane filtration techniques.

2.4 Electrically charged membranes

2.4.1 Introduction

The presence of an electrical charge in any membrane depends mainly on the properties of that membrane towards charged solutes.

It is generally recognized that separation properties of porous membranes are not only related to their physical properties such as pore size distribution, thickness, and porosity but also on their surface charge properties. This additional transport mechanism can lead to improved membrane separation efficiency.

Therefore, understanding the electrokinetic mechanisms that might occur during the filtration of a solution containing a charge species appears to be an important step to assess the filtration performance and predict the behaviours of ionic transfer inside nanofiltration membranes [47], [48].

In the asymmetric or composite ceramic membranes which usually consist of several layers of one or more different ceramic materials having different transport properties, the overall performance may be related to the contributions from each of the different layers. For instance, in nanofiltration membranes, the outer dense active skin layer normally shows high salts rejection that specifies membrane properties.

However, there is also a contribution of the membrane intermediate layers, so based on this fact the separation performance of asymmetric ceramic membrane can be demonstrated by the combination of surface charge and size exclusion effects [28].

Electrokinetic measurements are usually used to describe the sign and magnitude of a charged membrane. As mentioned previously in section (2.2.4), the acquired membrane charge could be attributed to the amphoteric behaviour of the ceramic membrane coming in contact with water. As a result of the Donnan exclusion effect, the charge interaction in porous membranes can improve the ion's rejection even when the dimensions of the membrane pore's size are larger than the size of the ions.

This section reviews the electrical double-layer and Gouy-Chapman theories and the techniques of measuring the zeta potential of membranes. Additionally, it explains the available models for evaluating a membrane's surface charge density and the Donnan potential of the membrane.

2.4.2 Electrical double layer theory

The theory of the electrical double layer (EDL) is the basis that can be used to interpret the membrane's electrokientic phenomena.

The formation of EDL can be affected mainly by the structure of the mineral oxide membrane such as the pore size and porosity, besides the nature of the electrolyte solutes such as the molar ionic concentration, valance and size of ions [47].

Israelachvili [48] defined the theory of EDL as "the separation of charges at the interface between two phases since most oxide membranes acquire electric surface charge when they are placed in a polar or aqueous medium through several mechanisms". These mechanisms include the dissociation of surface functional groups and adsorption of ions from the solution.

According to Dukhin et al. [49], the EDL generally refers to two parallel layers of charge surrounded by the surface of a solid material, in which the ions of an opposite charge (counter-ions) are attracted towards the surface and the ions of the same charge (co-ions) are excluded and repelled away from the surface. The equilibrium in EDL is reached when the absolute values of both counter-ions and co-ions are equal. This theory assumed that the electric field is formed and located only inside the EDL, which means that there is no ion transport (or ionic flux) between the electrolyte and the electrical double layer.

The electrical double layer around a charged oxide surface consists of two regions [50], [51], [28]:

- The "Stern layer" inner region of adsorbed ions. The chemical interactions of this layer reflect the specific properties of the counter-ions and the nature of the surface. This layer is located immediately next to the solid surface and might also be described as the compact layer since the ions in this layer are immobile and strongly attracted to the solid surface.
- The "Gouy layer" outer region of extended diffused ions. This layer is made of free mobile ions that still exhibit Brownian movement (further information about this layer in the Gouy-Chapman theory, see section 2.4.4).

Many researchers such as Bandini [51] and Blank et al. [52] agreed that the description of a double layer formation on oxide surfaces in the existence of an electrolyte solution can be applied to a pore's wall in nanofiltration membranes.

Figure (2.9) illustrates a schematic representation of an electric double layer formation in the presence of electrolytes at a negatively-charged membrane surface.

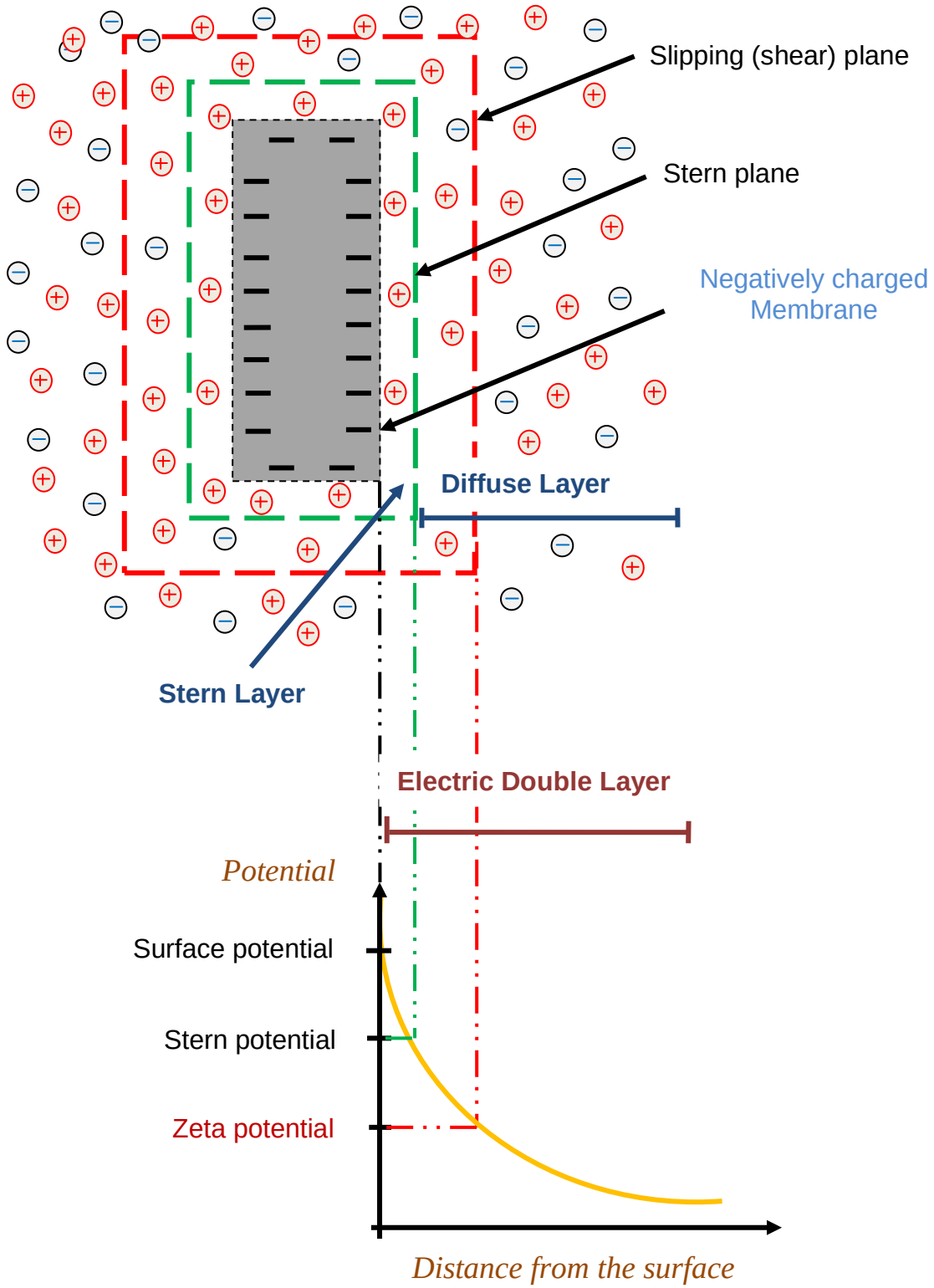

Figure 2.9: Schematic representation of electric double layer formation in the presence of electrolytes (adopted from [47]).

2.4.3 Zeta potential measuring techniques

As shown in the previous sections, the filtration performances of the ceramic membranes are usually affected by the electrochemical properties of that membrane towards charged solutes. This membrane electrokinetic phenomenon can result from the relative motion between an electrolyte solute and a charged membrane surface. The Stern potential at the boundary between the Stern and Gouy layers (see Figure 2.9) represents a very important parameter in the EDL, but this potential cannot be measured directly; however, the electrokinetic zeta potential is usually considered as a suitable substitution [53].

Hagmeyer and Gimbel [54] defined the zeta potential (ζ-potential) as "the potential at the plane of shear between the charged surface and liquid moving with respect to each other". The ζ-potential is used to recognize sign and magnitude of the surface charge and depends mainly on the concentration of the bulk solution. The amount of ζ-potential is directly proportional to the electrostatic repulsions.

ζ-potential is a commensurable parameter that can be linked to the membrane charge and electrical double layer of surfaces in aqueous solutions. The determination of membrane electrokinetic properties is often expressed in terms of zeta potential which can be determined from any of the following procedures [55], [56], [57], [58]:

2.4.3.1 Microelectrophoresis method

Microelectrophoresis analysis represents a very common electrokinetic method that is used to characterise the ζ-potential at a membrane-electrolyte interface.

In this analysis, a portion of the membrane is crushed in a rock mill. The sub-micrometer's size fragments of the grinded membrane were mixed with certain colloidal or electrolyte solutions, then, a laser Doppler electrophoretic mobility analyser is used to obtain the electrophoretic motilities on colloidal suspensions of a pulverized membrane [59], [60].

This method is widely effective for studying powder dispersions. However unlike other methods, this procedure requires destroying the membrane and allows determining the zeta potential of a membrane sample after grinding, but the newly formed surface can differ considerably from the membrane surface especially for measuring the ζ-potential of an asymmetric (composite) ceramic membrane in which the supporting layer's metal oxides differ from the surface active layer of the membrane.

2.4.3.2 Electro-osmosis method

In this method, an electric field is applied across a charged porous membrane. The charges in the mobile part are then moved to pull the water molecules along with them. An electro-osmotic flow is then generated at a certain velocity in the electric field, which is usually known as electrophoretic mobility which can be measured by using a laser Doppler velocimetry analyser. The volume of liquid transported per unit time can be used to determine the ζ-potential on a pore's wall [21].

2.4.3.3 Streaming potential method

Streaming potential is the potential difference at zero current caused by convective flow of a charge due to the pressure gradient in a charged membrane [59]. In this process, the electrolyte is forced through the pore by applying a pressure to one side of the membrane. The charges present in the mobile part of the double layer are carried towards the pore end. The accumulation of charges set up an electric field. The resulting electric potential difference (ΔE) on both sides of the membrane per unit of hydrodynamic pressure difference (ΔP), is called the streaming potential [60].

Alfonso et al. [61] explained that among all available techniques, streaming potential is the most suitable to determine the ζ-potential for a solid membrane surface. This method is preferred over electro-osmosis when measuring zeta potential because it is more convenient to measure small electrical potentials rather than a small rate of liquid flow.

Peeters et al. [62] showed that the electrokientic properties of mineral oxide membranes are frequently characterised in terms of ζ-potential and iso-electric points. The membrane zeta potential can be evaluated as a function of (pH) and ionic strength, whereas the iso-electric point represents the pH value when the ζ-potential is zero. In other words, zeta potential can be defined as the pH value at which the net charge of the membrane is globally zero.

The membrane ζ–potential can be determined (based on the measured streaming potential) from the well known Helmoholtz-Smoluchowski equation (H-S Equation) outlined as follows [61], [62], [63]:

$$\zeta = \frac{\Delta E_{stre}}{\Delta P} \frac{\mu}{\varepsilon_r \varepsilon_\circ} k \qquad \textbf{2.18}$$

Where:

ζ: Zeta potential (V).

ΔE_{stre}: Measured electrical (streaming) potential in the flow cell used to force the electrolyte to flow over the charged membrane (V).

ΔP: Applied pressure increment (Pa).

μ: Dynamic viscosity of the solution (Pa. s).

ε_r: Relative permittivity of water (78.54 at 25 ℃).

$\varepsilon_\circ$: Permittivity of free space (8.854×10^{-12} C. m^{-1}. V^{-1}).

k: Bulk conductivity of circulating electrolyte, (S. m^{-1}).

This equation applies for electrolyte concentrations larger than 0.001M. In case of lower concentrations, the surface conductivity effect contributes as well and the above equation needs to be multiplied by a correction factor [2], [63]. Takagi et al. [64] stated that the accuracy of measuring the ζ-potential by using this method is very high.

2.4.4 Gouy-Chapman theory

As discussed previously in section (4.2.4), the extended diffusive outer regions or Gouy layer represent one of the two main regions of the EDL theory, and also might be called the Gouy-Chapman layer. This layer has a complex structure; hence, the quantitative characterisation of the outer diffusive layer is difficult [65].

Gouy-Chapman devised a theory for hard surfaces to study the structure of the interface of the diffuse double layer. The basic assumptions of the Gouy-Chapman theory are summarised as follows [66], [49]:

- The solid surface is assumed to be flat and uniformly charged.
- The ions in the diffuse layer of the electrical double layer are assumed to be distributed according to the Boltzmann distribution.
- The dielectric constant (ε) is assumed to be constant inside the diffuse layer.
- The electrolyte of charge (z) is assumed to be single and symmetric.

The existence of a bulk concentration for electrolyte ions has a major effect not only on the electrostatic potential but also on the force between charged surfaces, so, understanding the double-layer interaction between two surfaces will lead to understanding the ionic distribution adjacent to a nanoporous surface in contact with an electrolyte solution. However, based on the above assumptions, this theory is applicable only for solutes under certain conditions.

Figure (2.10), (a) and (b) illustrates the charge and potential distribution in a negatively charged solid surface in contact with an aqueous solution based on the electrical double layer theory.

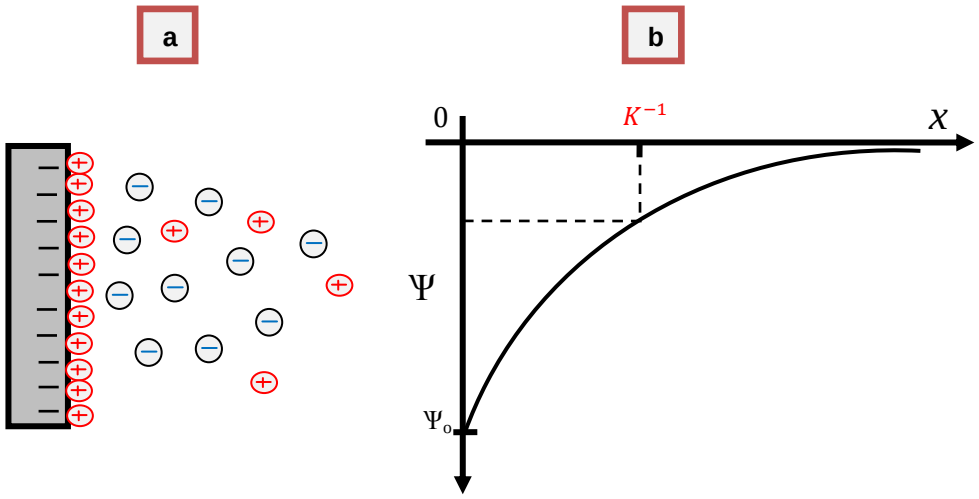

Figure 2.10: Schematic of the charge (a) and potential distribution (b) inside the electrical double layer of negatively charged surface in contact with aqueous solution [49].

It can be seen from Figure (2.10) for a negatively charged surface, the accumulation of cations (counterions) on the solid surface as a result of electrostatic attraction and the depletion of anions (coions) as a result of the electrical repulsion. Figure (2.11) shows the equilibrium of cations (C^+) and anions (C^-) inside a field of an electric double layer where ($C_\circ$) represents the bulk concentration of the electrolyte at distance (x) equal to infinity (∞).

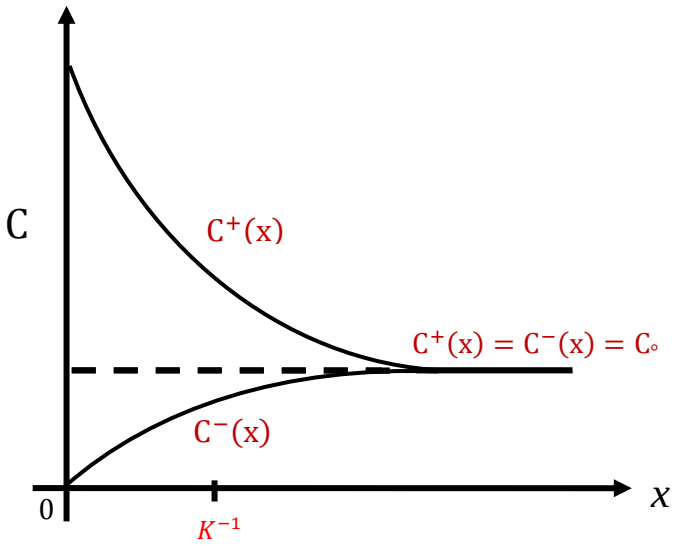

Figure 2.11: Distribution of counterions (C^+) and coions (C^-) in a negatively charged surface [49].

Applying the Boltzmann probability distribution to the ionic number concentration of positive and negative ions (number per unit volume), gives [48], [67]:

$$\mathrm{C}^{+} = \mathrm{C}_{\circ}.exp\left(-\frac{ze\Psi}{k_B T}\right) \quad \textbf{2.19}$$

$$\mathrm{C}^{-} = \mathrm{C}_{\circ}.exp\left(+\frac{ze\Psi}{k_B T}\right) \quad \textbf{2.20}$$

Here, (C^{+}) and (C^{-}) represent the ionic number concentrations for cations and anions at a given location in the electrolyte, while $(\mathrm{C}_{\circ})$ represents the bulk concentration of the electrolyte, and:

Ψ: Electrical field potential at a given position of the electrolyte (V).

z: Absolute value of the ionic valance.

e : Elementary charge (1.6022×10^{-19} C).

k_B: Boltzmann constant (1.3806×10^{-23} J/K).

T: Absolute temperature (289 K).

The net charge density (σ^d) at any point in the double layer is proportional to the concentration difference between the cations and anion, thus [48]:

$$\sigma^d = ze(\mathrm{C}^{+} - \mathrm{C}^{-}) \quad \textbf{2.21}$$

Substituting equation (2.21) with the equations (2.19) and (2.20), gives:

$$\sigma^d = -2ze\mathrm{C}_{\circ}.sinh\left(\frac{ze\Psi}{k_B T}\right) \quad \textbf{2.22}$$

The relationship between the net charge density and the electrical potential (Ψ) is described by the Poisson equation, which takes the following form:

$$\frac{d^2\Psi}{dx^2} = \frac{\sigma^d}{\varepsilon_r \varepsilon_{\circ}} \quad \textbf{2.23}$$

Substituting Equation (2.22) with the Poisson equation and solving it gives a relationship between the electrical potential (Ψ) and the Debye length ($1/K$ or K^{-1}). Figure (2.10) and Figure (2.11) show the location of the Debye length.

$$\Psi = \frac{2k_B T}{ze} ln\left(\frac{1 + \gamma \exp(-Kx)}{1 + \gamma \exp(-Kx)}\right) \quad \textbf{2.24}$$

With,

$$\gamma = \frac{\exp\left(\frac{ze\Psi_\circ}{2k_BT}\right) - 1}{\exp\left(\frac{ze\Psi_\circ}{2k_BT}\right) + 1} \quad \textbf{2.25}$$

And,

$$K = \left(\frac{2z^2e^2\mathrm{C}_\circ}{\varepsilon_r\varepsilon_\circ k_BT}\right)^{1/2} \quad \textbf{2.26}$$

This is known as the Gouy-Chapman theory for the diffuse double layer.

When the term $(ze\Psi_\circ/2k_BT) < 1$, then Equation (2.24) reduces to the so-called Debye-Huckel equation [48]:

$$\Psi = \Psi_\circ\, exp[-Kx] \quad \textbf{2.27}$$

The Debye length $1/K$ or (K^{-1}) normally refers to the "thickness of the diffuse double layer as a function of the electrolyte concentration". This parameter is independent of solid surface properties and can be evaluated based on the properties of the electrolyte (such as bulk ionic concentration and valance of the electrolyte).

2.4.5 Membrane surface and effective charge density

According to Israelachvili [4] and Peeters et al. [62], the relationship between the membrane net surface charge density (σ) and the membrane ζ-potential for low potentials (usually below 50 mV) can be described by using the following simplified Grahame equation:

$$\sigma = \frac{\varepsilon_\circ\varepsilon_r\zeta}{K^{-1}} \quad \textbf{2.28}$$

Here:

σ: Surface charge density, $(\mathrm{C.\,m^2})$.

$\varepsilon_\circ$: Permittivity of free space.

ε_r: Relative permittivity of water.

ζ: Zeta potential (V).

K^{-1}: Debye length (m), in which:

$$K^{-1} = \sqrt{\frac{\varepsilon_\circ\varepsilon_r k_BT}{4e^2N_A\,I}} \quad \textbf{2.29}$$

N_A: Avogadro number $(6.022 \times 10^{-23}/\mathrm{mol})$.

I: Ionic strength, where [50]:

$$I = 0.5 \sum z_i^2 \, c_i \qquad \textbf{2.30}$$

z_i: Valance of ion i.

c_i: Concentration of species i.

Israelachvili [48] showed that at 25 ℃, the Debye length (nm) of aqueous solutions can be determined based on the bulk ionic concentration and valance of the electrolyte as follows:

- For 1 : 1 electrolytes (such as, NaCl)

  $K^{-1} = 0.304 \sqrt{\text{NaCl}}$

- For 2 : 1 and 1 : 2 electrolytes (such as, $CaCl_2$ and Na_2SO_4)

  $K^{-1} = 0.176 \,/\, \sqrt{Na_2SO_4}$

- For 2 : 2 electrolytes (such as, $CaSO_4$)

  $K^{-1} = 0.152 \,/\, \sqrt{CaSO_4}$

For example, for NaCl solution, K^{-1} = 30.4 nm at 10^{-4} M, and 0.3 nm at 1.0 M.

Also, according to the Gouy-Chapman theory, the membrane surface charge density can be related to zeta potential by the following equation [61]:

$$\sigma^s = \left(2\varepsilon_\circ \varepsilon_r k_b T \sum\nolimits_{=1}^{n} c_i N_A \left(exp\left(-\frac{ze\zeta}{k_B T}\right) - 1\right)\right)^{0.5} \qquad \textbf{2.31}$$

Where:

σ^s: Electrical charge on membrane surface (C.m^2).

c_i: Concentration of ion i in the salt solution (mol.m^3).

The effective membrane fixed charge density X^m represents the concentration of electrically charged groups on the membrane surface. This parameter can be obtained from converting the membrane surface charge density σ^s to concentration units by assuming that the membrane surface charge is uniformly distributed in the void volume of cylindrical pores; as shown in the given equation [48], [68]:

$$X^m = \frac{2\sigma^s}{r_p F} \qquad \textbf{2.32}$$

Where:

X^m: Concentration of electrical charged groups on the membrane surface (mol.m^3).

σ^s: Electrical charge on the membrane surface (C.m^2).

r_p: Effective membrane pore radius (m).

F: Faraday constant (9.64867×10^4 C.mol).

2.4.6 Donnan potential

The electrostatic interaction and repulsion between ions of the solute and surface charge of the membrane represent one of the mechanisms that could explain the rejection behaviour of ions in nanofiltration membranes. This mechanism can be explained by the Donnan potential [69].

Based on the fundamentals of electrokientic effects, if a charged membrane is coming in contact with an electrolyte solution, equilibrium occurs between the membrane and the electrolyte solution due to the presence of the effective membrane fixed charge density [61].

According to Scheap et al. [47], there is a difference between the ionic concentrations in the bulk solution compared to these in the membrane. The counterions (opposite charge sign to the fixed charge of the membrane) concentration is higher in the membrane phase than in the bulk solution, whereas, the coions (same charge sign as the fixed charge of the membrane) is lower in the membrane phase. As a result of this difference, an electrical potential at the membrane interface is built-up to counteract the transport of coions to the membrane phase and the transport of the counterions to the solution phase. This potential is called the Donnan potential.

By applying a pressure gradient across the membrane, the effect of the Donnan potential is to repulse the coions from passing through the membrane. In order to achieve the system electroneutrality requirements, the counterions are rejected as well and salt retention occurs. This behaviour might also be called the Donnan equilibrium formalism.

Peeters et al. [62] explained that the determination of the Donnan potential depends mainly on the following important factors:

- Concentration of solutes.
- Effective fixed charge concentration in the membrane.
- Valence of both counterion and coion.

For the ideal solution, the standard generalisation equation that describes the Donnan potential ($\Delta\psi_{Don}$) is given by [2], [61], [70]:

$$\Delta\psi_{Don} = \frac{R_g T}{z_i F} ln\,(a_i / a_i^m) \qquad \textbf{2.33}$$

Here, a_i represents the activity of ion i in the bulk solution and a_i^m is the activity of ion i inside the membrane pores. This formula is known as the Nernst equation.

The ion i in Equation (2.33) might refer either to the cation or the anion of the solute (such as Na^+ or Cl^- in case of using a NaCl solution as a background electrolyte).

For diluted monovalent salt the activity of ion i in Equation (2.33) can be replaced by the concentration of ion i [2], [61].

This equation is correct when applied for uniform and non-uniform charge distribution associated with any phase equilibrium along the domain. The standard Donnan potential equation decreases to the usual Donnan potential in the particular case of homogenous charge distribution (described by constant voltage and concentration distribution).

As shown previously, the Donnan potential equilibrium at the interface between both sides of membrane and the solution exists in the presence of the effective fixed membrane charge concentration (X^m) that originally relates to the membrane surface charge density (σ^s).

Available literatures show that there are some approaches that can be used to determine the value of the Donnan potential. But all these methods depend on the determination of the membrane effective fixed charge density.

Based on Theorell, Meyer, and Sievers (TMS) model [71], [47]; the Donnan potential for 1:1 electrolytes can be determined as follows:

$$\Delta\psi_{Don} = \frac{R_g T}{F}\left(ln\frac{c_2}{c_1} ln\frac{\phi X + \sqrt{4c_2^2 + \phi^2 X^2}}{\phi X + \sqrt{4c_1^2 + \phi^2 X^2}}\right) \quad \textbf{2.34}$$

Where:

$\Delta\psi_{Don}$: Donnan potential (V);

R_g: Universal gas constant ($8.314\ \mathrm{J.mol^{-1}.K^{-1}}$);

c_2: Concentration of ion at the permeate side ($\mathrm{mol.m^3}$).

c_1: Concentration of ion at feed side ($\mathrm{mol.m^3}$).

X: Membrane effective charge density ($\mathrm{mol.m^3}$).

ϕ: Parameter refers to the characteristics of the membrane–electrolyte pair considered, and mainly depends on the type of the electrolyte and the electrolyte concentration.

ϕ In this equation represents an extra parameter, which in the TMS model is always equals to 1 [47].

Unlike the previous two Donnan potential equations which mainly depend on the activity (or concentration) of the ions in both the bulk and permeate sides, in 1990 Ohahima and Kondo [72], [73] derived an expression to evaluate the Donnan potential of an-ion-penetrable membrane immersed in a symmetrical electrolyte solution based on the uniform distributed membrane fixed charge density, bulk concentration and valency of the charged groups. This expression is used by many authors to determine the Donnan potential such as Yee et al. [74] and Wonders et al. [75].

In 2009, this formula was developed by Chein et al. [76] for a cylindrical pores membrane. In this formula, the Donnan equilibrium must occur in order to satisfy the system electro-neutrality conditions; this can be written as follows:

$$z_f c_f + \sum_{i=1}^{N} z_i c_i = 0 \qquad \textbf{2.35}$$

Where (f) denotes the firmly bound ions on the pore wall.

According to the Boltzmann distribution, the ion concentration distribution c_i of valence z_i can be expressed as [77]:

$$c_i = C_{i,bulk}\, exp\left(-\frac{z_i F}{R_g T}\Delta\psi_{Don}\right) \qquad \textbf{2.36}$$

By choosing ion 1 as the reference ion, the well known expression for the Donnan potential of the membrane (in volt) can be evaluated based on the bulk concentration $C_{i,bulk}$ of each ion and the effective membrane fixed charge concentration from the substituting and solving of Equations 2.35 and 2.36 as follow [76]:

$$\Delta\psi_{Don} = \frac{R_g T}{F} sinh^{-1}\left(\frac{z_f X^m}{2C_{i,bulk}\, F}\right) \qquad \textbf{2.37}$$

Equation (2.37) applied only for 1:1 electrolytes with bulk molar concentration of $C_{i,bulk}$ (mol/l) and valance z_f [76] while the effective charge density X^m (mol. m^3) can be calculated from Equation 2.32 based on the value of the membrane surface charge density σ^s (C. m^2).

2.5 Membrane fouling

The typical reduction of membrane permeates flux with time to levels below their actual capacity as a result of fouling represents one of the main problems that negatively affects the performance of membrane filtration processes.

According to Mulder [21], membrane fouling can be defined as "the accumulation of materials at the surface, or in the membrane pores, which decreases the permeate flux of the membrane".

Considerable studies have been performed in the last two decades to explore the fouling behaviours and the related permeate volume flux drop in membranes. The flux decline in membranes can be attributed to several factors that might cause an additional resistance on the feed side, such as: concentration polarisation, adsorption, cake formation, and plugging of the pores.

Many factors that govern the rejection in NF membrane can also play an important role in the fouling and cleaning of a membrane as follows [11], [78]:

- Membrane structural properties, such as; pore size distribution, thickness, porosity, and charge type.
- The chemistry of a treated solution, such as; solute compositions, pH, ionic strength, valence and the fouling affinity of the solute towards the membrane.
- The system design parameters, such as; the capacity, the dimensions, and the type of flow operation mode.
- The process operation conditions, such as; flow rate, applied trans-membrane pressure, temperature, cross velocity and flow patterns.

Schäfer et al. [2] stated that reducing (or eliminating) the membrane fouling started by identifying the foulants because once the foulants are identified, applicable control strategies can be adopted.

2.5.1 Concentration polarisation

Bian et al. [79] defined the concentration polarisation (CP) as the accumulation of the solutes (or particles) immediately adjacent to the membrane surface being higher than that in the bulk side. This phenomenon can lead to serious problems during membrane operation processes such as: deterioration in the quality of permeates, increase in the risk of fouling and possibility of scale development, furthermore, it increases the overall resistance to solute flow and thus decreases the permeate flux.

Several quantitative models have been used to investigate the behaviour of the CP layer. The film theory provides a simple analytical approach that works well for most RO/NF separations [33], [79]. This model assumes that the permeation driving force is the gradient in the chemical potential of the solution, therefore; the concentration of solution at the surface of the membrane can be evaluated based on the mass transfer film theory [21].

In the boundary layer, the net solute flux J_{v,C_p} is equal to the convection flux of the solute towards the membrane $J_{v,C}$ minus the diffusive flux of solute back into the bulk, expressed by diffusion law as $D(dc/dx)$, thus; the transport of a solute at any point inside the boundary layer can be expressed as follows [33]:

$$J_{v,C} - D(dc/dx) = J_{v,C_p} \quad \textbf{2.38}$$

Figure (2.12) shows a schematic of a concentration profile in concentration polarisation phenomena. According to the definition of the concentration polarisation phenomena, the solute concentration at membrane (C_m) is higher than that in the bulk (C_b), and the back-diffusion occurs from the membrane surface into the bulk side, while (C_p) represents the solute permeate concentration.

Integration of Equation (2.38) over the thickness of the boundary layer leads to the following concentration polarisation equation [80], [33]:

$$(C_m - C_p)/(C_b - C_p) = \exp(J_v/k) \quad \textbf{2.39}$$

Here, (J_v) is the volume flux in the boundary layer, and the mass transfer coefficient (k) represents the ratio of solute diffusivity (D) to boundary layer thickness (δ).

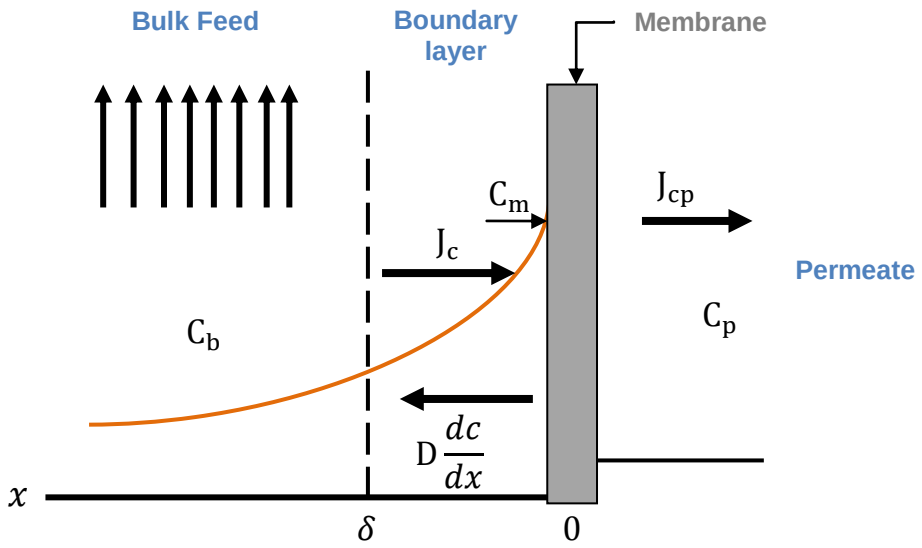

Figure 2.12: Schematic of concentration profile in concentration polarisation phenomena [21].

From Equation (2.39), it can be concluded that this phenomena depends mainly on the membrane morphology and related permeate flux, in addition to the solute properties, such as the viscosity and diffusivity.

As the occurrence of CP at the membrane surface is inevitable, the selection of appropriate operating conditions can reduce the negative effects of mass accumulation on the separation process efficiency [81].

According to the definition of membrane fouling, CP is not considered as fouling although it is also responsible for the flux decline because when the filtration is stopped, the concentration polarisation disappears.

2.5.2 Classification of membrane fouling

Generally, there are three types of fouling, these are [82], [83]:

- Organic fouling (as a result of natural or synthetic organic matters).
- Biofouling (as a result of living and non-living microorganisms).
- Inorganic fouling (as a result of inorganic salt deposits).

The term "mineral scale" is used to distinguish the inorganic fouling from any other membrane fouling types. The salt precipitates when the solubility product of the constituent ions is reached or exceeded.

Calcium sulphate ($CaSO_4$), calcium carbonate ($CaCO_3$), and silica (SiO_2) are some of the most common inorganic salts responsible for scaling on the membrane surface [11]. Also, flux decline caused by membrane fouling can generally be classified as reversible or irreversible; depending mainly on the effectiveness of the fouling control and cleaning technology.

For porous membranes, the reversible fouling can be described as the portion that can be recovered by backwashing (or back flushing) process. However, backwashing is normally not available for non-porous membranes.

The decline of flux due to irreversible fouling cannot be recovered unless the membrane is replaced or cleaned by chemical reagents.

Unlike reversible fouling, irreversible fouling is normally caused by strongly adherent films or material trapped within the porous substructures of the membrane.

The fouling of most salts such as calcium sulphate or calcium carbonate in a nanofiltration membrane is usually reversible [11], [82].

Figure 2.13 (a) and (b) shows the filtration cycles of reversible and irreversible fouling in porous membrane.

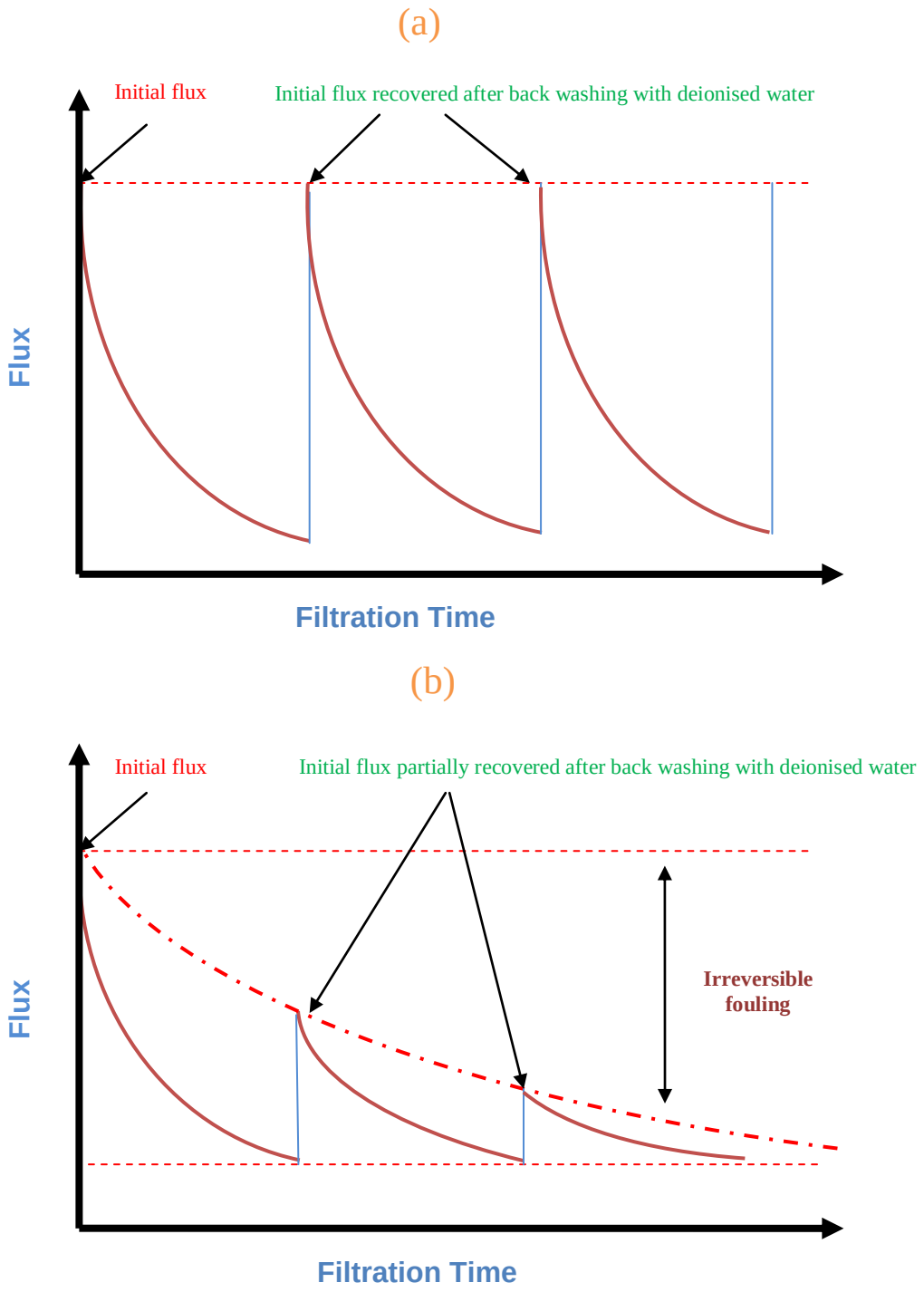

Figure 2.13: Schematics of reversible and irreversible fouling of porous membranes (a) reversible fouling and (b) irreversible fouling [11].

2.5.3 Critical flux theory

The reductions of the membrane permeate flux with time as a result of fouling represents a major problem in many pressure-driven membrane processes. This problem needs to be solved before the membrane filtration processes become technically and economically viable [84], [85].

The critical flux (CF) hypothesis is considered as one of the most helpful methods for characterisation and controlling membrane fouling. This concept can be used to describe the lowest flux for which fouling appears on a membrane [86].

Workings below certain permeate flux or at a sub-critical flux can permit operations over a long time period without any significant occurring of fouling [87], [88], [89].

As the fouling can alter the selectivity of the membrane, thus the CF can have effects on the membrane efficiency. Based on the critical flux theory, operating at sub-critical flux can lead to reducing the energy consumption, but in the meantime, keeping the same permeate flux requires a larger membrane area. This must be subjected to optimisation procedure, for critical flux; the decrease in the running costs is partially offset by an increase in the investment cost [90].

The critical flux value depends mainly on various factors, such as; membrane characteristics, feed water composition properties, the hydrodynamic of the system, and the applied process conditions [84], [88].

On the other hand, some authors such as Bacchin et al. [91], Stoller and Chianese [92] pointed out that operating below the critical flux may not be enough to avoid long-term fouling, thus they introduced the concept of sustainable flux, at which the desired separation can be operated in a profitable manner, only minimising but not eliminating fouling entirely.

For pressure driven membrane filtration processes, the critical flux concept is considered as an important parameter when design, characterise, and quantify the magnitude of fouling.

2.5.3.1 Critical flux definitions

In 1995, three key papers defining the critical flux concept were published. Field et al. [84] defined the CF for microfiltration membranes in the form of a theory: *"*The critical flux hypothesis for MF is that on start-up there exists a flux below which a decline of flux with time does not occur; above it fouling is observed. This flux is the critical flux and its value depends on the hydrodynamics and probably other variables."

Bacchin et al. [93] proposed a theoretical model for colloidal particles flux. From this model, a critical flux is defined as "the flux below which no fouling occurs". On the other hand, Howell [94] defined the critical flux as "the flux below which there is no deposition of colloids on the membrane". This definition allows using the term "sub-critical flux" which indicated that below the critical flux no fouling is observed.

Nowadays, the most common definition of critical flux is the flux of a membrane system under which fouling is first observed for a given feed concentration and given cross-flow velocity [88].

The critical flux theory discriminates between any kind of fouling and when fouling does not occur (or occurs relatively slowly), therefore it might be a good indicator for the membrane system to maintain its constant productivity with the advantage of operational cost. This concept provides a logically theoretical combination of fouled NF membranes [92].

Field et al. [84] identified two forms regarding this concept; these are the "strong form" and "weak form" of critical flux.

The strong form of the critical flux represents a comparison between the permeability of the fouling solution and the permeability of the pure water. Based on the flux-pressure relationship, the strong form is reached when the permeate flux of the fouling solutes starts to swerve from the pure water (flux-pressure) line; whereas the weak form of the critical flux supposed that in the beginning of the process there is a rapid fouling building up, therefore in the flux-pressure relationship the fouling solutes line is beneath that of pure water.

It is important to mention that the strong form of critical flux is rarely observed in real world feed.

Figure (2.14) shows a schematic illustration of the strong form and weak form of critical flux.

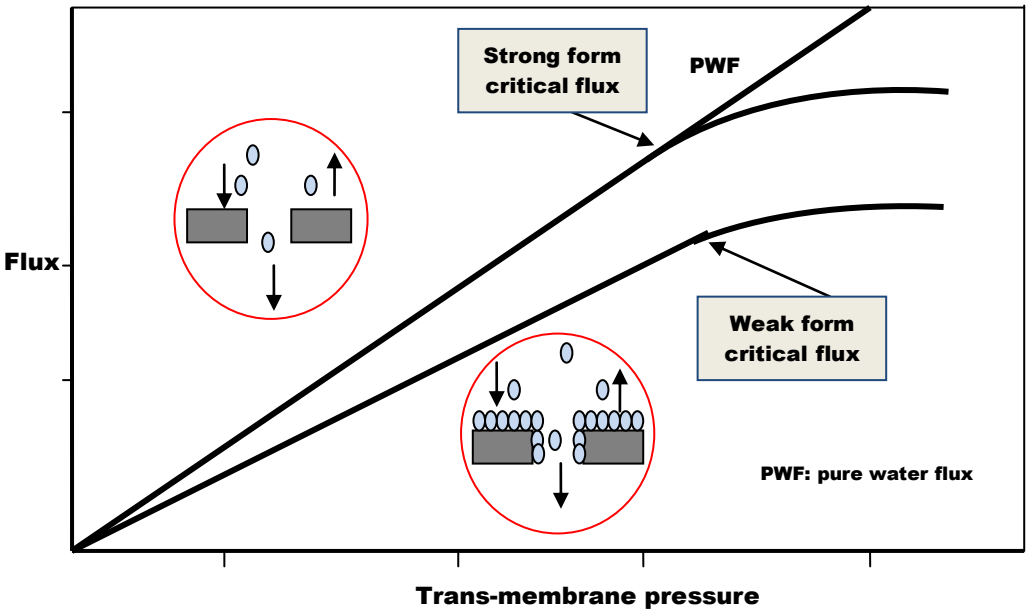

Figure 2.14: Schematic illustration of strong form and weak form of the critical flux concept [5].

Espinasse et al. [95] and Manttari et al. [96] used a different form for the critical flux that is "the critical flux for irreversibility". This form refers to the first process flux that results in irreversible fouling in which above the critical flux for irreversibility, the cleaning action is not sufficient to completely remove the foulant from the membrane.

In the real world applications the complete prevention of fouling is not possible especially for long process time, thus the term of "sustainable flux" has been established. The measurement of this term is based on the rate of fouling and mainly related to the reduction in the possible occurrence of fouling.

A sustainable operation depends on many factors such as the economic evaluation of the selected filtration process or the actual cost of the cleaning method, therefore the sustainable flux is not a solid number as the critical flux [91].

2.5.3.2 Critical flux measuring techniques for crossflow filtration

The critical flux concept has been used extensively in crossflow filtration. Based on available literatures [97], [98], [99] various methods can be found to determine the membrane critical flux depending on the accuracy, reliability, complexity, and experiment length.

Generally, for the cross flow filtration process; the CF can be measured by using one of the three following common methods:

- **Determination of critical flux from flux-pressure linearity**

In this method, the flux-pressure experiments can be made either by imposing the pressure and measuring the flux or by imposing the flux and measuring the pressure. A constant pressure procedure allows to determine the permeate flux in which the pressure is increased stepwise and the flux decline is monitored and measured over time which leads to reliable results with no time dependence (for sufficient duration for each pressure step). While for a constant flux procedure the trans-membrane pressure is measured and above the critical flux the pressure will increase with time. If the clean water permeate flux is known, then both the weak and strong forms of the critical flux can be determined by using this technique [100], [91].

According to Chiu and James [6], the critical flux from this method represents the average between the last time independent flux step and the first time dependent step.

Bacchin et al. [91] and Gesan-Guizion et al. [100] recommended using the constant pressure experiment when working with suspension solutions due to the sensitivity to detect small changes for any trace fouling.

The limiting flux (the maximum flux that can be achieved, regardless of an increase in operating pressure) is also determined as well as determining the critical flux using this method. According to Bacchin et al. [91], [90] work, the critical flux can be estimated as two thirds of the limiting flux (see Figure 2.15).

Based on the membrane permeability (L_P) definition (see section 1.2.4.5), Le-Clech et al. [102] and Guglielmi et al. [103] estimated the weak form of the critical flux at which the permeability decrease below 90% of the initial permeability ($L_{P_\circ}$). The critical flux can then be determined as the average of the maximum flux at which the permeability is higher than ($0.9\,L_{P_\circ}$) and the sub sequent flux-step value, as both these measurements represent the lower and upper boundaries of the critical flux region. In this method, the critical flux value can be determined based on the two different forms whether it is strong or weak. For the strong form of the critical flux, the solute permeate flux was compared to that of pure (deionised) water at the same pressures, and in this case the critical flux is exceeded when the solute permeate flux started to diverge from the pure water flux. Whereas with regard to the weak form, the critical flux is exceeded when the solute permeate flux is no longer linearly dependent.

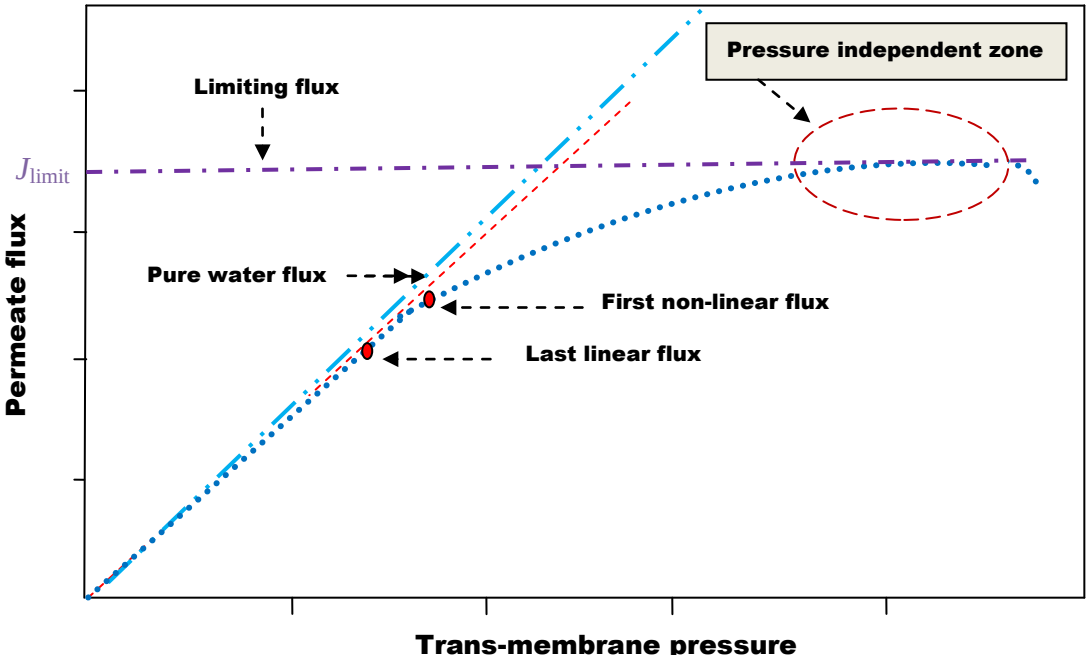

Figure 2.15: Schematic representation of flux-pressure linearity method and the limiting flux concept [101].

- **Determination of critical flux using the standard step-method**

The standard step method was improved by Espinasse et al. [95] and Mantarri et al. [104]. In this measuring method, an alternating step-pattern was applied where the pressure is alternatively increased and decreased which makes it possible to determine the flux where the critical flux was exceeded. The flux is measured for each increased or decreased pressure and then, compared to pure water flux.

In this method the pressure was alternatively increased and decreased, and the critical flux represents the average of two of the flux's steps values (based on the selected time interval), with one below the critical flux value and another above the critical flux value.

When the solute permeates flux's values for the increased and decreased pressure were the same, then in this case the critical flux has not yet been attained. Based on this (for each certain pressure step), the critical flux was exceeded when the decreased pressure does not give the same flux value that has already been obtained from the increased pressure. Both strong and weak forms of the critical flux can be estimated from this method, as it gives a strong form if the difference between the flux and the pure water flux is zero at low flux values while the weak form occurred if there is a difference between flux and pure water flux before the flux starts to increase [105].

The reversibility of the fouling beyond the critical flux can also be determined by using this method [95], [106].

Figure (2.16), shows a schematic representation of a flux-pressure standard step method.

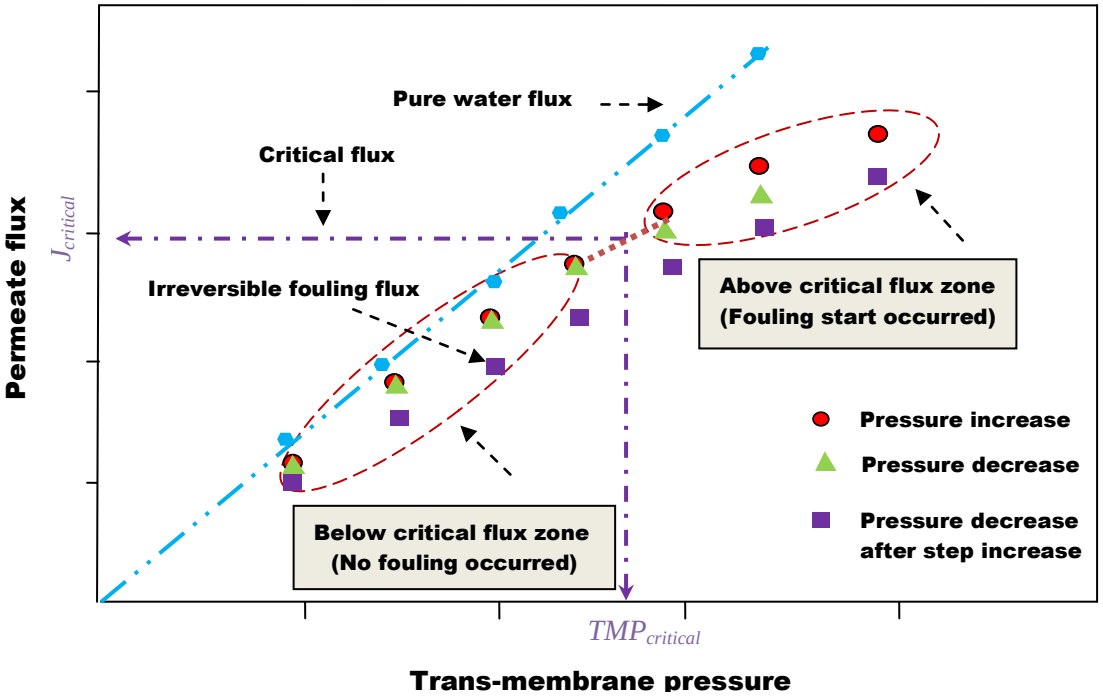

Figure 2.16: Schematic representation of flux-pressure standard step method (adopted from [93]).

- **Determination of critical flux from mass balance**

Kwon et al. [107] determined the critical flux based on particle mass balance over the membrane by monitoring the concentration of particle in feed and retentate. The idea is that since the concentration of particles in the feed and retentate is not changed, then the assumption is made that deposition on the membrane does not occur therefore, the critical flux has not been reached.

Obviously, this method does not depend on the measurements of the pressure and related flux, therefore a distinction between the strong and weak form of the critical flux cannot be achieved. The major limitation of this method results from the assumption that all particles are retained by the membrane ignoring the effect of other lost particles in the system by adsorption to tubing or to other system equipment.

Gesan-Guizou et al. [100] shows that this method needs to be corrected by combining this method with the flux-pressure step method in order to approve the validity of this method.

2.5.4 Fouling of calcium sulphate

Calcium sulphate represents one of the greatest scaling potential species in NF (and RO) membranes [2]. A serious problem resulted from the increased concentration of one or more species beyond their solubility limits and their precipitation onto the membrane surfaces.

The term membrane fouling is commonly used when the precipitate formed is a hard scale [11], [108].

The naturally occurring dihydrate calcium sulphate (or gypsum) (molecular weight of 172.172 g/mol and density of 2.32 gm/cm^3) differs from other calcium sulphate minerals by the numbers of water molecules in its crystalline structure [109].

Calcium sulphate depositions form an aqueous solution in three different crystalline forms, these are:

- Dihydrate (so-called gypsum) ($CaSO_4.2H_2O$).
- Hemihydrate $\left(CaSO_4.\frac{1}{2}H_2O\right)$.
- Anhydrite ($CaSO_4$).

Gypsum is the most common potential scaling that precipitates at room temperature, whereas the solubility of the other phases occurs in relatively higher temperatures.

The solubility of gypsum increases corresponding to increase in temperature up to (40 ℃), but above this temperature the gypsum solubility starts to decrease [110].

The intensity of scale formation on the membrane is generally governed by [111]:

$$S_{m\ (CaSO_4)} = \frac{\left[Ca^{2+}\right]_m\left[SO_4{}^{2-}\right]_m}{K_{SP\ (CaSO_4)}} \quad \textbf{2.39}$$

Where:

S_m : Super saturation ratio at membrane surface.

K_{SP}: Thermodynamic solubility product.

$\left[Ca^{2+}\right]_m\left[SO_4{}^{2-}\right]_m$: Bulk ion concentrations of Ca^{2+} and $SO_4{}^{2-}$ (at membrane surface).

Super saturation can be defined as the condition where a greater concentration of a substance exists in solution than would exist at equilibrium conditions.

The constitutional water of the gypsum crystal, together with already stressed solubility, gives gypsum unique properties among the rock-forming and soil-forming minerals. These properties explain the labiality of gypseous material [10].

The calcium sulphate solubility is highly affected by the existence of other ions in a certain system. In order to investigate the effect of ionic strength on the potential of scale formation of calcium sulphate, a highly soluble in water sodium chloride could be used to increase the ionic strength of the solution.

Ionic compounds normally dissociate to their constituent ions when they are dissolved in water, for example the dissociation of calcium sulphate [112]:

$$CaSO_{4(s)} \leftrightarrows {Ca^{2+}}_{aq} + {SO_4}^{2-}{}_{aq}$$

And the equilibrium expression is:

$$K_{(eq)} = \frac{\{{Ca^{2+}}_{(eq)}\}\{{SO_4}^{2-}{}_{(eq)}\}}{\{CaSO_{4(s)}\}}$$

Here $K_{(eq)}$ represents the solubility or equilibrium constant and the curly brackets indicate the substance activity.

Generally, for low soluble salts, the activity coefficients of the ions in the solution are assumed to be equal to 1. In this case, the above equilibrium expression can be reduces to the following solubility product formulation:

$$K_{(SP)} = \left[{Ca^{2+}}_{(eq)}\right]\left[SO_4^{2-}{}_{(eq)}\right]$$

According to this formulation, the solubility product $K_{(SP)}$ of an aqueous solution (in an equilibrium state) depends on the concentrations of ions in this solution.

The solubility product $K_{(SP)}$ of calcium sulphate at 20 ℃ is equal to 4.93×10^{-5} [113].

When Ca^{2+} and ${SO_4}^{2-}$ are the only dissolved ions in the $CaSO_4$ solution, then the solubility of the calcium sulphate solution and the concentration of each ion can be represented as follow:

$$\sqrt{K_{(SP)}} = \sqrt{4.93 \times 10^{-5}} = 7.02 \times 10^{-3} = \left[Ca^{2+}\right]\left[{SO_4}^{2-}\right]$$

2.5.5 Chemical cleaning and regeneration of fouled NF membranes

As mentioned in section (2.5.2), the fouling in pressure driven membranes is caused by organic matters or inorganic salts deposits present in water. This could lead to reduce the membranes efficiencies in addition to other related consequences such as increasing of the cost and required energy due to the reduction of membrane permeate flux [114].

The feed stream quality plays an important role in determining foulant-membrane interaction with foulant-foulant interactions.

Membrane surface foulant provides a good guide for the selection of the cleaning agent in the membrane regeneration process.

Chemical cleaning is an effective method to remove the fouling materials accumulated on the membrane surface when there is a considerable drop in permeates flux or salt rejection.

The factors that can be taken in consideration during any chemical cleaning process include: the cleaning agent type, concentration, pH, temperature, flow rate, pressure, and cleaning time [114].

For a particular membrane cleaning situation, it is significant to select a suitable cleaning agent because some cleaning agents are incompatible with certain types which could cause an adverse effect on the performance of the membrane.

The cleaning agents should be chosen in a way that it is not only effective in removing fouling materials but also restoring membrane performance.

A considerable number of chemical cleaning agents are available and commonly used for inorganic membrane fouling; these agents are basically falling into three main categories, which are [115]:

- Alkalis.
- Acids.
- Metal chelating agents.

The choice of preferred cleaning products depends on feed characteristics, for example, acid cleaning is appropriate for the removal of precipitated salts such as calcium carbonate, while, alkaline cleaning is used to remove adsorbed organics [7].

Wei et al. [116] showed that for an inorganic $CaSO_4$ type of foulant in NF membranes, the following chemical cleaning agents are recommended by different manufactures:

- Citric acid (CA).
- Hydrochloric acid (HCl).
- Sodium hydroxide (NaOH).
- Tetra-sodium salt of ethylene tetra actic acid (EDTA).

In order to quantify the membrane cleaning efficiency, the flux recovery ratio (FRR) can be used according to the following equation [2], [115]:

$$FFR\% = \frac{J_{cw} - J_{fw}}{J_{iw} - J_{fw}} \times 100 \qquad \textbf{2.40}$$

Where:

J_{cw} : Pure water flux after cleaning.

J_{fw}: Pure water flux after fouling.

J_{iw}: Pure water flux before fouling.

A cleaning agent should react with an inorganic foulant to lessen foulant-membrane and foulant-foulant interactions and finally form a lessened fouling layer that can be removed from the membrane surface by means of mass transfer.

In cases of cleaning with citric acid or hydrochloric acid, the FRR ratio increased with increasing the cleaning time due to their efficiency in dissolving the inorganic salts.

Metal chelating agents (such as EDTA) or acids can react with the inorganic fouling materials closest to the membrane surface to lessen foulant-membrane interaction and make the whole fouling layer looser and easier to remove via mass transfer [116], [115].

Wei et al. [116] proved that the strong metal chelating agent of EDTA represents the most favourable cleaning agent for a membrane fouled by calcium or sulphate ions with high FRR ratio during the cleaning process, as it can react with calcium ions in the sulphate and carbonate of calcium to form a soluble complex.

2.6 Previous studies

There are a very limited number of investigations which have been made to study the behaviour of calcium sulphate in nanofiltration membranes, despite the fact that the control of sparingly inorganic soluble salts such as gypsum represents one of the greatest scaling potential species in the nanofiltration membrane process which might present a major challenge in the development of membrane processes for desalination of saline water.

Several studies have been made to study the effects of operational conditions parameters on the mechanism of calcium sulphate scale formation in nanofiltration membranes. Lee and Lee [8] investigated the effect of hydrodynamic operating conditions on $CaSO_4$ scale formation mechanisms using a film Tec (NF−45) polyamide and plate-and-frame membrane modules. The flux decline in that study was attributed to the formation of calcium sulphate scale which greatly influenced the crystallisation mechanism.

Lin et al. [7] reported the effects of pressure and flow velocity on cake formation of calcium sulphate by using a flat sheet polyamide and plate-and-frame membrane module. The major finding from this study indicated that the fouling of $CaSO_4$ was strongly dependent on operating parameters and the fouling of calcium sulphate was most sensitive to applied filtration pressure followed by cross flow velocity.

A study conducted by Jawor and Hoek [9] was interested in the effects of feed water temperature on the inorganic fouling of calcium sulphate in the brackish water desalination process by using a reverse osmosis flat sheet membrane module. This study suggested that the scale formation was inhibited at high temperature but when the brine became super-saturated, gypsum formed rapidly.

Le Gouellec and Elimelech [10] investigated the scaling mechanism of calcium sulphate compared to a calcium carbonate scaling mechanism by using a low pressure fully flat sheet aromatic polyamide NF membrane (NF−90, film Tec). The major finding from this work indicated that both ($CaSO_4.2H_2O$) and ($CaCO_3$) scales might result from particulate deposition rather than surface (wall) crystallisation.

Shih et al. [12] investigated the morphmetric characterisation of gypsum scale by using an aromatic polyamide composite RO membrane and plate and frame RO system in order to study the morphology of gypsum crystal.

From the above mentioned researches, it can be noticed that all previous researches which were related to calcium sulphate were conducted on polymeric membranes.

On the other hand, considerable researches have been made in the last decade to investigate the performance of the ceramic Titanium dioxide nanofiltration membranes in different separation processes; however, most researchers focused either on the development of membrane properties or the factors which affected the separation behaviour of different electrolytes, for instance;

Both Weber et al. [5] and Tsuru et al. [117] used the streaming potential measurements to characterise the surface charge of a flat sheet TiO_2 NF membrane by using an electro-kinetic analyser and $Ag/AgCl$ electrodes.

Weber et al. [5] determined the salt retention for $NaCl, KCl, Na_2SO_4$ and $NaNO_3$ as single electrolyte solutions at different pH values and at pressure range of $4-15$ bar.

While Tsuru et al. [8] studied the rejection behaviour of four salts ($NaCl$, Na_2SO_4, $MgCl_2$ and $MgSO_4$) at adjusted pH from $3-10$ and applied pressure differences ranging from $2-10$ bar.

Puhlfürb et al. [118] indicated that the surface charge of the tubular ceramic TiO_2 NF membrane had a major influence on the retention efficiency of $NaCl$ and Na_2SO_4 as a single salt at different pH values and at an applied pressure range from $6-15$ bar. The rejection of sulphate ions at pH above 5.8 is more than 90 %.

Also, Labbez et al. [119] studied the rejection measurements of single salt solutions of ($KCl, LiCl, K_2SO_4, MgCl_2$ and $MgSO_4$) as a function of permeate volume flux using a commercial Titania NF membrane. The effect of both pH and salt concentration was also described.

Furthermore; Van Gestel et al. [120] determined the zeta potential of a tubular ceramic TiO_2 NF membrane from measuring the electrophoretic mobility of the membrane (as powder). The results from this study confirmed the amphoteric behaviour of the Titania membrane. Also, salt retention was investigated for five single salts ($NaCl, KCl, LiCl, Na_2SO_4$ and $CaCl_2$) at pH ranges from $2-11$ and applied pressure of 5.0 bar.

Narong [121] used the streaming potential method to determine the charge of a ceramic TiO_2 ultrafiltration membrane by measuring the instantaneous potential deference per applied pressure because the observed potential changes quite rapidly due to the polarisation of the electrodes.

Narong and James [122] studied the relationship between the rejection of sodium chloride and the electrokientic potentials at pH ranges from $3-7$ and maximum applied pressure of 2.0 bar.

Finally, Hajarat [20] investigated the rejections of NaCl, $Na_2SO_4, MgCl_2, NaNO_3$ and $CaCl_2$ by using two different pore size tubular ceramic TiO_2 NF membranes at pressure range $0.1-2.0$ bar.

Based on these studies, it can be seen that the rejection or fouling of calcium sulphate (as gypsum) at Titania membranes has not been studied yet.

The critical flux measurements represent an efficient tool to choose a specific operation condition to gain a better control of fouling in the membranes. The critical flux of calcium sulphate solutions in any type of membrane (not only in present the ceramic TiO_2 NF membrane) has not been investigated yet.

2.7 Summary

This chapter reviews the background literature that is related to the present work. The membranes filtration processes, classifications, flow operation modes, fundamental performance criteria, specifications of ceramic membranes, membrane structures, manufacturing techniques of ceramic membrane, and amphoteric behaviour of ceramic NF are explained and discussed. Also, the properties of nanofiltration membranes are compared to the conventional RO membranes. The methods of measuring the zeta potential, surface and effective charge density and Donnan potential for the present NF membrane are described. Relevant theories that the present study depends on such as electrical double-layer theory (used to interpret the membrane's electrokientic phenomena), Gouy-Chapman theory (study the structure of the interface of the diffuse double layer), critical flux theory (used to describe the lowest flux for which fouling appears on a membrane) and mass transport theory in NF membrane (illustrates the main factors that the salt rejection in microporous membrane mainly depends on) are outlined.

Furthermore, the cleaning and regeneration of fouled ceramic by inorganic salts and especially by calcium sulphate solutions are presented.

CHAPTER 3

MATERIALS AND METHODS

3.1 Introduction

This chapter provides details of the membrane and chemical reagents used in the experimental part of the study; equipment and accessories employed; properties and specifications of the tubular ceramic membrane used in this work; the NF membrane filtration rigs; in addition to a detailed explanation of the experimental procedures and re-generation method.

Three different types of experiment were used in the present research with regard to:

- Measurements of the electrokinitic zeta potential using a streaming potential technique.
- Determination of the rejection behaviour of calcium sulphate compared to other salts.
- Determination of the critical flux at different ionic strengths of calcium sulphate solutes.

Some important points are discussed in this chapter such as: the reason behind choosing the shape of tubular membrane type from among other various membrane configuration types, and why the titanium dioxide membrane was used rather than other types of mineral ceramic oxide membranes, and why the pore diameter of 1.0 nm was used rather than other lower ceramic NF membrane pore diameters.

The scanning electron microscopy (SEM) images allows for visual and quantitative characterisation of the membrane morphology where the active skin layer and the sub-supported layers were specified.

Also, energy dispersive X-ray spectroscopy (EDAX) analysis was used to identify the elements of the present work membrane and quantify its relative concentrations and map its distribution.

3.2 Membrane

A composite mono-channel tubular ceramic titanium dioxide NF membrane with mean pore size of 1 nm supported by aluminium dioxide sub-layers (produced by Inopor® GmbH, Veilsdorf-Germany) [31] was used in this work.

According to the manufacturer's information, the main specifications of this membrane are [31]:

- Number of channels: 1
- External diameter (mm): 10
- Channel diameter (mm): 7
- Total length (mm): 190
- Open porosity: 30−40%
- Mean pore diameter (nm): 1
- Filtration area (m^2): 4.178×10^{-3}
- Inflow area per tube (mm^2): 38

The tubular membrane configuration was used in the present work despite the availability of other membrane configuration types which can be attributed to two main reasons based on the characteristics of tubular membranes, which are [4], [21]:

- The fouling tendency in this type of membrane is considerably low compared to other types of membrane such as plate and frame, spiral wounds, and hollow fibre.
- The cleaning and regeneration for the tubular configuration is very effective and efficient, whereas for other types it is either poor or not applicable.

According to many researchers, the titanium dioxide TiO_2 (or titania) membranes have received significant attention because of their unique characteristics compared to other mineral oxides such as $\gamma - Al_2O_3$, SiO_2 or ZrO_2 . These characteristics can be summarised as follows [123], [124], [125]:

- High water flux due to their amphiphilic surface properties.
- Good resistance to fouling.
- Stability and chemical resistance under harsh conditions towards extreme pH ranges.
- Commercial availability.
- Ease of preparation.

- Lower fabrication costs due to their reduced sintering temperatures.
- Semi conductor, oxygen sensor, antimicrobial coating.

The reason for having chosen a pore diameter 1 nm for the present research (in spite of the availability of pores lower than this diameter (such as 0.9 nm) which could lead to an improvement in the rejection results) was because the initial rejection experiment tests for our newly designed membrane filtration rig showed that using lower than this diameter would decrease the solutes permeate flux, and in this case; the applied trans-membrane pressure would need to be increased up to 10 bar which it is not applicable for the present bench scale filtration rig.

Figure (3.1) shows a picture for a virgin ceramic TiO_2 NF membrane used in the present work.

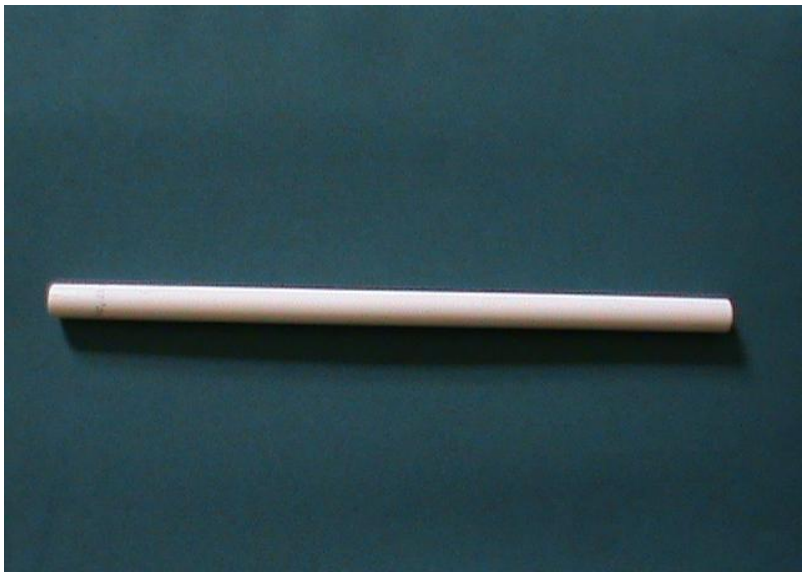

Figure 3.1: Virgin ceramic TiO_2 NF membrane with pore size of 1 nm.

3.2.1 SEM micrograph of ceramic Titania NF membrane

The morphology and the composite structure of the present work's 1 nm ceramic TiO_2 NF membrane was microscopically scanned using scanning electron microscopy (SEM) (FEI QUANTA 200, Purge, Czech Republic) with an accelerating voltage of 20-30 kV. The analysis of the cross-section SEM micrograph images allows for visual and quantitative characterisation of the membrane morphology where the active skin layer and the sub-supported layers can be clearly seen.

Figure (3.2) shows typical SEM images for present work's ceramic TiO_2 NF membrane. The SEM images reveal that the membrane surface has a complex nanoscale morphology which could significantly impact the rejection behaviour.

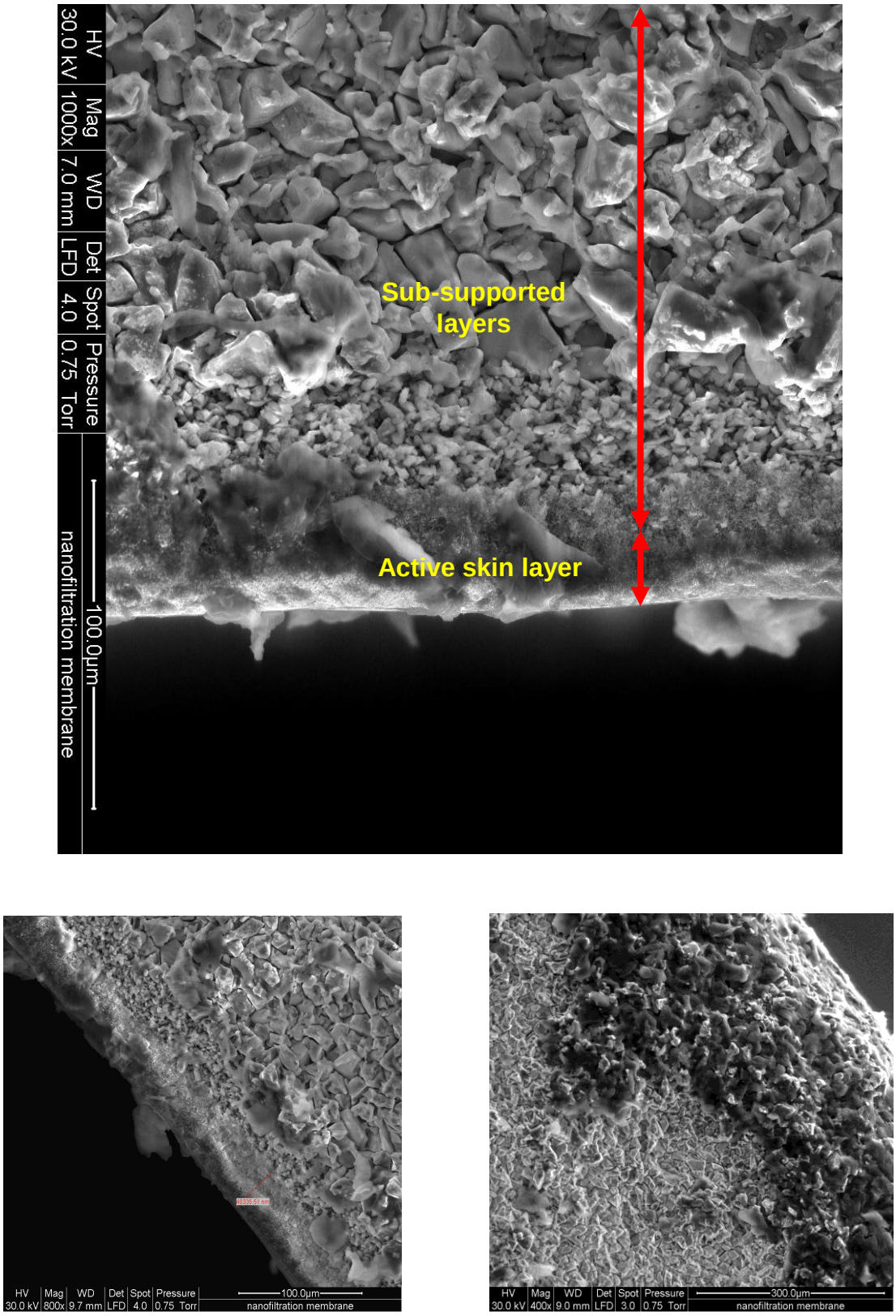

Figure 3.2: SEM cross-section images of 1 nm ceramic titanium dioxide NF membrane.

3.2.2 EDAX spectrum of ceramic Titania NF membrane

The solid state X-ray detector or EDAX (energy dispersive X-ray spectroscopy) represents a valuable tool used for quantitative elemental micro-analysis.

In the present work, the EDAX analysis was used to identify the main elements that exist in the ceramic titanium dioxide NF membrane and also to quantify their relative concentration and map their distribution.

The present TiO_2 membrane was cut into small pieces and only the active skin surface layer of the membrane was investigated by using an X-ray detector (Model: AMERTEK Inc, PA - USA).

Figure (3.3) shows the specific spectrums of the active skin layer of a 1 nm tubular TiO_2 NF membrane obtained by using EDAX analysis.

The EDAX (and SEM) results confirm that the membrane used in the present work is a composite membrane and the membrane active layer contains at least three mineral elements (aluminum, titanium, and zirconium).

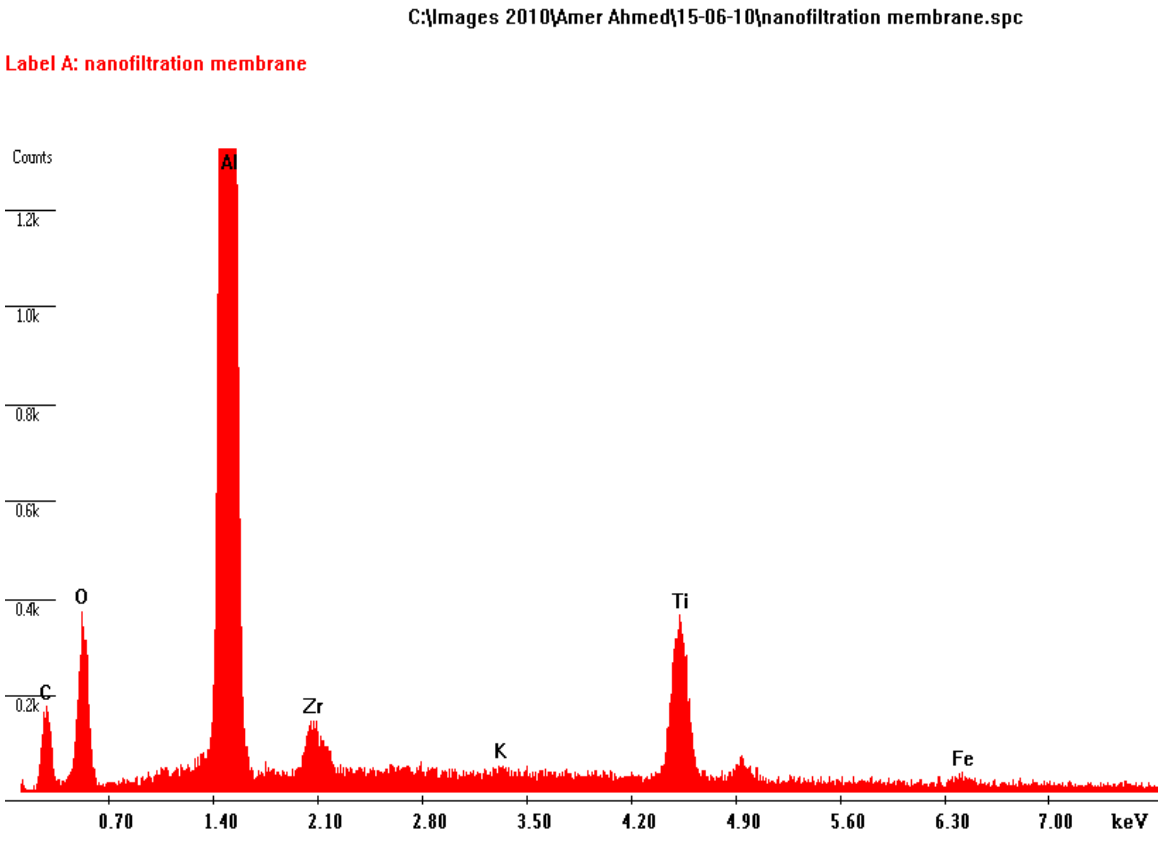

Figure 3.3: The EDAX specific spectrums of the active surface for 1 nm tubular ceramic TiO_2 NF membrane.

3.3 Membrane module

The present work constructed a new vertical module to house the ceramic TiO_2 nanofiltration membrane inside. The vertical position of the module was preferred as this further reduced the pH gradient effects between the solute permeate flux and membrane [9]. The present module was used in rejection and fouling experiments and also to determine the electrokinetic membrane zeta potential (ζ) using the streaming potential method after adding some technical modifications. This type of vertical module was originally designed by Baldeón [126].

The module structure was divided into three main sections inlet, middle, and outlet. The middle section was made from Perspex (a transparent material, in order to monitor the accumulation of the cross flow solutes permeate droplets), while the inlet and outlet sections were made from PVC with same inner diameter of the titania NF membrane used in order to give same velocity and flow pattern inside the membrane. The module was tested and proved to be capable of tolerating relatively high pressures (up to 8.0 bars). This range covered the typical working pressure for the pressure driven NF membranes (5.0−6.0 bar) [24].

The selection of Perspex and PVC as module construction materials was done in order to prevent any reaction or accumulation of chemicals or saline water salts inside the module. The zeta potential experiments set required very highly accurate measurements for the membrane potential (in milli-volts), so based on this, the module should be made from an isolating material in order to avoid any possible distortion in membrane potential that might occur during the experiments.

In order to measure the membrane streaming potential, the module was supplied with two platinum electrodes (Alfa Aesar, Johnson Matthey chemicals, UK); one was placed along the centreline of the tubular membrane and the other electrode was wrapped around the external surface of the membrane.

For rejection and fouling experiments, underwater epoxy resin was used as a sealing agent in order to prevent any possible direct leakages of solutes inside the module due to high applied pressure, whereas for streaming potential measurements a normal set of O-rings were used as a sealing agents because of low applied pressure (normally less than two bars).

Figure (3.4), shows schematic of the tubular membrane module used in the present work and the structure of the inlet, middle, and outlet sections.

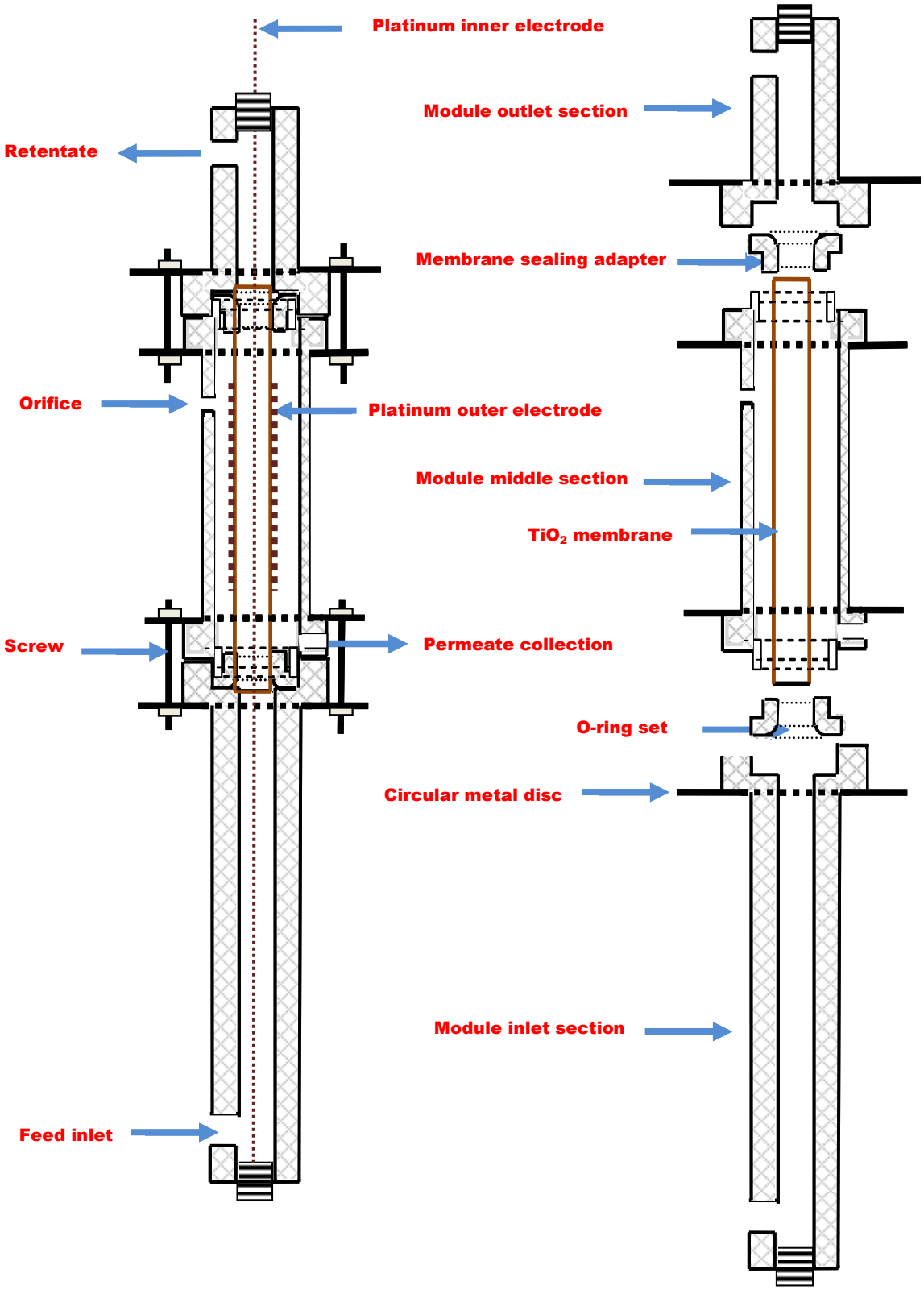

Figure 3.4: Schematic of tubular membrane module used in the present study accompanied with the structure of main three sections of the module.

3.4 Materials

3.4.1 Zeta potential experiments

- An electrolyte solution of analytical grade (NaCl) sodium chloride (Fisher Scientific, UK) with ionic strength of 0.01M was prepared by using deionised water (Millpore, EL1X5 – cartridges type/Automatic sanitisation module, France).
- 0.1 M (NaOH) (Fisher Scientific, UK) was used for pH adjustments.
- 0.1 M (HCl) (Fisher Scientific, UK) was used for pH adjustments.
- 0.1 M (NaOH) sodium hydroxide solution was also used as a chemical cleaning agent for membrane regeneration after each set of experiments.

3.4.2 Rejection experiments

- Electrolyte solutions of analytical grade ($CaSO_4.2H_2O$) dihydrate calcium sulphate (Fisher Scientific, UK) with ionic strength of 0.001, 0.005, 0.01 M, and at saturation concentration were prepared using deionised water (Millpore, EL1X5–France).
- Electrolyte solutions of analytical grade (NaCl) sodium chloride (Fisher Scientific, UK) with ionic strength of 0.001, 0.005, and 0.01 M.
- Electrolyte solutions of analytical grade (Na_2SO_4) anhydrous sodium sulphate (Fisher Scientific, UK) with ionic strength of 0.001, 0.005, and 0.01 M.
- Electrolyte solutions of analytical grade ($CaCl_2.2H_2O$) dihydrate calcium chloride (Fisher Scientific, UK) with ionic strength of 0.001, 0.005, and 0.01 M.
- 0.1 M (NaOH) was used as a chemical cleaning agent for membrane regeneration after each set of experiments.

3.4.3 Critical flux experiments

- Electrolyte solutions of analytical grade ($CaSO_4.2H_2O$) dihydrate calcium sulphate (Fisher Scientific, UK) with ionic strength of 0.001, 0.005, and 0.01 M and at saturation concentration were prepared using deionised water.
- 0.1 M (NaOH) was used as a chemical cleaning agent for membrane regeneration after each set of experiments.
- 0.1 M EDTA **(**ethylene di-amine tetra-acetic acid) (Fisher Scientific, UK) was also prepared and used as a cleaning agent for membrane regeneration.

3.5 Membrane filtration rig

3.5.1 Zeta potential experiments

Figure (3.5) shows a schematic diagram of a filtration rig experiments installation used to characterise the surface charge sign and magnitude for the present ceramic Titania NF membrane. The main equipment in this rig include: (10 liters) glass container as a reservoir, magnetic stirrer (RW20, IKAMAG, UK), variable speed peristaltic pump (type 603S, Watson−Marlow, UK), Flow meter (Gemü Gebr Müller−Germany), two pressure gauges (RS components, UK), cross-flow membrane modules, permeate storage beaker, digital balance (model: Oerlting/RC52, UK), high impedance milli-voltmeter (Wavetek Meteman, RS components, UK).

Also, for pH adjustment, a small dosing pump (RS components, UK) was used to inject the (0.1 M NaOH) or (0.1 M HCl). This dosing pump was connected electrically to pH/ORP controller (Oakton, 800 series, Singapore), and was used to measure the pH values inside the main reservoir via a probe and to send an electrical signal to stop the pump when the desired pH value has been reached.

In addition to the reinforced PVC flexible piping with various fittings and connectors, on-off gate valves, a back pressure control valve, a pH/conductivity meter (Model: accument 50−Fisher Scientific, USA), and a stop watch were used. The pH/ conductivity meter and the pH controller were re-calibrated by using special standard solutions.

3.5.2 Rejection and critical flux experiments

Figure (3.6) shows a schematic diagram of the filtration rig experiments installation used to study the rejection and fouling behaviour of calcium sulphate for the 1.0 nm TiO_2 NF membranes. The main equipment in this rig include: (10 liters) glass container as a reservoir, magnetic stirrer (RW20, IKAMAG, UK), variable speed peristaltic pump (type DFBa 013, ProMinent, Germany), flow meter (Gemü Gebr Müller, Germany), two pressure gauges (RS components, UK), cross-flow membrane modules, permeate storage beaker, digital balance (model: Oerlting/RC52, UK).

In addition to the reinforced PVC flexible piping with various fittings and connectors, on-off gate valves, a back pressure control valve, a variable speed peristaltic pump (type 603S, Watson-Marlow,UK), pH/conductivity meter (Model: accument 50 Fisher Scientific,USA) and a stop watch were used. (Figure 3.7 shows the bench scale of rig)

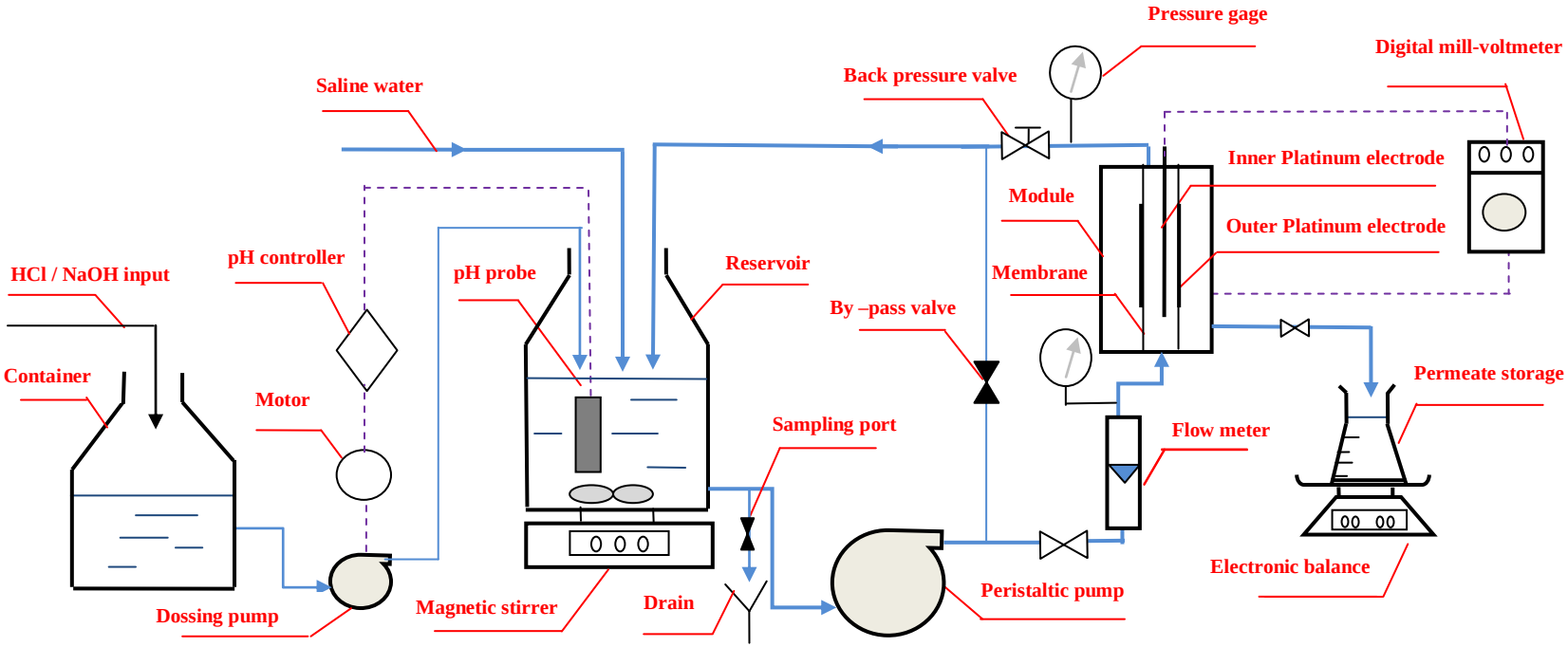

Figure 3.5: Schematic diagram of tubular ceramic TiO_2 NF membrane filtration rig for zeta potential experiments installation.

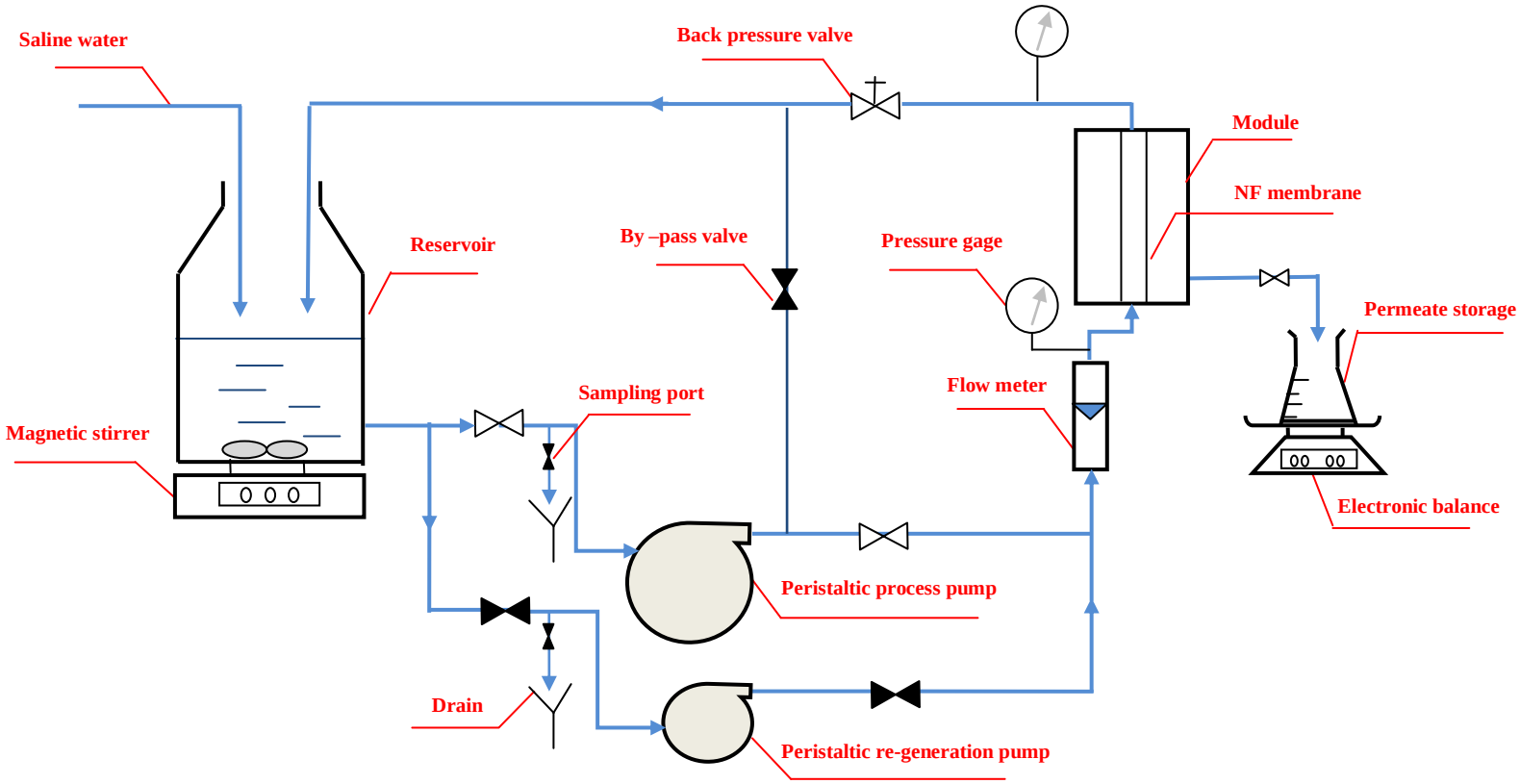

Figure 3.6: Schematic diagram of tubular ceramic TiO_2 NF membrane filtration rig for rejection and fouling experiments installation.

Figure 3.7: Bench scale of tubular ceramic TiO_2 NF membrane filtration rig.

3.6 Experimental methods

3.6.1 Zeta potential experiments

The streaming potential is among the most widely used techniques for studying the surface electrokinetic properties of the membranes. This procedure includes the main following steps:

- 0.01M sodium chloride (NaCl) solution was prepared using a solid dried form of analytical grade with ultra pure deionised water.
- Streaming potential measurements were made on a NF membrane over a ranged of pH $(3 - 9)$.
- Initial streaming potential measurements were carried out at pH of 6.0.
- Two sets of (NaCl) solution were used, 4 litres of total volume each, one set for streaming potential measurements at pH less than 6 and the other for pH more than 6.
- The electrical potential difference across the membrane was measured at a range of applied pressure driving forces of 0.5, 0.75, 1.0, 1.25, and 1.5 bar.
- At the beginning of the experiments and on each set of pressure values, pH

and conductivity of both retentate and permeate were continuously monitored to ensure that stable streaming potential was achieved.

- The applied pressure was monitored by the pressure gauges at either ends of membrane module and controlled by manual closing of the control valve (at the discharge part of the membrane module) to generate the required back-pressure.
- The two platinum electrodes were connected to the voltmeter which recorded the potential difference (in milli-volts) that was generated by the electrolyte flow.
- The measuring of the electrical potential difference (ΔE) started upon the injections of 0.1 M hydrochloric acid (HCl) to the NaCl electrolyte using the dosing pump for the sets of pH less than 6.0 (pH at 5.0, 4.5, 4.0, 3.5 and 3.0). The same procedure was repeated for the injections of 0.1 M (NaOH) sodium hydroxide for the sets of pH more than 6.0 (pH at 7.0, 8.0, and 9.0).
- The flow velocities for streaming potential measurements were conducted at 0.7 m/s (for average flow rate of 100 l/h) which corresponded to a Reynolds number of about 5000 (turbulent flow regime).
- The applied pressure through the membrane was gradually increased with an interval of (0.25 bar) and the corresponding electrical potential under each pressure were recorded.
- Experiments were carried out at room temperature (an average of 20 ℃).
- The streaming potential measurements showed a high reproducibility and to insure this each filtration experiment was repeated at least twice and the results showed in the present work were mean values.
- The estimated SP in present work is defined as the instantaneous potential deference per applied pressure; that is because the observed potential changes quite rapidly due to the polarisation of the electrodes [121], [127], [122].

The use of instantaneous potential provides a useful means of estimating both streaming potential and filtration potential [10].

In order to study the effects of solute ionic strength on membrane zeta potential values, the streaming potential measurements were also applied for 0.025, 0.05, and 0.075 M sodium chloride solution at unadjusted (fixed) pH value of 6 ± 0.2 by using exactly the same procedure for a background electrolyte of 0.01 M (NaCl).

3.6.2 Salts rejection experiments

In order to determine the retention efficiency of $CaSO_4.2H_2O$ (below and at the saturation concentration) as a single salt compared to other naturally occurring salts that typically dominate in saline soils ($NaCl, Na_2SO_4$ and $CaCl_2.2H_2O$), the procedure includes the main following steps:

- Five litres from the required salt molar concentration was prepared in the 10 litre glass container using a solid dried form of analytical grade with ultra pure deionised water.
- The magnetic stirrer was turned on for a certain period of time (depending on the ionic strength used) to assure the full solubility of the salt. Special attention should be paid to the calcium sulphate solutions (for further details see section 3.6.3)
- The experiment started when the variable speed peristaltic high pressure pump was turned on and the applied pressure was set by regulating the back pressure valve at 0.5 bar for about 10 minutes. During this period the retentate and permeate fluxes were continuously monitored to ensure that the system is stable after getting rid of all the air bubbles that might exist inside the system. Also, the conductivity and pH of the solute feed were measured.
- The system flow rate was monitored by the flow meter and set to be at 120 l/h (the design flow rate of the present work pump is 125 l/h) from the manual regulating of the variable speed peristaltic high pressure pump.
- For each salt concentration, the rejection was conducted for different applied pressures in the range from 1.0 to 5.0 bar.
- The applied pressure was monitored by the pressure gauges at either ends of the membrane module and controlled by manual closing of the control valve (at the discharge part of membrane module) to generate the required back-pressure.
- Experiments were carried out first by increasing the pressure up to 5.0 bars in order to estimate the maximum salt rejection because the membrane was not yet fouled then; the pressure was decreased in increments of 1.0 bar until the minimum pressure (1.0 bar) was attained. After that, the filtration was continued by increasing the pressure in steps of 1.0 bar until the highest pressure (5.0 bar) was attained.

- The mean ion rejection value was taken for each certain increased or decreased pressure.
- For each applied pressure, the filtration time was one hour and the permeate sample was collected for analysis after the solute permeation reached 20 ml.
- Experiments were carried out at room temperature (an average of 20 ℃).
- The cross flow velocities for streaming potential measurements were conducted at $0.85\ \mathrm{m/s}$ which corresponded to a Reynolds number of about 6000 (turbulent flow regime).
- The permeate flux in $\mathrm{m^3/m^2.s}$ (or $\mathrm{m/s}$) was measured using a digital balance for each decreased or increased pressure step. In the meantime, the conductivity of permeate was also measured.
- The rejection measurements showed a good reproducibility and each filtration experiment was repeated at least once and twice for some non identical experiment results.

3.6.3 Critical flux experiments

The critical flux experiments for the present TiO_2 NF membrane were conducted based on two different techniques, these are: step by step technique (pressure increase) and standard step technique (pressure increase and decrease) by using four different concentrations (0.001, 0.005, and 0.01M and at saturation concentration) of calcium sulphate (as $CaSO_4.2H_2O$).

The procedure includes the main following steps:

- In order to get an accurate permeate flux measurement and before the starting of each experiment, the entrance and exit junctions between the membrane and the module were sealed tightly using a flexible under water epoxy resin.
- Five litres from the calcium sulphate salt at the required molar concentration was prepared in the 10 litre glass container using a solid dried form of analytical grade with ultra pure deionised water.
- The prepared calcium sulphate solute was left (covered) on a magnetic stirrer until the total solubility of the salt was ensured. The time period depends mainly on the ionic strengths of the salt. Preparing of a calcium sulphate solution at saturation concentration required a special technique (for further details see section 4.3.5).

- The applied pressure was monitored by the pressure gauges at either ends of the membrane module and controlled by manual closing of the control valve (at the discharge part of membrane module) to generate the required back-pressure.
- The variable speed peristaltic high pressure pump was turned on and the applied pressure was set up by regulating the back pressure valve at 0.5 bar for about 10 minutes. During this period the retentate and permeate fluxes were continuously monitored to ensure that the system is stable after getting rid of all the air bubbles that might have existed inside the system.
- The system flow rate was monitored by the flow meter and set at 120 l/h from the manual regulating of the variable speed peristaltic high pressure pump.
- For each pressure step duration, the permeate flux was measured with a digital balance. In order to get more accurate permeate flux measurements, the permeate flux was recorded three times during each time interval (every 10 minutes for the step by step technique and every 5 minutes for the standard step technique).
- For the step by step technique, where the pressure was increased and related permeate flux was measured, the filtration time at each applied pressure was 30 minutes. When the filtration for the first pressure was completed, then, the pressure was increased in increments of 1.0 bar until the highest pressure of 6.0 bar was attained.
- For the standard step technique, where the pressure was increased and then decreased, the filtration time at each applied pressure was 15 minutes. At the beginning, the pressure was increased in increments of 1.0 bar until the highest pressure of 6.0 bar was reached. Subsequently, the pressure was decreased in reduction of 1.0 bar until the starting pressure of 1.0 bar was reached. Afterwards, the filtration process was continued by increasing the pressure in steps of 2.0 bar and decreasing by 1.0 bar until reaching the highest pressure of 6.0 bar again. At the end, the applied pressure was decreased again in reduction of 1.0 bar until the starting pressure of 1.0 bar was attained.

- In order to maintain the desired calcium sulphate molar concentration, the collected permeate was returned to the main process glass container after each step.
- The permeate flux measurements showed a good reproducibility after each filtration experiment and were repeated at least once and twice for some non identical experiment results.

3.7 Titania membrane re-generation procedure

The general procedure that has been used in the present work for the cleaning and re-generation of the Titania ceramic membrane after each rejection or fouling experiment can be summarised as follows:

- After the installation of the new TiO_2 ceramic nanofiltration membrane in the rig, the deionised water was used as a feed solution and re-circulated at applied increment pressures of 1.0, 2.0, 3.0, 4.0, and 5.0 bar.
- The pure water permeability was measured for each pressure in order to determine a relationship (normally linear) between the applied increment pressure and the permeate flux of deionised water.
- At low pressure peristaltic re-generation pump (see Figure 3.6) was used to conduct the regeneration process.
- After the conducting of each rejection or fouling experiment, the solution of 0.1M (NaOH) was prepared to be used as a chemical cleaning agent for the TiO_2 membrane re-generation. (Same procedure when EDTA has been used)
- Five litres of 0.1M sodium hydroxide solution was used as a feed solution and re-circulated in the rig. At the beginning of the re-generation process the pressure was set to be less than 0.5 bar to ensure that the system is stable after getting rid of all the air bubbles that might have existed inside the system. Then, the pressure was increased to 1.0 bar and the permeate flux was monitored and measured every 15 minutes until reaching the same pure water permeate flux at the pressure of 1.0 bar.
- After the re-generation process has been ended, the main reservoir was isolated and the re-generation peristaltic pump was turned on again in order to clean the system (piping and equipment) from the traces of NaOH solution.
- In order to remove any possible traces in the membrane filtration rig as a

result of the presence of sodium hydroxide solution or of the used salt before conducting the re-generation, a new quantity of deionised water (about 8.0 liters) was again re-circulated in the system at a pressure of 1.0 bar.

- The first three litres was not returned to the main pure water reservoir but was collected in a separate container as disposal waste water, and then the pure water retentate was returned to the main reservoir and re-circulated continuously for about 8 hours.
- The conductivity and pH of permeate and retentate of the pure water flux was monitored and checked to be cleaned from ions.
- The re-generation process was conducted at a constant flow rate of 100 l/hr.
- Re-generation processes were carried out at room temperature.
- In order to estimate the re-generation efficiency, new deionised water was used as a feed solution in the rig and the same first two steps above were repeated again to determine a new relationship between the applied increment pressure and the permeability of deionised water in order to compare the permeation of the pure water before and after the re-generation process.

3.8 Summary

This chapter shows the specifications of the tubular TiO_2 membrane, module, and the chemical reagents used in the experimental part of the present work. The fouling tendency of the tubular configuration is considerably low compared to other types of membranes such as plate and frame, spiral wounds and hallow fibre. Besides, the cleaning and regeneration of this type is very effective. The Titania membranes have received special attention due to their unique characteristics compared to other mineral oxides membranes such as Alumina, Zirconia, and Silica membranes as a result of its good resistance to fouling, high water flux and commercial availability. Detailed descriptions of the experimental materials and membrane filtration rig apparatus are presented in this chapter. The methodology of three different bench scale experiments used to evaluate the membrane zeta potential (by using streaming potential technique), salts rejection, and critical flux are explained. The re-generation procedure for the TiO_2 membrane is also described.

CHAPTER 4

EXPERIMENTAL RUSULTS AND DISCUSSIONS

4.1 Introduction

This chapter provides details related to the experimental analysis conducted in this work with extensive discussions for the obtained results.

In this work, three different sets of measurements have been carried out:

- Membrane electrokientic measurements. In this set of experiments the membrane zeta potential was obtained from streaming potential measurements by using the Helmoholtz-Smoluchowski equation to characterise the surface charge (type and magnitude) of the tubular ceramic TiO_2 NF membrane.
- Membrane rejection measurements. In this set of experiments the rejection behaviour of calcium sulphate solutes were studied and compared to the following naturally occurring single salts solutions: sodium chloride, sodium sulphate, and calcium chloride at three different initial concentrations of 0.001, 0.005 and 0.01 M and five different applied trans-membrane pressures ranging from 1.0 to 5.0 bars.
- Critical flux measurements. In this set of experiments the critical flux of calcium sulphate solutes at the present tubular TiO_2 NF membrane were described and compared by using two different flux-pressure techniques with four different ionic concentrations for each measuring technique at step heights covering applied trans-membrane pressure ranging from 1.0 to 6.0 bars.

In this chapter, the concept of critical flux (CF) was introduced based on cross-flow filtration (CFF) mode experiments in order to describe the fouling behaviour of calcium sulphate at different molar concentrations below saturation concentration (0.001, 0.005, 0.01 M) and at saturation concentration to identify the form and the onset of fouling in the present work ceramic titania NF membrane.

4.2 Membrane electrokientic measurements

Streaming potential measurements have been carried out to determine the membrane zeta potential in order to characterise the type and magnitude of the surface charge for a tubular ceramic TiO_2 NF membrane.

4.2.1 Zeta potential from streaming potential

The zeta potential was calculated from streaming potential measurements for a background electrolyte concentration of 0.01 M NaCl across a range of pH values from (3 – 9).

Streaming potential was measured from the applied pressure increment (ΔP) of (0.5, 0.75, 1.0, 1.25, and 1.5 bar) at each pH value to one side of the membrane and by measuring the variation of the resulting instantaneous electrical potential difference (ΔE) on both sides of the NF membrane.

This electrical potential difference per unit of applied pressure is the streaming potential ($SP = \Delta E/\Delta P$). The measured electrical potential varies linearly versus the applied pressure increments. Figures 4.1, 4.2, 4.3, 4.4, 4.5, 4.6, 4.7, 4.8, and 4.9 show the streaming potential measurements versus the applied pressure increments at pH values of 9, 8, 7, 6, 5, 4.5, 4, 3.5 and 3 respectively.

Initial experiments were performed to ensure that the electrical potential varies linearly versus the applied pressure increment, and then the streaming potential can be deduced from the slope of ($\Delta E = f\ \Delta P$).

The zeta potential can be calculated from the Helmoholtz-Smoluchowski equation; (see Equation 2.18); based on the relationship between the measurable streaming potential (V) and the ζ-potential (V), then:

$$\zeta^{sp} = slope\,\frac{\mu k}{\varepsilon_r \varepsilon_\circ}$$

In this equation, the dynamic viscosity ($Pa.s$) and the bulk conductivity of the circulating electrolyte ($S.m^{-1}$) according to the experiment results are equal to 8.9×10^{-4} and (0.1) respectively.

Table (4.1) illustrates the estimated membrane zeta potential (mV) over a range of pH values for a background electrolyte fixed at 0.01 M NaCl.

Figure (4.10) shows a plot of the measured zeta potential over a range of pH values from (3 – 9) by using 0.01 M NaCl as a background electrolyte.

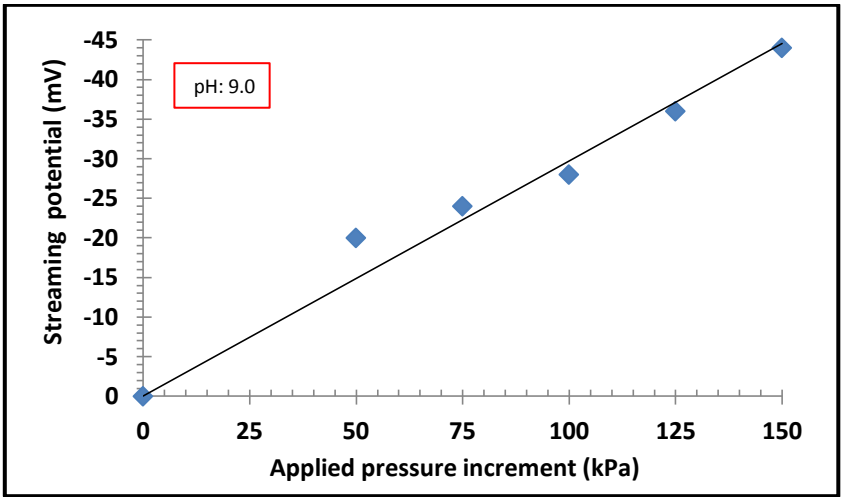

Figure 4.1: Streaming potential measurements versus applied pressure increment at pH = 9.

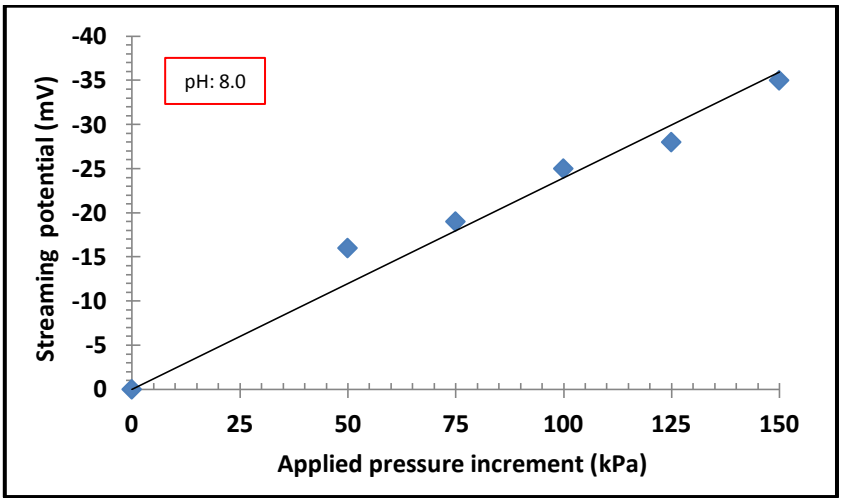

Figure 4.2: Streaming potential measurements versus applied pressure increment at pH = 8.

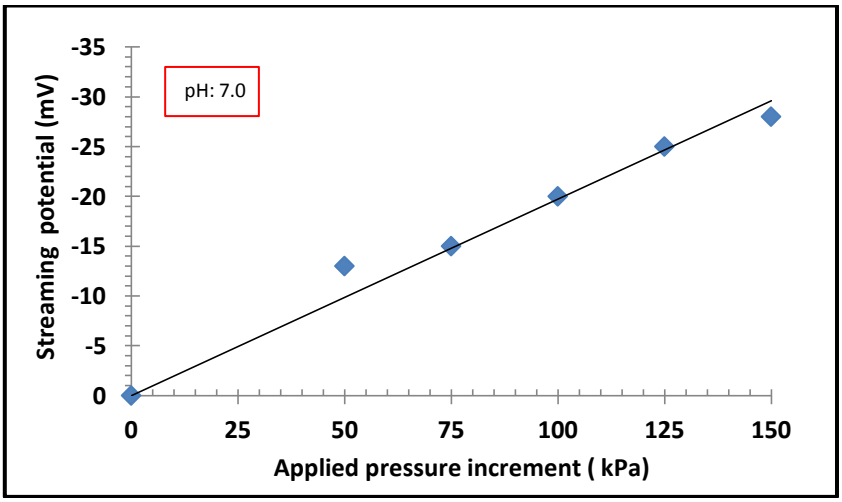

Figure 4.3: Streaming potential measurements versus applied pressure increment at pH = 7.

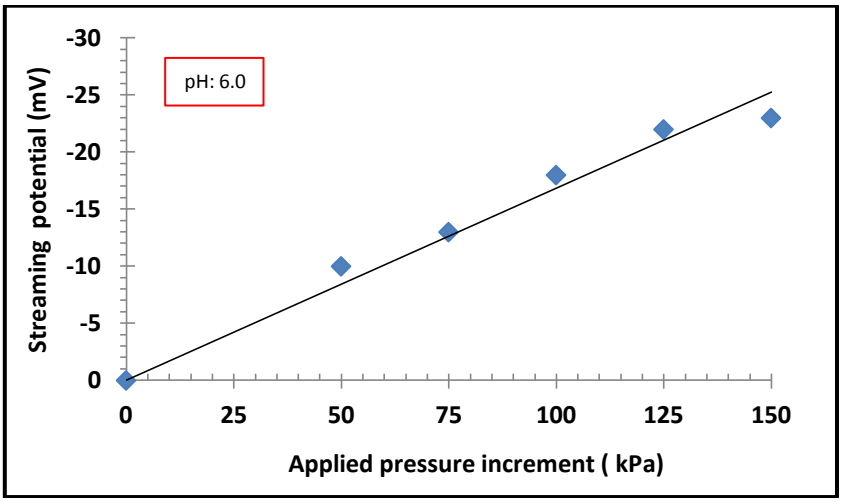

Figure 4.4: Streaming potential measurements versus applied pressure increment at pH = 6

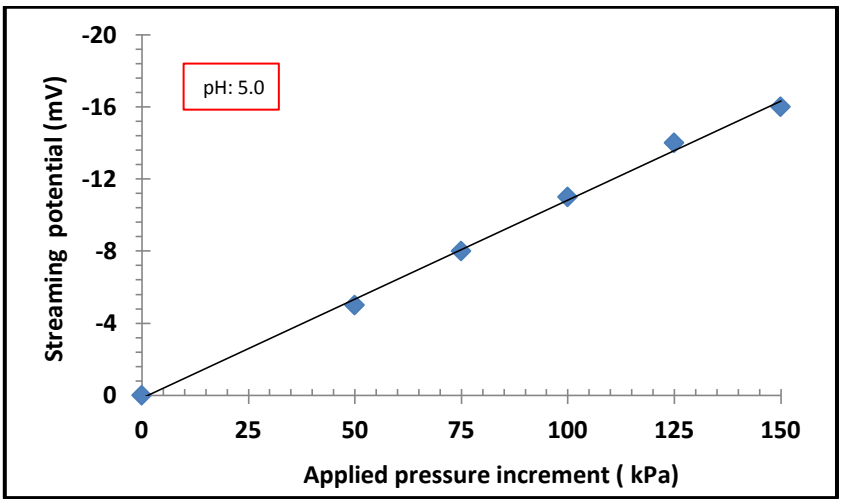

Figure 4.5: Streaming potential measurements versus applied pressure increment at pH = 5

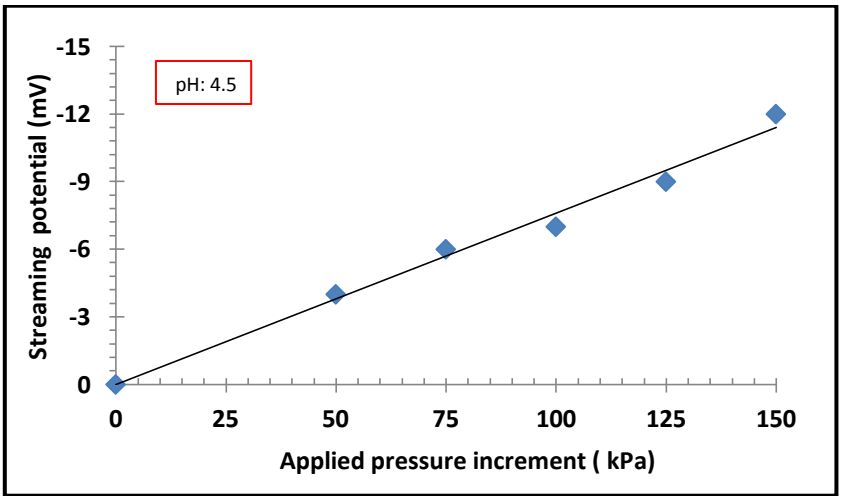

Figure 4.6: Streaming potential measurements versus applied pressure increment at pH = 4.5

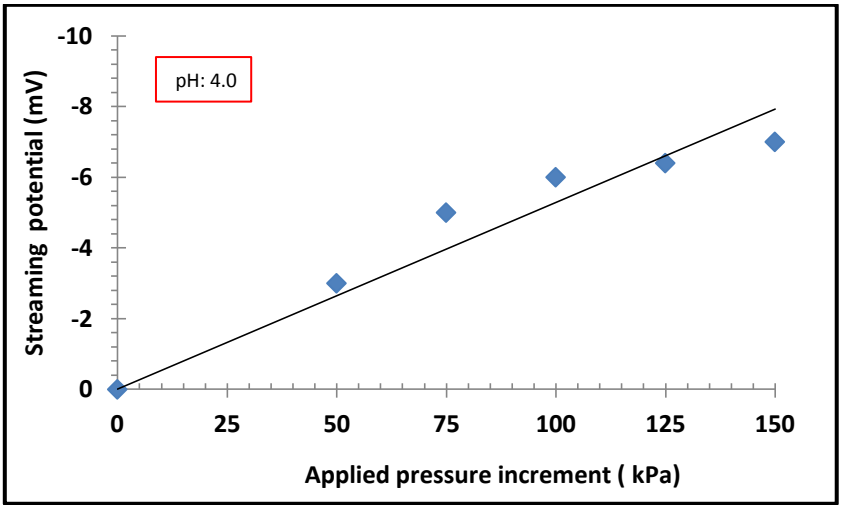

Figure 4.7: Streaming potential measurements versus applied pressure increment at pH = 4

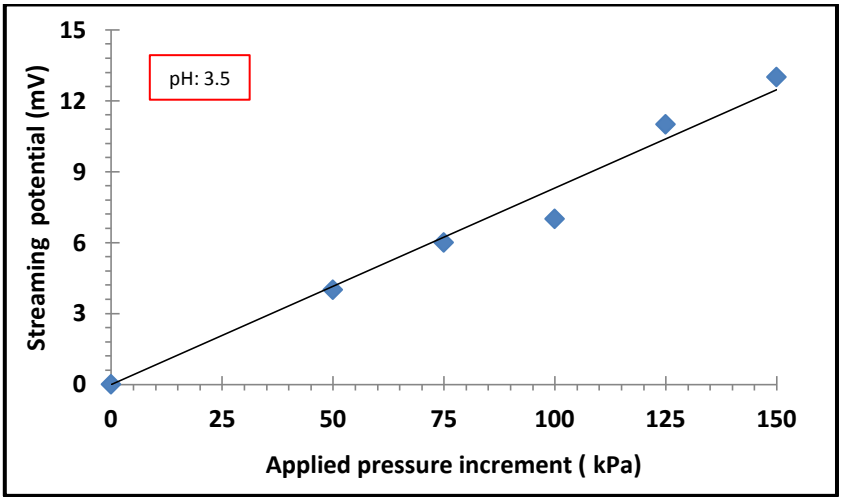

Figure 4.8: Streaming potential measurements versus applied pressure increment at pH = 3.5

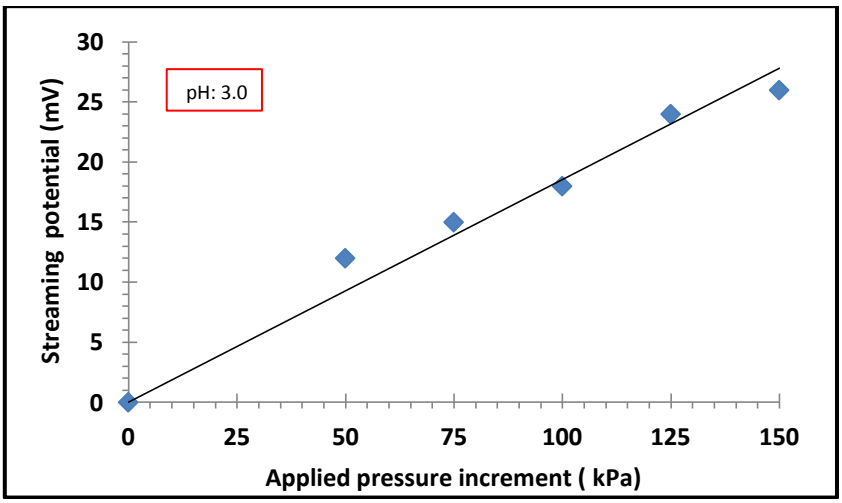

Figure 4.9: Streaming potential measurements versus applied pressure increment at pH = 3

Table 4.1: Estimated membrane zeta potential (mV) for ceramic TiO_2 NF over a range of pH values for background electrolyte fixed at 0.01 M NaCl.

pH	Charts slope	Charts R^2	ζ^{sp}(mV)
9.0	-2.97×10^{-4}	0.970	−38.39
8.0	-2.40×10^{-4}	0.968	−30.71
7.0	-1.97×10^{-4}	0.975	−25.59
6.0	-1.68×10^{-4}	0.973	−21.75
5.0	-1.08×10^{-4}	0.997	−14.07
4.5	-7.60×10^{-5}	0.987	−9.37
4.0	-5.29×10^{-5}	0.930	−6.65
3.5	$+8.31 \times 10^{-5}$	0.978	+10.64
3.0	$+1.85 \times 10^{-4}$	0.971	+24.31

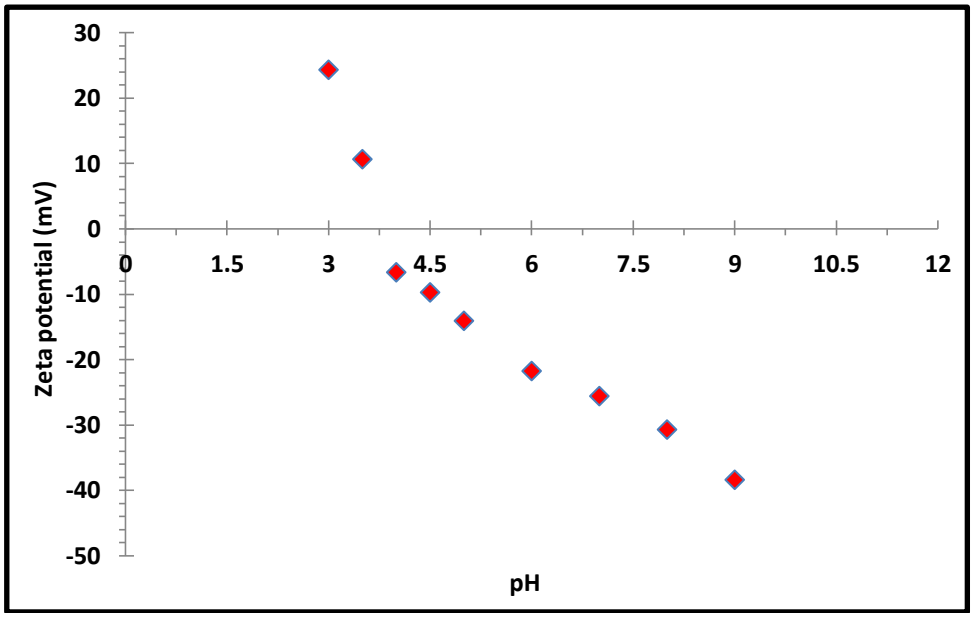

Figure 4.10: Zeta potential of 1 nm ceramic TiO_2 NF membrane determined from streaming potential plotted against pH for background electrolyte fixed at 0.01 M NaCl with i.e.p of 4.0.

The reason behind choosing the diluted background concentration of 0.01 M for conducting streaming potential experiments in this work can be attributed to the following:

- Most researches [62], [128], [129] consider this concentration as a standard zeta potential measurement value in order to ensure the achievements of the linearity relation of electrical potential measurements (ΔE) versus the applied pressure increment (ΔP).

- Based on the Darcy equation, using this diluted concentration in order to neglect the effects of osmotic pressure.
- The Helmoholtz-Smoluchowski equation normally applies for electrolyte concentrations larger than 0.001 M [2], [55]. Thus, for experiments with diluted solutions (less than 0.001 M) the surface conductivity effect would be contributed as well. In this case, the H-S equation needs to be multiplied by a correction factor based on electrolyte resistance of the electrolyte solution to that of concentrated solution (0.1 M KCl) [54], [62].

The behaviour of the streaming potential process can be explained based on the definition of the streaming potential which can be defined as the potential difference caused by the convective flow of charges as a result of applied pressure; this potential is generated by exerting a force on the electrical double layer that has been built up in the solution near the charged surface (see Figure 2.9).

Since an excess of counter charges are present, movement of those counter charges causes a current. This current which is streaming through the double layer is normally called streaming current. The accumulation of counter charges downstream generates a streaming potential across the membrane, which in its turn causes a conduction current through the membrane in the reverse direction.

In the mean time, the effect of pH on the membrane potential for most oxide materials (such as TiO_2, ZrO_2 and Al_2O_3) can be interpreted due to the fact that the potential determining ions in an aqueous medium are normally (H^+) and (OH^-); therefore, the total potential drop across the double layer is determined based on the pH of solute.

Based on the Debye-Huckel theory, the electric double layer at the plane interface can be described by ($d^2\Psi/dx^2 = K^2\Psi$), where Ψ is the potential and x is the dimension in which the potential varies (see Figure 2.9).

The extension of the double layer is characterised by Debye-Huckel length K^{-1}, which is expressed in terms of the concentration and valence of ions in the bulk solution (as shown in Equations 2.29 and 2.30).

Many researchers [51], [55], [130] believed that the separation mechanism of charged species in NF membranes is assumed to be a combination of several processes and membrane charge (Donnan) exclusion is one of the important parameters in addition to the size exclusion parameter.

As mentioned previously, the characteristics of ceramic membranes are affected by the electrokinetic phenomena of the solid surface when comes in contact with water. This could have an effect on the nature and magnitude of the interaction between the membrane and liquid feed which might affect the permeate flux and rejection behaviour of the ions.

These electrokinetic properties are frequently characterised in terms of zeta potential and iso-electric point (the pH value at which the net charge of the membrane is globally zero).

Figure (4.10) shows the dependence of streaming potential on the pH. The curve is typical of the amphoteric behaviour of metal oxide and results from proton equilibrium that occurs at the membrane surface when the pH shifts.

It can be seen from Figure (4.10) that the zeta potential changes its sign from negative to positive with decreasing pH; at pH of 9 the ζ-potential equals to -38.39 mV whereas, at pH of 3 the ζ-potential becomes positive with magnitude of 24.31mV.

The experimental results show that the commercial 1 nm ceramic TiO_2 NF membrane is negatively charged at neutral pH and its iso-electrical point is at pH value of 4.0 ($\pm$ 0.1). This means as pH of the solute increases, the zeta potential becomes more negative.

The obtained results show that for pH values from 9 to 4 there is a significant drop in zeta potential values from -38.39 to -6.65 mV which reflects the effect of the amphoteric behaviour of the present work's ceramic Titania membrane.

The results of the present work are in good agreement with the work done by Narong [120] where the iso-electrical point for a 0.005 μm Titania ceramic membrane (characterised as ultrafiltration membrane) was found to be at pH values of 3.8.

Also, Puhlfürb et al. [118] determined the zeta potential of a flat ceramic TiO_2 NF membrane from streaming potential measurements performed with NaCl and KCl solutions at two different concentrations (0.01 M and 0.05 M); the estimated i. e. p for both electrolytes were found to be at pH of 3.3.

By comparing the obtained membrane zeta potential results from using the streaming potential technique in the present work with the previous work done by Hajarat [11] where the micro-electrophoresis technique was used to measure zeta potential (for the same 1nm ceramic TiO_2 NF membrane and same background concentration of 0.01 M NaCl), it can be noticed that there is a clear shift in the i. e. p from 5.0 to 4.0.

The shift in the iso-electric point between the present work and Hajarat's work [20] can be attributed to the difference between the two techniques used in measuring the zeta potential. In terms of membrane characterisation, the present study used the streaming potential method which it is non-destructive in situ method, whereas, the measurements in the micro-electrophoresis method which requires particles of membrane material, can only be obtained from grinding the membrane.

The micro-electrophoresis method is widely effective for studying powder dispersions, unlike any other methods; this procedure requires destroying of the membrane but the newly formed surface can differ considerably from the original membrane surface. For a homogenous symmetrical membrane (made up from only one type of material) this method might be effective, but for an asymmetric (composite) ceramic membrane in which the supporting layers are made of metal oxides which differ from the surface active layer of the membrane.

As shown in Figure (3.3), the EDAX specific spectrums of the active skin layer of 1 nm tubular NF Titania membrane used in this work include many elements and components such as (aluminum, titanium, and zirconium) that compromise the membrane. The final properties of the membrane were identified due to the type and thickness of the active skin layer of the membrane, and based on this; the membrane's outer surface charge would definitely be affected by the material of the outer skin layer.

In the micro-electrophoresis method, the surface skin layer does not exist and the materials in the supported sub-layers were mixed with each other, which could explain the shift in the iso-electric point between the two studies. Also, there is an important limitation in the use of the electrophoresis method when studying the effect of fouling materials on the membrane zeta potential is needed.

Based on these reasons, the obtained membrane zeta potential from streaming potential measurements resulting in this work could be considered as more accurate than the previous work done by Hajarat [20].

The main difference of this work compared to other previous studies done by Narong [120] and Chiu [127] is that these works conducted the streaming potential experiments and the rejection of NaCl solution in different concentrations at the same time, while in the present work, the streaming potential measurement was separated from the NaCl rejection experiments.

4.2.2 Zeta potential at fixed pH with changed ionic strength

In order to study the influence of solution ionic strength on the electrokientic surface (zeta) potential, the streaming potential was also measured at 0.025, 0.05 and 0.075 M sodium chloride (NaCl) solution by using exactly the same procedure which is used for the background electrolyte of 0.01 M (NaCl).

The streaming potential measurement was conducted at an unadjusted pH of 6 ± 0.2.

The results show that as salt concentration increased, the zeta potential value decreased. It can be seen from the previous section that at solute pH of 6.0, the estimated membrane zeta potential value for 0.01 M NaCl was (-21.75 mV), whereas, at solute concentrations of 0.025, 0.05 and 0.075 M the membrane zeta potentials were -18.279, -15.296 and -13.022 mV respectively.

Figure (4.11) shows a plot of the measured zeta potential determined from streaming potential at unadjusted pH of 6 ± 0.2 by using 0.01, 0.025, 0.05 and 0.075M NaCl as a background electrolyte for a 1 nm ceramic NF TiO_2 membrane.

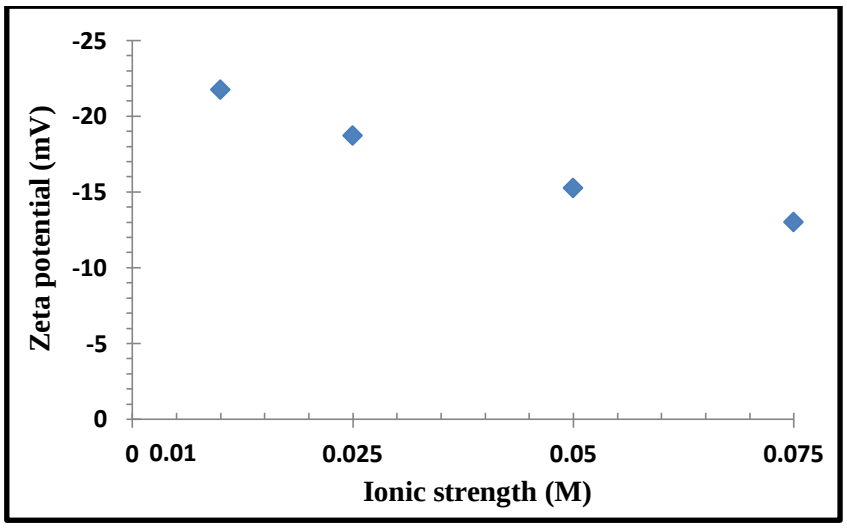

Figure 4.11: Zeta potential of 1 nm ceramic TiO_2 NF membrane determined from streaming potential plotted against pH (fixed at 6 ± 0.2) for background electrolytes of 0.01, 0.025, 0.05 and 0.075 M NaCl.

Figure (4.11) shows that the zeta potential values were decreased with the increasing of the salt concentration. This result is in agreement with other researchers [20], [127], [129]. The decreasing in the zeta potential magnitude as electrolyte concentration increases can be explained according to the electrical double layer theory, in which the effective thickness of the diffuse layer (K^{-1}) decreases as the ionic strength increases.

4.3 Membrane rejection measurements

The separation mechanisms in NF are not dependant on a sieving (size exclusion) mechanism only, for instance, in the NaCl solution; the ionic radius for cation Na^+ and anion Cl^- equal to 0.181 and 0.098 nm respectively [48]. The ionic radius of both sodium and chloride are smaller than the membrane pore size used in the present study (1nm), therefore the membrane pore is still large compared to the ionic radii. Based on this, there must be other mechanisms that govern the rejection of ions in NF membranes. For charged membranes, the Donnan exclusion mechanism is definitely one of these mechanisms.

Regarding the composite NF membrane, another mechanism can be added since the NF membrane is an asymmetric membrane type with a microporous skin layer and porous supporting sub-layers. Such a composite type leads to diffusion potential due to the concentration gradient in the porous layers based on the theory of a solution diffusion model (the same separation principle as in the RO membrane, see section 2.3.3); which could increase the rejection efficiency. This effect can be added to the other two main parameters that govern transport in a porous membrane (size exclusion and Donnan exclusion mechanisms).

In this section, the retentions behaviour of calcium sulphate were studied compared to other predominate naturally occurring single salts that usually accumulate in soil ($NaCl, Na_2SO_4$ and $CaCl_2$) by using a tubular ceramic TiO_2 nanofiltration membrane with a pore size of 1 nm at three different initial concentrations of 0.001, 0.005 and 0.01 M. The rejection experiments were carried out at five different feed pressures in the range from 1.0 to 5.0 bar.

The rejection behaviour of calcium sulphate based on the salt solubility saturation concentration (below and at saturation concentration) was also investigated.

The concentrations of the cations (sodium or calcium) were measured using inductively coupled plasma atomic emission spectroscopy (ICP-AES) while the concentrations of the anions (chloride or sulphate) were measured using ion chromatography (IC). The minimum sample volume needed for analysis is 12 ml.

The ion chromatography (type: Dionex DX 600-dual IC system) was used for anion analysis with column Dionex AS4A-SC, using a conductivity cell as a detector and the mixture of ($NaCO_3/NaHCO_3$) as the mobile phase was used to perform the anion's analysis measurements.

In the present IC device, the sample solutions passed through a pressurised chromatographic column, in which ions are absorbed. An ion extraction liquid, known as the eluent, is passed through the column and the absorbed ions are separated. By analysing the retention time, the ionic concentrations in the sample can be determined. Ion chromatography equipment normally contained an ion-exchange resin to separate atomic or molecular ions based on the interaction between ions in the solution and the oppositely charged functional group on the column resin. Its greatest utility is for analysis of anions for which there are no other rapid analytical methods, also the simplicity and high selectivity of this measuring technique.

The dilution of the sample in the IC device is normally performed when the concentration of the analyst of interest exceed the working capacity of the chosen separation column. Also, in order to avoid any possible blockages in the column(s) of the device, all samples were filtered prior to injection with a 0.2 μm filter.

The ICP-AES equipment (type: Perkin-Elmer Optima 5300 dual view**)** was used to conduct the analysis of the present work's cations. Liquid samples should normally be aqueous, acidified (typically $2\%\ HNO_3$ or equivalent), and filtered (removing particles > 0.45 μm). Analysis of water samples that containing $Na, K, Ca, Mg, Si, S, P, Fe,$ and Mn might typically conducted in this device.

The ICP device is one of the most recently developed techniques for trace elemental analysis in which the sample is usually transported into the instrument as a stream of liquid sample. Inside the instrument, the liquid is converted into an aerosol, then the sample aerosol is transported to the plasma where it is vaporised, atomised, and excited (or ionised) by the plasma. The excited ions and atoms emit their characteristic radiation which is collected by a device that sorts the radiation by wavelength. The radiation is detected and turned into electronic signals that are converted into concentration information for the analyst [131].

All the anion and cation's analysis for the rejection experiments samples of the present work were conducted at the laboratories of School of Earth, Atmospheric and Environmental Sciences (University of Manchester).

Studying the effects of pH on the salts rejection is not among the objectives of the present research.

4.3.1 Rejection of sodium sulphate

The retention of sodium sulphate as a single electrolyte in the 1nm tubular ceramic TiO_2 nanofiltration membrane as a function of applied trans-membrane pressure with emphasis on the effect of feed concentration has been studied experimentally. The rejection experiments were carried out at five different feed pressures in the range from 1.0 to 5.0 bar with solute feed concentrations of 0.001, 0.005 and 0.01 M by following the major steps that have already been mentioned in section (3.6.2) for each Na_2SO_4 concentration.

Figures (4.12, 4.13 and 4.14) show the rejection of sodium sulphate at 0.001, 0.005 and 0.01 M respectively as a function of applied trans-membrane pressure. From these figures, it can be concluded that the rejections of sodium (Na^+) and sulphate (SO_4^{-2}) were increased as the applied trans-membrane pressure increased.

Also, in all three figures the rejection of sulphate ions (SO_4^{-2}) was noticeably higher than the rejection of sodium ions (Na^+). At the highest applied trans-membrane pressure (5.0 bar); the rejection of sulphate ions was 30.77%, 25.53% and 19.79% for Na_2SO_4 feed concentration of 0.001, 0.005 and 0.01 M respectively whereas the rejection of sodium ions at the same concentrations was 26.22%, 21.71% and 16.94% respectively.

Figures (4.12, 4.13 and 4.14) show that the rejection of Na_2SO_4 salt solutions by the TiO_2 NF membrane was decreased with the growth of salt concentrations.

Figures (4.15, 4.16 and 4.17) show the conductivity of sodium sulphate permeates at 0.001, 0.005 and 0.01 M respectively as a function of applied trans-membrane pressure. These figures show that the conductivity of sodium sulphate permeates for each concentration was decreased with the increased applied pressure.

The permeate conductivity of 0.001M Na_2SO_4 was significantly decreased from 192 $\mu S/cm$ at 1.0 bar to 149 $\mu S/cm$ at 5.0 bar while the feed conductivity was 228 $\mu S/cm$ (see Figure 4.15).

The same behaviour occurred for other two concentrations in which the permeate conductivity of 0.005 M Na_2SO_4 was noticeably decreased from 942 $\mu S/cm$ at 1.0 bar to 730 $\mu S/cm$ at 5.0 bar while the feed conductivity was 1030 $\mu S/cm$ (see Figure 4.16). Whereas for 0.01 M Na_2SO_4 the permeate conductivity was decreased from 1.41 mS/cm at 1 bar to 1.24 mS/cm at 5.0 bars with feed conductivity of 1.65 mS/cm (see Figure 4.17).

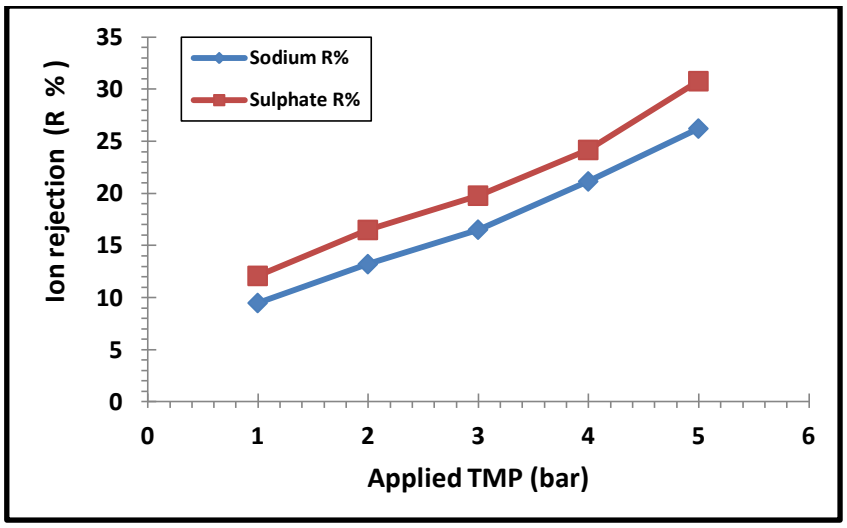

Figure 4.12: Sodium sulphate rejection (0.001 M) as a function of applied TMP (bar).

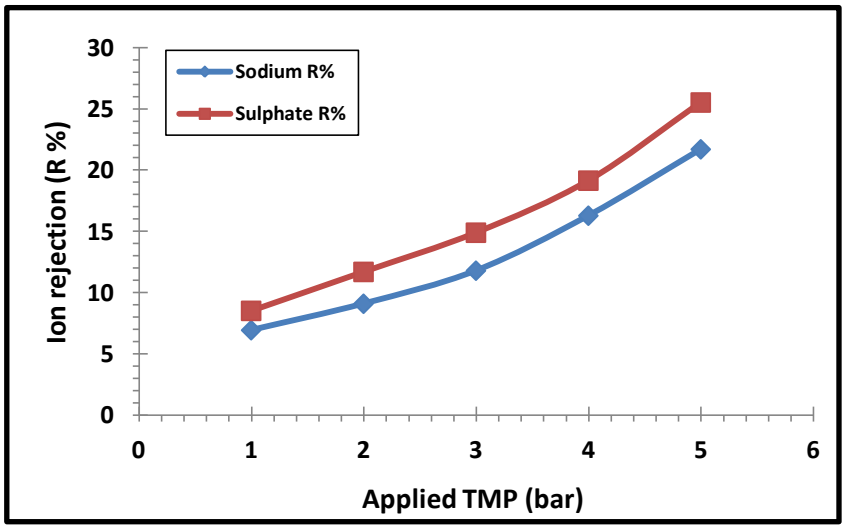

Figure 4.13: Sodium sulphate rejection (0.005 M) as a function of applied TMP (bar).

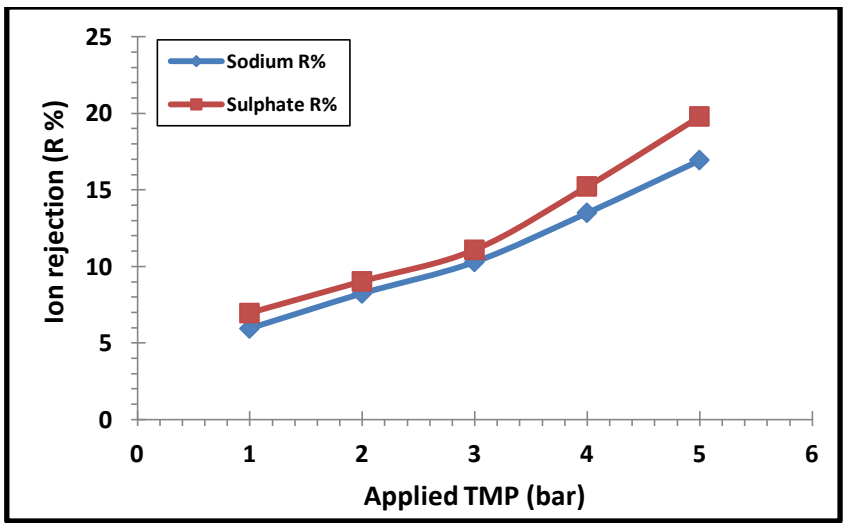

Figure 4.14: Sodium sulphate rejection (0.01 M) as a function of applied TMP (bar).

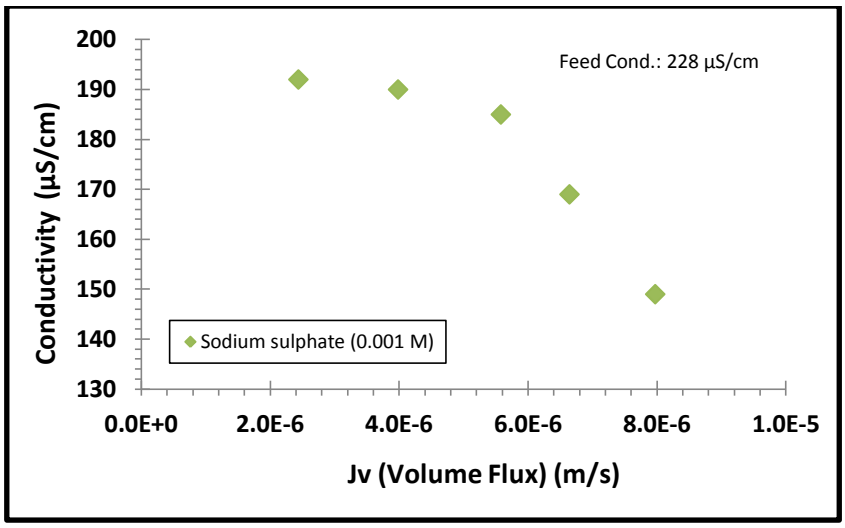

Figure 4.15: Permeate conductivity of Na_2SO_4 (0.001 M) vs. volume flux (m/s).

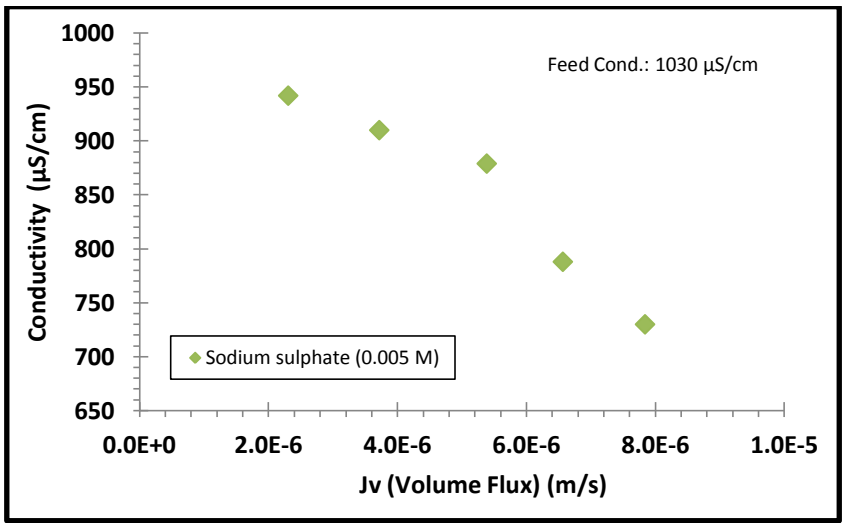

Figure 4.16: Permeate conductivity of Na_2SO_4 (0.005 M) vs. volume flux (m/s).

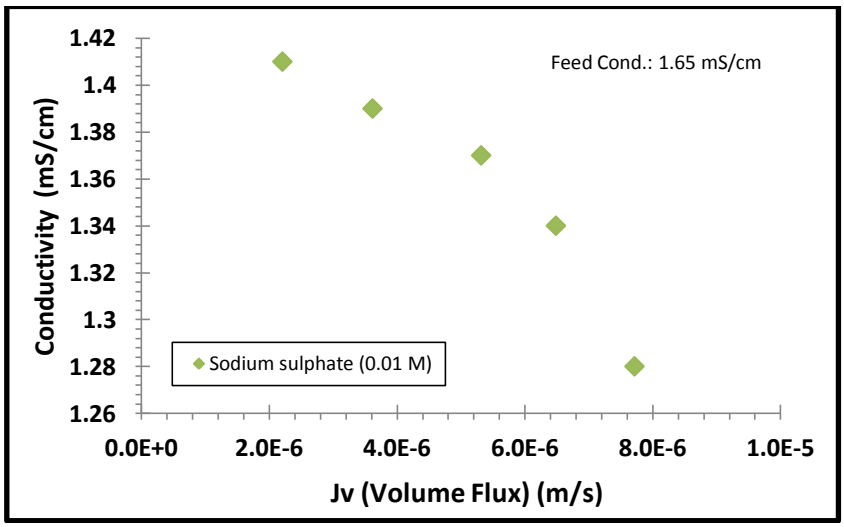

Figure 4.17: Permeate conductivity of Na_2SO_4 (0.01 M) vs. volume flux (m/s).

The measured conductivity on the permeate side might add other parameters as an important instantaneous indication that can be easily measured to show the changes that possibly occurred during the membrane filtration process.

The rejection (R %) of sodium sulphate solutes at 0.001, 0.005 and 0.01 M can be estimated based on the ionic strength equation (see Equation 2.30) depending on the ions valance and the measured rejection values (in mg/l) of sodium (Na^+) and sulphate (SO_4^{-2}) ions for each membrane operating pressure.

Figure 4.18 shows the rejection of sodium sulphate solutes at 0.001, 0.005 and 0.01 M as a function of applied trans-membrane pressure. From Figure (4.18) it can be seen that for each of the above concentrations there was a gradual rise in the rejection of Na_2SO_4 salt linked to the increased applied pressure. At the applied trans-membrane pressure of 5.0 bar; the rejection of sodium sulphate salt was 29.86%, 24.83% and 19.2% for feed concentration of 0.001, 0.005 and 0.01 M respectively.

The permeate volume flux (m/s) can be determined based on the mesured permeate flux in (m^3/s) divided by the Titania membrane area for the present study ($4.178 \times 10^{-3}\ m^2$).

Figure (4.18) shows the permeate volume flux of Na_2SO_4 at 0.001, 0.005 and 0.01 M as a function of applied trans-membrane pressure.

From Figure (4.19) it can be seen that there was a gradual rise of permeate volume flux for sodium sulphate salts solutions linked to the increased applied trans-membrane pressure. For each Na_2SO_4 salt concentration, there was a very slight change in permeate volume flux as a function of the applied trans-membrane pressure. At the applied trans-membrane pressure of 5.0 bars, permeates volume flux of sodium sulphate salt were 7.98×10^{-6}, 7.85×10^{-6} and 7.72×10^{-6} m/s for feed concentration of 0.001, 0.005 and 0.01 M respectively.

According to Figure (4.19) and for each sodium sulphate concentration, it can be concluded that the permeate volume flux was increased as the applied trans-membrane pressure increased whereas the permeate flux was decreased with the increased feed concentration.

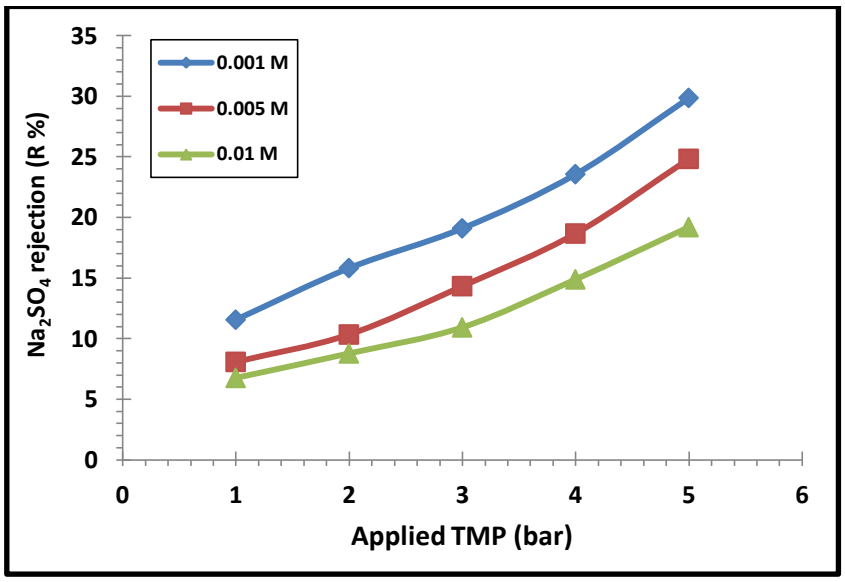

Figure 4.18: Rejection of Na_2SO_4 at (0.001, 0.005 and 0.01M) vs. applied TMP (bar).

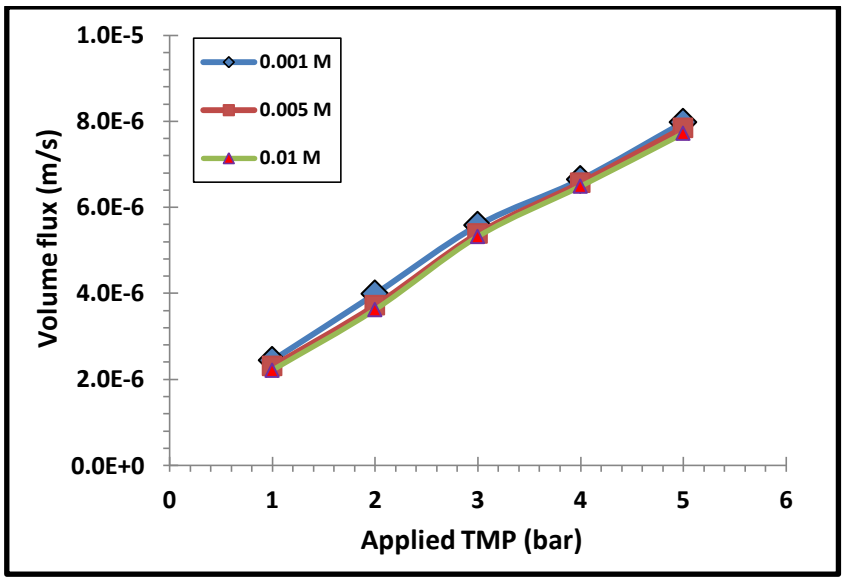

Figure 4.19: Permeate volume flux of Na_2SO_4 at (0.001, 0.005 and 0.01M) vs. applied TMP (bar).

4.3.2 Rejection of sodium chloride

The retention of sodium chloride as a single electrolyte in the 1nm tubular ceramic TiO_2 nanofiltration membrane as a function of applied trans-membrane pressure with emphasis on the effect of feed concentration has been studied experimentally.

Figures (4.20, 4.21 and 4.22) show the rejection of sodium chloride at 0.001, 0.005 and 0.01 M respectively as a function of applied trans-membrane pressure. From these figures, it can conclude that the rejections of sodium (Na^+) and chloride (Cl^-) were gradually increased as the applied trans-membrane pressure increased.

In all three figures the rejection of chloride ions (Cl^-) was slightly higher than the rejection of sodium ions (Na^+). At the highest applied trans-membrane pressure (5.0 bar), the rejection of chloride ions (Cl^-) was 12.43%, 7.83% and 5.1% for NaCl feed concentration of 0.001, 0.005 and 0.01 M respectively. On the other hand, the rejection of sodium ions (Na^+) at same concentrations was 11.35%, 7.4% and 4.65% respectively.

At the lowest applied trans-membrane pressure (1.0 bar), the rejection of chloride ions was 2.13%, 1.81% and 1.21% for NaCl feed concentration of 0.001, 0.005 and 0.01 M respectively. While, the rejection of sodium ions at same concentrations was 1.77%, 1.49% and 0.93% respectively.

Figures (4.20, 4.21 and 4.22) show that the rejection of NaCl salt solutions by the TiO_2 NF membrane was decreased with the growth of salt concentrations.

Figures (4.23, 4.24 and 4.25) show the conductivity of sodium chloride permeates at 0.001, 0.005 and 0.01 M respectively as a function of applied trans-membrane pressure. From these figures it can be concluded that the conductivity of sodium chloride permeate for each concentration was decreased with the increased applied trans-membrane pressure.

The permeate conductivity of 0.001 M NaCl was noticeably decreased from 97 μS/cm at 1.0 bar to 86.1 μS/cm at 5.0 bar while the feed conductivity was 100 μS/cm. The same behaviour occurred for other two concentrations in which the permeate conductivity of 0.005 M NaCl was noticeably decreased from 514 μS/cm at 1.0 bar to 485 μS/cm at 5.0 bar while the feed conductivity was 519 μS/cm. On the other hand, for 0.01 M NaCl the permeate conductivity was decreased from 996 μS/cm at 1 bar to 934 μS/cm at 5.0 bar with feed conductivity of 1.03 mS. cm.

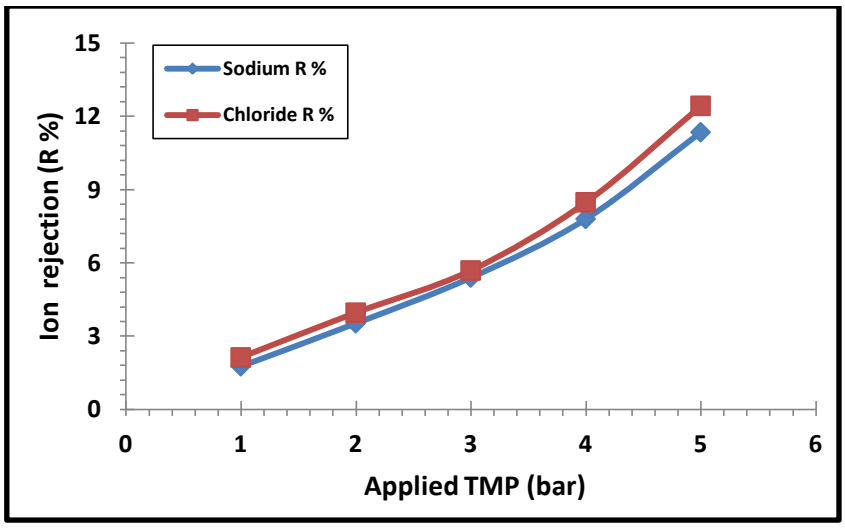

Figure 4.20: Sodium chloride rejection (0.001 M) as a function of applied TMP (bar).

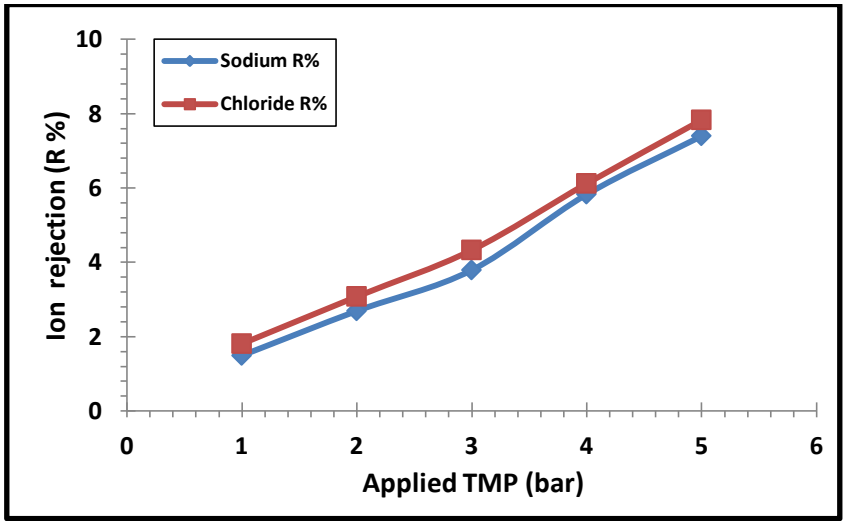

Figure 4.21: Sodium chloride rejection (0.005 M) as a function of applied TMP (bar).

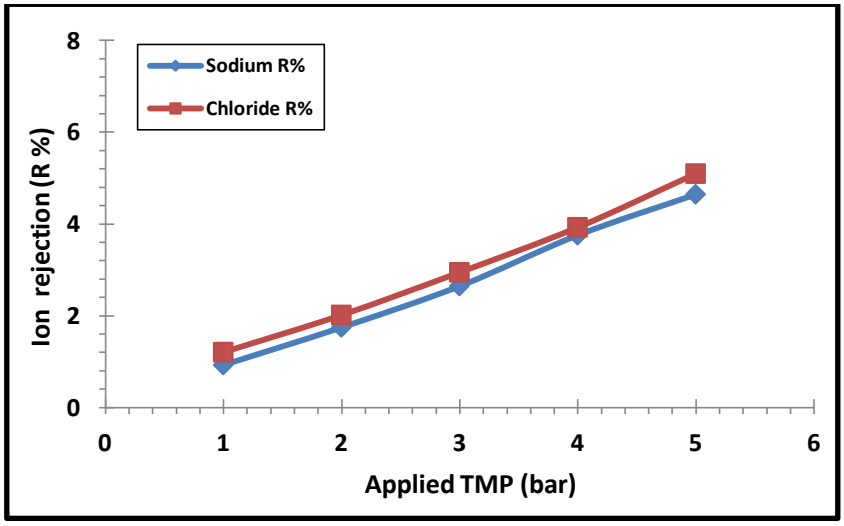

Figure 4.22: Sodium chloride rejection (0.01 M) as a function of applied TMP (bar).

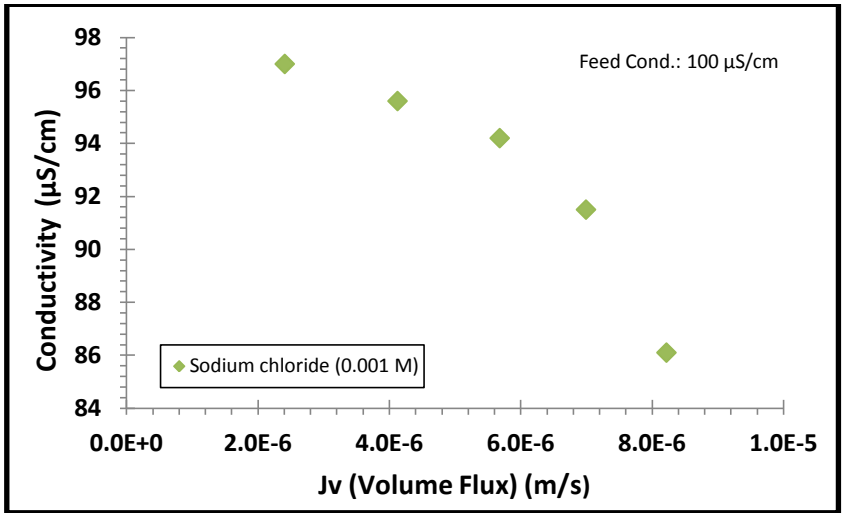

Figure 4.23: Permeate conductivity of NaCl (0.001 M) vs. volume flux(m/s).

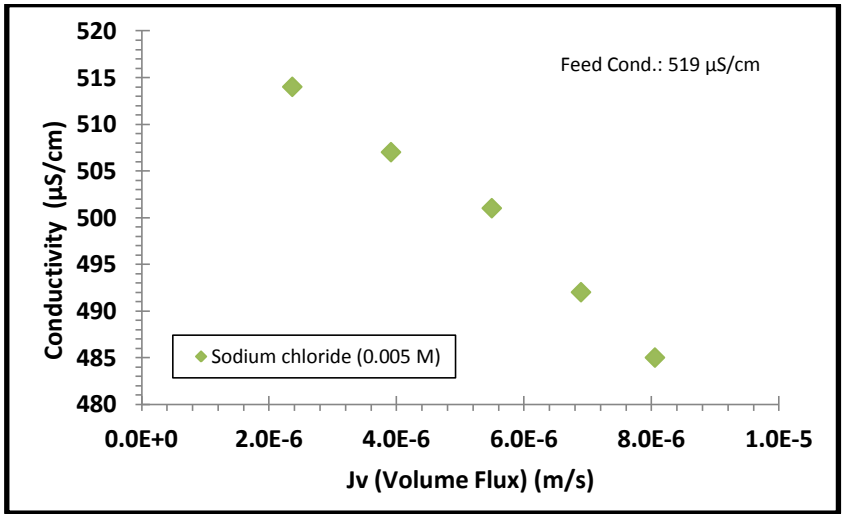

Figure 4.24: Permeate conductivity of NaCl (0.005 M) vs. volume flux (m/s).

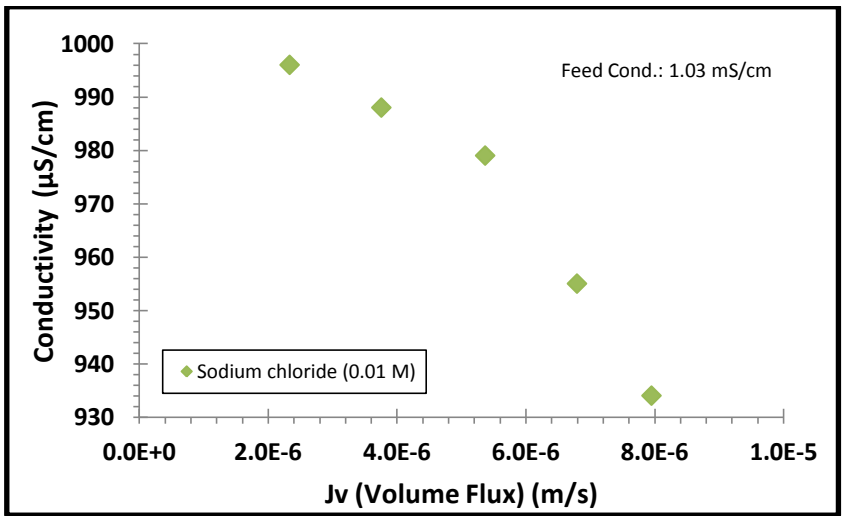

Figure 4.25: Permeate conductivity of NaCl (0.01 M) vs. volume flux(m/s).

Figure 4.26 shows the rejection of sodium chloride solutes at 0.001, 0.005 and 0.01 M as a function of applied trans-membrane pressure. From this figure it can be seen that for each of the above concentrations there was a gradual rise in the rejection of NaCl salt linked to the increased applied trans-membrane pressure. At the applied trans-membrane pressure of 5.0 bar; the rejection of sodium chloride salt was 11.27%, 7.7% and 4.95% for feed concentration of 0.001, 0.005 and 0.01 M respectively.

On the other hand, at the lowest applied trans-membrane pressure of 1.0 bar, the rejection of sodium chloride salts was 2.1%, 1.68% and 1.1% for NaCl feed concentration of 0.001, 0.005 and 0.01M respectively.

Figure (4.27) shows the permeate volume flux of NaCl at 0.001, 0.005 and 0.01 M as a function of applied trans-membrane pressure.

It can be seen from the Figure (4.27) that there is a steadily increase of permeate volume flux of sodium chloride salts solutions linked to the increased applied trans-membrane pressure. For each NaCl salt concentration, there was a very slight change in permeate volume flux as a function of the applied pressure. At the applied pressure of 5.0 bars, permeates volume flux of sodium chloride salt were 7.96×10^{-6}, 7.83×10^{-6} and 7.76×10^{-6} m/s for feed concentration of 0.001, 0.005 and 0.01 M respectively.

While at the lowest applied trans-membrane pressure of 1.0 bar, permeates volume flux of sodium chloride salt was 2.39×10^{-6}, 2.26×10^{-6} and 2.13×10^{-6} m/s for feed concentration of 0.001, 0.005 and 0.01 M respectively.

According to Figure (4.27) and for each sodium chloride concentration, it can be concluded that the permeate volume flux was increased as the applied trans-membrane pressure was increased, whereas the permeate flux was decreased with the increased feed concentration.

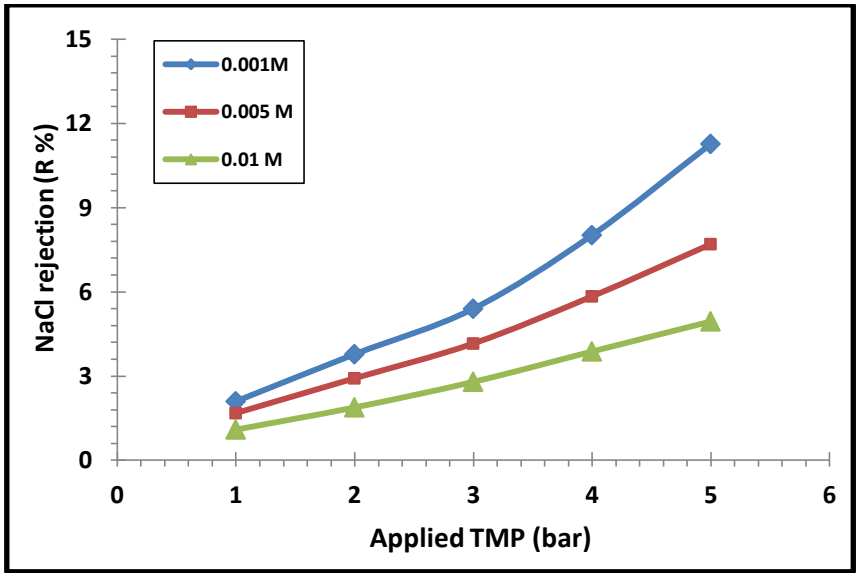

Figure 4.26: Rejection of NaCl at (0.001, 0.005 and 0.01M) vs. applied TMP (bar).

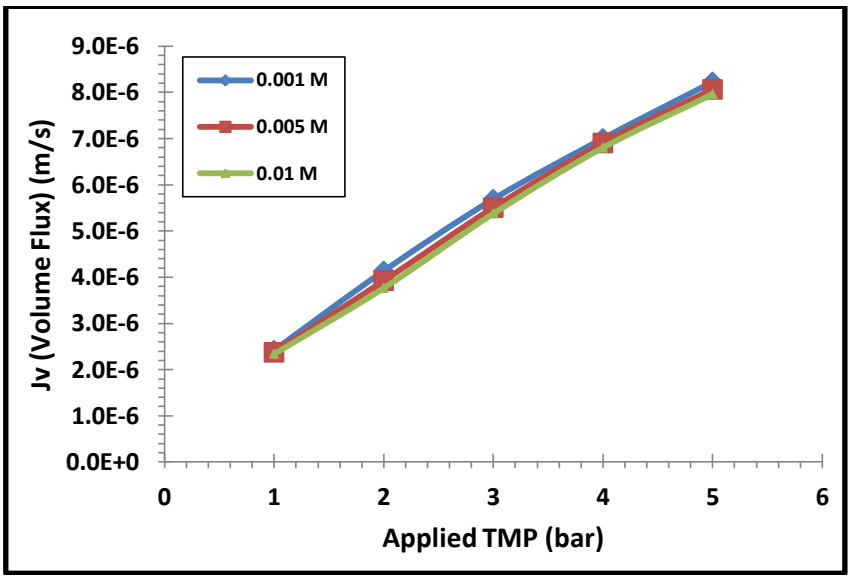

Figure 4.27: Permeate volume flux of NaCl at (0.001, 0.005 and 0.01M) vs. applied TMP (bar).

4.3.3 Rejection of calcium chloride

The rejection of calcium chloride as a single electrolyte in the 1nm tubular ceramic TiO_2 nanofiltration membrane as a function of applied trans-membrane pressure with emphasis on the effect of feed concentration has been studied experimentally.

Figures (4.28, 4.29 and 4.30) show the rejection of calcium chloride at 0.001, 0.005 and 0.01 M respectively as a function of applied trans-membrane pressure. From these figures, it can be concluded that the retentions of calcium (Ca^{+2}) and chloride (Cl^{-1}) were gradually increased as the applied trans-membrane pressure increased.

In all these three figures, the rejection of calcium ions (Ca^{+2}) was slightly higher than the rejection of chloride ions (Cl^{-1}). At the highest applied trans-membrane pressure (5.0 bar), the rejection of calcium ions was 25.14%, 20.47% and 12.7% for $CaCl_2$ feed concentration of 0.001, 0.005 and 0.01 M respectively. On the other hand, the rejection of chloride ions at the same concentration was 23.89%, 18.75% and 10.8% respectively.

At the lowest applied trans-membrane pressure of 1.0 bar, the rejection of calcium ions was 6.15%, 3.51% and 3.49% for $CaCl_2$ feed concentration of 0.001, 0.005 and 0.01 M respectively, while the rejection of chloride ions at the same concentrations was 4.5%, 3.13% and 3.08% respectively.

From Figures (4.28, 4.29 and 4.30), it can be seen that the rejection of $CaCl_2$ salt solutions by the TiO_2 NF membrane were decreased with the growth of salt concentrations.

Figures (4.31, 4.32 and 4.33) show the conductivity of calcium chloride permeates at 0.001, 0.005 and 0.01 M respectively as a function of applied trans-membrane pressure. From these figures it can be seen that the conductivity of $CaCl_2$ permeate for each concentration were decreased with the increased applied trans-membrane pressure.

The permeate conductivity of 0.001 M $CaCl_2$ was remarkably decreased from 207 $\mu S/cm$ at 1.0 bar to 176 $\mu S/cm$ at 5.0 bar while the feed conductivity was 233 $\mu S/cm$. The same behaviour occurred for other two concentrations in which the permeate conductivity of 0.005 M $CaCl_2$ decreased from 900 $\mu S/cm$ at 1.0 bar to 815 $\mu S/cm$ at 5.0 bar while the feed conductivity was 1130 $\mu S/cm$, while, for 0.01 M $CaCl_2$ the permeate conductivity was decreased from 1.9 mS/cm at 1.0 bar to 1.77 mS/cm at 5.0 bar with feed conductivity of 2.08 mS/cm.

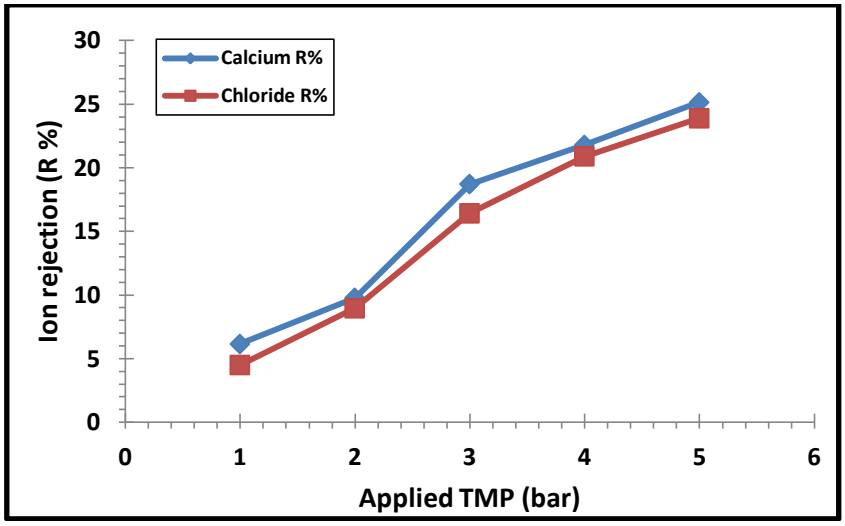

Figure 4.28: Calcium chloride rejection (0.001 M) as a function of applied TMP (bar).

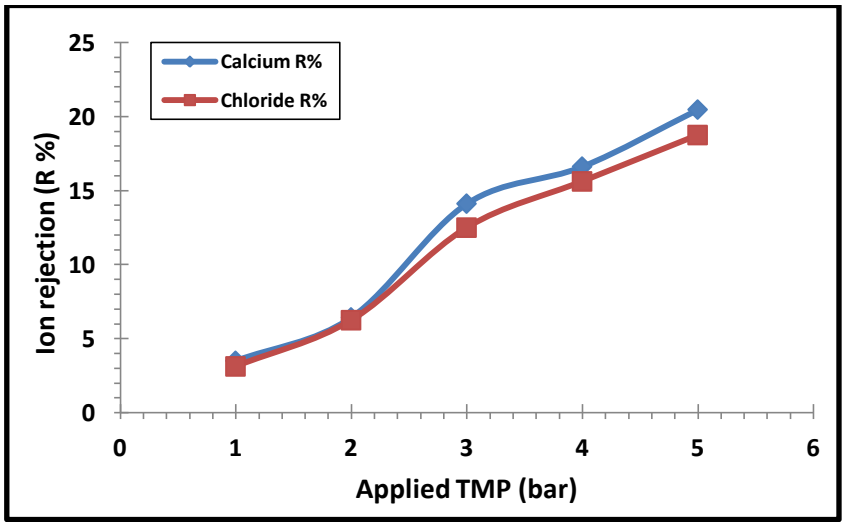

Figure 4.29: Calcium chloride rejection (0.005 M) as a function of applied TMP (bar).

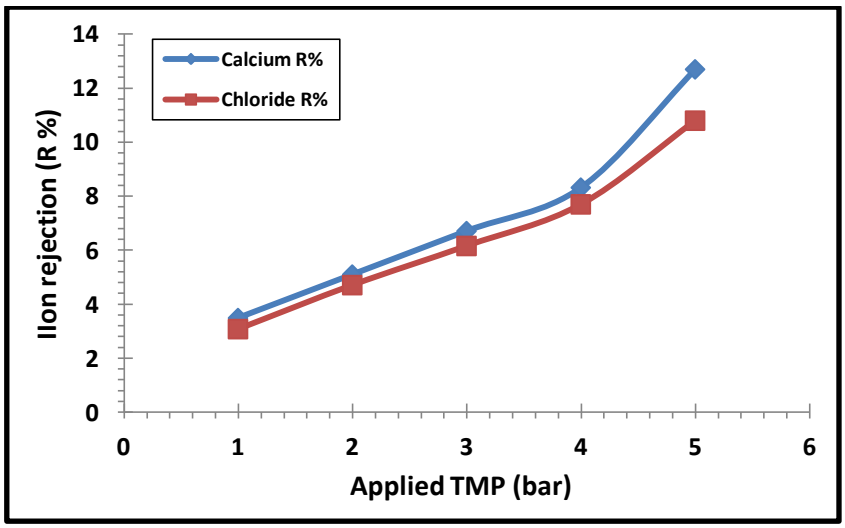

Figure 4.30: Calcium chloride rejection (0.01 M) as a function of applied TMP (bar).

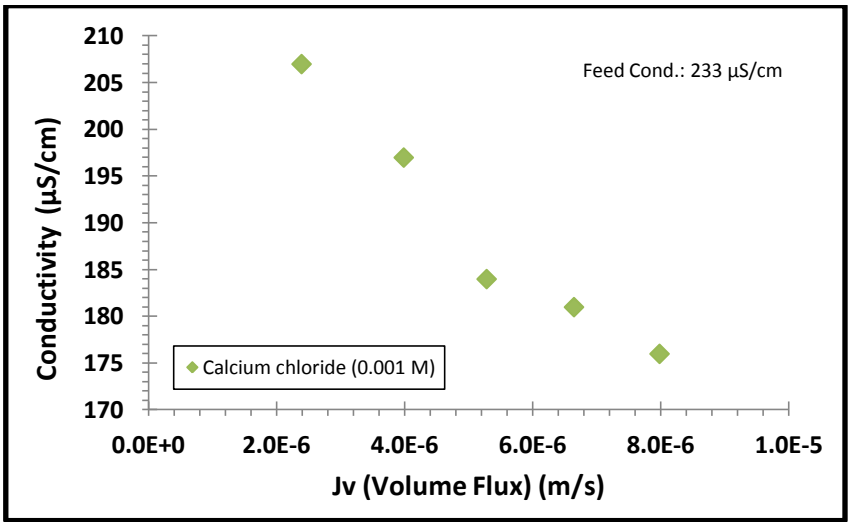

Figure 4.31: Permeate conductivity of $CaCl_2$ (0.001 M) vs. volume flux(m/s).

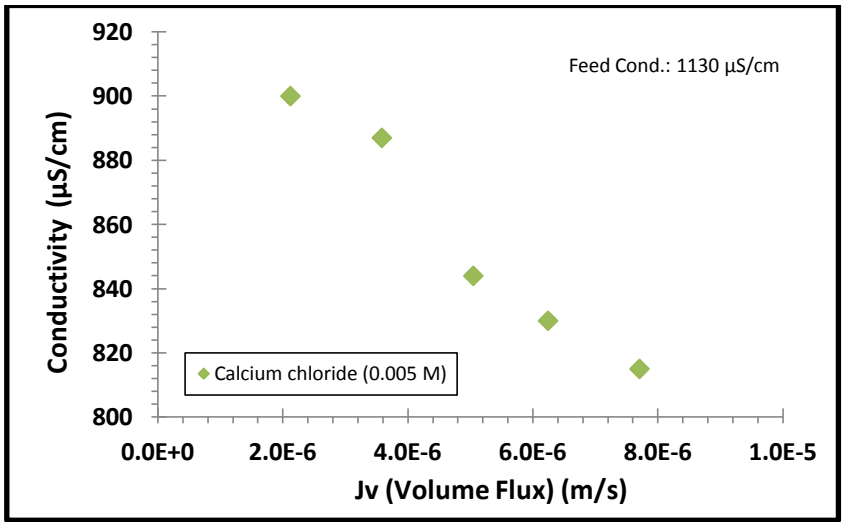

Figure 4.32: Permeate conductivity of $CaCl_2$ (0.005 M) vs. volume flux (m/s).

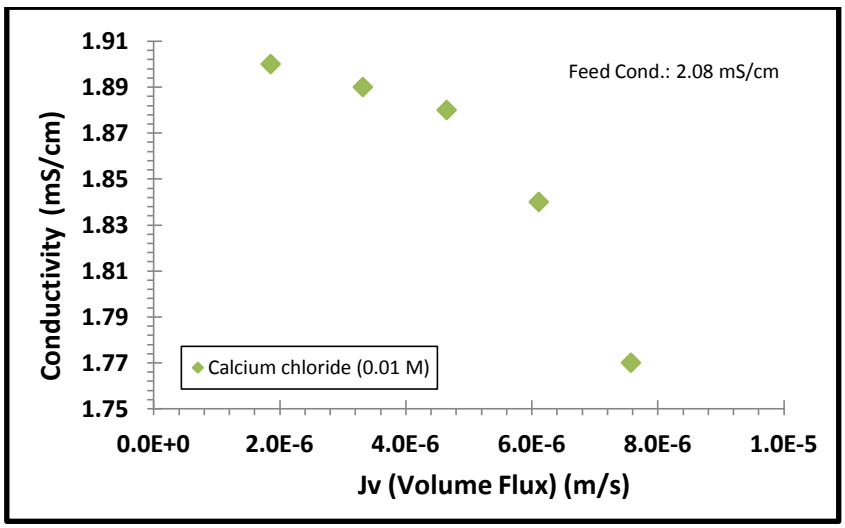

Figure 4.33: Permeate conductivity of $CaCl_2$ (0.01 M) vs. volume flux (m/s).

Figure 4.34 shows the rejection of calcium chloride solutes at 0.001, 0.005 and 0.01 M as a function of applied trans-membrane pressure. It can be seen from this figure that for each concentration used there was a gradual rise in the rejection of $CaCl_2$ salt linked to the increased applied trans-membrane pressure. At the applied trans-membrane pressure of 5.0 bar, the rejection of calcium chloride salt was 24.54%, 19.64% and 11.75% for the feed concentration of 0.001, 0.005 and 0.01 M respectively.

On the other hand, at the lowest applied trans-membrane pressure of 1.0 bar, the rejection of calcium chloride salts was 5.34%, 3.33% and 3.03% for $CaCl_2$ feed concentration of 0.001, 0.005 and 0.01 M respectively.

Figure (4.35) shows the permeate volume flux of calcium chloride at 0.001, 0.005 and 0.01 M as a function of applied trans-membrane pressure.

It can be seen from Figure (4.35) that there is a steadily increase of permeate volume flux of calcium chloride salts solutions linked to the increased applied trans-membrane pressure. For each $CaCl_2$ salt concentration, there was a slight change in permeate volume flux as a function of the applied trans-membrane pressure. At the applied trans-membrane pressure of 5.0 bar, permeates volume flux of calcium chloride salt were 7.99×10^{-6}, 7.71×10^{-6} and 7.58×10^{-6} m/s for feed concentration of 0.001, 0.005 and 0.01 M respectively.

While at the lowest applied trans-membrane pressure of 1.0 bar, permeates volume flux of calcium chloride salt were 2.39×10^{-6}, 2.13×10^{-6} and 1.86×10^{-6} m/s for feed concentration of 0.001, 0.005 and 0.01 M respectively.

Based on the measured $CaCl_2$ permeate volume flux and for each used calcium chloride concentration, it can be seen that the permeate volume flux was increased as the applied trans-membrane pressure increased, whereas the permeate flux was decreased with the increased feed concentration.

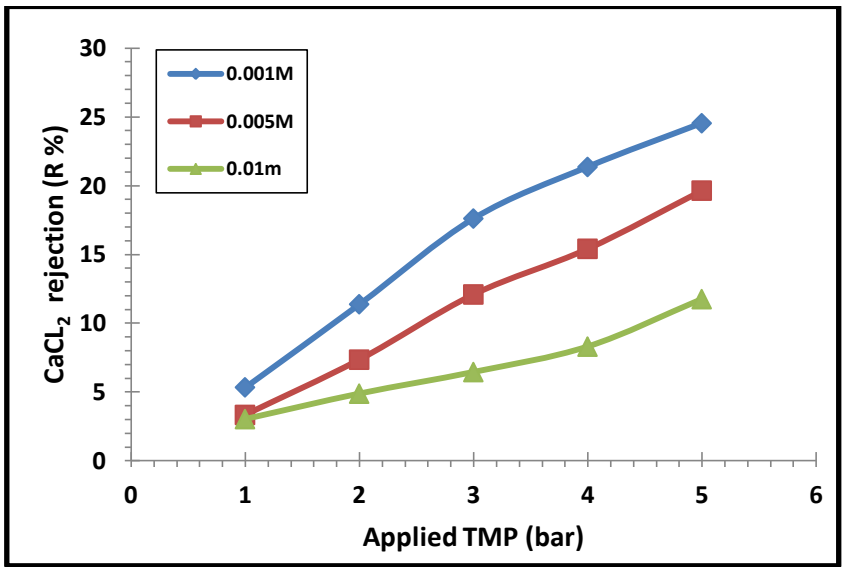

Figure 4.34: Rejection of $CaCl_2$ at (0.001, 0.005 and 0.01M) vs. applied TMP (bar).

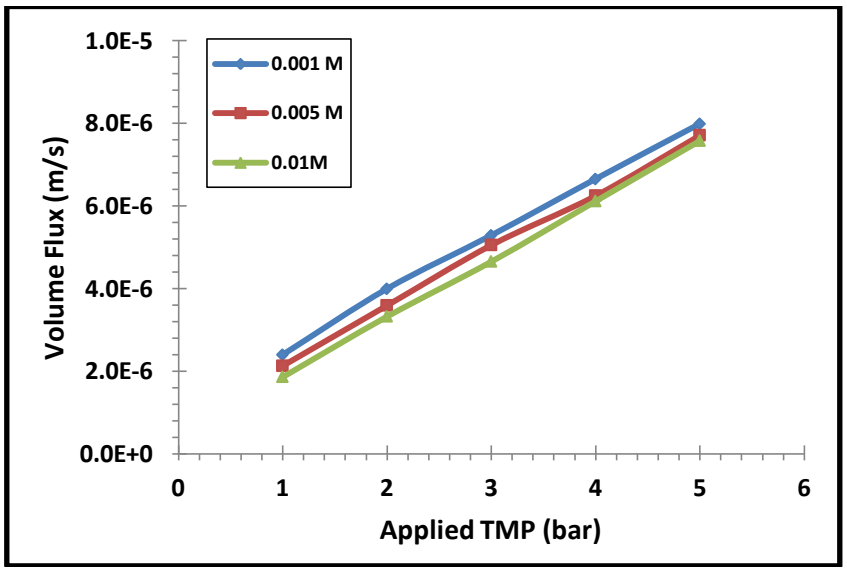

Figure 4.35: Permeate volume flux of $CaCl_2$ at (0.001, 0.005 and 0.01 M) vs. applied TMP (bar).

4.3.4 Rejection of calcium sulphate

The rejection of calcium sulphate as a single electrolyte in the 1nm tubular ceramic TiO_2 nanofiltration membrane as a function of applied trans-membrane pressure with emphasis on the effect of feed concentration has been studied experimentally.

Figures (4.36, 4.37 and 4.38) show the rejection of calcium sulphate at 0.001, 0.005 and 0.01 M respectively as a function of applied trans-membrane pressure. It can be seen from these figures that the retentions of calcium ions (Ca^{+2}) and sulphate ions (SO_4^{-2}) were steadily increased as the applied trans-membrane pressure increased.

In all these three Figures, the rejection of sulphate ions (SO_4^{-2}) was slightly higher than the rejection of calcium ions (Ca^{+2}). At the highest applied trans-membrane pressure (5.0 bar), the rejection of calcium ions was 41.23%, 31.58% and 23.42% for $CaSO_4$ feed concentration of 0.001, 0.005 and 0.01 M respectively. While the rejection of sulphate ions (SO_4^{-2}) at same concentrations was 44%, 34.1% and 25.5% respectively.

At the lowest applied trans-membrane pressure of 1.0 bar, the rejection of calcium ions was 9.65%, 6.67% and 5.16% for $CaSO_4$ feed concentration of 0.001, 0.005 and 0.01 M respectively. While, the rejection of sulphate ions at same concentrations was 11%, 7.7% and 5.89% respectively.

From Figures (4.36, 4.37 and 4.38), it can be seen that the rejection of $CaSO_4$ salt solutions by the TiO_2 NF membrane was decreased with the growth of salt concentration.

Figures (4.39, 4.40 and 4.41) show the conductivity of calcium sulphate permeates at 0.001, 0.005 and 0.01 M respectively as a function of applied pressure. From these figures it can be shown that the conductivity of $CaSO_4$ permeate for each concentration was decreased with the increased applied trans-membrane pressure.

The permeate conductivity of 0.001 M $CaSO_4$ was remarkably decreased from 221 $\mu S/cm$ at 1.0 bar to 169 $\mu S/cm$ at 5.0 bar while the feed conductivity was 248 $\mu S/cm$. The same behaviour was noticed for two other concentrations in which the permeate conductivity of 0.005 M $CaSO_4$ decreased from 878 $\mu S/cm$ at 1.0 bar to 755 $\mu S/cm$ at 5.0 bar while the feed conductivity was 936 $\mu S/cm$, whereas, for 0.01 M $CaSO_4$ the permeate conductivity decreased from 1.62 mS/cm at 1.0 bar to 1.42 mS/cm at 5.0 bar with feed conductivity of 1.65 mS/cm.

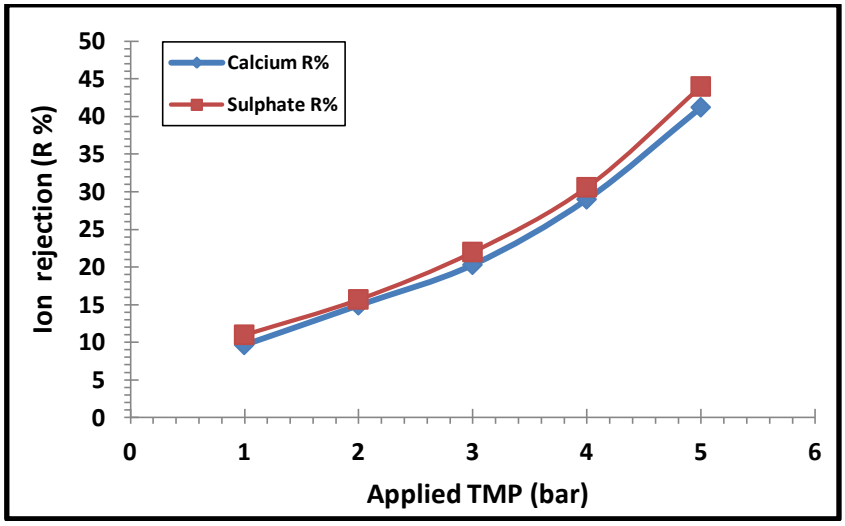

Figure 4.36: Calcium sulphate rejection (0.001 M) as a function of applied TMP (bar).

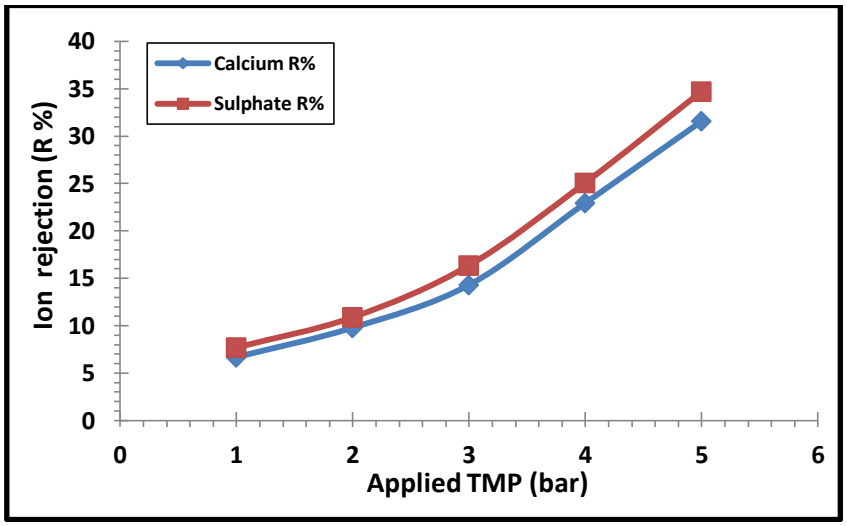

Figure 4.37: Calcium sulphate rejection (0.005 M) as a function of applied TMP (bar).

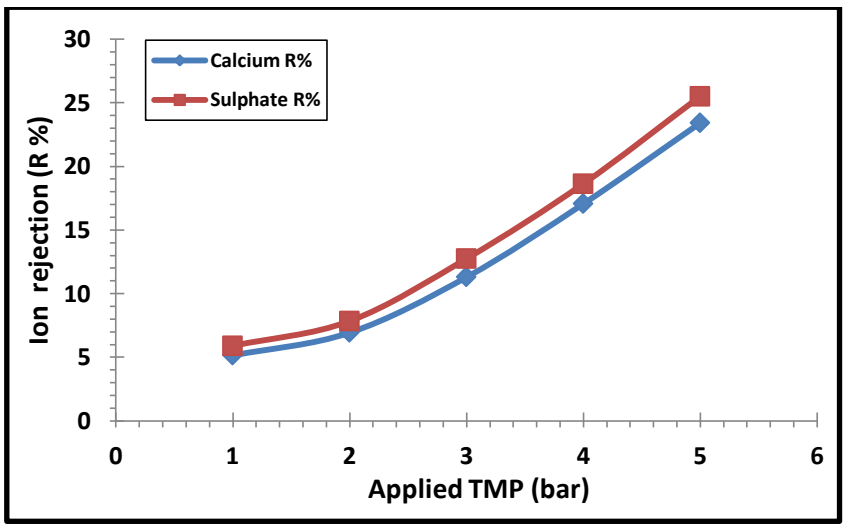

Figure 4.38: Calcium sulphate rejection (0.01 M) as a function of applied TMP (bar).

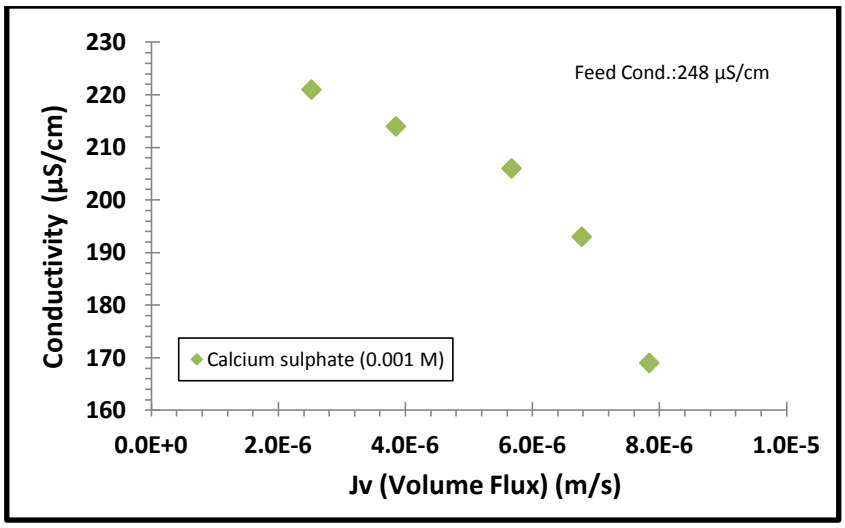

Figure 4.39: Permeate conductivity of $CaSO_4$ (0.001 M) vs. volume flux (m/s).

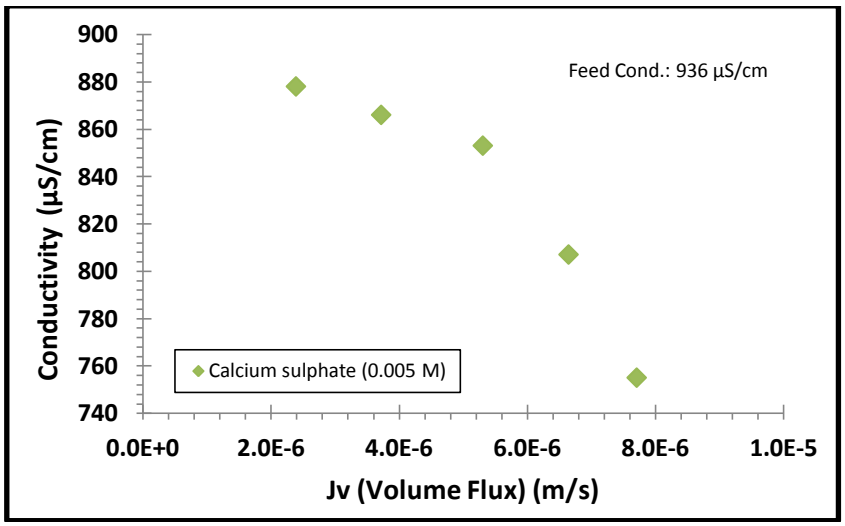

Figure 4.40: Permeate conductivity of $CaSO_4$ (0.005 M) vs. volume flux (m/s).

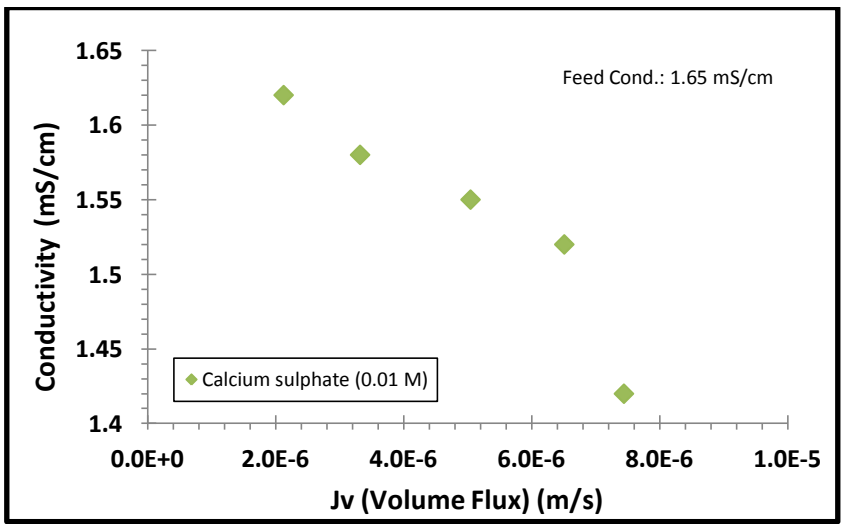

Figure 4.41: Permeate conductivity of $CaSO_4$ (0.01 M) vs. volume flux (m/s).

Figure 4.42 shows the rejection of calcium sulphate solutes at 0.001, 0.005 and 0.01 M as a function of applied trans-membrane pressure. It can be seen from this figure that for each of the concentrations used there was a steadily growth in the rejection of $CaSO_4$ salt linked to the increased applied trans-membrane pressure. At the applied trans-membrane pressure of 5.0 bars, the rejection of calcium sulphate salt was 43.13%, 33.24% and 24.88% for the feed concentration of 0.001, 0.005 and 0.01 M respectively.

On the other hand, at the lowest applied trans-membrane pressure of 1.0 bar, the rejection of calcium sulphate salts was 10.51%, 7.38% and 5.65% for $CaSO_4$ feed concentration of 0.001, 0.005 and 0.01 M respectively.

Figure (4.43) shows the permeate volume flux of calcium sulphate at 0.001, 0.005 and 0.01 M as a function of applied trans-membrane pressure.

In this figure the permeate volume flux of calcium sulphate salt solution for each concentration was gradually increased linked to the increased applied trans-membrane pressure. There was a slight change in $CaSO_4$ permeate volume flux as a function of the applied trans-membrane pressure. At the applied trans-membrane pressure of 5.0 bars, permeates volume flux of calcium sulphate salt were 7.85×10^{-6}, 7.71×10^{-6} and 7.45×10^{-6} m/s for feed concentration of 0.001, 0.005 and 0.01 M respectively.

While at the lowest applied trans-membrane pressure of 1.0 bar, permeates volume flux of calcium sulphate salt were 2.53×10^{-6}, 2.39×10^{-6} and 2.13×10^{-6} m/s for feed concentration of 0.001, 0.005 and 0.01M respectively.

According to the measured $CaSO_4$ permeate volume flux and for each used calcium sulphate concentration, it can be seen that the permeate volume flux was increased as the applied trans-membrane pressure increased, whereas the permeate flux was decreased with the increased feed concentration.

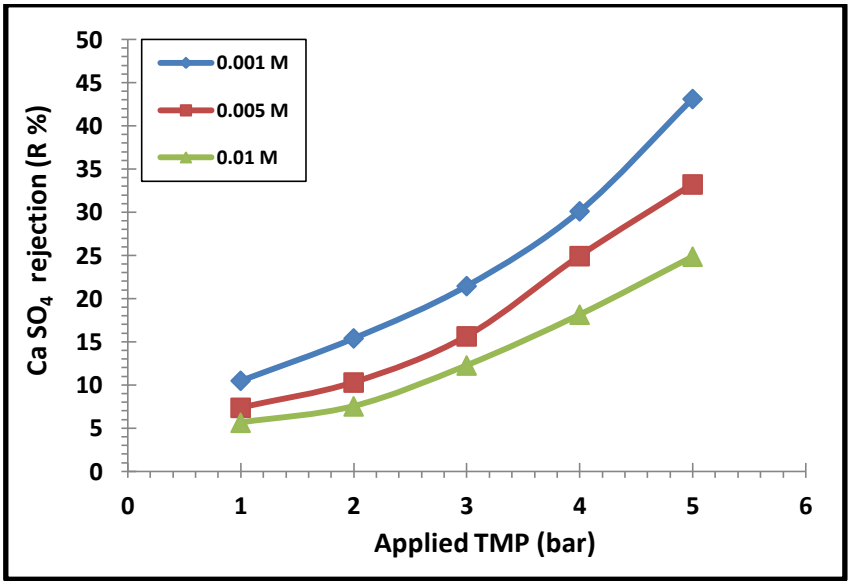

Figure 4.42: Rejection of $CaSO_4$ at (0.001, 0.005 and 0.01M) vs. applied TMP (bar).

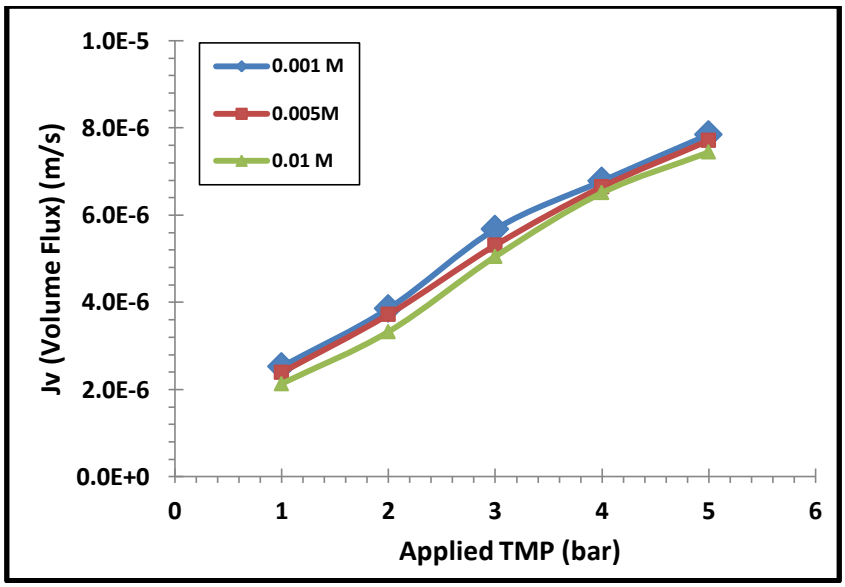

Figure 4.43: Permeate volume flux of $CaSO_4$ at (0.001, 0.005 and 0.01M) vs. applied TMP (bar).

Figure (4.44) shows the rejections of calcium sulphate, sodium sulphate, calcium chloride, and sodium chloride solutes in 1nm tubular ceramic TiO_2 NF membrane (as a function of feed concentration of 0.001, 0.005, and 0.01 M at applied trans-membrane pressure of 5.0 bar).

Salts retention measurements showed the following salt rejection sequence:

$R\ (CaSO_4) > R\ (Na_2SO_4) > R\ (CaCl_2) > R\ (NaCl)$.

The rejection for bivalent ions was the highest, whereas that of monovalent ions was the lowest.

From Figure (4.44) it can be concluded that the rejections (of the selected salts used in the present work) were decreased as the salts ionic strength increased.

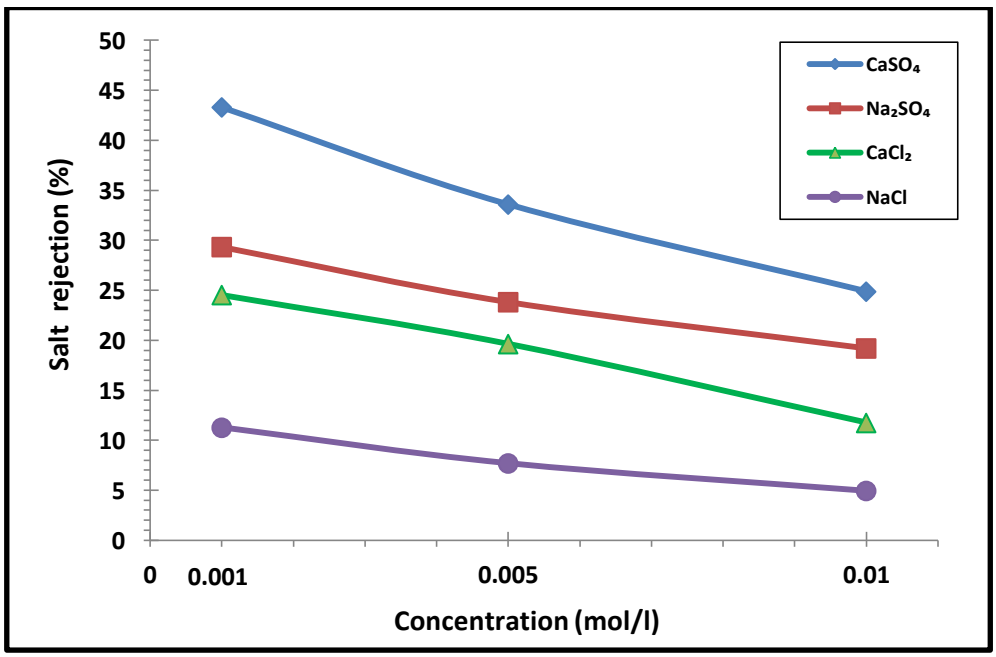

Figure 4.44: The rejections of $CaSO_4$, Na_2SO_4, $CaCl_2$ and NaCl solutes in TiO_2 NF membrane as a function of feed concentration at applied pressure of 5.0 bars.

4.3.5 Rejection of calcium sulphate at saturation concentration

Up to now all the previous established rejection experiments of calcium sulphate at 0.001, 0.005 and 0.01 M were conducted below the saturation concentration of $CaSO_4$ (as gypsum). This section represents an attempt to establish the rejection of calcium sulphate at saturation concentration.

In order to determine the saturation concentration of a $CaSO_4$ solution, the present work suggested the concentration of (0.015 M) calcium sulphate as a suspension solution since this concentration is definitely above the saturation concentration of calcium sulphate (as a gypsum) [132], [133].

This suspension solution was prepared in a 10 litre glass storage vessel where the analytical grade of $(CaSO_4.2H_2O)$ was dissolved in deionised water. The calcium sulphate suspension was stirred gently with a magnetic stirrer at room temperature for 7 days to establish equilibrium and to be sure that the maximum solubility of $CaSO_4$ solute was reached. During this period, the glass storage vessel was covered tightly to prevent the water from evaporating. Trace amount of insoluble $CaSO_4$ where observed as a sediment in the bottom of the glass vessel after this period.

The removal of insoluble calcium sulphate suspended particles from the solute was conducted according to the following procedure, after turning off the magnetic stirrer, the solute was left overnight. The insoluble calcium sulphate particles had been precipitated as sediments. A small metering pump had been used to transfer the $CaSO_4$ solute from the clear water area. Then, all the solute had been filtered by using a fine paper filter (Whatman™, type 42). In the mean time, several samples had been taken before and after the filtration process.

The present work estimated the saturation concentration of calcium sulphate salt as a gypsum (after filtration) to be around 2.35 g/ l at average temperature of 18 ℃ which is nearly the same result determined by the American Chemical Society (2006) [133] for saturation concentration of dihydrate calcium sulphate (2.4 g/l at 20 ℃).

After the preparation of the calcium sulphate solution, the same previous rejection experiment procedure was used as a function of applied pressure (up to 5.0 bar).

Figure 4.45 shows the rejection of the prepared calcium sulphate (0.015 M after filtration) as a function of applied trans-membrane pressure. It can be seen from this figure that the retentions of calcium ions (Ca^{+2}) and sulphate ions (SO_4^{-2}) were steadily increased as the applied trans-membrane pressure increased.

Also, the rejection of sulphate ions (SO_4^{-2}) was slightly higher than the rejection of calcium ions (Ca^{+2}) especially for applied trans-membrane pressure below 2.0 bar showing the same previous behaviour for the rejections experiments that were conducted below the saturation concentration.

At the highest applied trans-membrane pressure of 5.0 bar, the rejection of calcium ions was 16.91%, while the rejection of sulphate ions (SO_4^{-2}) at the same concentration was 18.55%. Whereas at the lowest applied trans-membrane pressure of 1.0 bar, the rejection of calcium ions was 4.07%, while the rejection of sulphate ions (SO_4^{-2}) at the same concentration was 4.84%.

From this figure, it can be concluded that the ionic retention of $CaSO_4$ solute was the lowest compared to $CaSO_4$ rejection results of 0.001, 0.005 and 0.01 M.

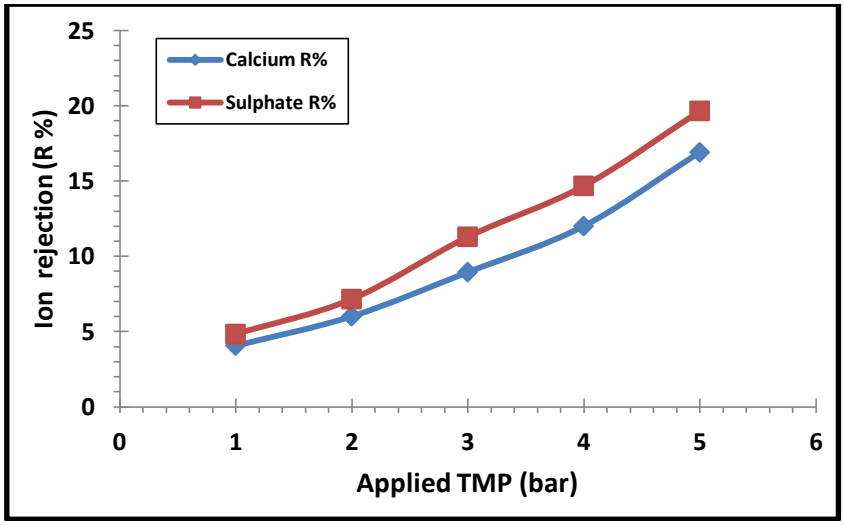

Figure 4.45: Calcium sulphate rejection (0.015 M after filtration) as a function of applied TMP (bar).

Figure 4.46 shows the rejection of the prepared calcium sulphate 0.015 M (after filtration) as a function of permeate flux and applied trans-membrane pressure.

In this figure the permeate volume flux of the calcium sulphate salt solution was steadily increased linked to the increased applied pressure and salt rejection. At the applied trans-membrane pressure of 5.0 bar, the permeate volume flux of calcium sulphate salt was 6.91×10^{-6} m/s with salt retention (R %) of 18.1% whereas at the lowest applied TMP of 1.0 bar; the permeate volume flux of calcium sulphate salt was 1.86×10^{-6} m/s with salt retention (R %) of 4.49%. It was found that the salt rejection and permeate volume flux of the prepared $CaSO_4$ solute was the lowest compared to the $CaSO_4$ rejection results of 0.001, 0.005 and 0.01 M.

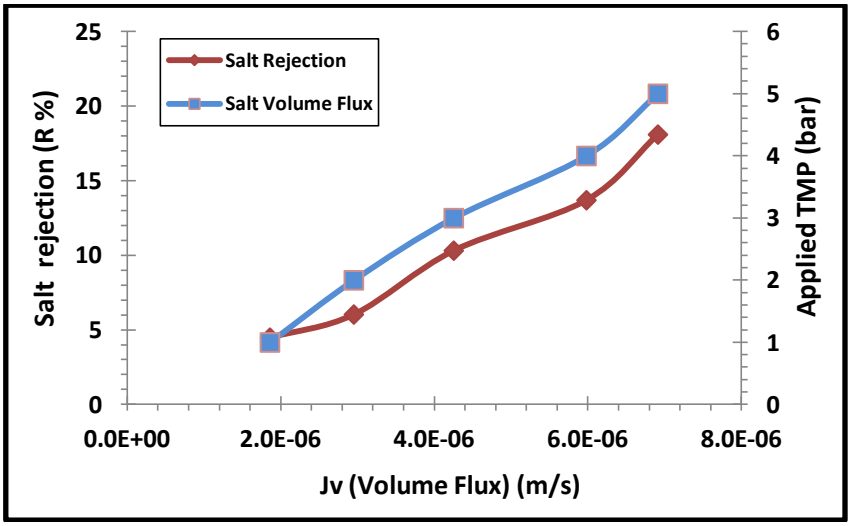

Figure 4.46: Calcium sulphate salt rejection (0.015 M after filtration) as a function of permeates volume flux and applied TMP (bar).

Figure 4.47 shows the rejection (*R* %) of calcium sulphate salt below the saturation concentration at 0.001, 0.005, and 0.01 M and at saturation concentration (0.015 M /after filtration) as a function of applied pressure.

From this figure it can be seen that the rejection of calcium sulphate salts in the TiO_2 NF ceramic membrane was decreased as salt concentration increased. The rejection behaviour of the $CaSO_4$ solution (at saturation concentration) was the same as the rejection of $CaSO_4$ solutions (below saturation concentration).

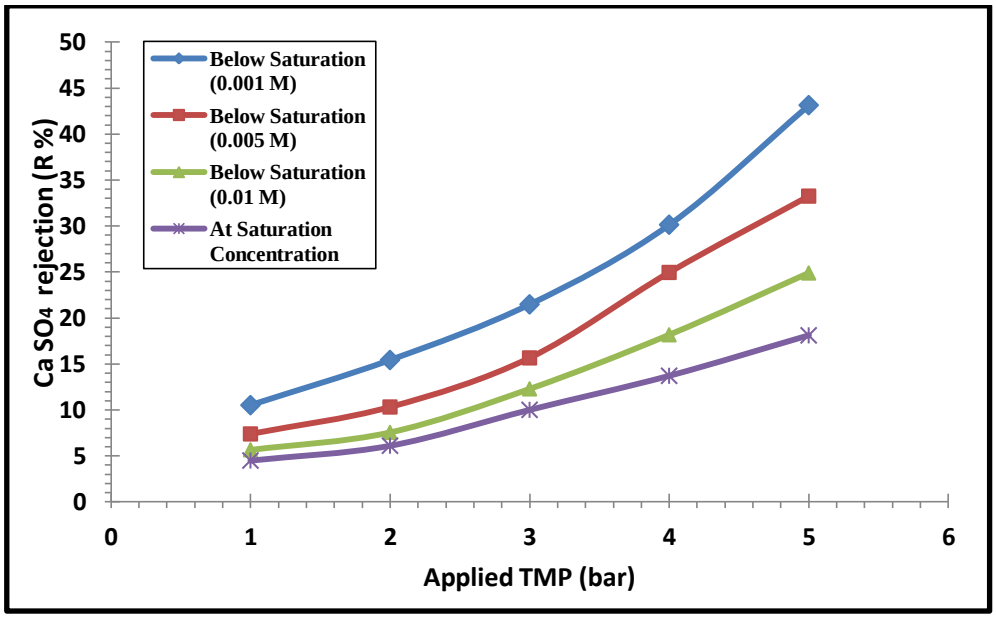

Figure 4.47: The rejection of $CaSO_4$ (*R* %) below (0.001, 0005, 0.01 M) and at saturation concentration as a function of applied TMP (bar).

4.3.6 Discussion of rejection experiments

There are three main effects related to the transport of solutes in nanofiltration membranes, which are:

- Convection effect (due to applied pressure inside the membrane).
- Diffusion effect (due to the concentration gradient across the membrane).
- Charge effect (due to electrostatic repulsions between the charged membrane and the charged ionic materials).

Most ceramic nanofiltration membranes are either negatively or positively charged, thus, when brought in contact with an aqueous solution acquired an electrical charge as a result of the dissociation of functional groups or adsorption of charged species from the solution into membrane pores.

In the case of nanofiltration membranes where the pores are very small, the electrostatic infraction between aqueous solution ions and membrane material can play a very important role on the electrolyte transport through membrane pores.

The combination of very small pore diameters (less than 2 nm for NF membranes) with electrically charged membrane materials indicate that the separation mechanisms of NF membranes involve both steric effect (size exclusion) and electrical effect (Donnan exclusion). This combination allows NF membranes to be effective in salt retention.

The transport mechanism of an uncharged solution is simple and well understood. The rejection of uncharged solutes are generally governed by the combination of a sieving effect and fractional forces, a convection effect due to pressure difference, and by a diffusion effect as a result of the concentration gradient across the membrane. Sieving (or steric hindrance) is a function of size exclusion where the solutes with a large molecular weight cut off (MWCO) will be retained.

The transport mechanism of charged solutions is mainly controlled by charge exclusion (Donnan effect). The Donnan effect depends mainly on the electrolyte valance type. The phenomenon involves the interaction between the rejection of co-ions and the fixed membrane charges attached the membrane matrix. The Donnan exclusion effect increases with the increasing of the co-ions charge and decreases with the increasing of counter-ions charge [51], [130].

The separation mechanism in NF membranes is normally explained in terms of charge and (or) size effect [134], [135].

The well-known Donnan exclusion mechanism was often used to give a possible explanation of solute ions rejection. According to Scheap et al. [47], the Donnan exclusion can be interpreted based on the potential difference at the membrane interface which can be described as follows:

When a charged membrane is in contact with a salt solution; equilibrium occurs between the membrane and solution as a result of the presence of a fixed membrane charge.

The ionic concentrations in the membrane and that in the solution are not equal. The counter-ions concentration (opposite sign of charge to the fixed charge of the membrane) is higher in the membrane phase than in the bulk solutions, whereas the co- ions concentration (same sign of charge to the fixed charge of the membrane) is lower in the membrane phase. As a result, a potential difference at the interface is created to counteract the transport of counter-ions to the solution phase and the co-ions to the membrane phase.

When the pressure is applied across the membrane, the water is transported through the membrane and the effect of Donnan exclusion is then to repel the co-ions from the membrane as a result of electroneutrality requirements. Based on the Donnan exclusion mechanism, the increment of salt concentration would lead to a decrease in the rejection because the counter-ions might shield the membrane charge.

On the other hand, reduction of the salt concentration would lead to an increase in the rejection because the membrane charge in this case is more effective.

Among many factors that might have an effect on the ions rejection in charged ceramic NF membranes, the pH of the solution can play an important role on salts rejection as pH could have an effect on the change of membrane charge type based on the iso-electric point of each membrane.

Also, the adsorption of solute particles that might occur inside membrane pores or on membrane surface should have an effect on salts rejection. As salt ionic strength increases, the effect of solute adsorption by the membrane increases which might have a negative effect on the rejection due to the increase in the possibility of membrane fouling.

The rejections behaviour of Na_2SO_4, $NaCl$, $CaCl_2$ and $CaSO_4$ as single salts for three different concentrations of 0.001, 0.005 and 0.01 M in a commercial ceramic TiO_2 NF membrane will be discussed based on the above transport mechanisms.

Table (4.2) shows the bare (pulling) ion radius and hydrate radius (in nm) of the hydrated ions (sodium, chloride, calcium, and sulphate) [48], [55], [136], [137].

Table 4.2: Bare ion radius (nm) and hydrate radius of sodium, chloride, calcium, and sulphate.

Ions	Bare Ion radius (nm)	Hydrate radius (nm)
Na^{+1}	**0.095**	**0.36**
Cl^{-1}	**0.181**	**0.33**
Ca^{+2}	**0.099**	**0.41**
SO_4^{-2}	**0.290**	**0.38**

In order to find out the possible effects of a sieving mechanism (steric hindrance effect) on the ions rejection of the four salts that have been used in this work, the bare ions radius and hydrate radius in (nm) for sodium, chloride, calcium and sulphate ions are presented in Table 4.2.

The bare ion radius (or pulling radius) can be defined as the bare ion crystal radius. According to Hussain et al. [137], this parameter has a strong influence on the diffusion properties of ions which significantly affect the ion rejections while the hydrated radius (or effective radius) represents the radius of an ion in water which is larger than its real crystal lattice radius (as shown in Table 4.2) because smaller ions are more hydrated so they tend to have larger hydrated radii than larger ions [48].

The estimated membrane effective pore radius (r_p) for the present 1 nm ceramic TiO_2 nanofiltration membrane based on the Donnan steric pore partitioning model (DSPM) was 0.68 nm (see section 6.2 of the present study).

By comparing the data presented in Table 4.2 for both the ionic radius and the hydrated radius of the four ions used in the present wok with the estimated (r_p) of the present Titania membrane, it can be seen that the estimated membrane pore radius is still larger than the ionic radii and the hydrated radius of the four hydrated ions.

It can be seen from Table 4.2 that the hydrated ionic radii of the sodium ion was (0.36 nm) and sulphate ion was (0.38 nm), while the estimated effective pore radius (r_p) of the present work's ceramic TiO_2 NF membrane was 0.68 nm. Thus for both sodium and sulphate, the ratio of hydrated radius to the estimated pore radius (r_p) was about 0.55.

This means that the convective ion transport through the membrane pore can be hindered for both sodium and sulphate ions and the hindered effect of sulphate ion is higher than sodium since the ratio of hydrated radius to (r_p) for (SO_4^{-2}) ion is closer to 1.0 (where the ions are totally hindered) than that of (Na^{+1}) ion.

Based on the ions hydrated radius it can be concluded that the sieving mechanism could have an effect on the rejection of both sodium and sulphate ions.

On the other hand because of the bare ion radius, this can play a less important role on the retention of sodium and sulphate ions as a result of its small pore radius compared to the hydrated radius (see Table 4.2). Here, it can also be noticed that the hindered possibility for sulphate ions is also higher than that of sodium ions since the bare ionic radius of sulphate (0.29 nm) is higher than that of sodium (0.095 nm).

The rejection of a single Na_2SO_4 solution at concentration of 0.001, 0.005 and 0.01 M in a TiO_2 NF membrane shows that the rejection of sulphate ions (SO_4^{-2}) was higher than that of sodium ions (Na^{+1}). This behaviour can be explained based on the Donnan exclusion theory as a result of the electrostatic interaction (repulsion and attraction) between the electrolyte ions and the charge of the membrane.

As shown previously, the present TiO_2 NF membrane possessed a weak negative charge for pH above than 4, hence the SO_4^{-2} ions represent co-ions and Na^{+1} ions represent the counter-ions relative to the charge sign of the TiO_2 membrane.

The repulsion of co-ions and the membrane is the control factor of the rejection of Na_2SO_4 by the TiO_2 membrane; the higher the valance of co-ions, the stronger the repletion of co-ions and the TiO_2 membrane and the higher the rejection to the electrolyte.

The lower rejection of cation Na^{+1} than that of anion SO_4^{-2} can be explained based on the definition of the electro-neutrality condition on both sides of the membrane. The electro-neutrality means for every removed anion, one cation must be removed. Since sulphate ion (SO_4^{-2}) has a double charge compared to that of sodium ions (Na^{+1}) then, in order to achieve the electro-neutrality condition a lesser amount of SO_4^{-2} ion is needed to pass through the membrane compared to that of Na^{+1} ion. This reason can explain the relatively low rejection of both ions.

In addition, the possible formation of ion complex due to the presence of SO_4^{-2} ion in water can lead to the formation of more anions such as HSO_4^{-1} which can result from the interacting of SO_4^{-2} ions with H^{+1} ions from dissociated water.

This could increase the repulsion between this new formed anion and the negatively charged TiO_2 membrane thus; more sulphate ion would be rejected based on the Donnan effect mechanism whereas more sodium ions had to pass through the membrane to achieve the electro-neutrality condition.

Figures (4.12, 4.13 and 4.14) show that the rejection of Na_2SO_4 salt solutions by the TiO_2 NF membrane was decreased with the growth of salt concentration.

According to the interpretation of Pontalier et.al [138] and Wang et.al [139] and based on the Donnan exclusion model, the repulsion and attraction effects are reduced with the increased feed electrolyte concentrations. So, the electrostatic effect is the major factor involved at low salt concentrations, whereas at high salt concentrations the steric-hindrance effect is the major factor that governs the rejection process. The membrane charge will be extensively shielded which can lead to a reduction in the effective membrane charge and consequently the retention was decreased.

Also, the increasing of the electrolyte concentration would encompass the thickness of the electrical double layers at the interface of the membrane and that of the bulk solution, which can lead to destabilized conditions around the membrane. Therefore, the charge effect could become less effective with more salts permeating through the membrane. As a result, the rejection rate for the ions was then reduced.

According to Figure (4.19), it can be seen that the permeate volume flux for the three different Na_2SO_4 concentrations was increased as the applied pressure increased while the permeate flux was decreased with the increased feed concentration.

This behaviour can be explained based on the integral form of Darcy's law in which the convective flux through the membrane can be defined as the driving forces (applied pressure) divided by the multiplication of the viscosity with total resistance.

At the beginning of the filtration process, the term total resistance can be referred to the membrane hydraulic resistance which is mainly affected by the adsorption that could occur on the surface or at the membrane pores and the concentration polarisation resistance in which the solute concentration in the vicinity of the membrane surface is higher than that in the bulk.

Increasing the solute concentration will affect both the adsorption of the membrane and the membrane concentration polarisation which can lead to flux decline or decreases of the permeation rate.

The rejection of the single NaCl solution in the TiO_2 NF membrane at concentrations of 0.001, 0.005 and 0.01 M, shows that the rejection of chloride ions (Cl^{-1}) is higher than sodium ions (Na^{+1}).

This behaviour can also be explained based on the Donnan exclusion theory as a result of the electrostatic repulsion and attraction between the electrolyte ions and the negatively charged TiO_2 membrane used in the present work.

The chloride ions represent the co-ions whereas the sodium ions represent the counter-ions relative to the charge sign of the Titania membrane.

The low rejection of both sodium Na^{+1} and chloride Cl^{-1} ions can be interpreted based on the electro-neutrality condition across both membrane sides. Both ions have to diffuse through the membrane to neutralize the charge at the permeate side.

Furthermore, it can be seen from Table 4.2 that the bare ionic radius of (Na^{+1}) and (Cl^{-1}) were still lower than the estimated effective membrane pore radius for the 1 nm Titania membrane which could indicate that the sieving (or size exclusion) mechanism is insignificant in the rejection of sodium chloride solutes. This may give another possible reason why the rejection of NaCl solutions was low.

On the other hand, it can be seen from Table 4.2 that the hydrated ionic radii of sodium ion was (0.36 nm) and chloride ion was (0.33 nm) while the estimated effective pore radius (r_p) of the present work's ceramic TiO_2 NF membrane was 0.68 nm, thus for both sodium and chloride ions; the ratio of hydrated radius to the estimated pore radius (r_p) were 0.53 and 0.48 respectively.

Based on the hydrated radii of sodium and chloride ions, it can be indicated that the convective ion transport through the membrane pore can be hindered for both sodium and chloride ions and the hindered effect of sodium ion is higher than that of chloride ion since the ratio of hydrated radius to (r_p) for Na^{+1} ion is closer to 1.0 (where the ions are totally hindered) than that of Cl^{-1} ion. In this case, it can be concluded that the sieving mechanism (or size exclusion) could affect the rejections of both sodium and chloride ions.

By comparing the rejection behaviour of (Na^{+1}) ions in both the sodium sulphate solutions and sodium chloride solutions for all the three selected concentrations, it can be concluded that the rejection of sodium ions in Na_2SO_4 solutes was higher than that in NaCl solutes. In other words, the rejection of Na^{+1} was significantly higher in the solutions containing sulphate ions than that containing chloride ions.

This rejection behaviour of Na^{+1} in Na_2SO_4 and NaCl solutions can be explained based on the fact that the rejection of the sodium ion has enhanced with the presence of a bivalent anion which can be interpreted by the Donnan exclusion theory. Since the membrane is negatively charged, thus; the anions are excluded. As a result, the cations are also rejected, together with the anions in order to achieve the electro-neutrality condition at both permeate and retentate sides.

The rejection of sodium ions has enhanced with the more negative anion since sulphate ion (SO_4^{-2}) has a double charge when compared to that of a mono valance chloride ion (Cl^{-1}) which can lead to an increase in the electrostatic repletion by the Titania membrane.

The obtained rejection results of Na^{+1} as a common ion in NaCl and Na_2SO_4 solutions in the present work are in agreement with other researcher's results [139], [140], [141].

The rejection of single $CaCl_2$ solutions in the TiO_2 NF membrane at concentrations of 0.001, 0.005 and 0.01 M, shows that the rejection of calcium ions (Ca^{+2}) is higher than that of chloride ions (Cl^{-1}).

This behaviour cannot be explained by the Donnan exclusion mechanism and electrostatic attraction theory because in this case the calcium ions (counter-ions) have an opposite sign from that of the negatively charged membrane, while the chloride ions (co-ions) have the same membrane charge, based on the definition of the Donnan effect. The rejection of the chloride ions should be higher than that of calcium ions which did not occur in the present set of the calcium chloride rejection experiments.

In the meantime, it can be seen from Table (4.2) that the bare ion radius of both calcium (0.099 nm) and chloride (0.181 nm) was noticeably lower than the estimated effective membrane pore radius of the present work's TiO_2 membrane (0.68 nm) which could give an indication that the sieving or size exclusion mechanism is not effective in this case.

But on the other hand, if the hydrated radius of ions were taken in consideration, then; it can be seen from Table (4.2) that the hydrated radius of the calcium ion (0.41 nm) is higher than any other hydrated radius of other ions used in the present work; whereas the hydrate radius of the chloride ion (0.33 nm) is lower than any other hydrated radius of other ions used in the present work.

So, based on the steric hindered pore model (SHP) [142], the steric hindrance effect

increases with increasing the ratio of the hydrated ionic radius to the effective membrane pore radius (r_p). For calcium ions, the ratio of hydrated radius to (r_p) was 0.6 whereas for chloride ions; the ratio of hydrated radius to (r_p) was 0.48.

This can indicate that the convective ion transport through the membrane pore can be hindered for both calcium and chloride ions and the hindered effect of calcium ions is higher than that of chloride. It can be seen that the ratio of hydrated radius to (r_p) for Ca^{+2} ion is much closer to 1.0 than that of Cl^{-1} ion.

This could indicate that the steric hindrance effect is very effective because in this case the ion size that transported by convection will be greatly hindered even without taking into consideration the effect of the membrane charge. This could give a possible interpretation to explain why the rejection of calcium is higher than that of chloride in the rejection of single calcium chloride solutions and the size exclusion mechanism can play an important role in the rejection behaviour.

The higher rejection of (Ca^{+2}) ions compared to that of (Cl^{-1}) ions for the electrolytes solutions of calcium chloride can be related to the Titania membrane's electro-neutrality condition, since the Ca^{+2} ion has a higher charge than that of Cl^{-1} ion, thus fewer amount of calcium ions have to permeate through the membrane to achieve the electro-neutrality conditions.

From the rejection results of calcium chloride solutions in the TiO_2 NF membrane, it can be concluded that the resulting membrane surface charge was not effective to establish the Donnan effect mechanism.

Also, it can be seen that the rejection of Ca^{+2} ion as a bivalent ion was higher than the rejection of the chloride ion as a monovalent ion which agreed with the basic specifications of ions rejection efficiencies in NF membranes (see Table 2.2).

The rejection of single calcium sulphate solutions in a TiO_2 NF membrane at concentrations of 0.001, 0.005 and 0.01 M shows that the rejection of sulphate ions (SO_4^{-2}) is higher than that of calcium ions (Ca^{+2}).

This behaviour can be explained based on the Donnan exclusion theory as a result of the electrostatic interaction between the electrolyte ions and the membrane charge.

The sulphate ions represent the co-ions whereas the calcium ions represent the counter-ions relative to the charge sign of the Titania membrane, thus the SO_4^{-2} ions were repelled by the negative membrane charge whereas the Ca^{+2} ions were attracted by the membrane (and can pass through it).

Beside this, the rejection of calcium sulphate can be affected by the formation of new charged complexation materials that could be resulted from the interaction of anionic and cationic species in the aqueous solution. It can be seen from the following equation that several ions would exist from dissolving the dihydrate $CaSO_4$ in deionised water.

$$CaSO_4.2H_2O + H_2O \longrightarrow Ca^{+2} + SO_4^{-2} + H^{+1} + OH^{-1}$$

For instance, the presence of SO_4^{-2} ions in water can lead to the formation of more anions such as HSO_4^{-1} which can result from the interacting of SO_4^{-2} ions with H^{+1} ions from water dissociation.

Other possible weak anions such as $CaSO_4^{-2}$, $CaOH(SO_4)^{-}$, $Ca(SO_4)OH^{-}$, and $Ca(SO_4)_2^{-2}$ can also be formed. The presence of these anions could increase the repulsion between this newly formed anion and the negatively charged TiO_2 membrane thus; more sulphate ions will be rejected based on the Donnan exclusion theory. On the other hand, weak cations such as $CaOH^{+}$ and $Ca_2SO_4^{+2}$ might also be formed.

The presence of these complexation ions depends mainly on the solute concentration, pH, and temperature. The rejection of such complex species depends mainly on the charge and radius of the formed ion [143], [120], [144], [145].

In order to interpret the high rejection of $CaSO_4$ solutions compared to other pervious salts that have been used in the present work, Schaep et al. [55] explained that the Donnan exclusion mechanism leads to prevention of the movement of counter-ions (Ca^{+2} ions) to the solution and the co-ions (SO_4^{-2} ions) to the membrane phase, thus in order to achieve the electro-neutrality conditions of the membrane, the rejection of the counter-ions is also required which is represented as the total salt rejection.

When comparing the rejection results of (SO_4^{-2}) ions as a common ion for each selected concentration in both calcium sulphate and sodium sulphate solutions, it was noticed that the rejection of (SO_4^{-2}) was higher in calcium sulphate solutions than that of sodium sulphate. This behaviour means that the rejection of (SO_4^{-2}) ions was enhanced by the presence of bivalent calcium ion (Ca^{+2}) which has a double charge when compared to that of monovalent sodium ions (Na^{+1}), which can lead to increasing the repletion and attraction by the Titania membrane.

Also, the rejection results of Ca^{+2} ions as a common ion in both calcium sulphate and calcium chloride solutions showed that the rejection of Ca^{+2} is higher in calcium

sulphate solutions than that of calcium chloride. From these results it can be concluded that the rejection of calcium ions enhanced with the presence of more negatively charged anion since sulphate ion (SO_4^{-2}) has a double charge when compared to that of the mono valance chloride ion (Cl^{-1}) which can increase the electrostatic interaction by the membrane.

From Table 4.2 it can be seen that the bare ionic radius of SO_4^{-2} (0.29 nm) is higher than that of Ca^{+2} (0.099 nm), which could give a possible interpretation to explain why the rejection of sulphate was slightly higher than calcium rejection. However this parameter was not effective since the ionic radii of both ions were still lower than the estimated effective membrane pore radius for the present work's ceramic Titania membrane (0.68 nm) which could indicate that the sieving mechanism related to the ionic radii was insignificant.

On the other hand, the effect of the hydrated ion size on its retention can be estimated based on the steric hindered pore model (SHP) [142]. The steric hindrance effect increases with the increasing ratio of the hydrated ionic radius to the effective membrane pore radius (r_p).

It can be seen from Table 4.2 that the hydrated ionic radii of calcium ion is (0.41 nm) and sulphate ion is (0.38 nm) while the estimated effective pore radius (r_p) of the present work's ceramic TiO_2 NF membrane was 0.68 nm, thus for calcium; the ratio of hydrated radius to (r_p) was about 0.6 whereas for sulphate; the ratio of hydrated radius to (r_p) was about 0.55.

This means that the convective ion transport through the membrane pore can be hindered for both calcium and sulphate ions and the hindered effect of calcium ion is higher than that of sulphate since the ratio of the hydrated radius to (r_p) for Ca^{+2} ions is much closer to 1.0 than that of SO_4^{-2} ions.

When the ratio of the hydrated pore radius to the effective pore radius is close to 1.0, this means that the steric hindrance effect is very effective because in this case the ion size that is transported by convection will be greatly hindered even without taking into consideration the effect of membrane charge.

In order to give a possible explanation for the rejection behaviour of $CaSO_4$ solution in the present work's ceramic TiO_2 NF membrane as a function of feed concentrations of 0.001, 0.005, and 0.01 M at applied pressure of 5.0 bars compared to the rejection of Na_2SO_4, $CaCl_2$, and NaCl solutes.

Figure 4.44 shows the following salts rejection sequence:

$R(CaSO_4) > R(Na_2SO_4) > R(CaCl_2) > R(NaCl)$.

Form the sequence; it can be concluded that the rejections for bivalent ions were the highest, whereas that of monovalent ions were the lowest.

Table (4.3) shows the bulk diffusion coefficients of selected ions used in this work.

Table 4.3: Bulk diffusion coefficients (m^2/s) of selected ions (used in present work).

Ion	$D_{bulk} \times 10^{-9}$ ($m^2.s^{-1}$)	Ref.
Na^{+1}	**1.33**	[12]
Cl^{-1}	**2.03**	[146]
Ca^{+2}	**0.92**	[147]
SO_4^{-2}	**1.06**	[148]

According to Schaep et al. [13], [14] the salt diffusion coefficient can be calculated from the bulk diffusion of the related ion based on the following formula:

$$D = (z_+ - z_-).D_{bulk^+}.D_{bulk^-}/(z_+.D_{bulk^+} - z_-.D_{bulk^-}) \quad \textbf{4.1}$$

Table (4.4) shows the diffusion coefficients of selected salts used in the present work calculated from the bulk diffusion coefficient for each ion (presented in Table 4.3) according to the above formula.

Table 4.4: Diffusion coefficient (m^2/s) of present study salts in water

Salt	Diffusion coefficient $\times 10^{-9}$ ($m^2.s^{-1}$)	Ref.
NaCl	**1.61**	[120]
$CaCl_2$	**1.45**	[149]
Na_2SO_4	**1.23**	[120]
$CaSO_4$	**1.0**	[150]

As shown in Table (4.4), the diffusion coefficients decrease going from NaCl, $CaCl_2$ and Na_2SO_4 to $CaSO_4$. It can be indicated from this order of diffusion coefficients that it is inversely reflected in the salt rejection sequence. It can be seen that the salt with the lowest diffusion coefficient exhibits the higher rejection, while the salt with the higher diffusion coefficient exhibits the lowest rejection. The effect of the solute diffusion coefficient on salt rejection was previously discussed in section (2.3.3).

4.4 Critical flux measurements

The critical flux measurments represent a major tool for assessing membrane fouling. The aim of this work is to achieve a better understanding of the generated impacts from using different molar concentrations of calcium sulphate in a 1 nm ceramic titania nanofiltration membrane.

The simulation or theoretical prediction of critical flux of certain solutes based on its physio-chemical properties only is still impossible as the theory dealing with surface interaction cannot be applied to complex fluids. Moreover, it is quite common to mention that the stability of any solutes is hardly controllable in most filtration systems.

Based on this, the measurements of the critical flux seem to be essential since this tool can lead to choosing the specific operation conditions that achieve a better control of fouling.

In this work, the concept of critical flux was introduced based on cross-flow filtration (CFF) experiments in order to describe the fouling behaviour of calcium sulphate at different molar concentrations below saturation concentration (0.001, 0.005, 0.01 M) and at saturation concentration to identify the form and the onset of fouling.

Two different flux-pressure techniques have been applied to determine the critical flux of calcium sulphate (as $CaSO_4.2H_2O$) using a 1nm tubular TiO_2 NF membrane, which are: the step by step technique (flux-pressure increase) and the standard stepping technique (flux-pressure increase and decrease).

In this work, the resulting critical flux measurements from using the above two techniques for calcium sulphate solutions were compared and discussed.

It is important to mention here, that there is no existence to a unique or precise method which can be used directly to determine the critical flux for any solute because choosing a measuring procedure normally depends on many factors such as: the type of membrane, filtration operation mode (whether it is cross or dead end flow), type of solute (for instance; organic, inorganic or combined solutions), the affinity between solute and membrane, step time interval, step height (or the range of applied pressure) and the status of the membrane as to whether it is a new or backwashed.

4.4.1 Step by step technique (flux-pressure increase)

The step by step technique was used to estimate the critical flux values for calcium sulphate solutions in a 1 nm ceramic Titania NF membrane below saturation concentration (0.001, 0.005, and 0.01 M) and at saturation concentration (0.015 M after filtration).

For each of the four sessions, there were six step heights covered applied pressure ranged from 1.0−6.0 bars. For each session, the trans-membrane pressure or the average applied pressure across the membrane (see section 2.1.4.3) was estimated based on the recorded inlet and outlet pressure of the membrane module while the permeate side pressure was ignored.

In this method, the permeate flux-pressure profile of the calcium sulphate solution (represented with red dots) was compared to that of pure water flux (represented by the blue rhombus shape). The permeate flux is represented by a series of red dots. The red dotted line represents a tangent to the permeate flux-pressure profile which is used normally for indicating the point where the profile deviates from linearity.

Figure 4.48 shows the permeate flux of both calcium sulphate (0.001 M) and pure water as a function of trans-membrane pressure using a step by step technique.

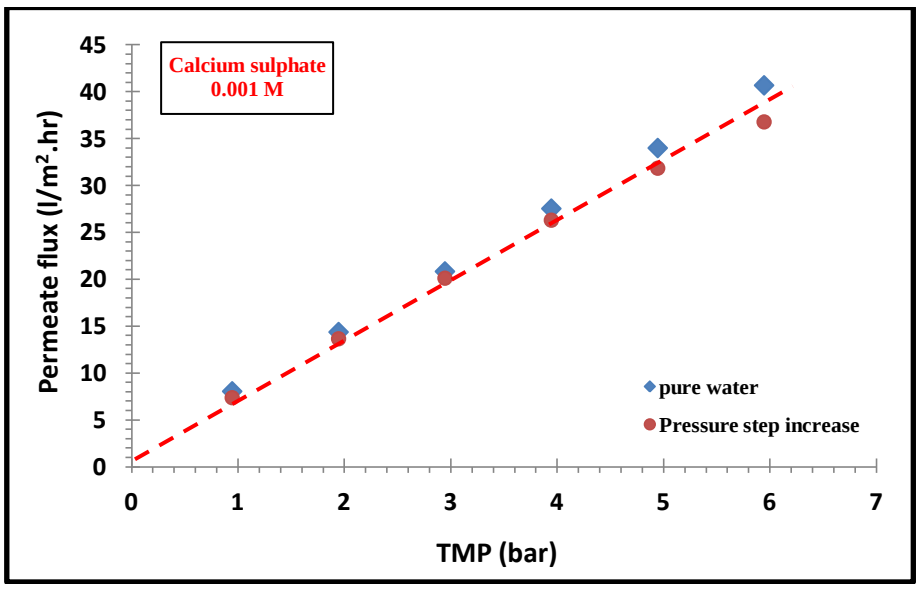

Figure 4.48: Permeate flux of calcium sulphate (0.001 M) and pure water as a function of trans-membrane pressure using step by step technique for 1 nm ceramic Titania NF membrane.

It can be seen from Figure 4.48 that, at the same pressures, the permeate flux of (0.001 M) calcium sulphate started to deviate from the pure water linear flux at trans-membrane just below 5.0 bars. Above this pressure, the critical flux was exceeded since the calcium sulphate permeate flux was clearly diverged from the pure water flux. In this case the strong form of the critical flux was achieved. Based on the definition of the step by step method, the critical flux (J_{crit}) of calcium sulphate (0.001 M) in a 1 nm ceramic Titania NF membrane equals to 33 ($\mathrm{l/m^2.hr}$).

Figure 4.49 shows the permeate flux of both calcium sulphate (0.005 M) and pure water as a function of trans-membrane pressure using the step by step technique.

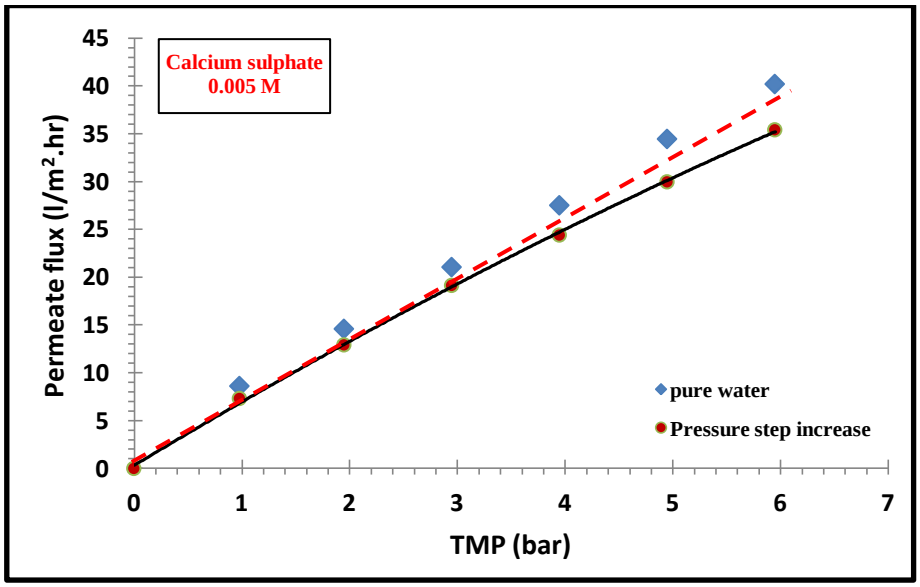

Figure 4.49: Permeate flux of calcium sulphate (0.005 M) and pure water as a function of trans-membrane pressure using step by step technique for 1 nm ceramic Titania NF membrane.

According to Figure (4.49), it can be seen that the permeate volume flux of (0.005 M) calcium sulphate was not identical to that of pure water flux even at the lowest trans-membrane pressure. Based on this, the weak form of critical flux can be observed. It can be seen from this figure that critical flux was exceeded above the trans-membrane pressure of 4.0 bar where the solute permeate flux was no longer linearly dependent.

According to the definition of the step by step method, the critical flux (J_{crit}) of calcium sulphate (0.005 M) in a 1 nm ceramic Titania NF membrane equals to 26 ($\mathrm{l/m^2.hr}$).

Using the same procedure but for different concentrations, Figure (4.50) shows the permeate flux of both calcium sulphate (0.01 M) and pure water as a function of trans-membrane pressure.

At this concentration, the permeate flux of calcium sulphate was noticeably lower than that of pure water flux at the same pressures, therefore; the critical flux is of the weak form. It can be seen from this figure that critical flux was exceeded above the trans-membrane pressure of 3.5 bar where the solute permeate flux was no longer linearly dependent. Based on this, the critical flux of (0.01 M) calcium sulphate seems to be 21 ($l/m^2.hr$).

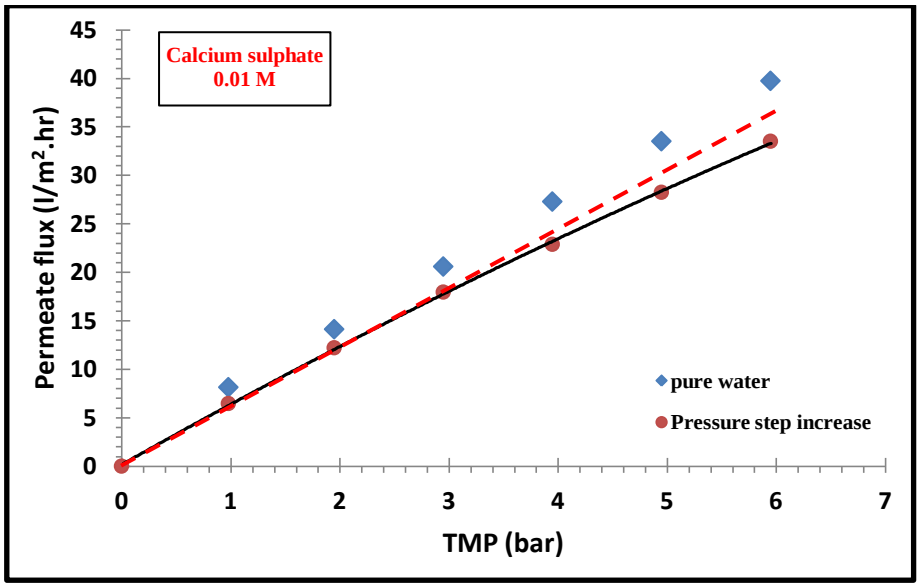

Figure 4.50: Permeate flux of calcium sulphate (0.01 M) and pure water as a function of trans-membrane pressure using step by step technique for 1 nm ceramic Titania NF membrane.

By using the same procedure as previously mentioned procedure to prepare calcium sulphate solute at saturation concentration (see section 4.3.5), Figure 4.51 shows the permeate volume flux of both calcium sulphate at saturation concentration and pure water as a function of trans-membrane pressure using the step by step technique.

It can be seen from this figure that the calcium sulphate permeates flux at saturation concentration was significantly lower than that of pure water flux starting from the lowest trans-membrane pressure. Therefore, the weak form of critical flux was clearly observed at this concentration. The critical flux was exceeded above the trans-membrane pressure of 2.5 bar where the solute permeates flux was no longer linearly dependent. Based on the step by step technique, the critical flux of calcium sulphate at this concentration in a ceramic titanium NF membrane was then 17 ($l/m^2.hr$).

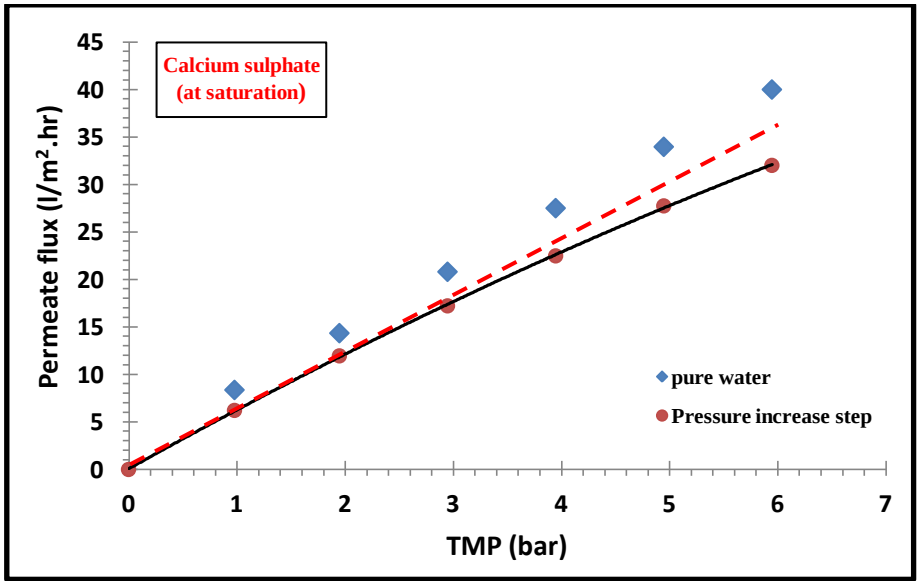

Figure 4.51: Permeate flux of calcium sulphate (at saturation concentration) and pure water as a function of trans-membrane pressure using step by step technique for 1 nm ceramic Titania NF membrane.

4.4.2 Standard stepping technique (flux-pressure increase and decrease)

A standard stepping technique was used to estimate the critical flux values for calcium sulphate solutions in a 1 nm ceramic Titania NF membrane below saturation concentration (0.001, 0.005, and 0.01 M) and at saturation concentration.

In this technique the pressure was increased stepwise and decreased in order to find the flux where the critical flux was exceeded. This flux can be identified when the decreased pressure flux does not give the same increased pressure flux. For each of the four sessions, there were six step heights covering an applied pressure ranged from 1.0−6.0 bar.

Figure 4.52 illustrates the process of the standard stepping technique used in the present work (increasing and decreasing pressure step height of 1.0 bar and 15 minutes time interval for each step).

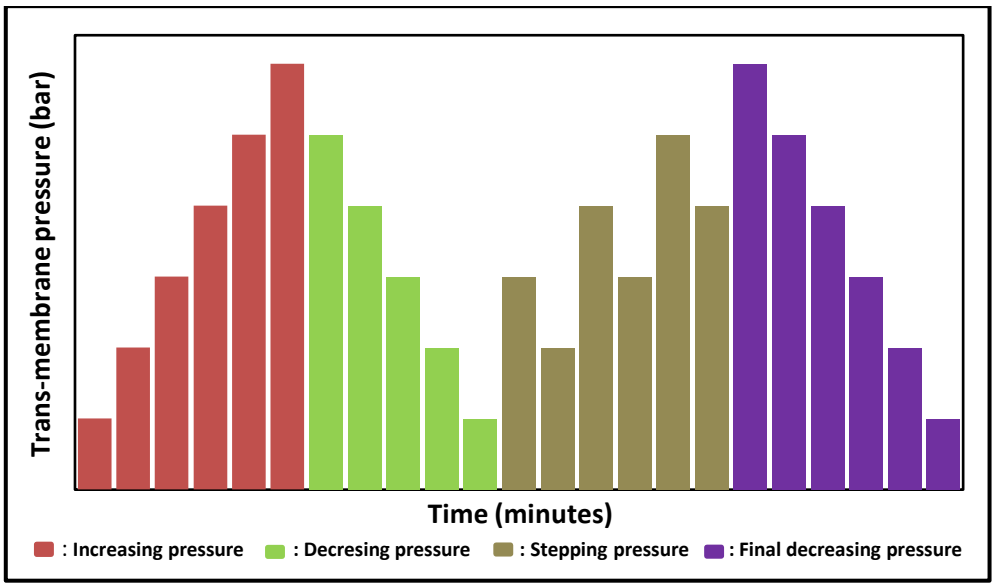

Figure 4.52: Illustration for standard stepping technique used in present work (1 bar pressure step height and 15 minutes time interval).

In this method, the pure water flux (before calcium sulphate filtration) was represented by a series of connected blue rhombus shapes. The permeate flux-increased pressure profile (up to 6.0 bar) of the calcium sulphate solution was represented with red dots while the permeate volume flux-decreased pressure profile (down to 1.0 bar) was represented by green triangular shapes. The purple squares represent the calcium sulphate permeates flux of the final continuously decreased pressure from 6.0 to 1.0 bar (after stepwise pressure increased and decreased).

Figure 4.53 shows the permeate flux of 0.001 M calcium sulphate as a function of the increased and decreased trans-membrane pressure and pure water flux using a standard stepping technique.

In order to identify the critical flux form, it can be seen from this figure that, at same pressures (up to 5.0 bar), the permeate volume flux–increased pressure profile of 0.001 M solute was almost the same as that of pure water. At TMP less than 6.0 bars, the solute permeate flux was noticeably lower than that of pure water which could give an indication that the CF for 0.001 M calcium sulphate was of a strong form.

The critical flux from this method represents the average of two flux steps values where one is below the critical flux value and another is above the critical flux value.

It can be seen from this figure that, below 4.0 bar, the solute permeates flux's values for the increased and decreased pressure were almost the same; this can indicate that the critical flux was not reached. Whereas the decreased pressure at TMP of 5.0 bar did not give the same flux value that had already been obtained from the increased pressure which can indicate that the critical flux was exceeded.

Based on this, the critical flux value of calcium sulphate (0.001 M) in a Titania ceramic NF membrane then equals to 31($l/m^2.hr$).

Also, it can be seen from Figure 4.53 that the purple squares represent the rate of reversibility of the fouling beyond the critical flux which shows the irreversibility behaviour of 0.001M calcium sulphate. This indicates that the Titania membrane was a bit fouled.

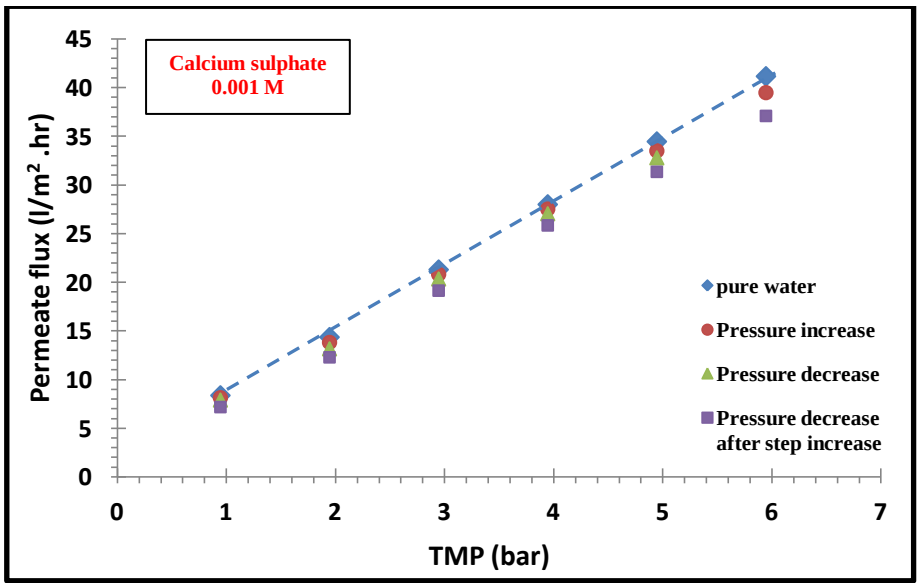

Figure 4.53: Permeate flux of calcium sulphate (0.001 M) and pure water as a function of trans-membrane pressure using standard stepping technique for 1 nm ceramic Titania NF membrane.

Figure 4.54 shows the permeate flux of 0.005 M calcium sulphate as a function of increased and decreased trans-membrane pressure and pure water flux using a standard stepping technique.

As can be seen from this figure, the permeate flux–increased pressure profile of a 0.005 M solute was a bit lower than that of pure water flux starting from the lowest up to the highest applied trans-membrane pressure. Therefore, the weak form of critical flux was observed for 0.005 M calcium sulphate.

It can be seen from this figure that, below 3.0 bar, the 0.005 M solute permeates flux's values for the increased and decreased pressure remained almost the same; this can be indicated that the critical flux was not reached. The decreased pressure at TMP of 4.0 bar and above was not given the same flux value that was obtained from the increased pressure which can indicate that the critical flux was exceeded.

Based on this, the critical flux value of (0.005 M) calcium sulphate in a ceramic Titania NF membrane was then 25 ($l/m^2.hr$).

The purple squares from this figure represent the rate of reversibility of the fouling beyond the critical flux which shows the irreversibility behaviour of 0.005 M calcium sulphate. This indicates that the Titania membrane was slightly fouled.

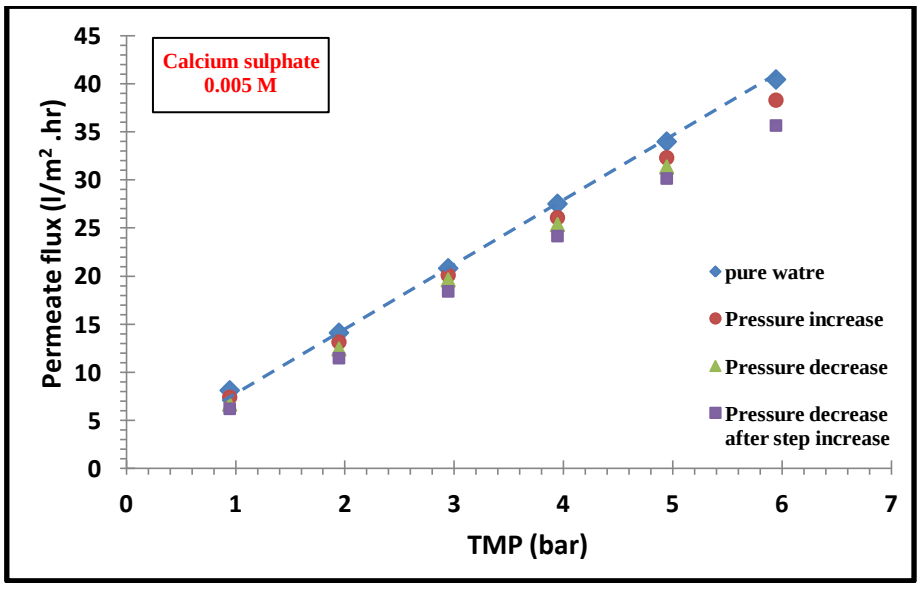

Figure 4.54: Permeate flux of calcium sulphate (0.005 M) and pure water as a function of trans-membrane pressure using standard stepping technique for 1 nm ceramic Titania NF membrane.

Using the same procedure but for different concentrations, Figure 4.55 shows the permeate flux of 0.01 M calcium sulphate as a function of increased and decreased trans-membrane pressure and pure water flux.

For the purpose of identifying the type of critical flux form, Figure (4.55) indicate that the permeate flux-increased pressure profile (red dots) of 0.01 M solute was noticeably lower than that of pure water flux (compared to 0.005 M solute) starting from the lowest up to the highest applied trans-membrane pressure. Based on this, the weak form of critical flux can be seen for 0.01 M calcium sulphate.

According to this figure, it can be seen that the 0.01 M calcium sulphate permeates fluxes values for the increased and decreased pressure remained almost the same below 3.0 bar; this can indicate that the critical flux was not reached. Whereas, at applied trans-membrane pressure of 4.0 bar and above, the decreased pressure was not given the same flux value that was obtained from the increased pressure which can indicate that the critical flux was exceeded.

Based on the standard stepping method, the critical flux value of (0.01 M) calcium sulphate in a Titania NF membrane was then 22 ($l/m^2.hr$). On the other hand, the irreversibility behaviour of 0.01M calcium sulphate solution indicated that the titanium dioxide membrane was noticeably fouled.

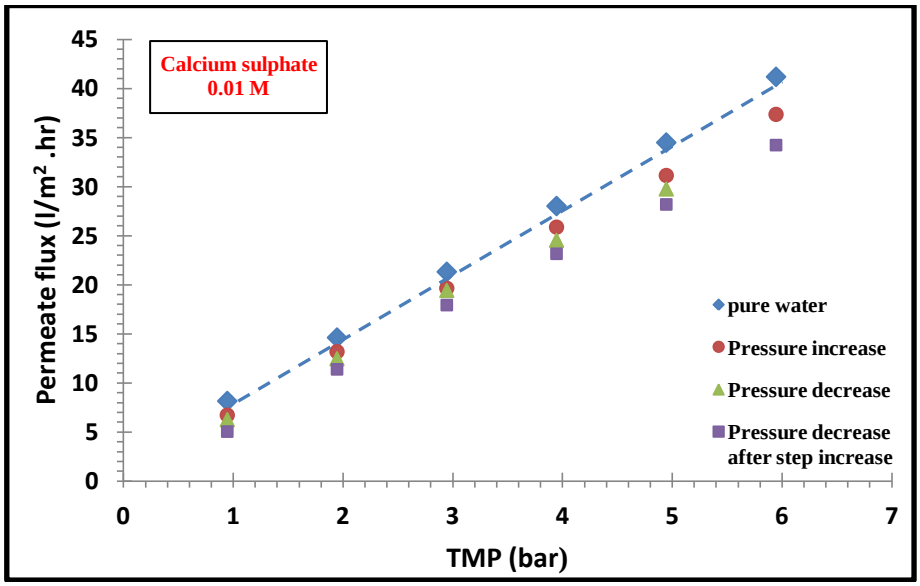

Figure 4.55: Permeate flux of calcium sulphate (0.01 M) and pure water as a function of trans-membrane pressure using standard stepping technique for 1 nm ceramic Titania NF membrane.

Figure 4.56 shows the permeate volume flux of (0.015 M after filtration) calcium sulphate solution (at saturation concentration) as a function of increased and decreased trans-membrane pressure and pure water flux using a standard stepping technique.

It can be clearly noticed from Figure 4.56 that the critical flux for 0.015 M solute was of the weak form since the (permeate flux-increased pressure) profile of the solute was significantly lower than that of pure water flux. This could be attributed to the rapid fouling that occurred during the early stages of filtration.

Also, it can be seen that below 2.0 bar the difference between the increased (red dots) and decreased (green triangles) permeate flux's values for applied TMP remained almost the same; this can indicate that the critical flux was not attained. Whereas, the decreased pressure at TMP of 3.0 bar and above did not give the same flux value that was obtained from the increased pressure which indicated that the critical flux was exceeded.

Based on this, it can be clearly seen that the critical flux value of calcium sulphate at saturation in a TiO_2 NF membrane then equals to 16 ($l/m^2.hr$).

The rate of reversibility of a calcium sulphate solute at saturation beyond the critical flux (purple squares) in this figure indicated that the Titania NF membrane was significantly fouled compared to all previous calcium sulphate concentrations used in the present study.

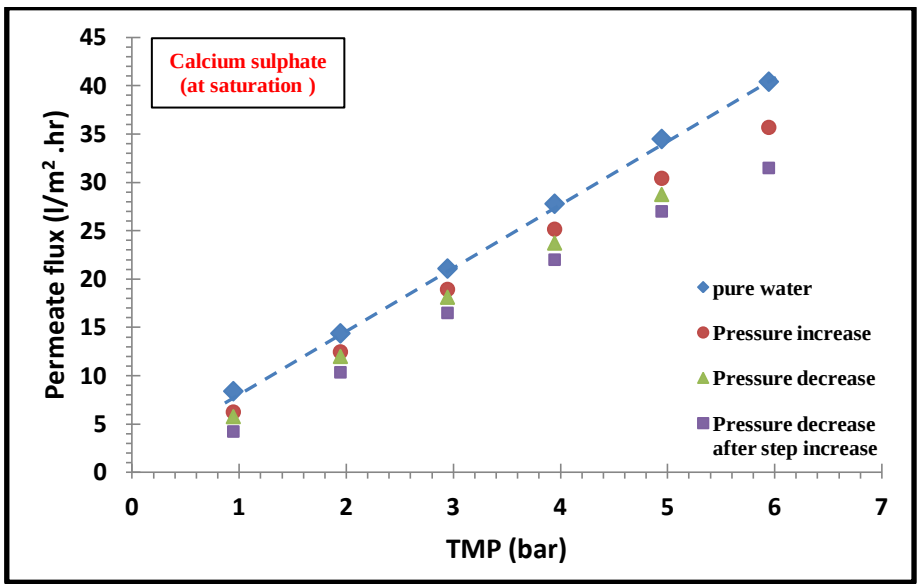

Figure 4. 56: Permeate flux of calcium sulphate (at saturation concentration) and pure water as a function of trans-membrane pressure using standard stepping technique for 1 nm ceramic Titania NF membrane.

Figures 4.53, 4.54 and 4.55 confirm that the critical flux for the (0.001, 0.005 and 0.01 M) $CaSO_4$ solutes in a ceramic Titania nanofiltration membrane using the standard stepping technique has been reached and exceeded. In order to add more evidences for the achievement of the critical flux theory, the following debate on this matter is based on the simplest definition of the critical flux concept (the flux below which no fouling is observed). As mentioned previously in section (2.5.3), the critical flux theory discriminates between any kind of fouling and when fouling does not occur (or is relatively slow).

Figures 4.57, 4.58 and 4.59 represents the permeate flux of 0.001, 0.005 and 0.01 M calcium sulphate solutions all below (or at sub-critical) the estimated critical flux value of each concentration obtained from using the standard stepping technique.

In these Figures, the red columns represent the permeate fluxes of calcium sulphate when the pressure increased, while the green columns represent the permeate fluxes of calcium sulphate when the pressure decreased and the brown columns represent the permeate fluxes of calcium sulphate when the pressure is stepped.

It can be seen from Figures 4.53, 4.54 and 4.55 that there is a clear distinction between two different zones; one below the estimated critical flux values (where no fouling occurred) and the other was above the estimated critical flux values (where fouling occurred). In Figures 4.57, 4.58 and 4.59, it can be clearly observed that below the estimated CF values the solute permeates flux remains almost the same at each selected increased, decreased or stepped TMP.

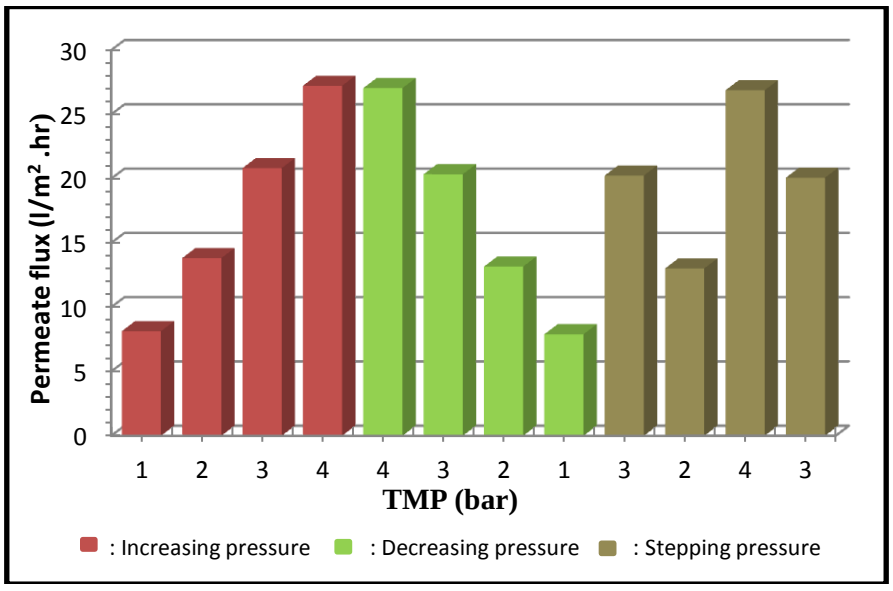

Figure 4.57: Permeate flux of calcium sulphate (0.001 M) as a function of (increasing, decreasing and stepping) trans-membrane pressure below the estimated critical flux value.

This behaviour can be considered as important evidence for the existence of a time independent zone below the estimated critical flux values even when the TMP were changed (increased, decreased, or stepped) with time, whereas above the critical flux values the time dependent zone can be clearly seen in Figures (4.52, 4.53, 4.55 and 4.56).

The existence of such a time independent zone below the estimated critical flux value would add a significant proof for the existence of the critical flux phenomenon.

The reason why these figures do not refer to the final decreasing trans-membrane pressure (the purple columns in Figure 4.52) is because the calcium sulphate solution at this stage had already spent so much time above the critical flux value (or at the time dependent zone). In other words, the membrane at this stage has already been fouled as a result of permeate flux reduction due to the accumulation of calcium sulphate ions, thus, it is not possible to compare the permeate flux for the final decreasing pressure stage after stepping increase (purple columns) with the previous three stages.

The estimation of the critical flux of calcium sulphate at saturation concentration (Figure 4.56) shows that, below 3.0 bar, the permeate flux for the first increasing stage (red dots) and the decreasing pressure stage (green dots) were almost the same, but the permeate flux of the stepping stage cannot be compared with the previous two stages as a result of a noticeably fouled membrane and low estimated critical flux value.

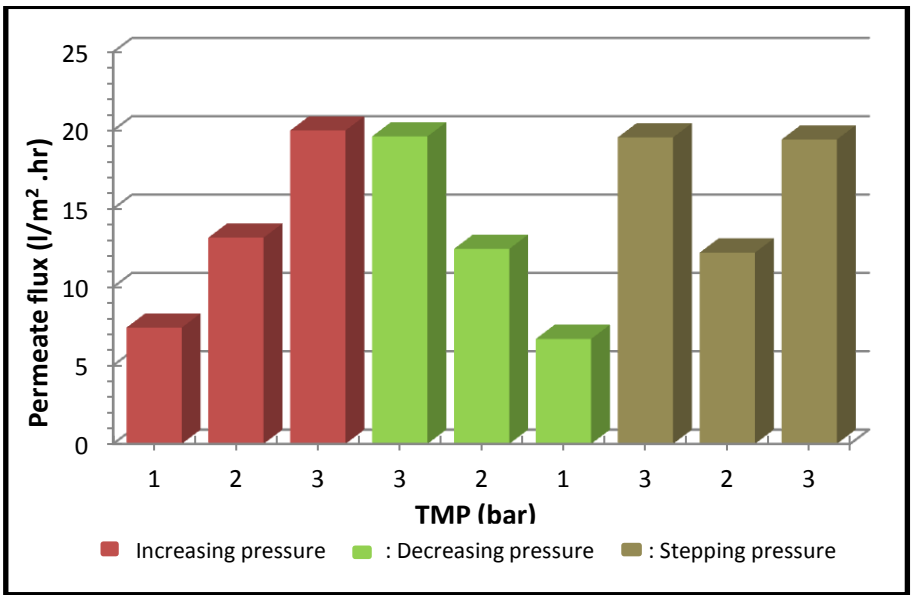

Figure 4.58: Permeate flux of calcium sulphate (0.005 M) as a function of (increasing, decreasing and stepping) trans-membrane pressure below the estimated critical flux value.

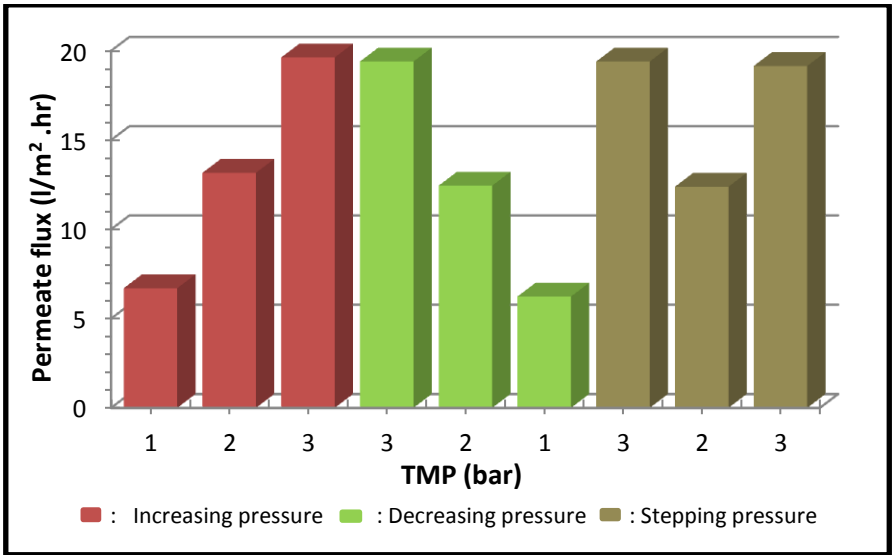

Figure 4.59: Permeate flux of calcium sulphate (0.01 M) as a function of (increasing, decreasing and stepping) trans-membrane pressure below the estimated critical flux value.

4.4.3 Discussion of critical flux experiments

In this work, two approaches were used to evaluate the critical flux using four different calcium sulphate concentrations based on a cross-flow operation mode of a 1 nm ceramic TiO_2 NF membrane.

As mentioned previously in section (2.5.3), the critical flux concept can be considered as an intrinsic solution to the problem of membrane fouling.

From this theoretical definition, the critical flux is a result of force balance between drag forces and surface interaction in a mass boundary layer; therefore, depending on the hydrodynamics effects and surface interactions of the cross flow filtration, critical flux appears. Beyond this critical regime, the increase of the applied pressure leads to increasing the flux which means more deposit growth.

Usually the critical flux occurred with a rather low applied pressure, thus, in order to avoid this problem, large membrane areas must be used. Here, the optimisation factor is very important because working within the sub-critical flux can change the filtration process to be sustained. In this case, the cleaning costs are removed and energy saving can be achieved as well.

As stated before in the previous studies section of the present work (see section 2.6), the fouling behaviour of calcium sulphate (as gypsum) in this type of TiO_2 membrane has not been studied yet.

From this point of view, it seems that there is no other available work which has attempted to determine critical flux of calcium sulphate in any type of membrane, since the majority of relevant published works examined the filtration of colloids, mostly organic matter such as paper mill effluent, lactic acid, yeast and latex; as a result, a direct comparison between the data obtained from the experimental procedures and any other previous work is not applicable.

The estimation of the critical flux in this work depends mainly on the measuring of the permeate flux of calcium sulphate at different concentrations. The permeate flux in any membrane filtration process could be subjected to a wide number of parameters, for instance:

- Type and constituent of the solute.
- Concentration of the solute.
- Membrane charge (electrokientic effects).
- Membrane effective pore radius.
- Membrane porosity.
- Flow operation mode.
- Active skin layer and sub-layers materials.
- Process operating conditions, such as applied pressure, cross-flow velocity and temperatures.
- Membrane status (virgin or back washed).

According to the above points, the present work concluded that the assumption that the critical flux would be the same even if the systems are different is not necessarily valid. Therefore, the present work suggested a comparison between two different experimental procedures which could be used to determine the critical flux values.

The deduction of critical flux in this work was obtained from flux's-pressure experiments (imposing pressure and measuring the flux). According to the process specifications of the present membrane filtration rig, it can be seen that it is easier to operate the filtration system by controlling the applied pressure instead of trying to set the flux.

Two different techniques have been used, which are: the step by step technique (where the pressure is only increased) and the standard stepping technique (where the pressure is increased and decreased).

In order to discuss the main difference between the two methods, it can be seen that the standard step method is preferred over the step by step method since it provides a better control of the flow of calcium sulphate solutions on the membrane surface; also, the standard stepping method represents an improved method since the required data from this method allow more accurate values of the critical flux, and also, this method shows the rate of irreversibility of the created deposits on the membrane.

The standard stepping method allows discrimination between two distinct zones; one where no deposit build-up appears in the membrane thus, there is no need to be cleaned and the other one for which cleaning will be necessary.

In contrast, the step by step technique provides useful data on comparative fouling tendency with less time and a less complicated procedure than the prolonged standard stepping method. Also, the discrimination between the strong and weak form of the critical flux can be easily made by using this technique.

But in this method, any decline in the solute permeate flux indicates that fouling might have occurred and that the critical flux has been exceeded, taking in consideration ignoring the effect of other important parameters which could decrease the flux as well, such as the effect of solute concentration polarisation. In the meantime, this method does not give a clear indication about how the membrane is really getting fouled.

It was observed from Figures (4.48, 4.49, 4.50 and 4.51) that the critical flux was reached and exceeded (where the solutes permeate flux starts to deviate from linearity). Other important parameters that might have an effect on determining the critical flux such as the cross-flow velocity and the temperature were stable for each calcium sulphate concentration.

The strong form of the critical flux was observed only in 0.001 M calcium sulphate solutions for both measuring techniques. Since the flux was below the critical level at which the applied TMP starts to deviate from the pure water line, this form presents non-deposition conditions. Then, by ignoring the adsorption between the calcium sulphate solution and the Titania membrane, the strong form can differentiate the states between zero-fouling and any other type of fouling.

According to the definition, the weak form of critical flux was observed for calcium sulphate solutions of 0.005 M, 0.01 M and that at saturation.

The weak form indicates a rather low but non-zero rate of membrane fouling which was detected even under sub-critical flux conditions.

Comparing the estimated critical flux values that resulted from using both techniques for each selected calcium sulphate concentration it showed that the critical flux values (J_{crit}) were almost the same in spite of the differences in measuring technique and in step duration of each time interval. However, there were some changes of about 0.5 bars in related applied critical trans-membrane pressures ($\mathrm{TMP_{crit}}$) for the calcium sulphate concentrations of 0.001, 0.005 and 0.01 M. While for saturation concentration, the determined ($\mathrm{TMP_{crit}}$) from both measuring techniques was the same.

The experiment's results indicated that the critical flux values in TiO_2 membranes depend mainly on the ionic strength of the calcium sulphate. The present work pointed that the resulting critical flux values from both measuring procedures were decreased as the ionic strengths of the calcium sulphate solutes were increased.

According to the obtained results from the step by step technique, it can be seen that the determined critical flux values were 33, 26, 21 and 17 ($\mathrm{l/m^2.hr}$) while the determined critical flux values from the standard stepping technique were 31, 25, 22, 16 ($\mathrm{l/m^2.hr}$) for calcium sulphate solute concentrations of 0.001, 0.005, 0.01 M and at saturation concentration respectively.

Based on these results, it can be seen that the critical flux values were reduced up to half when the concentration of calcium sulphate increased from 0.001 M to that at saturated concentration.

The same behaviour has been reported by other researchers, such as; Chiu and James's [101] work which studied the effects of critical flux for different molar concentrations of potassium chloride (KCl) salt where a drop of 35% in the critical flux was observed despite using micro-filtration membranes.

Similar trends have been reported by Kwon et al. [107] and Espinasse et al. [95] although both groups of workers used latex particles.

In fact this behaviour is quite understandable since the critical flux value depends mainly on the obtained permeate flux for calcium sulphate (discussed previously in section 4.3.6) which has already decreased as the solute concentrations increased and as a consequence the critical flux would be reduced as well.

The obtained critical flux results from the standard stepping method (for all the four sessions) confirm that the critical flux values were exceeded since the recorded permeate flux of the decreasing pressure did not give the same values when compared to that of increasing pressure. This can be considered as strong evidence that fouling did occur in the membrane.

As expected, for the relationship between the calcium sulphate solutes flux and the increased applied trans-membrane pressure can be linear for only a limited range of values, as fouling induces the decline of flux regardless of any increase of the pressure. However, this behaviour can be attributed to the formation of a compact concentration polarisation layer.

In fact this could have been possible when the first step by step technique was used. However when using the standard stepping technique where the critical flux was determined by comparing the recorded fluxes from the increasing (red dots) and decreasing (green triangles) applied pressure, the concentration polarisation layer was not re-dispersed when the pressure was decreased after the highest trans-membrane pressure had been reached. Thus, the decrease in calcium sulphate permeate flux was not only because of the concentration polarisation layer but also as an indication of fouling occurrence.

Based on a sound theoretical basis, the critical flux represents the shift from repulsive interaction to attractive interaction. This shift then represents the change from (dispersed matter-polarised layer) into (condensed matter-deposit).

The experimental results of the stepping method shows that the purple squares which represent the final decreasing steps (after the consequence of increasing and decreasing of the applied pressure) did not give the same permeate fluxes for both increasing (red dots) and decreasing (green triangles) applied trans-membrane pressure.

This behaviour can be explained based on the fundamental idea from using this technique which depends mainly on forcing the membrane to work for a long period of time above the point where the critical flux was exceeded.

Therefore, it can be seen from Figures (4.52, 4.53, 4.55 and 4.56) that as the critical flux values were reduced by increasing the calcium sulphate concentrations; the TiO_2 membrane would be subjected to a long period of time above the CF value which definitely leads to increasing the possibility of more fouling occurrence (this behaviour was seen clearly in Figure 4.56).

The same behaviour was observed by other researchers such as Manttari et al. [105], [104] and Van der Bruggen [88], despite using different membrane type than that of the present Titania membrane (organic flat sheet membrane Desal-5) and paper mill and wood pulp effluent which have totally different chemical and physical properties compared to the present calcium sulphate solutions. However the pattern of both the pure water and the permeate flux-pressure profiles from these works was similar to the results achieved from the present study.

The major advantages of Manttari et al. [105] and Van der Bruggen et al. [88] researches were the ability to get more detailed data which extended over a much wider applied pressure range than was possible with the laboratory equipment utilised for the purposes of the present work. The experimental results (from both techniques used) shows that maximum or limiting flux (see Figure 2.15) was not reached and in this case, the applied trans-membrane pressure needs to be increased which is beyond the capability of the present rig.

Also, a similar trend has been reported by Espinasse et al. [95] in spite of using latex suspension as effluent and a ultrafiltration tubular Zirconia and Titania membrane.

It is important to mention here that the accuracy of the evaluation of the critical flux was based on flux linearity which was directly related to the step increment chosen for the experiments. Thus, the larger the pressure step applied, the higher the error in estimation of the critical flux. The chosen step height depended mainly on the membrane type, and the capability of the filtration rig.

The selection of the current calcium sulphate molar concentrations for the present work was subjected to many experimental tests before the present concentrations were been chosen based on calcium sulphate saturation concentration.

Also, for both critical flux measuring techniques used in this work, the selection of the step time interval was also subjected to many experimental tests before the present steps time period have been chosen.

Regarding the step by step measuring technique, the present work suggested the use of 30 minutes as a fixed step time interval for each applied pressure step even when the critical flux point was exceeded. This selected step time interval differs from the previous works done by Chiu and James [101] and Gesan-Guizion et al. [100]. In these studies (where a microfiltration membrane was used) the time steps were reduced to 15 minutes after exceeding the critical flux point.

In the same manner, the suggested time steps interval for the standard stepping technique for the present work was 15 minutes, whereas Manttari et al. [104], [105], and Van der Bruggen et al. [88] works used 10 and 5 minutes as filtration step times respectively.

4.5 Summary

This chapter focuses on the experimental results of electrokientic, rejection, and critical flux measurements in the present TiO_2 membrane. The streaming potential measurements were conducted in a background electrolyte comprising 0.01M NaCl which allowed characterising the type and magnitude of the surface charge for the membrane. The experimental results showed that the present study's membrane is negatively charged at neutral pH and its iso-electrical point is at pH of 4.0.

The solutes rejections (R %) at different molar concentrations (0.001, 0.005, 0.01 M) of Na_2SO_4, NaCl, $CaCl_2$ and $CaSO_4$ covering applied pressure ranged from 1.0−5.0 bar are evaluated and compared.

The rejection results showed that the salt with lowest diffusion coefficient ($CaSO_4$) shows the highest rejection (43.3 %), whereas that with highest diffusion coefficient shows lowest rejection. The ionic analysis for ($CaSO_4$) permeates indicated that the rejection for bivalent anion SO_4^{-2} was the higher, than that of the bivalent cation Ca^{+2}.

The concept of critical flux was introduced based on cross-flow (CF) nanofiltration experiments in order to describe the fouling behaviour of calcium sulphate at different molar concentrations below saturation concentration (0.001, 0.005, 0.01 M) and at saturation concentration, to identify the form and the onset of fouling. For each session, there were six step heights covering applied pressure ranged from 1.0−6.0 bars. The critical flux of calcium sulphate below and at saturated concentration using two different techniques (step by step and standard stepping methods) is studied.

The obtained critical flux results from the step by step method confirmed that the critical flux was reached and exceeded while the obtained CF results from the standard stepping method confirmed that the critical flux values were exceeded as the recorded permeate flux of the decreasing pressure did not give the same values when compared with that of increasing pressure.

Comprehensive discussion based on the combination of both size exclusion mechanism and Donnan exclusion mechanism including comparison with previous researches for each experimental result is presented.

CHAPTER 5
MODELLING

5.1 Introduction

Over the past few years, many researchers had worked on the modelling of the transport of electrolytes through NF membranes. At a fundamental level, the rejection of solutions by nanofiltration membranes is a very complex process because it is usually take place on a scale length of the order of one nano-metre (or less). As a result the calculations of such events would also be complex; therefore, it is very important to understand the main basic parameters that govern this process.

Modelling generally improves understanding, helps in experimental design, shows the ability for scaling up a process, and allows process optimisation. A practical, useful predictive method should provide quantitative process prediction from accessible physical data. This prediction should be physically realistic and require a minimum number of assumptions. For the present work, the modelling process is an attempt to predict the performance of the filtration process by understanding the main parameters that affect the transport of ions in a ceramic TiO_2 NF membrane.

Among all the membrane separation processes in the liquid phase, the innovative pressure driven nanofiltration membranes process is the latest developed process. This promising technique has attracted an increasing attention over recent years as a result of the development of several new applications for environmental and industrial purposes. The reclamation of salt-affected soil represents one of the new applications in this field.

This chapter provides details about the estimation of the effective pore radius (r_p) of a TiO_2 NF membrane by using two different models based on the rejection of glucose as a neutral solution. Also, the estimation of the related physio-chemical parameters that mainly depend on the estimated value of the membrane effective pore radius such as: the equivalent effective membrane active layer thickness, the ionic hindrance factors

for convection and diffusion, the steric partitioning coefficient and the hindered diffusivity.

Furthermore, this section will discuss the estimation of the Donnan potential based on the previous zeta potential measurements from chapter four; this estimation depends on the estimations of the membrane surface charge density and the effective membrane fixed charge density.

A numerical model based on the original Donnan steric pore model (DSPM) will be used in order to simulate the rejection of 0.01 M NaCl as a reference solution.

5.2 Estimation of TiO_2 membrane effective pore radius

There are several approaches proposed in the literature to characterise the membrane effective pore radius (r_p). The present work will determine the effective pore radius of the ceramic TiO_2 nanofiltration membrane based on transport equations of solutes inside membrane pores, the Hagen-Poiseuille equation and permeation test of uncharged solute (glucose) [151], [125], [153].

For the present work, the determination of the effective pore radius has been carried out based on two different models.

5.2.1 Donnan steric pore model

The first model was related to the Donnan steric pore partitioning model (DSPM) where the hindered nature of solute transport in the extended Nernst-Planck (ENP) equation provides the possibility of determining (r_p) of the TiO_2 membrane.

Ahmed and Ooi [152] and Bowen et al. [151], [153] proved that the retention measurements of an uncharged solute allows the characterisation of a membrane in terms of only two parameters: the membrane effective pore radius (r_p) and the effective ratio of membrane thickness to porosity ($\Delta x/A_k$).

The extended Nernst-Planck equation (ENP) forms the basis for the description of solute transport through NF membranes [154]. It describes transport in terms of diffusion under the action of the solute concentration gradient, migration under the action of a spontaneously arising electric field, and convection due to solute flow or the pressure gradient. The ENP equation has been modified by hydrodynamics coefficients in order to take the effect of finite pore size on both diffusion and convection into account.

The membrane is normally considered as a bundle of identical pores that length is much greater than their diameter, so that both volume flux and ions can be considered as one dimensional [130].

Based on the approximation of no direct coupling between ion fluxes and by using molar units for the electrochemical potential, Bowen et al. [154], [155] described the transport equation for ion fluxes through pores of NF membranes as follows:

$$J_i = -D_{i,p}\frac{dc_i}{dx} - \frac{z_i c_i D_{i,p}}{R_g T} F \frac{d\psi^m}{dx} + K_{i,c} c_i V \quad \textbf{5.1}$$

The terms on the right hand side of Equation (5.1) represents transport due to diffusion, the electric field, and convection respectively. Where:

J_i: Flux of ion i $(\mathrm{mol.\,m^{-2}.\,s^{-1}})$.

$D_{i,p}$: Hindered diffusivity of ion i $(\mathrm{m^2.\,s^{-1}})$.

c_i: Concentration of ion i in membrane $(\mathrm{mol.\,m^{-3}})$.

x: Distance normal to membrane (m).

z_i: Valence of ion i (dimensionless).

F: Faraday constant $(\mathrm{C.\,mol^{-1}})$.

R_g: Real gas constant $(\mathrm{J.\,mol^{-1}.\,K^{-1}})$.

T: Absolute temperature (K).

ψ^m: Electrical potential of the membrane (V).

$K_{i,c}$: Ionic hindrance coefficient for convection (dimensionless).

V: Solute velocity $(\mathrm{m.\,s^{-1}})$.

The pore size and the effective thickness divided by porosity can be determined by using the permeation test of the uncharged solute [152], [156].

For uncharged or neutral solutes (such as glucose), there will be no electrostatic term thus, only diffusion and convection flows affect the transport of solutes inside the membrane. As a result, the solute flux can be expressed as:

$$J_i = -D_{i,p}\frac{dc_i}{dx} + K_{i,c} c_i V \quad \textbf{5.2}$$

Routh et al. [15] described glucose as the most abundant neutral sugar. While Bowen et al. [155], [154] proved that in such narrow pores as those in nanofiltration membranes, the glucose has a reasonable range of rejection.

In order to obtain an expression for the rejection of the solute, Equation (5.2) is integrated across the membrane with solute concentrations at (x=0) which is on the

bulk side of the membrane and (x=Δx) which is on the permeate side of the membrane.

In terms of rejection (R), Equation (5.2) can be expressed as follows [158], [119], [159]:

$$R_i = 1 - \frac{C_i^{permeate}}{C_i^{feed}} = 1 - \frac{K_{i,c}\emptyset}{1 - \exp(-Pe_*)\left[1 - \emptyset K_{i,c}\right]} \quad \textbf{5.3}$$

Where:

Pe_*: Peclet number, which can be defined as follows:

$$Pe_* = \frac{K_{i,c}}{K_{i,d}} \frac{J_V \Delta x}{D_{i,\infty} A_k} \quad \textbf{5.4}$$

And:

$K_{i,d}$: Ionic hindered coefficient for diffusion (dimensionless).

J_V: Permeate volume flux ($\mathrm{m^3.m^{-2}.s^{-1}}$).

$D_{i,\infty}$: Molecular diffusion coefficient of ion i at infinite dilution ($\mathrm{m^2.s^{-1}}$).

Δx: Thickness of the membrane active layer (m).

A_k: Porosity of membrane (dimensionless).

The hindered diffusivity of ion i ($D_{i,p}$) can be determined as follows [141]:

$$D_{i,p} = D_{i,\infty}.K_{i,d} \quad \textbf{5.5}$$

$\emptyset$: Steric partitioning coefficient of ion i.

The steric partitioning coefficient accounts for the sieve effect due to the intrinsic porosity of the membrane. The steric partitioning coefficient is bounded between 0 and 1.

From the definition of the steric partitioning coefficient for cylindrical pores, it can be expressed as follows [155], [156]:

$$\emptyset_i = (1 - \lambda_i)^2 \quad \textbf{5.6}$$

Here λ_i represents the ratio of stocks radius of ion i (or solute) to the effective pore radius of the membrane.

Both of the hydrodynamic coefficients $K_{i,d}$ and $K_{i,c}$ depend on the solute to pore size ratio, λ_i in which [152]:

$$\lambda_i = \frac{r_i}{r_p} \quad \textbf{5.7}$$

r_i: Stokes' radius of ion i (or solute) (m).

r_p: Membrane effective pore radius (m).

It should be noticed that $K_{i,d}$ and $K_{i,c}$ are not dependant only on λ_i, but also on the radial position within the pore. However, the effect of the finite pore size on both diffusion and convection can be quite accurately estimated using the values of ($K_{i,d}$ and $K_{i,c}$) at the pore centre only [160].

Solutes moving in free solution experience a drag force exerted by the solvent, so, when solutes move in confined spaces such as membrane pores, the drag is modified and the transport may be considered to be hindered [161].

(r_i) can be obtained from the well-known Stokes-Einstein formula as follows [152]:

$$r_i = \frac{k_B T}{6\pi\eta D_{i,\infty}} \quad \textbf{5.8}$$

Here, k_B represents the Boltzmann constant (1.3806×10^{-23} J/K), while T and η represent the absolute temperature (K) and the dynamic viscosity of the solution (Pa. s) respectively.

The molecular diffusion coefficient of the glucose solute at infinite dilution equals to 0.69×10^{-9} ($m^2.s^{-1}$) [16]. So, by applying Equation 5.8, the Stokes radius of glucose solute then equals to 0.310×10^{-9} (m).

The extent to which the finite pore size acts on the diffusion and convection solute fluxes inside pores depends mainly on pore geometry [158].

For a cylindrical geometry (assuming that they can be applied to charge species) the values of $K_{i,d}$ and $K_{i,c}$ can be estimated as a function of ionic radius/pore radius ratio (for: $0 < \lambda_i \leq 0.8$) as follows [155], [156]:

$$K_{i,d} = 1.0 - 2.3\left(\frac{r_i}{r_p}\right) + 1.154\left(\frac{r_i}{r_p}\right)^2 + 0.224\left(\frac{r_i}{r_p}\right)^3 \quad \textbf{5.9}$$

$$K_{i,c} = (2 - \emptyset)(1.0 + 0.054\left(\frac{r_i}{r_p}\right) - 0.988\left(\frac{r_i}{r_p}\right)^2 + 0.441\left(\frac{r_i}{r_p}\right)^3) \quad \textbf{5.10}$$

Also, the hindrance factors according to Bowen and Mukhtar [162] for any ion i can be determined as follows:

$$K_{i,d} = -1.705\,\lambda_i + 0.946 \quad \textbf{5.11}$$

$$K_{i,c} = -0.0301\,\lambda_i + 1.022 \quad \textbf{5.12}$$

The Hagen-Poiseuille equation gives the relationship between the pure water flux (J_w) and the applied pressure across the membrane as follows [152], [163]:

$$J_w = VA_k = \frac{r_p^2\, P}{8\mu(\Delta x/A_k)} \qquad \textbf{5.13}$$

P: Applied pressure (Pa).

μ : is the dynamic viscosity of solution (Pa. s).

Rejection experiment for glucose solution (as an uncharged solute) at concentration of 300 mg/l [152] was conducted using the present work ceramic titanium dioxide nanofiltration membrane at different applied pressure ranged from 1.0 to 5.0 bars.

The rejection of glucose was estimated based on its bulk and permeate concentrations (the left hand side of Equation 5.3) by applying exactly the same previous procedure that has been used for salts rejection experiments (see section 3.6.2).

Glucose concentrations were analysed using the glucose analyser (Model: GL6 ANALYSER), the assay kit being supplied by Analox Instruments Ltd, UK.

Figure (5.1) shows the permeate flux of (m/s) versus the applied pressure/8μ (s^{-1}) in the present work's ceramic Titania membrane.

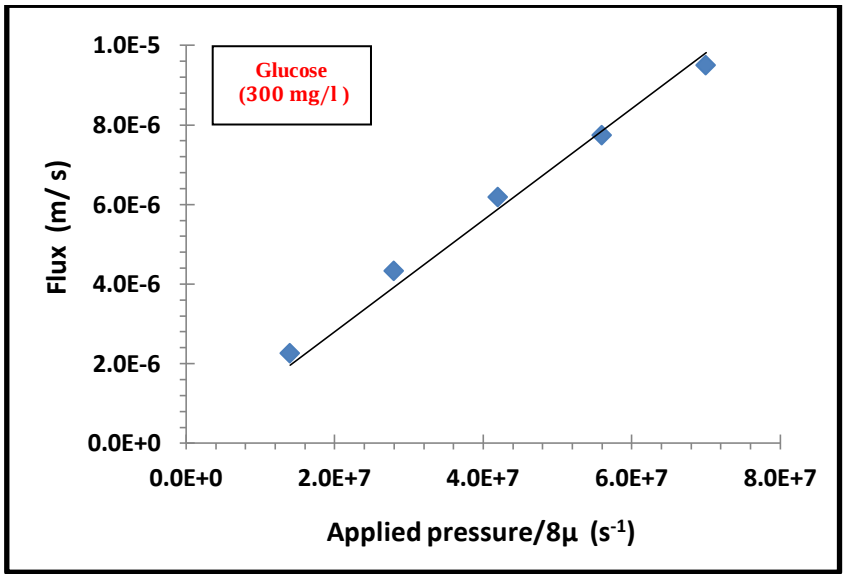

Figure 5.1: The permeate flux of glucose as a function of applied pressure.

Based on the Hagen-Poiseuille equation, the obtained slope $({r_p}^2/\Delta x)$ from Figure (5.1) equals to 1.4×10^{-13} (m). Therefore, the effective membrane thickness (Δx) can be easily determined from the estimated slope as a function of the estimated effective pore radius $\left(\Delta x = {r_p}^2/slope\right)$.

Figure (5.2) shows the rejection of glucose versus the permeate flux of glucose (m/s) in the present work's ceramic Titania membrane.

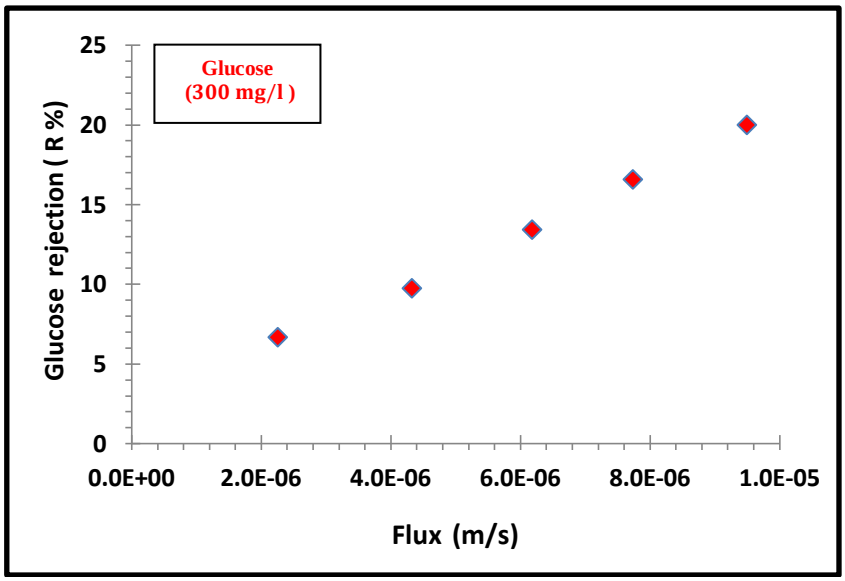

Figure 5.2: The rejection of glucose as a function of volumetric permeates flux.

The retention data of glucose show, as expected, that the rejection increases as the permeate flux increases.

By using Microsoft's spreadsheet *solver*™ add-in, Microsoft Excel™ and substituting Equations (5.4), (5.6), (5.7), (5.8), (5.9) and (5.10) in Equation (5.2) and solved to determine the effective membrane pore radius of the Titania nanofiltration membrane based on the resulting rejection value of the glucose. The effective membrane active layer thickness can be substituted in terms of effective membrane pore radius which was already stated in the slope equation of Figure (5.1).

The estimated result of the effective pore radius for the present ceramic Titania membrane from using the Donnan steric pore model showed that the effective pore radius for the present Titania membrane was found to be equal to 0.68 nm.

By knowing the value of the effective pore radius, the membrane thickness can then be easily obtained from the slope equation stated in Figure (5.1). The estimated thickness of the Titania membrane based on the Donnan steric pore model was equal to 3.256 μm.

The obtained results of the effective membrane pore radius and effective membrane thickness from applying this model are in good agreement with the results reported by Bowen et al. [162], [151], [153], [155].

5.2.2 Uncharged solute hydrodynamic model

According to Bowen and Welfoot [155], [164], [165] another hydrodynamic model can be applied to estimate the effective pore radius (r_p**)** which is generally based on fundamental transport models but in terms of partial molar volume for uncharged solute. In this model, as a result of the solute-membrane interactions, the porous membranes are represented as a bundle of straight cylindrical pores and the transport of solute is corrected for hindered convection and hindered diffusion [160].

Thus, for a neutral solute (glucose), the transport Equation can be expressed as:

$$J_s = K_c c V - \frac{c D_p}{RT}\frac{d\epsilon}{dx} \quad \textbf{5.14}$$

Here, (ϵ) represents the chemical potential of an uncharged solute, which can be defined as follows:

$$\epsilon = RT\ ln\ a + V_s P + const. \quad \textbf{5.15}$$

Here a represents the activity of the uncharged solute (mol.m^{-3}).

V_s: Partial molar volume for the uncharged solute $(\text{m}^3.\text{mol}^{-1})$.

If the solute concentration is low, then, the solution can be assumed to behave ideally. So, the differentiation of Equation 5.15 and substitution in Equation 5.14 yields:

$$J_s = K_c c V - D_p\frac{dc}{dx} - \frac{c D_p}{RT} V_s \frac{dP}{dx} \quad \textbf{5.16}$$

The solute flux can also be expressed as:

$$J_s = V C^{permeate} \quad \textbf{5.17}$$

$C^{permeate}$: Concentration of solute in permeates (mol.m^{-3}).

The solvent velocity V (m.s^{-1}) within the pore is related to the pressure gradient through the pore (which is assumed to be constant) that can be determined according to the rearranged Hagen-Posuille equation:

$$J_s = \frac{r_p^2}{8\mu}\frac{dP}{dx} \quad \textbf{5.18}$$

Substitution of Equation 5.17 and 5.18 in Equation 5.16 and rearrangement, the concentration gradient inside the membrane pores can be expressed as follows [155]:

$$\frac{dc}{dx} = \frac{V}{D_p}\left(\left(K_c - \frac{D_p}{RT}V_s\frac{8\mu}{r_p^2}\right)c - C^{permeate}\right) \quad \textbf{5.19}$$

Here, c represents the uncharged solute concentration within pore (mol.m^{-3}).

The integration of the above equation over the membrane thickness ($0< x < \Delta x$) using the following boundary conditions yields an expression that can be applied for uncharged solute rejection at charged nanofiltration membrane:

$C_{x=0} = \emptyset C^{feed}$

$C_{x=\Delta x} = \emptyset C^{permeate}$

For simplicity, Bowen and Welfoot [155], [164] suggested the following dimensionless group which can be considered independent of solute concentration by assuming that both V_s (the uncharged solute partial molar volume, $\mathrm{mol.\,m^{-3}}$) and D_p (the uncharged solute pore diffusion coefficient, $\mathrm{m^2.\,s^{-1}}$) are independent of concentration:

$$Y = \frac{D_p}{RT} V_s \frac{8\mu}{r_p^2} \quad \textbf{5.20}$$

Birch et al. [166] estimated the partial molar volume for glucose to be 1.1×10^{-4} $\mathrm{m^3.\,mol^{-1}}$.

Substitution of Equation 5.20 in Equation 5.19 and integration of the concentration gradient with respect to the above boundary conditions, gives:

$$\frac{C^{permeate}}{C^{feed}} = \frac{[\{K_c - Y\}\emptyset] exp(Pe^*)}{\{K_c - Y\}\emptyset - 1 + exp(Pe^*)} \quad \textbf{5.21}$$

By the substitution of Equation 5.21 into the normal definition of solute rejection, then:

$$R = 1 - \frac{C^{permeate}}{C^{feed}} = 1 - \frac{\{K_c - Y\}\emptyset}{1 - [1 - \{K_c - Y\}\emptyset] exp(Pe^*)} \quad \textbf{5.22}$$

Here, (Pe^*) represents a modified Peclet number, which can be defined as follows:

$$Pe^* = \frac{\{K_c - Y\} r_p^2 P}{8\mu D_p} \quad \textbf{5.23}$$

By using Microsoft's spreadsheet *solver*™ add-in, Microsoft Excel™ and substituting Equations (5.5), (5.6), (5.7), (5.8), (5.9), (5.10) , (5.20) and (5.23) in Equation (5.22) and solved to determine the effective pore radius of the Titania nanofiltration membrane based on the resulted rejection value of the glucose (see Figure 5.2).

The estimated result of the effective pore radius for the present nanofiltration membrane from using the uncharged solute hydrodynamic model was found to be equal to 0.74 nm.

By comparing the estimated effective pore radius for the TiO_2 membrane for both models used in the present work, it can be seen that both results were very similar. However according to Bowen et al. [152] who proposed both the above models, the predictive Donnan steric pore partitioning model (DSPM) has proved to be very successful in the characterisation of NF membranes in which the rejection data are analysed as a function of volumetric flux. As a result, many researchers such as [152], [167], [156] used this method to determine the effective pore radius but for different types of NF membranes.

The present work also adopted the estimated effective pore radius (r_p) that has been determined based on the Donnan steric pore partitioning model (0.68×10^{-9} m) for the following reasons: It can be seen from Equations 5.22 and 5.23 that the rejection of the uncharged solute depends on the applied pressure only, with ignoring the effects of membrane thickness (Δx) on rejection.

In the DSPM model, the rejection data are analysed as a function of volumetric flux and are dependent on two main parameters: the effective pore radius (r_p) and the effective ratio of membrane thickness to porosity ($\Delta x/A_k$) whereas the uncharged solute hydrodynamic model depends mainly on (r_p).

As mentioned before, Equation 5.20 and Equation 5.22 were based on the assumption that the dimensionless group (Y) was considered to be independent on the solute concentration, with further assumptions for (V_S) and (D_p) (which is an important parameter in Equation 5.23) which will be independent on the solute concentration, and that is absolutely incorrect. In the meantime, by comparing these assumptions with the DSPM model, this means that the first term from the ENP equation which is related to the concentration gradient was ignored.

Furthermore, the prediction model of ion transport through the present work's Titania membrane will be based on using the DSPM model.

5.3 Estimation of Donnan potential

This section can be divided into three main sections; the first one is related to the estimation of the membrane surface charge density while the second and third parts are related to the estimation of the effective membrane fixed charge density and the Donnan potential respectively.

5.3.1 Membrane surface charge density estimation

Although zeta potential (the membrane / electrolyte interface parameter) is more widely used for electrokientic characterisation, the electrokientic surface charge density (σ^d) or net surface charge density at the plane shear can be obtained from the zeta potential data based on the Gouy-Chapman theory.

Based on the electrical double layer and in the case of relatively low potential (less than 50 mV) [17], the relationship between the surface charge density at the hydrodynamic shear plane and the zeta potential is given in Equation (2.28).

The Debye length (K^{-1}) value for 1:1 electrolytes (such as NaCl) can be calculated from the simplified Graham equation (see section 2.4.5). The membrane surface charge density can then be obtained from the Graham equation by substituting the values of zeta potential that were already estimated for each pH number (see Table 4.1) and (K^{-1}) value at 0.01 M NaCl.

Table (5.1) shows the calculated surface charge density (σ^d) in (mC/m^2) over a range of pH values from (3.0 – 9.0) by using 0.01 M NaCl as a background electrolyte for a 1 nm ceramic TiO_2 NF membrane.

Table 5.1: Membrane surface charge density, effective membrane charge, and Donnan potential at pH from 3 to 9 determined from zeta potential measurements for background electrolyte fixed at 0.01M NaCl.

pH	Membrane surface charge density (mC/m^2)	Effective membrane charge (mol/m^3)	Donnan potential (mV)
3.0	**+ 5.55**	**+ 170.09**	**+ 2.26**
3.5	**+ 2.42**	**+ 73.76**	**+ 0.98**
4.0	**− 1.52**	**− 46.33**	**− 0.61**
4.5	**− 2.22**	**− 67.67**	**− 0.89**
5.0	**− 3.21**	**− 98.15**	**− 1.30**
6.0	**− 4.97**	**− 151.49**	**− 2.01**
7.0	**− 5.85**	**− 178.32**	**− 2.37**
8.0	**− 7.02**	**− 213.98**	**− 2.85**
9.0	**− 8.19**	**− 249.65**	**− 3.32**

The membrane zeta potentials which can be determined from electrokinetic measurements gives information about the net charge of the surface and thereby, about the charge distribution inside the electrochemical double layer. This net membrane charge density (σ^d) can be estimated from zeta potential data based on the theory of Gouy-Chapman and Graham equations.

The results from Table (5.1) show that as the pH values increase, the surface charge density becomes more negative being found at a pH of 9 which is equal to -8.19 ($\mathrm{mC/m^2}$), whereas, at a pH of 3 the surface charge density becomes positive with a magnitude of 5.55 ($\mathrm{mC/m^2}$), which is exactly the same behaviour of the related zeta potential.

The results also show that for the pH values from 9 to 4, there is significant drop in the net surface charge values from $-8.193\ \mathrm{mC/m^2}$ to $-1.520\ \mathrm{mC/m^2}$ which would reflect the effect of pH on the results of the surface charge density.

The estimated membrane surface charge density obtained from the present work is in a good agreement with the previous work done by Hurwitz et al. [129].

Hurwitz et al. [129] results showed that for zeta potential of 20.6 mV, the related surface charge density was equal to $5.0\ \mathrm{mC/m^2}$, whereas in the present work, for a measured membrane zeta potential of 24.317 mV, the related estimated membrane surface charge density was equal to $5.55\ \mathrm{mC/m^2}$, and that can confirm the consistency in results between the obtained results of this work compared with Hurwitz et al.'s work.

This agreement in results between the above two studies means that there were also agreements in other important calculated parameters such as the Debye length (K^{-1}) value for 1:1 electrolytes, which was originally determined in this work based on a simplified Graham equation and represents the thickness of the diffuse layer in the electrical double layer theory.

5.3.2 Effective membrane charge estimation

The membrane surface charge density (σ^d) or net surface charge density at the plane shear was determined based on the Gouy-Chapman and Graham equations. So, the determined membrane surface charge can be subsequently converted to concentration units by using Equation (2.32).

The effective membrane fixed charge density (X^m) represents the concentration of electrical charged groups on the membrane surface in ($\mathrm{mol.\,m^{-3}}$).

Equation (2.32) assumes that the membrane surface charge is uniformly distributed in the void volume of cylindrical pores. In this equation, the effective membrane pore radius (r_p) for the ceramic Titania nanofiltration membrane used in this work is equal to 0.68 nm (based on pore radius estimated from DSPM model, see section 5.2).

Table (5.1) shows a calculated effective charge density X^m in ($\mathrm{mol.\,m^{-3}}$) over a range of pH values from (3.0 – 9.0) by using 0.01 M NaCl as a background electrolyte for a 1 nm ceramic TiO_2 NF membrane. In order to estimate the effective charge density X^m for the membrane in ($\mathrm{mol.\,m^{-3}}$), the determined membrane surface charge should be subsequently converted to concentration units. This can be done by assuming that the membrane surface charge is uniformly distributed in the void volume of the cylindrical pores.

The membrane effective charge is actually representing the concentration of electrical charged groups on the membrane surface in ($\mathrm{mol.\,m^{-3}}$).

The results from Table (5.1) show that at pH of 3.0, the effective membrane charge was equal to 170.09 $\mathrm{mol.\,m^{-3}}$ related to surface charge density of 5.55 $\mathrm{mC/m^2}$. It can be easily realised that this parameter is also dependant on pH magnitude.

5.3.3 Donnan potential estimation

The Donnan potential or the potential at the membrane-solution interface can occur as a result of the difference in ionic concentrations in membrane pores to those in the bulk solution.

Equilibrium occurs between the membrane and solution due to the presence of the effective membrane charge density in order to achieve electroneutrality (for every removed anion, one cation must be removed).

The ions repulsion at the surface of a charged membrane can be described by the Donnan potential [70].

When a charged membrane is coming in contact with a salt solution, equilibrium occurs between the membrane and solution due to the presence of the effective membrane charge density, based on the fact that the ionic concentrations in the membrane are not equal to these in the bulk solution.

The determination of the Donnan potential for each membrane type, pH and electrolyte concentration are very important especially in the modelling of the

transport performance in a NF membrane since all the available partitioning models were based on the values of the Donnan potential.

In the present work, the Donnan potential values in (mV) were estimated from Chein formalism (see Equation 2.37) based on the values of the effective membrane charge X^m in (mol. m^{-3}) for bulk concentration $C_{i,bulk}$ of 0.01 M NaCl solution.

Table (5.1) shows the estimated Donnan potential in (mV) determined from the effective membrane charge over a range of pH values from (3.0 – 9.0) by using 0.01 M NaCl as a background electrolyte for a 1 nm ceramic TiO_2 NF membrane.

Results from Table (5.1) show that as pH values increase, the Donnan potential becomes more negative (at pH of 9.0 is equal to − 3.32 mV), whereas at a pH of 3.0, the Donnan potential becomes positive with a magnitude of + 2.26 mV, which reflects the effect of pH on the Donnan potential.

Also, the results show that for the pH values from 9 to 4, there is a significant drop in the estimated Donnan potential values from – 3.32 mV to − 0.61 mV.

The estimated Donnan potential values obtained from the present work are in consistent with the previous work done by Pivonka et al. [168]. The results from this work show that; at same background electrolyte concentration of 0.01 M and at normal pH; the Donnan potential values for cations and anions are equal to −5.43 (mV) and −2.96 (mV) respectively.

The Donnan potential is mainly dependant on salt bulk feed concentration, effective fixed charge concentration in the membrane (X^m), and valence of both counter and co- ions.

All these parameters exist in Equation (2.37), thus by applying this equation, a direct value for the Donnan potential can be obtained, whereas the estimation of the Donnan potential values from the other two Equations (2.33) and (2.34) required conducting an experiment to estimate the ion concentration (such as Na^+ or Cl^- in the case of using a NaCl solution as a background electrolyte) in the bulk and permeate side, which may lead to obtaining two different values for the Donnan potential due to the difference in rejection for each ion, which is obviously incorrect.

5.4 Interface partitioning models

For the purpose of describing the rejection performance of NF membranes, the literatures showed the existence of two main models, which are, the Kedem-Spiegler model (KSM) and Donnan equilibrium models [137], [169].

The Kedem-Spiegler model normally depends on the irreversible thermodynamic of the membrane. This model was initially applied for RO membranes and for a single salt solution [169]. In this model the membrane is assumed as a black box and can be characterised only in terms of solute permeability. The assessment of ions transport by (KSM) is conducted without any information related to membrane structure [18]. Hussain et al. [137] showed that these types of models are only effective at high rejection rates of solutes and fail to describe the ion transportation at low rejection rates.

Donnan distribution models belong to mechanistic models which are more interested in membrane structure and the chemical and physical effects of the membrane and electrolyte solutions. This type of model can be used to predict the ion transportation across the membrane based on convective, electric and diffusive transport. In the mean time, it can also provide more information about membrane charge, thickness and effective pore size. Therefore, these types of models can give a better understanding of the main mechanisms and parameters that could govern the transport in NF membranes.

In order to describe the mass transport inside the active skin layer of NF membranes, the extended Nernst-Planck (ENP) equation is the most efficient and commonly used.

Solving the ENP equation requires knowing the boundary conditions at the pore inlet (feed side) and outlet (permeate side). For a NF membrane, the present work discussed the two most common models that have normally been used to evaluate the boundary conditions at membrane-interface partitioning.

The rejection in nanofiltration membranes is often modelled by using the following three steps model [171] as shown in Figure (5.3):

- The partitioning distribution between the bulk at the feed side and the pore entrance (step 1).
- The transport inside the pore is described with the extended Nernst-Planck equation (step 2).
- The partitioning distribution is again applied at the permeate side (step 3).

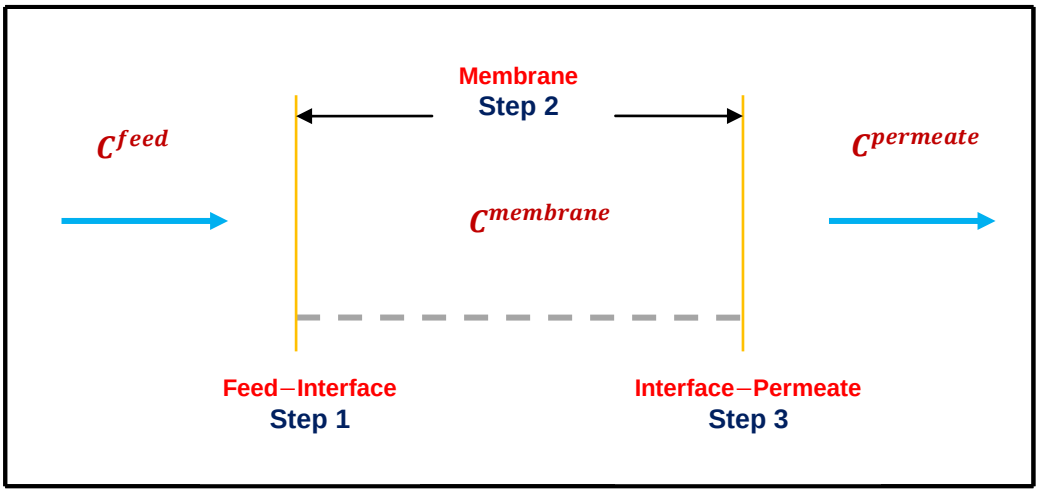

Figure 5.3: Schematic diagram of partitioning in feed and permeate interface.

The ion partitioning distribution between the bulk solution and the pore (step 1) and the ion partitioning distribution at the permeate side (step 2) can be influenced by several parameters such as the Donnan equilibrium and steric partitioning [172], [173].

5.4.1 Donnan equilibrium distribution model

The transport equation was initially coupled with the so- called Donnan equilibrium by Bowen and Mukhtar [162].

This model assumed that all the ions freely penetrate the membrane, and because of the membrane charge, a potential difference relative to the external bulk electrolyte must be established in order to satisfy the electroneutrality condition.

According to Boltzmann distribution, ion concentration c_i^m can be expressed as:

$$c_i^m = \frac{\gamma_{i,sol}}{\gamma_{i,pore}} C_i^{feed} exp\left(-\frac{z_i F}{R_g T}\psi_{Don}\right) \quad \textbf{5.24}$$

Where:

c_i^m: Concentration of ion i in membrane (mol. m^{-3}).

C_i^{feed}: Concentration of ion i in the bulk (mol. m^{-3}).

z_i: Valence of ion i (dimensionless).

F: Faraday constant (96487 C. mol^{-1}).

R_g: Universal gas constant (8.314 J. mol^{-1}. K^{-1}).

T: Absolute temperature (K).

ψ_{Don}: Donnan potential (V).

$\gamma_{i,sol}$: Activity coefficient of ion i in the solution side of the interface (dimensionless).

$\gamma_{i,pore}$: Activity coefficient of ion i in the pore side of the interface (dimensionless).

The activity coefficients can be calculated according to the extended law of the Debye-Huckel theory by using the well-known Davies equation that is related to the ionic strength of the solution to the activity coefficient through the following semi-empirical relationship [174]:

$$ln(\gamma_i) = Az_i^2\left(\frac{\sqrt{I}}{1+\sqrt{I}} - 0.3\,I\right) \quad \textbf{5.25}$$

Here, (I) represents the ionic strength (see Equation 2.30) and the temperature dependent parameter (A) is given by:

$$A = \frac{e^3.N_A^{1/2}}{ln10(4\pi)\sqrt{2(\varepsilon_\circ\varepsilon_r k_b T)^{3/2}}} \quad \textbf{5.26}$$

Where:

e : Electronic charge, (1.602×10^{-19} C).

N_A: Avogadro number.

k_b: Boltzmann constant.

$\varepsilon_\circ$: is the permittivity of free space.

ε_r: is the relative permittivity of water

Equation (5.25) can be used to calculate the activity coefficients both in the solution and inside the membrane by using an adequate ion concentration.

The activity coefficient of ion i inside the membrane pore can be estimated based on the average concentration inside the pore, which can be defined as [141]:

$$c_{i,avg} = \frac{c_{i,(x=0)} - c_{i,(x=\Delta x)}}{2} \quad \textbf{5.27}$$

$c_{i,(x=0)}$: Concentration of ion i at feed-membrane interface.

$c_{i,(x=\Delta x)}$: Concentration of ion i at membrane-permeate interface.

Many authors assumed that for diluted solutions, the activity coefficients ratio for a certain ion in the solution to that in pore side of the interface (as shown in Equation 5.24) is equal to one (unity) [162], [137], [155].

5.4.2 Donnan steric pore partitioning model (DSPM)

The Donnan steric pore partitioning model improves the partitioning between the bulk solution and the solution in membrane pores by taking into account the steric effect which was developed by Bowen and Mukhtar [162]. The DSPM model was originally based on the fixed charge theory proposed by Teorell, Meyer and Sievers [71].

According to many researchers such as Labbez et al. [158] and Wang et al. [53], the DSPM has been shown to be successful in the prediction of a nanofiltration membrane's performance.

In this model, the transportation of ions inside NF membrane can be described based on the extended Nernst-Planck (ENP) equation and membrane equilibrium partitioning. The original Nernst-Planck equation is modified to include the hindered transport and the membrane equilibrium partitioning resulted from the combination of electrical (Donnan) and steric (sieving) mechanisms.

The mathematical derivation of the DSPM model is based on the following essential assumptions [175], [176], 177]:

- The porous membrane is considered to consist of a parallel association (or bundle) of identical straight cylindrical pores.
- The effective membrane volume charge density is constant in the axial direction and mainly controlled by feed concentration.
- The effective membrane volume charge is assumed to be sufficiently small and the salt solutions are sufficiently diluted in order to consider that both electrical potential and ion concentrations are radially constant.
- Since solutions are considered to be diluted, then the difference between various average velocities (mass, molar and volume) and any coupling that might arise from the motion of ions can be ignored. Also, the ion activities can be replaced by a concentration.
- The main components of a DSPM model (including: ion concentration, permeate volume flux and electrical potential) are all defined in terms of average quantities.
- The separation at the pore interface is only due to Donnan and steric effects taking in consideration ignoring the effect of dielectric interaction.

According to the DSPM model, the concentration of ion i at feed-membrane interface can be estimated as follows:

$$c_{i(x=0)}^{m} = \frac{\gamma_{i,sol}}{\gamma_{i,pore}} \emptyset_i C_i^{feed} exp\left(-\frac{z_i F}{R_g T} \psi_{Don}\right) \quad \textbf{5.28}$$

Here ($\emptyset_i$) represents the steric partitioning coefficient of ion i.

This partitioning term can be defined as the ratio between the available section (i.e. taking into account the zone inside the pore) and the pore cross section.

Furthermore, the concentration of ion i at membrane−permeate interface in DSPM model can be expressed as follows:

$$C_i^{permeate} = \frac{\gamma_{i,pore}}{\gamma_{i,sol}} \frac{c_{i(x=\Delta x)}^{m}}{\emptyset_i exp\left(-\frac{z_i F}{R_g T} \psi_{Don}\right)} \quad \textbf{5.29}$$

The characterisation of a NF membrane using DSPM is normally analysed as a function of permeates volume flux and salts rejection data.

The assessment of ions transport through nanofiltration membranes based on a DSPM model depends on the following three main parameters:

- Effective pore radius (r_p).
- Equivalent thickness of the membrane active layer (Δx_e).
- Effective membrane surface charge density (X^m)

This predictive model has proved to be successful in predicting a single system such as organic molecules and univalent electrolytes [137], [155], [178].

5.5 Numerical solution of the transport model

There are several approaches proposed in the literature to describe the mass transport through nanofiltration membranes but the approach based on the extended Nernst-Planck (ENP) equation is the most commonly used due to the effective representation that this equation could give.

When the extended Nernst-Planck (ENP) equation is applied to a membrane pore, the hindrance factors are used to correct the diffusion coefficient [130].

The ionic concentration gradient within the pore (dc_i^m/dx) can be obtained by assuming that all partitioning effects are located at the feed-membrane and membrane-permeate interfaces. The substitution of Equation (5.5) in Equation (5.1) and the rearrangement yields [153], [140], [162]:

$$\frac{dc_i^m}{dx} = \frac{J_v}{D_{i,p}A_k}(K_{i,c}c_i^m - C_i^{permeate}) - \frac{z_i c_i^m}{R_g T} F \frac{d\psi^m}{dx} \qquad \textbf{5.30}$$

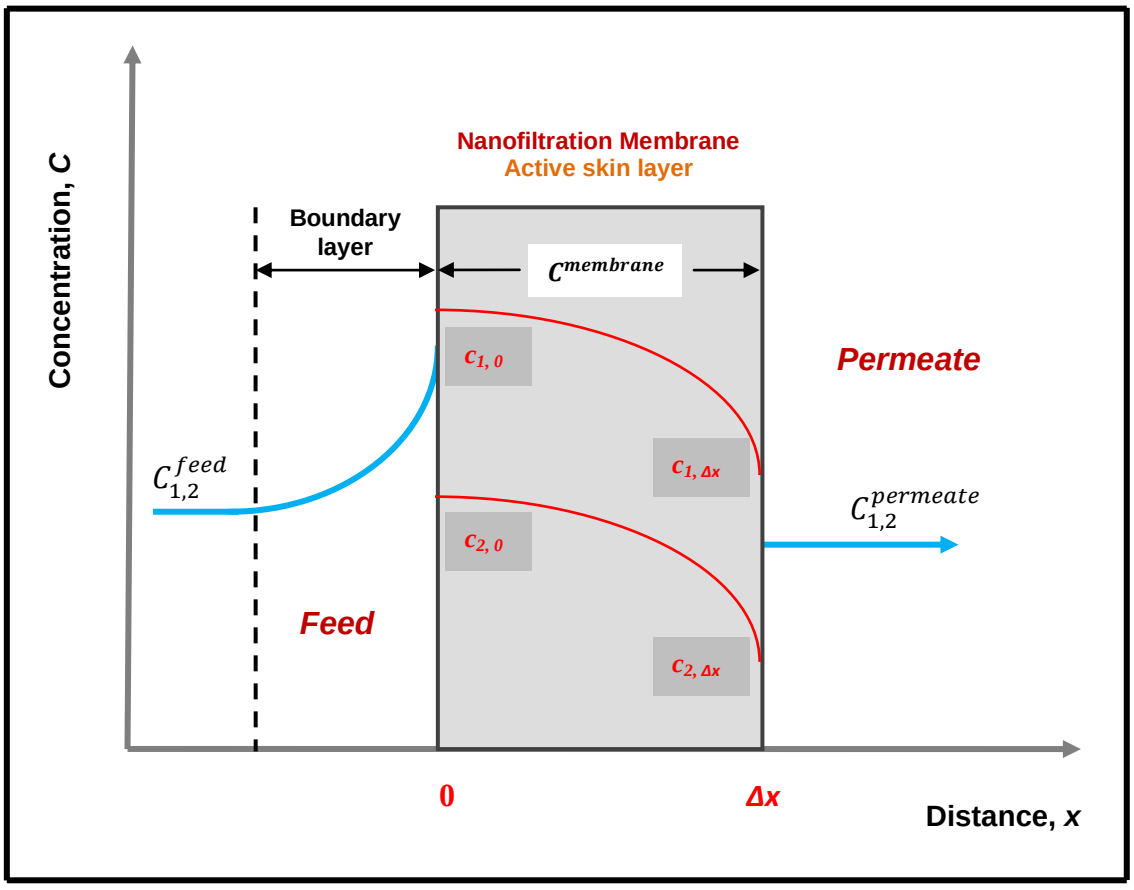

Figure 5.4: Schematic of ions transport in nanofiltration membranes.

The electro-neutrality condition inside pores is given by:

$$\sum_{i=1}^{n} z_i c_i^m = -X^m \quad \textbf{5.31}$$

For $0 \leq X^m \geq \Delta x$ (where X^m represents the membrane volume charge density).

Furthermore, in an external bulk solution, the condition of electric-neutrality is expressed as follows:

$$\sum_{i=1}^{n} z_i c_i^b = 0 \quad \textbf{5.32}$$

And for no overall electrical current passing through the membrane:

$$I = \sum_{i=1}^{n} F z_i J_i = 0 \quad \textbf{5.33}$$

The axial potential gradient inside pores ($d\psi^m/dx$), can be derived from equations (5.33), (5.31), and (5.30) as follows:

$$\frac{d\psi^m}{dx} = \frac{\sum_{i=1}^{n} \frac{z_i J_v}{D_{i,p}} (K_{i,c} c_i^m - C_i^{permrate})}{\frac{F}{R_g T} \sum_{i=1}^{n} z_i c_i^m} \quad \textbf{5.34}$$

Based on interface membrane partitioning models, Equation (5.30) and Equation (5.34) can be solved with the following boundary conditions:

$x = 0 \rightarrow c_i^m = C_i^{feed}$

$x = \Delta x \rightarrow c_i^m = C_i^{permeate}$

Then, the rejection of ion i can be determined from the following equation:

$$R_i = 1 - \frac{C_i^{permeate}}{C_i^{feed}} \quad \textbf{5.35}$$

In the present work, the DSPM model was used to assess the permeate volume fluxes and the rejection of a 0.01 M NaCl solution in a commercial ceramic NF membrane.

Figure (5.4) shows a schematic diagram of ions transport in nanofiltration membranes.

The numerical solution of Equations (5.30), (5.34), (5.28) and (5.29) indicated that for each ion there are main physio-chemical parameters which need to be identified, they are: hindered coefficient for diffusion ($K_{i,d}$), hindered coefficient for convection ($K_{i,c}$), the ratio of stocks radius to the effective pore radius (λ_i), hindered diffusivity ($D_{i,p}$) and steric coefficient ($\emptyset_i$).

The estimation of all these parameters values were related to the estimated effective

pore radius of a TiO_2 NF membrane (see section 5.2).

All these parameters can be determined by the substitutions of the estimated effective membrane pore radius (r_p = 0.68 nm) in Equations 5.5, 5.6, 5.7, 5.8, 5.9 and 5.10 (or 5.11 and 5.12). Table (5.2) shows the ionic properties with hindrance factors and steric coefficients for each ion used in the present work.

The programme was run by using (0.01 M) sodium chloride solutions as a feed concentration for different permeate volume flux (m/s) at each pressure step from 1.0 to 5.0 bars.

As a verification case study to simulate the original DSPM model, the present work used the (0.01 M) sodium chloride solute as a reference solution depending on the real rejection of this solute in the Titania NF membrane.

Solving the present DSPM model was done based on the following assumptions:

- Since the present work deals with diluted salts at very low concentrations (less than 0.1 M), therefore; the effect of osmotic pressure can be ignored [162]. At high salt concentration, the osmotic pressure can be a very important parameter that can lead to permeate volume flux decline especially when compared with pure water flux.
- Since the solutions were assumed to be at infinitely diluted, thus the activity coefficients of ions along the pore is very low, therefore; the activity coefficients at the solution and at the pore side of the interface were considered as unity [20].
- The effective charge density (or surface potential) is constant throughout the NF membrane and depends only on the concentration of the feed solution.
- The difference in viscosity between the bulk solution and the solution inside the membrane pores is negligible [137].
- Concentration polarisation across the surface of the membrane is neglected [137].

Table 5.2: Ionic properties with hindrance factors and steric coefficients (for an estimated effective membrane pore radius equals to 0.68 nm)

Ionic type	*Diffusivity at infinite dilution [155], [149]* $(D_{i,\infty})$ $(\mathbf{m/s}) \times \mathbf{10^{-9}}$	*Stokes radius [155], [37]* (r_i) $(\mathbf{m}) \times \mathbf{10^{-9}}$	*Ratio of Stokes radius to effective pore radius* $(\lambda_i = r_i/r_p)$ **(dimensionless)**	*Hindered coefficient for diffusion* $(K_{i,d})$ **(dimensionless)**	*Hindered coefficient for convection* $(K_{i,c})$ **(dimensionless)**	*Steric coefficient* $(\emptyset_i)$ **(dimensionless)**	*Hindered diffusivity* $(D_{i,p})$ $(\mathbf{m^2/s}) \times \mathbf{10^{-9}}$
$\mathbf{Na^{+1}}$	1.333	0.184	0.270	0.456	0.925	0.531	0.606
$\mathbf{Cl^{-1}}$	2.031	0.120	0.177	0.644	0.942	0.672	1.307

Equations (5.30), (5.34), (5.28) and (5.29) were solved numerically by applying the *forth order Range-Kutta method* (*with adjustable step size technique*) using FORTRAN programme codes (F95) in order to solve the one-dimensional first order ordinary differential equation (ODE) to describe the changes in ionic concentration inside the active skin layer of the present ceramic TiO_2 NF membrane.

The present work chose to write the mathematical model using FORTRAN codes because this language is easy to learn, most common, useful in solving mathematic and scientific problems and also this language is very efficient when high accuracy is required [179], [180].

Figure (5.5) shows the algorithm developed for solving the equations of the present work's ions transport model where the flowchart graphically explains the modelling process pathway. In this figure it can be seen that the structure of the programme includes three main parts: model input, internal calculation, and output.

The estimation of the effective membrane pore radius (r_p) was used to determine the main membrane physio-chemical parameters while the estimation of the effective membrane active layer thickness (Δx) based on the DSPM model was used to determine the equivalent effective membrane active layer thickness (Δx_e) which can be defined as the ratio of the effective membrane thickness to the membrane surface porosity (A_k) [181], [151].

The estimation of the Donnan potential was based on the estimated membrane zeta potential and effective charge density as a result of measured streaming potential using the same sodium chloride concentration as above.

The numerical solution of the DSPM model was conducted according to the following algorithm:

- Input the effective membrane pore radius (r_p).
- Input the ions physio-chemical parameters: hindered coefficient factor of convection $(K_{i,c})$, hindered coefficient factor of diffusion $(K_{i,d})$, and hindered diffusivity $(D_{i,p})$.
- Input the estimated steric coefficient $(\emptyset_i)$ for each ion.
- Input the equivalent thickness of the membrane active layer (Δx_e).
- Input the estimated membrane Donnan potential.
- Input the operating parameters: ionic bulk concentration (C_{bulk}), permeate flux (J_V), number of ionic species, and temperature.

- Input the numerical parameters: number of steps (or iteration) 300, under-relaxation factor (0.8), and error ratio (less than or equal to 10^{-3}).
- Initialise (c_i^m) for each ion at feed-membrane interface using Equation (5.28).
- Since the permeate concentration ($C_i^{permeate}$) must be initialised, the present work assumes that the initial permeate concentration is equal to the bulk concentration.
- Estimate the electrical potential gradient of each ion in the solute inside the pore ($d\psi^m/dx$) using Equation (5.34).
- Estimate the concentration gradient of each ion in the solute within the pore (dc_i^m/dx) iteratively after the estimated electrical potential gradient of the ion within the pore is substituted in Equation (5.30).
- The ionic concentration gradient inside the membrane active skin layer for each ion changes from ($c_{x=0}^m$) (at feed-membrane interface) to ($c_{x=\Delta x_e}^m$) (at membrane-permeate interface).
- The $\left(c_{x=\Delta x_e}^m\right)$ represents the ionic final concentration at the maximum iteration number based on the estimated equivalent effective membrane active layer thickness.
- The new permeate concentration ($C_{i,new}^{perm}$) of each selected ion was determined when the ionic final concentration $\left(c_{x=\Delta x_e}^m\right)$ was substituted in Equation (5.29).
- For each ion, the change ratio between the new permeate concentration and the assumed old permeate concentration at the beginning of the programme was estimated as follows:

$$ratio_i = \frac{C_{i,old}^{perm} - C_{i,new}^{perm}}{C_{i,old}^{perm}}$$

- If the error in the above ratio was less than (or equal to) 10^{-3}, then; end the programme and estimate the rejection of each ion for each solute flux based on its feed concentration from Equation (5.35).
- In case of not achieving the above error condition, then; use the under relaxation factor for each ion to correct and recalculate the new permeate concentration in the following relation and continue solving:

$$C_{i,new}^{perm} = relax \times C_{i,old}^{perm} + (1 - relax) \times C_{i,new}^{perm}$$

- The rejection (R %) of each ion can be estimated directly from the programme without any further calculations.
- The average calculation time for integrating the ordinary differential model programmed using (FORTRAN/95) codes in Pentium IV (2.4 GHz, 4 GB RAM and 500 HDD) was 3 seconds.

The Runge-Kutta method normally deals with a specified number of sequenced steps with equally spaced intervals. For many scientific researchers, the fourth order Rung-Kutta method is quite competitive, especially when combined with an adjustable step size technique. This method can be used to integrate the ODE at highly acceptable accuracy [182], [180], [179].

The concentration of ions as a function of the membrane active skin layer thickness in the present FORTRAN program is changed from $C(i,1)$ to $C(i,k+1)$ where i and k represent the number of variables and the adjusted steps size value respectively.

In this work, the step size (h) mainly depends on equivalent membrane active layer thickness and the selected number of steps (N_{steps}) as shown in the following:

$$h = \frac{(X_2 - X_1)}{N_{steps}}$$

Here, (X_2) and (X_1) represent the equivalent membrane active layer thickness at $(X = \Delta x)$ and at $(X = 0)$ respectively.

Table (5.3) shows the main DSPM model parameters that have been used in the present work, while Table (5.4) shows the main parameters used in the present work and the techniques used to assess them.

In this work, a computer programme has been proposed based on the original DSPM model for describing the one-dimensional transport of a reference solution of sodium chloride 0.01 M (as a univalent single solute) through nanoporous media.

In this computer programme the ENP equations are solved inside the porous active layer of the commercial titanium dioxide ceramic NF membrane. (The FORTRAN programme codes can be found in Appendix 1 of this work)

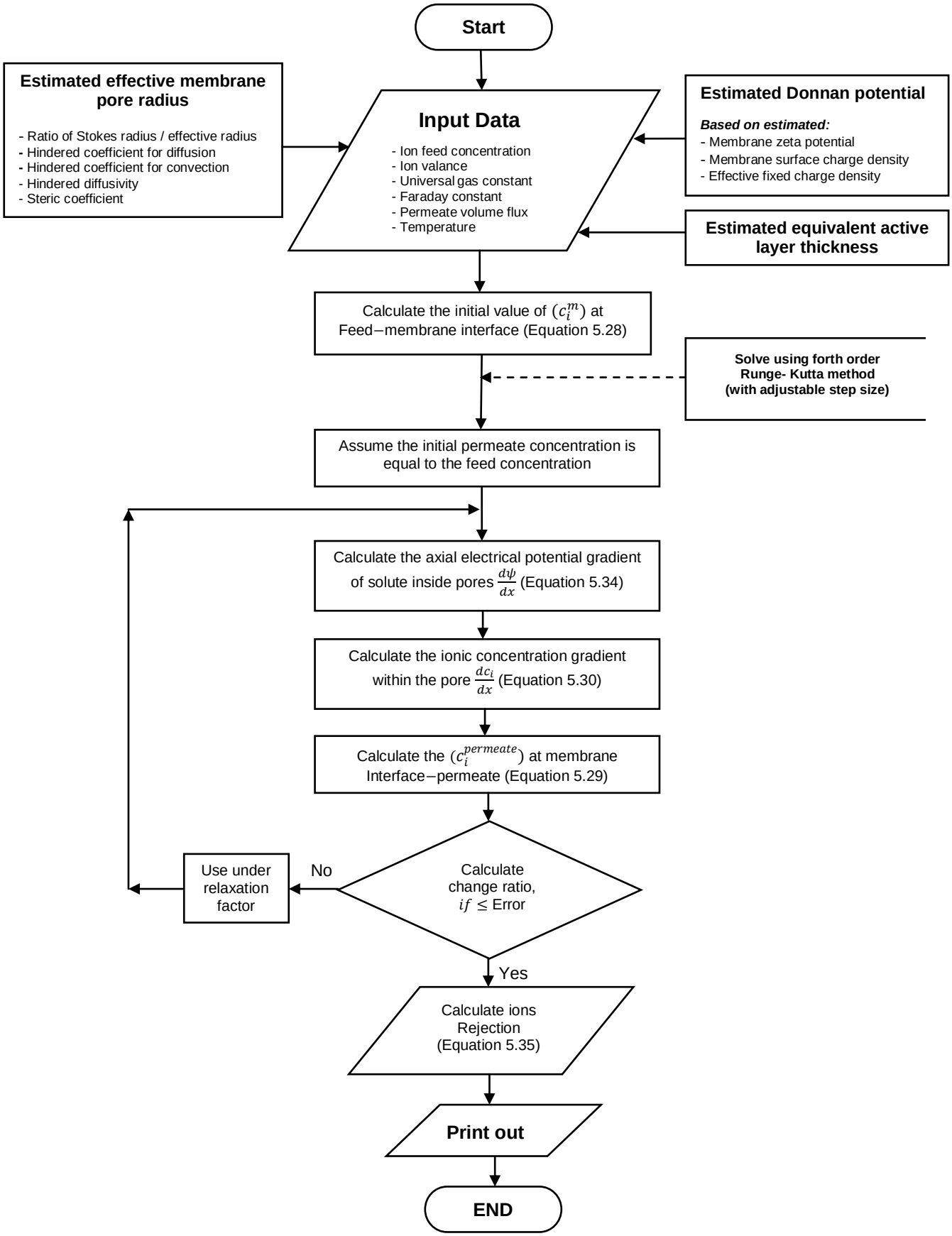

Figure 5.5: Algorithm developed for solving the ions transport model.

Table 5.3: Model main parameters.

Salt	NaCl
Bulk concentration	$0.01\ (\mathrm{M})$
Membrane effective pore radius	$0.68\ (\mathrm{nm})$
Effective membrane active layer thickness	$3.256 \times 10^{-6}\ (\mathrm{m})$
Surface porosity	0.4
Equivalent membrane active layer thickness	$8.14 \times 10^{-6}\ (\mathrm{m})$
Permeate volume flux	$2.34 - 7.96 \times 10^{-6}\ (\mathrm{m^3/m^2.s})$
Trans-membrane pressure	$1.0 - 5.0\ (\mathrm{bar})$
Temperature	$298\ (\mathrm{K})$
pH	6.2
Activity coefficients	1.0
Osmotic pressure	1.0
Faraday constant	$96487\ (\mathrm{C.mol^{-1}})$
Universal gas constant	$8.314\ (\mathrm{J.mol^{-1}.K^{-1}})$
Viscosity	$0.89 \times 10^{-3}\ (\mathrm{Pa.s})$
Membrane charge density	$-4.97\ (\mathrm{mC/m^2})$
Donnan potential	$-2.01\ (\mathrm{mV})$

Table 5.4: Model main parameters and the techniques used to assess them.

Parameters	Characterisation method
Membrane effective pore radius	Rejection of uncharged solute (glucose)
Membrane effective thickness	Calculated from effective pore radius value and Hagen−Poiseuille equation
Equivalent membrane thickness	Estimated from effective membrane thickness and surface porosity
Donnan potential	Estimated membrane zeta potential, surface and effective membrane charge density
Steric coefficient	Calculated from Stokes−Einstein formula and effective pore radius
Permeate volume flux	Experimental work of the present study
Initial ions feed concentrations	Experimental work of the present study
Membrane surface Porosity	Manufacturer

5.5.1 Model results

The simulated results of the sodium and chloride ions concentrations versus (x) steps inside the membrane active skin layer of the titanium dioxide ceramic NF membrane based on a selected number of steps can be seen in Figures 5.6 and 5.7 respectively.

As can be observed from these Figures 5.6 and 5.7, the concentrations of both sodium and chloride ions decreased as both ions passed through the membrane active layer thickness (towards the outer permeate side). It also can be seen from these Figures that the concentration of chloride ions inside the membrane active skin layer was slightly higher than that of sodium ions.

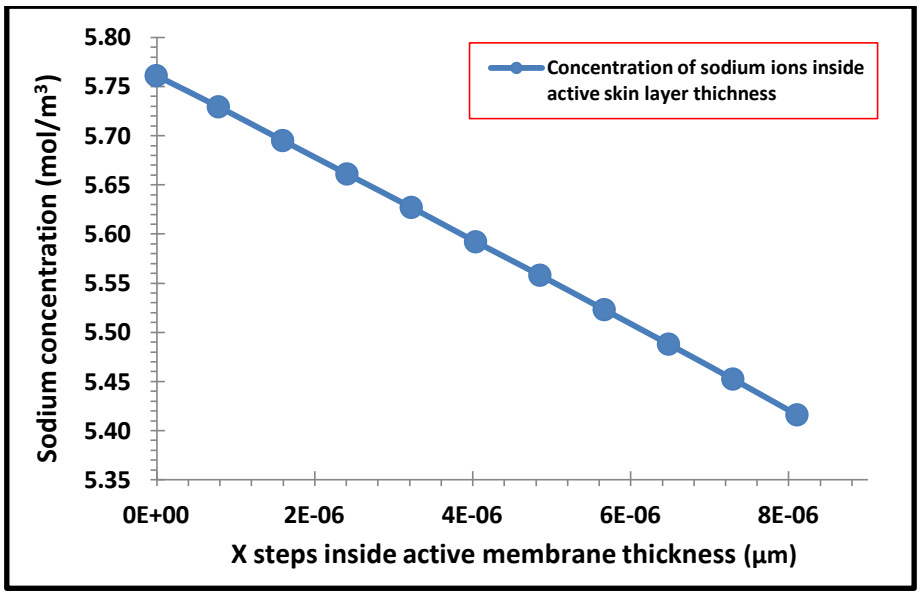

Figure 5.6: Concentration of sodium ions (mol/m^3) vs. (X) steps inside membrane active layer.

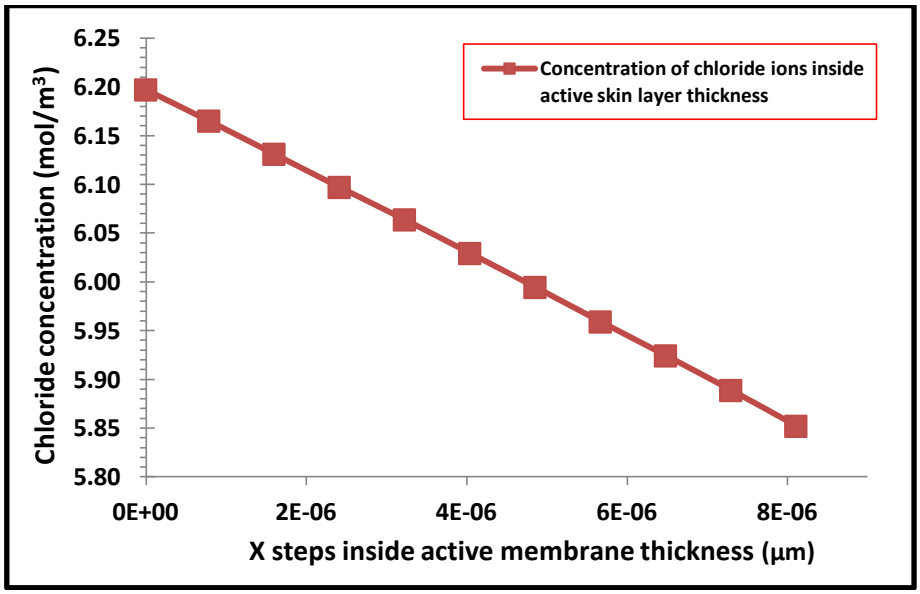

Figure 5.7: Concentration of chloride ions (mol/m^3) vs. (X) steps inside membrane active layer.

Regarding the concentrations of sodium and chloride ions, it is worthwhile to note that the obtained results show that there are no big shifts between the two ions. This could reflect the same behaviour that was already observed in the results of the experimental work for the rejection of sodium chloride solutes (see section 4.3.2).

As mentioned previously, the present work chose the number of steps (or nodes) to be equal to 300; this number was selected in order to gain further details to describe the transfer of sodium chloride solute inside the equivalent active skin layer thickness (as shown in Figures 5.6 and 5.7) and to ensure that the predicted ions concentration cover the estimated range of the equivalent active skin layer thickness of the present titania membrane. It is worthwhile to mention that the number of nodes do not change the model results.

From Figures 5.6 and 5.7, it can be seen that the concentrations of (Na^{+1}) and (Cl^{-1}) ions inside the estimated equivalent active skin layer thickness of 8.1 μm decreased as both ions moved towards the outer permeate side. Also, it can be noted that the concentration of sodium ions inside the membrane was lower than that of chloride ions.

The obtained results which were related to the decreases in ions concentrations as the ions passed through the membrane active layer thickness (from the feed side towards the outer permeate side) are supported by theory and in agreement with the results reported by Bowen et al. [162], [155] and that of Geraldes and Ana Maria [181].

Predictive results from the present model were compared with the actual experimental conditions of a 0.01M sodium chloride solute at a different permeate volume flux.

The permeate volume flux measurements of ($NaCl$) solution in (m/s) were already estimated based on the area of the present ceramic titanium dioxide NF membrane (see section 3.2).

Regarding to the rejection of (Na^{+1}) ions (see Figure 5.8), it can be seen that the results obtained from the numerical solution of the DSPM model indicate that the rejection of sodium ions was gradually increased as the permeate volume flux increased.

At the highest permeate volume flux (at applied pressure of 5.0 bars), Figure (5.8) shows the rejection value (R %) of sodium ions was 5.93%. Such behaviour is fully supported by theory [4], [51], [162]. For further details on this behaviour see section 2.3.3 of this work (transport theory of NF membrane).

Figure 5.8 shows the numerically simulated results for the rejection (R %) of (Na^{+1}) ions in the present Titania membrane based on the DSPM model as a function of permeate volume flux.

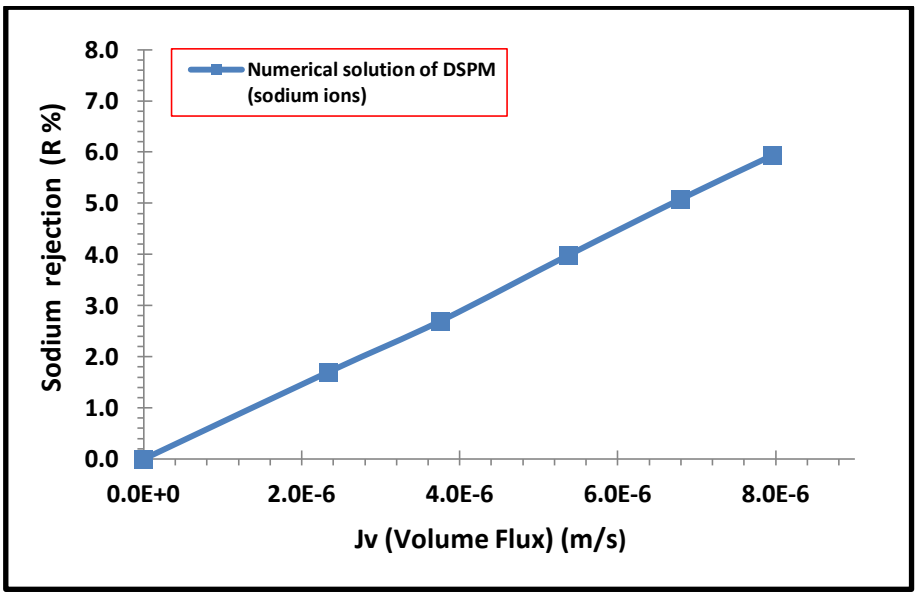

Figure 5.8: Rejection (R %) of sodium ions numerically predicted based on DSPM model as a function of permeates volume flux.

Regarding to the rejection of (Cl^{-1}) ions, it can be seen from Figure 5.9 that the results obtained from the numerical solution of the DSPM model indicated that the rejections of both chloride ions and sodium ions had the same behaviour.

It can be noted from Figure (5.9) that the rejection (R %) of chloride ions was also gradually increased as the solute permeates volume flux (which actually depends on the area of the present Titania membrane) increased. As mentioned before, for the rejection of sodium ions, this behaviour can be supported by theory and is fully understood [4], [51], [162].

Also it can be seen from this figure that at the highest solute permeate volume flux (at applied pressure of 5.0 bar) the rejection value (R %) of chloride ions was 5.51%.

Figure 5.9 shows the numerically simulated results for the rejection (R %) of (Cl^{-1}) ions in the present Titania membrane based on the DSPM model as a function of permeate volume flux.

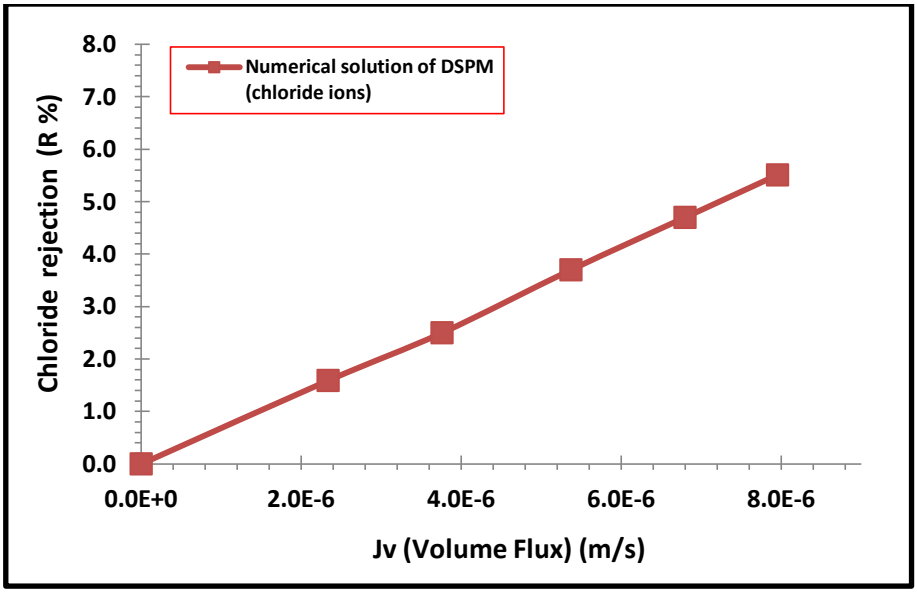

Figure 5.9: Rejection (R %) of chloride ions numerically predicted based on DSPM model as a function of permeates volume flux.

According to Bowen et al. [162], the comparison between the experimental and assessed model results should be done based NaCl as a solute. The rejection of NaCl solute inside the active porous layer of the present work can be estimated based on the ionic strength equation (see Equation 2.30).

The estimation of NaCl as a solute depends mainly on the ions valance and the assessed rejections values for (Na^{+1}) and (Cl^{-1}) ions that were already obtained from the numerical solution of the DSPM model at each membrane permeate volume flux.

Figure (5.10) shows a comparison between the assessed model results and that determined from experimental rejection data of sodium chloride solute for the present Titania membrane (see section 4.3.2).

It can be seen from Figure (5.10) that the numerical solution of the DSPM model shows that rejection (R %) of sodium chloride solute was steadily increased as the solute permeates volume flux (and hence the applied pressure) increased. At the highest permeate volume flux (at applied pressure of 5.0 bar), the rejection (R %) of sodium chloride solute was 5.72% while the experimental results indicated that the rejection (R %) of sodium ions at the highest solute permeate volume flux was 5.24%. It can be observed that the theoretical prediction of the present model was found to be in agreement with the experimental data. The obtained linear relationship results from the present work model are in agreement with the results (at the same applied pressure range) reported by Bowen et al. [162], [151], [153], [155].

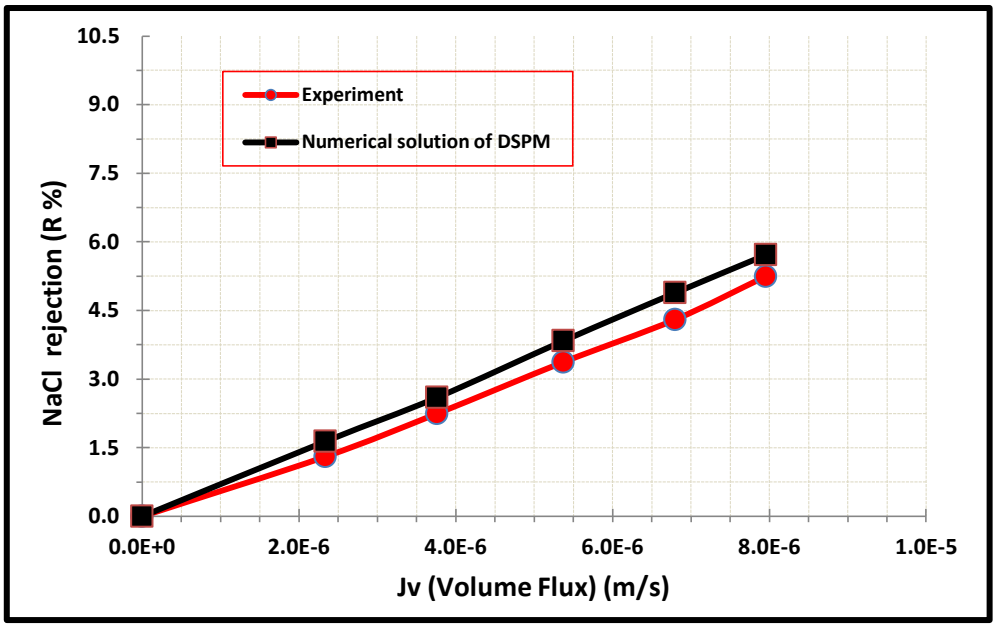

Figure 5.10: Experimental and numerically predicted rejection (*R* %) of 0.01 M sodium chloride solution in TiO_2 NF membrane as a function of permeates volume flux (m/s).

A sensitivity analysis (SA) represents a valid tool for characterising the uncertainty associated with a certain computational model. This technique studies how the uncertainty of a model's output can be divided to different sources of uncertainty by assessing the changes in the input variables under a given set of assumptions [183].

In other words, a sensitivity analysis is used to [184]:

- Quantify the effects of the input variables on a set of outputs.
- Identify which input parameters most significantly affect the model's obtained results.

Conducting such an analysis can support the decision maker, and can achieve a better understanding for the performance of the system, in addition to the development of the model by searching for possible errors.

The present work use the sensitivity analysis technique to investigate the rejection performance for the currently used Donnan steric pore model (DSPM) taking in consideration the effects of both ions steric coefficients and the Donnan potential of the membrane which can be considered as the most important parameters that could directly have an effect on the rejection of ions.

The model's input values for sodium and chloride steric coefficients were increased by 5% and 10% and decreased by 5% and 10% while the present model results were taken as a reference value.

The model rejection (R %) results (for each ion's increased or decreased values) of (0.01 M) sodium chloride solution at applied TMP of 5.0 bars was estimated as shown in Figure (5.11).

It can be seen from Figure (5.11) that the rejection (R %) of NaCl decreased from 5.72% (as a reference value) to 5.1% and 4.54% when the input values of the ionic steric coefficients increased by 5% and 10% respectively.

On the other hand, the rejection (R %) of sodium chloride increased from 5.72% (as a reference value) to 6.42% and 6.81% as the ionic steric coefficients decreased by 5% and 10% respectively.

It can be concluded from Figure (5.11) that as the ionic steric coefficients decreased the rejection (R %) of the NaCl solution increased.

This behaviour is supported by theory and can be explained based on the membrane effective pore radius (r_p). It can be seen from Equations (5.6) and (5.7) that the steric coefficient of ions depends mainly on the membrane effective pore radius (the membrane effective pore radius decreased as the ion steric coefficient decreased).

Schaep et al. [47] and Bowen et al. [153], [155] explained that in nanofiltration membranes, decreasing the membrane effective pore radius could lead to an improvement in the rejection performance of the membrane as a result of improving the steric-hindered effects (or size exclusion mechanism).

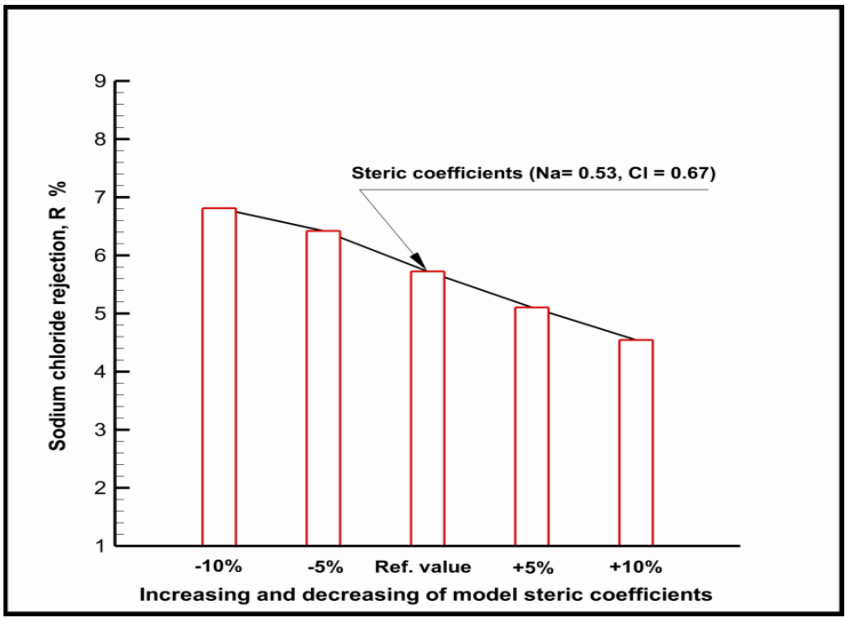

Figure 5.11: Effect of increasing and decreasing of the model ionic steric coefficients on the rejection of NaCl solution at applied TMP of 5.0 bars.

The same procedure was repeated for the membrane Donnan potential which represents the second important parameter in the present study's (DSPM) model. The estimated model's input value for the Donnan potential of the present ceramic TiO_2 membrane was increased by 5% and 10% and decreased by 5% and 10% while the present model values were taken as a reference value.

The model rejection (R %) results (for each increased or decreased Donnan potential values) of (0.01 M) NaCl solution at applied TMP of 5.0 bars was estimated as shown in Figure (5.12).

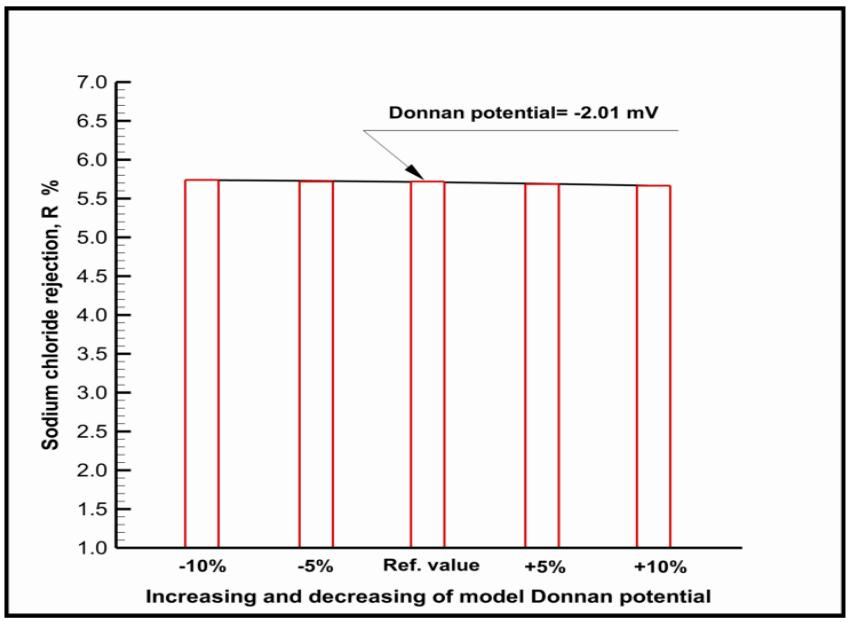

Figure 5.12: Effect of increasing and decreasing of the model Donnan potential on the rejection of NaCl solution at applied TMP of 5.0 bars.

It can be indicated from Figure (5.12) that the model rejection of sodium chloride solution was not affected by the proposed (5% and 10%) increasing or decreasing of the Donnan potential value.

This behaviour can be attributed to the estimated value of the present work's Titania membrane which seems to be too small to make a clear change in the rejection of the NaCl solution (because of the small membrane filtration area 4.178×10^{-3} m^2).

It can be concluded from Figures (5.11) and (5.12) that the steric coefficients of sodium and chloride ions were found to have much more effect than the Donnan potential of the membrane.

5.5.2 Discussion

The assessment of the salts rejection in amphoteric nanofiltration membranes represents a real challenge because different mechanisms such as adsorption, steric-hindered effects, and electrostatic effects could occur at the same time. In order to simulate the transport of ions through nano-porous membranes correctly, these mechanisms represent the main pathways that must be taken in consideration.

The description of the solute rejection performance in a NF membrane normally depends on:

- Composition and concentration of the feed solution.
- Operation parameters of the system.

Therefore, any further accurate models must consider in account the membrane charge and the steric effects.

The (DSPM) model represents the conventional approach in simulating the transport inside NF membranes. Many authors proved that the Donnan steric pore model was very successful in the prediction of salts rejection [155], [158], [[176], [185].

In the DSPM model, the partitioning distribution (at the feed and permeate sides) can be attributed to the combination of electrical (Donnan) and sieving (steric) mechanisms, whereas the ionic transportation inside the NF membrane is based on the extended Nernst-Planck (ENP) equation.

The effective representation of the (ENP) equation can be attributed to the contributions of three mechanisms (diffusion, electro-migration, and convection). This equation was modified to account for the effect of the finite pore size on the hindered transport coefficient of both convection ($K_{i,c}$) and diffusion ($K_{i,d,}$) (see Equation 5.1).

In this work, the Donnan steric pore model was also proposed to estimate the membrane effective pore radius (r_p) for the present (TiO_2) membrane based on the transport equations of a solute inside membrane pores, the Hagen-Poiseuille equation, and the permeation test of an uncharged solute (glucose).

The numerical solution of the DSPM model required the estimation of the main physio-chemical parameters. The estimation of all these parameter's values were related to the estimated effective pore radius of a TiO_2 NF membrane (see Table 5.2).

The steric coefficient $(\emptyset_i)$ which mainly depends on the ratio between the size of the molecule i and that of the pore was included in the present DSPM model.

According to Bowen et al [162], the original Donnan steric pore model (DSPM)

allows simulating the rejection rate of a single salt (monovalent ions) solution.

The novelty of the proposed approach lies with the estimation of the Donnan potential from the surface charge density based on the estimation of zeta potential of the present titanium dioxide NF membrane.

In the present work, the same solute concentration of 0.01 M sodium chloride was used (as a reference solution) to estimate the:

- Type and magnitude of membrane charge.
- Zeta potential and effective membrane charge density
- Donnan potential (based on precise relationship made for monovalent ions).
- Numerical simulation of the (DSPM) with the compared experimental data.

The normal numerical solution of a DSPM model based on fixed charge theory. The potential gradient over the membrane depends mainly on the following two assumptions [185], [158]:

- Assume the electroneutrality conditions inside and outside the membrane.
- Assume zero electric conditions inside the membrane.

In other words, all the previous DSPM model simulation work did not use a real value of the Donnan potential.

The present Titania membrane was characterised in terms of three parameters, which are: the effective membrane pore radius (r_p), the equivalent membrane active layer thickness (Δx_e), and the Donnan potential. The rejections of sodium and chloride ions were predicted in terms of these three parameters.

In Hajarat work [20], all these three parameters were not estimated. Hajarat assumed that the effective membrane pore was the same as the membrane pore diameter. The effective membrane active layer thickness was also assumed and the membrane surface porosity was ignored. Also, the Donnan potential for the present Titania membrane was again assumed without conducting any further calculations related to the membrane's electrokientic phenomena.

Furthermore, another two important parameters were also ignored in Hajarat work, which are, the membrane charge and the steric coefficient.

An accurate model requires dealing with all the governing parameters in order to achieve a reasonable agreement with the experimental results.

Compared to Hajarat's work [20], the following points have been added to the present simulation model:

- A mathematical model has been proposed based on the DSPM model to investigate the ionic transportation, whereas the Donnan equilibrium distribution model was used in Hajarat's work.
- Estimation of the effective pore radius r_p (by using two different models).
- Estimation of the main physio-chemical parameters values such as $(K_{i,c})$, $(K_{i,d,})$, and $(D_{i,P,})$ based on the estimated effective pore radius.
- Estimation of the steric coefficient $(\emptyset_i)$.
- Estimation of the Donnan potential based on the estimated membrane zeta potential and effective surface charge density.
- Estimation of the equivalent membrane active layer thickness (Δx_e) based on the estimated effective layer thickness (Δx) and (TiO_2) membrane surface porosity (A_k).
- The negatively charged of the present (TiO_2) membrane was included in the model.

According to many authors [158], [27], it is recommended that the porosity of a multilayer's composite membrane with microporous range (such as the present Titania membrane) to be measured by using the permporometry technique. This method discriminates between the active pores and dead end pores. The permporometry method is considered as a non-destructive test as there is no need to crush the membrane.

Permporometry is based on controlled blockage of pores by capillary condensation of a condensable gas and simultaneous measurement of noncondensable gas diffusional flux through the remaining opening pores. Since the present TiO_2 membrane manufacturer [31] used this technique to measure the porosity, the present model suggested using this porosity in order to assess the ionic transport performance.

The major finding from this study showed that the behaviour of the theoretical prediction is in an agreement with the experimental work, however, the obtained results were not identical. Regarding to the experimental work, this can be attributed to some limitations in the filtration process rig.

With regard to the results of the mathematical work, this can be classified in three main parts:

The first part is related to the adopted DSPM model, where the difference in the obtained results can be attributed either to ignoring the effects of some parameters in the DSPM model, such as, the osmotic pressure and the activity of coefficients of ions and the original DSPM model itself ignored the effects of some important phenomena's which could have an effect on the simulation procedure, such as, the effect of concentration polarisation or the effect of dielectric interactions inside the pores.

The second part is related to the estimation of the main DSPM model parameters, such as: the effective pore radius, the equivalent active layer thickness and the Donnan potential. The estimation of these parameters required conducting experimental work and afterward substituting the obtained results in certain models or relationships. As a result, the possibility of errors (or uncertainty) might increase.

The third part is related to the accuracy needed for the adopted numerical solution method. The choice of more accurate solution methods might lead to difficulties in programming and coding issues.

The simulated numerical results to predict the rejection of sodium chloride solution based on the present DSPM model showed good agreement with the previous studies done by Bowen et al [162], [151], [153], [155] over the same range of permeate volumetric flux but for different types of NF membranes.

When the present work model's results compared with Hajarat's work [20], two main differences can be clearly observed related to the assessed concentrations of sodium and chloride ions inside the membrane in spite of using the same solute concentration of 10 mol/m^3 and the same titania membrane. The first difference is related to the reduction of the assessed sodium and chloride ions concentrations inside the membrane. It can be noticed that the sodium concentration at the membrane-permeate interface decreased from 8.59 (mol/m^3) in Hajarat's work compared to 5.42 (mol/m^3) in the present work, whereas the chloride concentration at the membrane-permeate interface decreased from 11.63 (mol/m^3) in Hajarat's work (for bulk concentration of 10 mol/m^3) compared to 5.85 (mol/m^3) in this work.

Whereas the second remark can be concluded from the above models results, it can be seen that the assessed concentrations values for sodium and chloride ions in this work

were much closer to each other than that in Hajarat's work. This result is important because it is compatible with the experimental work of this study.

The differences between this work's results and Hajarat's [20] work can be attributed either to the addition of more affective parameters as a result of using the DSPM model or the estimations of other important parameters that have been assumed in Hajarat's work. Parameters such as the steric (or sieving) effects, membrane charge effects, and surface porosity represent important additions for this work, while the estimations of other parameters such as the effective pore radius, equivalent active skin layer thickness, and the Donnan potential represent an attempt to reduce the possible errors and get more accurate results.

As mentioned previously, the steric effect (or size exclusion mechanism) can be considered as one of the important pathways that governed the transport of the ionic solutions inside NF membranes. Furthermore, the results of the present study indicated that parameters such as the equivalent membrane active layer thickness, membrane charge and permeate volumetric flux can affect the model rejection results.

In order to improve the process understanding, the present work suggests as future work the studying of the possible effects for other parameters which have been ignored in the present original DSPM model. Parameters like the dielectric interactions inside pores membrane or concentration polarisation phenomenon might have an effect on the present simulation procedure results.

Other models can be used to study the possible effects of these parameters such as the Donnan steric partitioning pore and dielectric exclusion model (DSPM-DE model) [167] and the differential concentration polarisation and Donnan steric pore model (CP-DSPM model) [186], [174], [178].

It is worthwhile to mention that the present numerical simulation procedure can be used for any monovalent single salt solution to predict the rejection performance of any charged nanofiltration membranes.

Regarding to any other type of salts (such as the bivalent calcium sulphate solution), the present model can be applied directly except for the Donnan potential parameter. As future work, the present study suggests that further investigations will be needed to evaluate the Donnan potential based on feed concentration and effective surface charge density of the membrane separately for each case.

The derivation of new relationships or formulas to fit this parameter can be done by using the NaCl solution (as a background or reference solution) to determine the membrane charge, membrane zeta potential, and membrane iso-electric point (as shown in section 2.4.3). These electrokinetic measurements should then be repeated for the new solution and compare with the results in terms of the sodium chloride solution.

5.6 Summary

The present study's tubular ceramic Titanium dioxide NF membrane has been characterised in terms of three main parameters: effective membrane pore radius, equivalent active skin layer thickness and effective membrane surface charge density. The first and second parameters were estimated based on the rejection data of uncharged solutes of glucose, while the third parameter was estimated from the electrokientic measurements of membrane zeta potential and related surface and effective charge density of the present Titania membrane. A mathematical model has been proposed based on the original DSPM model to simulate the rejection of 0.01 M sodium chloride as a reference solution.

In the DSPM model, the transportation of ions inside the NF membrane was characterised based on the ENP equation in conjunction with the Donnan and steric effects at the membrane-solution interface. Formulation of the DSPM model allows the hindered nature of the transport inside the NF membrane to be taken into account, thus this model can be considered as a useful means of characterising, analysing and assessing the performance of NF membranes.

The Donnan potential or the potential at the membrane-solution interface was determined for each electrically charged nanofiltration membrane based on two main parameters. The first one was related to the physical properties of the 1:1 background electrolytes such as ionic strength and pH number while the second parameter was related to the estimation of the effective membrane fixed charge density.

The present work adopted the estimated (r_p) that has been determined based on the DSPM model because the uncharged solute hydrodynamic model ignored the effects of membrane thickness (Δx) on rejection. Also, the dimensionless group (Y) in this model was considered to be independent of the solute concentration. Furthermore, the DSPM model was used to predict the ions transport through the present work's Titania membrane.

The estimation of the main physio-chemical parameter's values for the present titanium dioxide NF membrane such as ($K_{i,c}$), ($K_{i,d,}$) and ($D_{i,P,}$) have been determined based on the estimated effective pore radius (r_p).

The ionic steric coefficients (for cylindrical pores) have been estimated based on the ionic Stokes' radius and effective pore radius. The Stokes' radius of each ion in the present TiO_2 membrane was estimated based on the Stokes-Einstein formula.

The theoretical rejection of the sodium chloride solute in the present numerical model was found to be in agreement with the experimental data.

A sensitivity analysis was performed in terms of rejection performance of the sodium chloride solution to study the effect of the most significant parameters on the rejection of ions in the present TiO_2 NF membrane based on present work's Donnan steric pore model. The steric coefficients of sodium and chloride ions were found to have much more effect than the Donnan potential of the membrane.

CHAPTER 6

CONCLUSIONS AND RECOMMENDATIONS

This chapter summarises the main conclusions drawn from this research, also gives recommendations for process improvement and suggestions for future work. All of the main goals of this study outlined in Chapter one (section 1.3) have been successfully met.

6.1 Conclusions

This study was set out to study the rejection and fouling behaviour of calcium sulphate in 1 nm ceramic TiO_2 NF membrane. The presence of calcium sulphate solutions in any membrane filtration unit could cause an adverse effect on the rejections performance of the system as a result of its high fouling tendency.

The unique specifications of the ceramic NF membranes as the most newly developed technology compared to the conventional RO membranes encourage many researchers to use such membranes in the new applicable processes and the remediation of salt-effected soils is one of these applications.

The good fouling resistance, high water flux, stability under extreme pH ranges in addition to commercial availability and low fabrication cost represent the main properties that led to prefer using the TiO_2 NF membrane for the present study in spite of the availability of other types of mineral oxide membranes.

The present work had two major aims, the first one was to show the rejections efficiency of the present TiO_2 NF membrane and its ability to separate the $CaSO_4$ solutions at different concentrations (below and at the saturation concentration) compared to other naturally occurring single salts such as $NaCl$, Na_2SO_4 and $CaCl_2$. While the second aim was to explore the fouling trend of the $CaSO_4$ solutions in term of the critical flux concept by using the same concentrations that already used in the rejection sets in order to identify the forms and the onset of the fouling in a way that could lead to adopt a suitable controlling strategy.

This study has also sought to characterise the electrokinetic effects of Titana membrane in the present work especially the parameters that could have a direct impact on the rejections performance such as: membrane charge type and magnitude, iso-electric point of the membrane, in addition to the surface and effective membrane charge density. Evaluation of all these parameters can be led to estimate the Donnan potential of the membrane.

Finally, the modelling part of this study was performed in order to investigate the effect of the Donnan and size exclusion mechanisms (as the most significant parameters in DSPM model) on the rejections performance of the ions.

The conclusions of the present work have been divided into the following four broad parts:

6.1.1 Membrane electrokientics

The conducted electrokinitic measurements of TiO_2 NF membrane in the present study showed that it is a negatively charged membrane at neutral pH and its iso-electrical point is at pH of 4.0. The obtained results proved that the estimated membrane zeta potential values were strongly dependant on pH of the electrolyte as a result of the amphoteric behaviour of the present composite ceramic TiO_2 NF membrane.

The conducting of streaming potential measurements at unadjusted pH for different background electrolyte ionic strengths showed that as the electrolyte ionic strength increased the electrokinetic membrane zeta potential decreased.

The effective membrane fixed charge density (or the concentration of the electrically charged membrane) could be evaluated based on the estimated surface charge density of the membrane by assuming that the surface charge of the membrane normally distributed in a void volume of cylindrical pores.

The present work pointed that the electrokinetic effect of the TiO_2 NF membrane can play a very important role in the elucidation of the rejection behaviour of each ion.

6.1.2 Membrane salts rejection

It can be concluded that the rejection and the permeate volume flux of all the four salts used in the present study increased as the applied trans-membrane pressure increased and decreased with the growth of salt concentration.

The main conclusions for the ionic rejections of the four salts can be summarised as follows:

- Regarding the rejection of sodium sulphate solutions, it was found that the rejection of sulphate ions was noticeably higher than the rejection of sodium ions for each selected concentration. The rejection behaviour of Na_2SO_4 solutions in the present TiO_2 NF membrane has been explained based on the theory of Donnan exclusion and size exclusion mechanisms.
- Regarding the rejection of sodium chloride solutions, it was found that the rejection of chloride ions was slightly higher than the rejection of sodium ions for each selected concentration. The rejection behaviour of NaCl solutions in the present TiO_2 NF membrane has been interpreted based on the theory of Donnan exclusion and size exclusion mechanisms.
- Regarding the rejection of calcium chloride solutions, it was found that the rejection of calcium ions was significantly higher than the rejection of chloride ions for each selected concentration. The rejection behaviour of $CaCl_2$ solutions in the present TiO_2 membrane cannot be explained according to the theory of Donnan exclusion. However based on the ions hydrated radius of the calcium chloride solution, the sieving or size exclusion mechanism could give a possible explanation.
- Regarding the rejection of calcium sulphate solutions, it was found that the rejection of sulphate ions was slightly higher than the rejection of calcium ions for each selected concentration. The rejection behaviour of $CaSO_4$ solutions in the present TiO_2 NF membrane has been explained based on the theory of Donnan exclusion and size exclusion mechanisms.

The salt rejection measurements found to have the following rejection sequence:

$R\ (CaSO_4) > R\ (Na_2SO_4) > R\ (CaCl_2) > R\ (NaCl)$.

It can be noticed from this sequence that the diffusion coefficient of the salt can play a significant effect in the rejection inside this type of membrane in which the lowest diffusion coefficient ($CaSO_4$) shows the highest rejection (43.3%), whereas that with the highest diffusion coefficient exhibits the lowest rejection.

The rejection behaviour of the calcium sulphate solution at saturated concentration showed the same behaviours as that of calcium sulphate solutions below the saturation concentration.

The rejection and permeate volume fluxes of the $CaSO_4$ solute at saturation concentration were the lowest compared to $CaSO_4$ rejection results of that below the saturation concentration. The saturation concentration of calcium sulphate salt (as gypsum) was found to be equal to 2.35 g/l at an average temperature of 18 ℃.

It can be concluded that the TiO_2 membrane could efficiently reject the $CaSO_4$ solutes compared to other salts used in this study and the concentration of the salt and the applied trans-membrane pressure are the most governing parameters. In addition, the present work approved that the sieving or size exclusion mechanism can be very effective in the explanation of salt rejection behaviour if the hydrate radius of ions were taken in consideration without ignoring the possible effect of the ionic bare radius.

6.1.3 Critical flux of calcium sulphate

The present work suggested a comparison between two different experimental procedures to determine the critical flux values at different molar concentrations below and at saturation concentration of calcium sulphate by using tubular ceramic TiO_2 NF membrane; these are step by step technique and standard stepping technique.

The obtained critical flux results from the step by step method (for all sessions) confirmed that the critical flux was reached and exceeded (where the solutes permeate flux started to deviate from linearity). While the obtained critical flux results from the standard stepping method (for all sessions) confirmed that the critical flux values were exceeded since the recorded permeate flux of the decreasing pressure did not give the same values when compared with that of increasing pressure.

The experimental results showed that the critical flux values depend mainly on the ionic strength of the calcium sulphate. The present work pointed out that the resulting critical flux values from both measuring procedures were decreased as the ionic strength of the calcium sulphate solutes was increased.

It was found that for each selected calcium sulphate concentration, the determined critical flux values from using both techniques were found to be close to each other despite the differences in measuring techniques and in step duration of each time interval.

For both critical flux measuring techniques that have been used in the present work, it was found that the strong form of the critical flux was observed only at 0.001 M calcium sulphate solution whereas the weak form of the critical flux was observed in

all other calcium sulphate concentrations. It can be noticed from the experimental results for both critical flux measuring techniques that the maximum (or limiting) flux was not reached. The applied trans-membrane pressure needed to be increased to reach this point which is beyond the capability of the present filtration rig.

The present study approved that the critical flux value depends mainly on the obtained permeate flux for calcium sulphate which is already decreased as the solute concentrations increased and as a consequence the critical flux would be reduced as well.

The high fouling tendency of calcium sulphate as the highest potential scaling salt could explain the up to half reduction of the estimated critical flux values when the concentration of calcium sulphate increased from 0.001 M to that at saturation concentration.

6.1.4 Mathematical model

A mathematical model has been proposed based on the original DSPM model to simulate the rejection of a reference solution of 0.01M sodium chloride in order to investigate the effect of the most significant parameters on the rejection of ions in the TiO_2 NF membrane. The membrane of the present study has been characterised in terms of three main parameters: effective membrane pore radius, equivalent active skin layer thickness and effective membrane surface charge density. The first and second parameters were estimated based on the rejection data of uncharged solutes of glucose, while the third parameter was estimated from the electrokientic measurements of membrane zeta potential and related surface charge density of the present Titania membrane.

Two different transport models have been used to determine the effective pore radius (r_p) for the present TiO_2 membrane, which are: the DSPM model and uncharged solute hydrodynamic model. It was found that the estimated (r_p) from both these two models were relatively close to each other.

The simulated model's results of ionic transport inside the titanium dioxide ceramic NF membrane showed that the concentrations of (Na^{+1}) and (Cl^{-1}) ions inside estimated equivalent active skin layer thickness of 8.1µm were decreased as both ions moved towards the outer permeate side and the concentration of chloride ions inside the membrane active skin layer was slightly higher than that of sodium ions.

The obtained results showed that there was no big shift between the concentrations of two ions. The same behaviour was seen in the rejection experimental work of 0.01 M sodium chloride solutes.

The numerical solution of the DSPM model indicated that the rejection of both sodium and chloride ions were gradually increased as the permeate volume flux increased.

It can be concluded that the theoretical rejection of the sodium chloride solute in the present numerical model was found to be in agreement with the experimental data and the obtained linear relationship resulted from the model of the present work is in agreement with the rejections obtained by other researchers considering the same applied pressure range.

In terms of rejection performance of the sodium chloride solution, the performed sensitivity analysis for the Donnan steric pore model of the present work showed that the steric coefficients of sodium and chloride ions were found to have much more effect than the Donnan potential of the membrane.

6.2 Recommendations

The present work's limitations and the possibilities of process improvements as well as future work studies can be summarised as follows:

6.1.2 Limitations and process improvement

Regarding the bench scale experimental work of the present nanofiltration membrane rig, there were a number of factors that needed to be improved in order to increase the reliability and accuracy of the acquired data. In terms of process improvement, avoiding these limitations would have a direct effect on the performance of the rig equipment and as a result reduce the uncertainty of the experimental work, especially if there is an attempt to scale-up the system or move to a prototype scale. These factors are outlined as follows:

- The manually regulated back pressure gate valve that sets the applied trans-membrane pressure had faced stability problems especially at high applied pressures, therefore; changing this valve with an automatically controlled pressure valve would increase the system's stability, and furthermore would avoid the continuous control and supervision that was done by the operator of the system.
- The section head of the present work's peristaltic process pump generally moved in a rotary manner. The pump rollers were used to squeeze the tube followed by a void. Repeating this mechanism (at high flow rate) causes the fluid to be pulsated rather than being continuous and smooth. Therefore to maintain a constant flow, installation of a pulse damper would be required which could be inserted into the pump discharge line to reduce the pulsation.
- The combination of the back pressure valve stability problem with the pulsation problem made it quite difficult to establish trans-membrane pressure increments less than 1 bar (which might have reduced the possible experimental errors). The pulsation of the peristaltic process pump (above 4.0 bars) could vary within a range of $(0.5 - 1.0$ bar) from the peak to the trough of the pulse.

- The design parameters of the present work's ProMinent™ peristaltic process pump stated that the maximum feed rate was up to 125 l/h at a back operating pressure of 6.0 bars, thus operation with a much wider range flow rate or applied trans-membrane pressure was not possible in this project. Therefore, changing present work's process pump to a more powerful pump that could reach an applied pressure of about $15 - 20$ bars and flow rate of about $400 - 500$ l/h would improve the experimental results of both the critical flux and salts rejection.
- Measuring the permeate volume flux is a very important issue for both the rejection and critical flux experiments. Despite the fact that the measurements of the present's work permeate flux were relatively accurate, the occurrence of potential errors could be expected due to human factors. In order to get more accurate measurements, an electronic digital scale with timer can be used to measure the permeate flux automatically.
- Scope for further studies in the same field can be conducted taking in consideration the effects of other parameters on the rejection and critical flux of calcium sulphate in the ceramic Titania NF membrane such as: temperature, flow rate, pH and cross flow velocity.

6.2.2 Future work

It is recommended that further future work is undertaken as follows:

- Characterise the type and magnitude of any charged ceramic nanofiltration membrane by using electrokientic SP measurements to estimate the zeta potential and the iso-electric point of the membrane, furthermore; develop new derivations to estimate the related surface charge density and Donnan potential when using any (1−2), (2−1) and (2−2) salts rather than the present work's (1−1) salt.
- Study and compare the rejection behaviour of calcium sulphate in the presence of mixed electrolyte systems with other predominate salts that typically accumulate in soils such as sodium chloride, sodium sulphate and calcium chloride in binary or tertiary salts.
- Study the effects of adding an effective anti-scaling additive(s) (typically polyelectrolyte's such as polycarboxylates, polyacrylates, polyphosphonates and polyphosphates) on the critical flux of calcium sulphate in the ceramic titanium dioxide NF membrane in order to decrease the membrane fouling and improve the rejection of calcium sulphate solutions.
- Apply different mathematical models to simulate the ionic transport through the Titania NF membrane such as the Donnan steric partitioning pore and dielectric exclusion model (DSPM-DE model) and the differential concentration polarisation and Donnan steric pore model (CP-DSPM model) to study the possible effects of other parameters that were ignored in the present original DSPM model.

REFERENCES

[1]. Me, X. M., Xie, Q. L., Xia, H. P. and Lan, W. G., *Application of nanofiltration process in 5′-GMP production.* Desalination, 2008. 225(1): p. 322-328.

[2]. A. I. Schäfer, A. G. Fan, and T. D. Waite, *Nanofiltration principles and applications*. 2007: Elsevier.

[3]. Qureshi, T. M., Aslam, M., Ashraf, M. Y. and Hussain, F., *Performance of Eucalyptus camaldulensis under different types of salt-affected soil*. Int. J. Agri. Biol, 2000. 2(1): p. 45.

[4]. Schäfer, A., A. G. Fane, and T. Waite, *Fouling effects on rejection in the membrane filtration of natural waters.* Desalination, 2000. 131(1-3): p. 215-224.

[5]. Weber, R., H. Chmiel, and V. Mavrov, *Characteristics and application of new ceramic nanofiltration membranes.* Desalination, 2003. 157(1-3): p. 113-125.

[6]. Bartels, C., Wilf, M., Casey, W. and Campbell, J., *New generation of low fouling nanofiltration membranes.* Desalination, 2008. 221(1-3): p. 158-167.

[7]. Lin, C., Shirazi, S., Rao, P. and Agarwal, S., *Effects of operational parameters on cake formation of $CaSO_4$ in nanofiltration.* Water research, 2006. 40(4): p. 806-816.

[8]. Lee, S. and C. H. Lee, *Effect of operating conditions on $CaSO_4$ scale formation mechanism in nanofiltration for water softening.* Water research, 2000. 34(15): p. 3854-3866.

[9]. Jawor, A. and E. Hoek, *Effects of feed water temperature on inorganic fouling of brackish water RO membranes.* Desalination, 2009. 235(1-3): p. 44-57.

[10]. Le Gouellec, Y. A. and M. Elimelech, *Calcium sulfate (gypsum) scaling in nanofiltration of agricultural drainage water.* Journal of membrane science, 2002. 205(1): p. 279-291.

[11]. Shirazi, S., C. J. Lin, and D. Chen, *Inorganic fouling of pressure-driven membrane processes — A critical review.* Desalination, 2010. 250(1): p. 236-248.

[12]. Shih, W. Y., Rahardianto, A., Lee, R. W. and Cohen, Y., *Morphometric characterization of calcium sulfate dihydrate (gypsum) scale on reverse osmosis membranes.* Journal of membrane science, 2005. 252(1): p. 253-263.

[13]. Gouellec, L. *High performance Nano- filtration membrane for agriculture waste water reclamation*. in *IDA world congress on desalination and water reuse*. 2007. Madrid, Spain.

[14]. Abdul-Halim, *Soil salinization and the use of halophytes for forage production in Iraq* Reclamation and Revegetation Research, 1986. 26(5): p. 75-82.

[15]. Rahi, K. A. and T. Halihan, *Changes in the salinity of the Euphrates River system in Iraq.* Regional Environmental Change, 2010. 10(1): p. 27-35.

[16]. J. Dieleman, P., *Reclamation of salt affected soil in Iraq, Soil hydrological and Agriculture studies*, International Institution for land Reclamation and Improvement, 3rd edition. 1977: Wageningen. Netherlands.

[17]. Pessarakli, M., *Handbook of plant and crop stress*. 1999: CRC.

[18]. Aljubouri, Z. A. and S. M. Aldabbagh, *Sinjarite ,a new mineral from Iraq.* Mineralogical Magazine, 1980. 43: p. 643-5.

[19]. CANDESAL® Corporation .*http://www.candesal.com*. Ottawa, Canada, 2012.

[20]. Hajarat, R. A., *The use of nanofiltration in desalinating brackish water*, in *School of Chemical Engineering and Analytical Science*. 2010, phD thesis, The University of Manchester.

[21]. Mulder, M., *Basic principles of membrane technology*. 1996: Springer.

[22]. Winston, W. and K. K. Sirkar, *Membrane handbook.* 1992: Van Hostrand Reinhold, New York.

[23]. Hoffman, E. J., *Membrane separations technology: single-stage, multistage, and differential permeation*. 2003: Gulf Professional Publishing.

[24]. Hughes, R., *Industrial membrane separation technology*. 1996: Springer.

[25]. Belfort, G., *Synthetic membrane processes ,Fundamentals and water application*. 1984: academic press INC.

[26]. J. A. Howell, V. S., and R. W. Field, *Membranes in Bio processing-Theory and Applications*. 1st edition. 1993: Chapman & Hall.

[27]. Li, K. and MyiLibrary, *Ceramic membranes for separation and reaction*. 2007: Wiley Online Library.

[28]. A. J. Burggraaf and L. Cot, *Fundamental of Inorganic Membrane Science and Technology*. Membrane Science and Technology Series 4. 2005, Elsevier Science: Netherlands.

[29]. Mansoor M. Amiji and Beverly J. S., *Applied Physical Pharmacy*. 2002: McGraw-Hill Professional.

[30]. Laitines, N., *Development of ceramic membrane filtration equipment and its applicability for different wastewater*. 2002, phD thesis, University of Technology: Lappeenranta.

[31]. Inopor® GmbH. *http://www.inopor.com*. Veilsdorf, Germany, 2012.

[32]. A .Larbot, S. Alami-Younssi, M. Persin, J. Sarrazin, and L. Cot, *Preparation of alumina nanofiltration membrane.* Journal of Membrane Science 1994. 97: p. 167–173.

[33]. Baker, R. W., *Membrane technology and applications*. 2004: Wiley.

[34]. Moritz, T., Benfer, S., Arki, P. and Tomandl, G., *Investigation of ceramic membrane materials by streaming potential measurements.* Colloids and Surfaces A: Physicochemical and Engineering Aspects, 2001. 195(1–3): p. 25-33.

[35]. Fievet, P., Labbez, C., Szymczyk, A., Vidonne, A., Foissy, A. and Pagetti, J., *Electrolyte transport through amphoteric nanofiltration membranes.* Chemical engineering science, 2002. 57(15): p. 2921-2931.

[36]. Timmer, J. M., *Properties of nanofiltration membranes: model development and industrial application*. 2001: Technische Universiteit Eindhoven.

[37]. Peeters, J. M. M., Boom, J. P., Mulder, M. H. V. and Strathmann, H., *Retention measurements of nanofiltration membranes with electrolyte solutions.* Journal of membrane science, 1998. 145(2): p. 199-209.

[38]. Van Rijn, C., *Nano and micro engineered membrane technology*. Vol. 10. 2004: Elsevier Science.

[39]. Bird, R. B., Stewart E. W. and Lightfoot N. E., *Transport phenomena.* 2nd edition, 2002: John Wiley & Sons, Inc.

[40]. Chaabane, T., Taha, S., Cabon, J., Dorange, G. and Maachi, R, *Dynamic modeling of mass transfer through a nanofiltration membrane using calcium salt in drinking water.* Desalination, 2003. 152(1–3): p. 275-280.

[41]. Sagle A., and Freeman B., *Fundamentals of membranes for water treatment in the future of desalination in Texas*, 2004, Texas Water Development Board: Austin, USA. p. pp. 137-154.

[42]. Wijmans, J. G. and R. W. Baker, *The solution-diffusion model: a review.* Journal of membrane science, 1995. 107(1–2): p. 1-21.

[43]. Mauviel, G., Berthiaud, J., Vallieres, C., Roizard, D. and Favre, E., *Dense membrane permeation: From the limitations of the permeability concept back to the solution-diffusion model.* Journal of membrane science, 2005. 266(1–2): p. 62-67.

[44]. Van Wagner, E. M., Sagle, A. C., Sharma, M. M. and Freeman, B. D, *Effect of crossflow testing conditions, including feed pH and continuous feed filtration, on commercial reverse osmosis membrane performance.* Journal of membrane science, 2009. 345(1–2): p. 97-109.

[45]. R. L. Riley, H. K. Lonsdale, C. R. Lyons, and U. Merten, *Preparation of ultrathin reverse osmosis membranes and the attainment of theoretical salt rejection.* Journal of applied polymer science 1967. 11(11): p. 2143-2158.

[46]. Gutman, R. G., *Membrane Filtration, The technology of pressure-driven crossflow processes*. 1987, Bristol, UK: IOP publishing Ltd.

[47]. Schaep, J. and C. Vandecasteele, *Evaluating the charge of nanofiltration membranes.* Journal of membrane science, 2001. 188(1): p. 129-136.

[48]. Israelachvili, J. N., *Intermolecular and surface forces*. 2007: Academic press.

[49]. Dukhin, S. S., R. Zimmermann, and C. Werner, *Charge density distribution at interfaces between polyelectrolyte layers and aqueous solutions—Experimental access and limitations of traditional electrokinetics.* Journal of Colloid and Interface Science, 2008. 328(2): p. 217-226.

[50]. Bowen, W. R. and X. Cao, *Electrokinetic effects in membrane pores and the determination of zeta-potential.* Journal of membrane science, 1998. 140(2): p. 267-273.

[51]. Bandini, S., *Modelling the mechanism of charge formation in NF membranes: Theory and application.* Journal of membrane science, 2005. 264(1–2): p. 75-86.

[52]. Blank, R., Muth, K. H., Proske-Gerhards, S. and Eberhard, S., *Electrokinetic investigations of charged porous membranes.* Colloids and Surfaces A: Physicochemical and Engineering Aspects, 1998. 140(1–3): p. 3-11.

[53]. Wang, D. X., Su, M., Yu, Z. Y., Wang, X. L., Ando, M. and Shintani, T., *Separation performance of a nanofiltration membrane influenced by species and concentration of ions.* Desalination, 2005. 175(2): p. 219-225.

[54]. Hagmeyer, G. and R. Gimbel, *Modelling the rejection of nanofiltration membranes using zeta potential measurements.* Separation and Purification Technology, 1999. 15(1): p. 19-30.

[55]. Schaep, J., Van der Bruggen, B., Vandecasteele, C. and Wilms, D., *Influence of ion size and charge in nanofiltration.* Separation and Purification Technology, 1998. 14(1–3): p. 155-162.

[56]. Bruni, L. and S. Bandini, *The role of the electrolyte on the mechanism of charge formation in polyamide nanofiltration membranes*. Journal of membrane science, 2008. 308(1–2): p. 136-151.

[57]. Tay, J. H., J. Liu, and D. Delai Sun, *Effect of solution physico-chemistry on the charge property of nanofiltration membranes.* Water research, 2002. 36(3): p. 585-598.

[58]. Xu, Y. and R. E. Lebrun, *Investigation of the solute separation by charged nanofiltration membrane: effect of pH, ionic strength and solute type.* Journal of membrane science, 1999 :(2–1)158 .p. 93-104.

[59]. Johnson, P. R., *A comparison of streaming and microelectrophoresis methods for obtaining the ζ potential of granular porous media surfaces.* Journal of Colloid and Interface Science, 1999. 209(1): p. 264-267.

[60]. Smith, R. W. and Y .Narimatsu, *Electrokinetic behavior of kaolinite in surfactant solutions as measured by both the microelectrophoresis and streaming potential methods.* Minerals Engineering, 1993. 6(7): p. 753-763.

[61]. Afonso, M. D., G. Hagmeyer, and R. Gimbel, *Streaming potential measurements to assess the variation of nanofiltration membranes surface charge with the concentration of salt solutions.* Separation and Purification Technology, 2001. 22–23(0): p. 529-541.

[62]. Peeters, J. M. M., M. H. V. Mulder, and H. Strathmann, *Streaming potential measurements as a characterization method for nanofiltration membranes.* Colloids and Surfaces A: Physicochemical and Engineering Aspects, 1999. 150(1–3): p. 247-259.

[63]. Afonso, M. D., *Surface charge on loose nanofiltration membranes.* Desalination, 2006. 191(1–3): p. 262-272.

[64]. Takagi, R., Hori, M., Gotoh, K., Tagawa, M. and Nakagaki, M., *Donnan potential and ζ-potential of cellulose acetate membrane in aqueous sodium chloride solutions.* Journal of membrane science, 2000. 170(1): p. 19-25.

[65]. Oldham, K.B., *A Gouy–Chapman–Stern model of the double layer at a (metal)/(ionic liquid) interface.* Journal of Electroanalytical Chemistry, 2008. 613(2): p. 131-138.

[66]. Rytwo, G., *Applying a Gouy–Chapman–Stern model for adsorption of organic cations to soils.* Applied Clay Science, 2004. 2 :(4–3)4p. 137-147.

[67]. Delgado, A. V., Gonzalez C., F., Hunter, R. J., Koopal, L. K. and Lyklema, J., *Measurement and interpretation of electrokinetic phenomena.* Journal of Colloid and Interface Science, 2007. 309(2): p. 194-224.

[68]. Hagmeyer, G. and R. Gimbel, *Modelling the salt rejection of nanofiltration membranes for ternary ion mixtures and for single salts at different pH values.* Desalination, 1998. 117(1–3): p. 247-256.

[69]. Dukhin, S. S., R. Zimmermann, and C. Werner, *Intrinsic charge and Donnan potentials of grafted polyelectrolyte layers determined by surface conductivity data.* Journal of Colloid and Interface Science, 2004. 274(1): p. 309-318.

[70]. Levenstein, R., D. Hasson, and R. Semiat, *Utilization of the Donnan effect for improving electrolyte separation with nanofiltration membranes.* Journal of membrane science, 1996. 116(1): p. 77-92.

[71]. Wang, X. L., Tsuru, T., Nakao, S. I. and Kimura, S., *Electrolyte transport through nanofiltration membranes by the space-charge model and the comparison with Teorell-Meyer-Sievers model.* Journal of membrane science, 1995. 103(1–2): p. 117-133.

[72]. Ohshima, H. and T. Kondo, *Relationship among the surface potential, Donnan potential and charge density of ion-penetrable membranes.* Biophysical Chemistry, 1990. 38(1–2): p. 117-122.

[73]. Ohshima, H. and T. Kondo, *Membrane potential and Donnan potential.* Biophysical Chemistry, 1988. 29(3): p. 277-281.

[74]. Yee, N., D. A. Fowle, and F. G. Ferris, *A Donnan potential model for metal sorption onto Bacillus subtilis.* Geochimica et cosmochimica acta, 2004. 68(18): p. 3657-3664.

[75]. Wonders, J. H. A. M., H. P. Van Leeuwen, and J. Lyklema, *Metal- and proton-binding properties of a core-shell latex: interpretation in terms of colloid surface models.* Colloids and Surfaces A: Physicochemical and Engineering Aspects, 1997. 120(1–3): p. 221-233.

[76]. Chein, R., H. Chen, and C. Liao, *Investigation of ion concentration and electric potential distributions in charged membrane/electrolyte systems.* Journal of membrane science, 2009. 342(1–2): p. 121-130.

[77]. J. T. Davies, E. K. Rideal, ed. *Electrostatic Phenomena*. 1961, Academic Press, Inc., New York and London.

[78]. Rice, G., Barber, A., O'Connor, A., Stevens, G., and Kentish, S., *Fouling of NF membranes by dairy ultrafiltration permeates.* Journal of membrane science, 2009. 330(1-2): p. 117-126.

[79]. Bian, R., K. Yamamoto, and Y. Watanabe, *The effect of shear rate on controlling the concentration polarization and membrane fouling.* Desalination, 2000. 131(1–3): p. 225-236.

[80]. C. Guizared, G. Rios,. *Transport and fouling phenomena in liquid phases separation with inorganic and hybird membranes.* 2005, Membrane Science and Technology Series 4: Netherlands.

[81]. Matthiasson, E. and B. Sivik, *Concentration polarization and fouling.* Desalination, 1980. 35(0): p. 59-103.

[82]. Potts, D. E., R. C. Ahlert, and S. S. Wang, *A critical review of fouling of reverse osmosis membranes.* Desalination, 1981. 36(3): p. 235-.264

[83]. M. Goosen, S.S., H. Al-Hinai, S. Al-Obeidani, and R. D. Jackson, *Fouling of reverse osmosis and ultrafiltration membranes: a critical review.* Separation science and technology, 2004. 39(10): p. 2261–2297.

[84]. Field, R., Wu, D., Howell, J. and GUPTA, B., *Critical flux concept for microfiltration fouling.* Journal of membrane science, 1995. 100(3): p. 259-272.

[85]. Chen, V., Fane, A., Madaeni, S. and Wenten, I., *Particle deposition during membrane filtration of colloids: transition between concentration polarization and cake formation.* Journal of membrane science, 1997. 125(1): p. 109-122.

[86]. Stoller, M. and M. Bravi, *Critical flux analyses on differently pretreated olive vegetation waste water streams: Some case studies.* Desalination, 2010. 250(2): p. 578-582.

[87]. Xu, J. and C. Gao, *Study of critical flux in ultrafiltration of seawater: New measurement and sub-and super-critical flux operations.* Chemical Engineering Journal, 2010. 165(1): p. 102-110.

[88]. Van der Bruggen, B., M. Mänttäri, and M. Nyström, *Drawbacks of applying nanofiltration and how to avoid them: A review.* Separation and Purification Technology, 2008. 63(2): p. 251-263.

[89]. Xu, J., Ruan, L. G., Wang, X., Jiang, Y. Y., Gao, X. L. and Gao, J. C., *Ultrafiltration as pretreatment of seawater desalination: Critical flux, rejection and resistance analysis.* Separation and Purification Technology, 2011.

[90]. Bacchin, P., P. Aimar, and V. Sanchez, *Influence of surface interaction on transfer during colloid ultrafiltration.* Journal of membrane science, 1996. 115(1): p. 49-63.

[91]. Bacchin, P., P. Aimar, and R. W. Field, *Critical and sustainable fluxes: theory, experiments and applications.* Journal of membrane science, 2006. 281(1): p. 42-69.

[92]. Stoller, M. and A. Chianese, *Optimization of membrane batch processes by means of the critical flux theory.* Desalination, 2006. 191(1): p. 62-70.

[93]. Bacchin, P., P. Aimar, and V. Sanchez, *Model for colloidal fouling of membranes.* AIChE journal, 1995. 41(2): p. 368-376.

[94]. Howell, J. A., *Sub-critical flux operation of microfiltration.* Journal of membrane science, 1995. 107(1): p. 165-171.

[95]. Espinasse, B ,.P. Bacchin, and P. Aimar, *On an experimental method to measure critical flux in ultrafiltration.* Desalination, 2002. 146(1-3): p. 91-96.

[96]. Mänttäri, M., J. Nuortila-Jokinen, and M. Nyström, *Influence of filtration conditions on the performance of NF membranes in the filtration of paper mill total effluent.* Journal of membrane science, 1997. 137(1): p. 187-199.

[97]. Li, H., Fane, A., Coster, H. and Vigneswaran, S., *An assessment of depolarisation models of crossflow microfiltration by direct observation through the membrane.* Journal of membrane science, 2000. 172(1): p. 135-147.

[98]. Tarabara, V. V., I. Koyuncu, and M. R. Wiesner, *Effect of hydrodynamics and solution ionic strength on permeate flux in cross-flow filtration: direct experimental observation of filter cake cross-sections.* Journal of membrane science, 2004. 241(1): p. 65-78.

[99]. Vera, L., Villarroel-Lopez, R., Delgado, S. and Elmaleh, S., *Cross-flow microfiltration of biologically treated wastewater.* Desalination, 1997. 114(1): p. 65-75.

[100]. Gesan-Guiziou, G., R. Wakeman, and G. Daufin, *Stability of latex crossflow filtration: cake properties and critical conditions of deposition.* Chemical Engineering Journal, 2002. 85(1): p. 27-34.

[101]. Chiu, T. and A. James, *Critical flux determination of non-circular multi-channel ceramic membranes using TiO_2 suspensions.* Journal of membrane science, 2005. 254(1): p. 295-301.

[102]. Le Clech, P., Jefferson, B., Chang, I. S., and Judd, S. J., *Critical flux determination by the flux-step method in a submerged membrane bioreactor.* Journal of membrane science, 2003. 227(1–2): p. 81-93.

[103]. Guglielmi, G., Saroj, D. P., Chiarani, D. and Andreottola, G., *Sub-critical fouling in a membrane bioreactor for municipal wastewater treatment: Experimental investigation and mathematical modelling.* Water research, 2007. 41(17): p. 3903-3914.

[104]. Mänttäri, M., K. Viitikko, and M. Nyström, *Nanofiltration of biologically treated effluents from the pulp and paper industry.* Journal of membrane science, 2006. 272(1): p. 152-160.

[105]. Mänttäri, M. and M. Nyström, *Critical flux in NF of high molar mass polysaccharides and effluents from the paper industry.* Journal of membrane science, 2000. 170(2): p. 257-273.

[106]. Mänttäri, M., Puro, L., Nuortila-Jokinen, J., and M. Nyström, *Fouling effects of polysaccharides and humic acid in nanofiltration.* Journal of membrane science, 2000. 165(1): p. 1-17.

[107]. Kwon, D., Vigneswaran, S., Fane, A., and Aim, R. B., *Experimental determination of critical flux in cross-flow microfiltration.* Separation and Purification Technology, 2000. 19(3): p. 169-181.

[108]. Peng, W., I. C. Escobar, and D. B. White, *Effects of water chemistries and properties of membrane on the performance and fouling—a model development study.* Journal of membrane science, 2004. 238(1): p. 33-46.

[109]. Lee, S., J. Kim, and C. H. Lee, *Analysis of $CaSO_4$ scale formation mechanism in various nanofiltration modules.* Journal of membrane science, 1999. 163(1): p. 63-74.

[110]. Atamanenko, I., A. Kryvoruchko, and L. Yurlova, *Study of the scaling process on membranes.* Desalination, 2004. 167: p. 327-334.

[111]. Her, N., G. Amy, and C. Jarusutthirak, *Seasonal variations of nanofiltration (NF) foulants: identification and control.* Desalination, 2000. 132(1-3 :(p. 143-160.

[112]. Yoon, S.H., Lee, C. H., Kim, K. J., and Fane, A. G., *Effect of calcium ion on the fouling of nanofilter by humic acid in drinking water production.* Water research, 1998. 32(7): p. 2180-2186.

[113]. Fradin, B. and R. Field, *Crossflow microfiltration of magnesium hydroxide suspensions: determination of critical fluxes, measurement and modelling of fouling.* Separation and Purification Technology, 1999. 16(1): p. 25-45.

[114]. Al-Amoudi, A., Williams, P., Mandale, S., and Lovitt, R. W., *Cleaning results of new and fouled nanofiltration membrane characterized by zeta potential and permeability.* Separation and Purification Technology, 2007. 54(2): p. 234-240.

[115]. Al-Amoudi, A., Williams, P., Al-Hobaib, A. and Lovitt, R. W., *Cleaning results of new and fouled nanofiltration membrane characterized by contact angle, updated DSPM, flux and salts rejection.* Applied Surface Science, 2008. 254(13): p. 3983-3992.

[116]. Wei, X., Wang, Z., Fan, F., Wang, J., and Wang, S., *Advanced treatment of a complex pharmaceutical wastewater by nanofiltration: Membrane foulant identification and cleaning.* Desalination, 2010. 251(1): p. 167-175.

[117]. Tsuru, T., Hlronaka, D., Yoshioka, T., and Asaeda, M., *Titania membranes for liquid phase separation: effect of surface charge on flux.* Separation and Purification Technology, 2001. 25(1–3): p. 307-314.

[118]. Puhlfürß, P., Voigt, A., Weber, R., and Morbe', M., *Microporous TiO_2 membranes with a cut off 500 Da*. Journal of membrane science, 2000. 174(1): p. 123-133.

[119]. Labbez, C., Fievet, P., Szymczyk, A., Vidonne, A., Foissy, A. and Pagetti, J., *Analysis of the salt retention of a titania membrane using the "DSPM" model: effect of pH, salt concentration and nature*. Journal of membrane science, 2002. 208(1): p. 315-329.

[120]. Van Gestel ,T., Vandecasteele, C., Buekenhoudt, A., Dotremont, C., Luyten, J., Leysen, R., Van der Bruggen, B. and Maes, G., *Salt retention in nanofiltration with multilayer ceramic TiO_2 membranes.* Journal of membrane science, 2002. 209(2): p. 379-389.

[121]. Narong, P., *The influence of electrokientics on membrane MICRO/ULTRA filtration of colloidal systems*, in *School of Chemical Engineering and Analytical Science*. 2006, phD thesis, The University of Manchester: Manchester,UK.

[122]. Narong, P. and A. E. James, *Sodium chloride rejection by a UF ceramic membrane in relation to its surface electrical properties.* Separation and Purification Technology, 2006. 49(2): p. 122-129.

[123]. Zhang, H., Quan, X., Chen, S., Zhao, H., Zhao, Y., and Li, W., *Zirconia and titania composite membranes for liquid phase separation: preparation and characterization.* Desalination, 2006. 190(1): p. 172-180.

[124]. Hagen, A., Barkschat, A., Dohrmann, J., and Tributsch, H., *Imaging UV photoactivity and photocatalysis of TiO_2 films.* Solar energy materials and solar cells, 2003. 77(1): p. 1-13.

[125]. Lee, H. S., Im, S. J., Kim, J. H., Kim, H. J., Kim, J. P., and Min, B. R., *Polyamide thin-film nanofiltration membranes containing TiO_2 nanoparticles.* Desalination, 2008. 219(1-3): p. 48-56.

[126]. Baldeón, T. L., *Studies of electrically enhanced membrane processe*, in *Department of Chemical Engineering*. 2002, phD thesis, University of Manchester, Institute of Science and Technology: Manchester.

[127]. Chiu, T. Y. and A. E. James, *Electrokinetic characterisation of cleaned non-circular multi-channelled membranes.* Desalination, 2006. 189(1–3): p. 13-20.

[128]. Childress, A. E. and M. Elimelech, *Effect of solution chemistry on the surface charge of polymeric reverse osmosis and nanofiltration membranes* .Journal of membrane science, 1996. 119(2): p. 253-268.

[129]. Hurwitz, G., G. R. Guillen, and E. M. Hoek, *Probing polyamide membrane surface charge, zeta potential, wettability, and hydrophilicity with contact angle measurements.* Journal of membrane science :(2–1)349 .2010 ,p. 349-357.

[130]. Garba, Y., Taha, S., Gondrexon, N., and Dorange, G., *Ion transport modelling through nanofiltration membranes.* Journal of membrane science, 1999. 160(2): p. 187-200.

[131]. Todolí, J. L. and J. M. Mermet, *Sample introduction systems for the analysis of liquid microsamples by ICP-AES and ICP-MS.* Spectrochimica Acta Part B: Atomic Spectroscopy, 2006. 61(3): p. 239-283.

[132]. Gehr, R., Zhai, Z. A., Finch, J. A. and Rao, S. R., *Reduction of soluble mineral concentrations in $CaSO_4$ saturated water using a magnetic field.* Water research, 1995. 29(3 :(p. 933-940.

[133]. American Chemical Society specifications, *Reagent chemicals: specifications and procedures:, official from*. 2006, Oxford University Press. p. p. 242.

[134]. Bandini, S., J. Drei, and D. Vezzani, *The role of pH and concentration on the ion rejection in polyamide nanofiltration membranes.* Journal of membrane science, 2005. 264(1): p. 65-74.

[135]. Yaroshchuk, A. E., *Negative rejection of ions in pressure-driven membrane processes.* Advances in colloid and interface science, 200 :(1)139 .8p. 150-173.

[136]. Hassan, A., Ali, N., Abdull, N. and Ismail, A., *A theoretical approach on membrane characterization: the deduction of fine structural details of asymmetric nanofiltration membranes.* Desalination, 2007. 206(1): p. 107-126.

[137]. Hussain, A. A., M. E. E. Abashar, and I. S. Al-Mutaz, *Influence of ion size on the prediction of nanofiltration membrane systems.* Desalination, 2007. 214(1–3): p. 150-166.

[138]. Pontalier, P. Y., A. Ismail, and M. Ghoul, *Mechanisms for the selective rejection of solutes in nanofiltration membranes.* Separation and Purification Technology, 1997. 12(2): p. 175-181.

[139]. Wang, D. X., Su, M., Yu, Z. Y., Wang, X. L., Ando, M. and Shintani, T., *Separation performance of a nanofiltration membrane influenced by species and concentration of ions.* Desalination, 2005. 175(2): p. 219-225.

[140]. Palmeri J., Blanc, P., Larbot, A. and David, P., *Theory of pressure-driven transport of neutral solutes and ions in porous ceramic nanofiltration membranes.* Journal of membrane science, 1999. 160(2): p. 141-170.

[141]. Yaroshchuk, A.E., Makovetskiy, A. L., Boiko, Y. P. and Galinker, E. W., *Non-steady-state membrane potential: theory and measurements by a novel technique to determine the ion transport numbers in active layers of nanofiltration membranes.* Journal of membrane science, 2000. 172(1): p. 203-221.

[142]. Wang, L., Tsuru, T., Nakao, S. and Kimura, S., *The electrostatic and steric-hindrance model for the transport of charged solutes through nanofiltration membranes.* Journal of membrane science, 1997. 135(1): p. 19-3.

[143]. Combe, C., Guizard, C., Aimar, P. and Sanchez, V., *Experimental determination of four characteristics used to predict the retention of a ceramic nanofiltration membrane* .Journal of membrane science, 1997. 129(2): p. 147-160.

[144]. Bouranene, S., Szymczyk, A., Fievet, P. and Vidonne, A., *Effect of salts on the retention of polyethyleneglycol by a nanofiltration ceramic membrane.* Desalination, 2009. 240(1–3): p. 94-98.

[145]. Szymczyk, A. and P. Fievet, *Investigating transport properties of nanofiltration membranes by means of a steric, electric and dielectric exclusion model.* Journal of membrane science, 2005. 252(1–2): p. 77-88.

[146]. Maria D. Alfonso, and Maria N. de Pinho, *Transport of $MgSO_4$, $MgCl_2$, and Na_2SO_4 across an amphoteric nanofiltration membrane.* Journal of membrane science 2000. 179: p. 137-154.

[147]. Ko, Y. W. and R. M. Chen, *Ion Rejection in Single and Binary Mixed Electrolyte Systems by Nanofiltration: Effect of Feed Concentration.* Separation science and technology, 2007. 42(14): p. 3071-3084.

[148]. Newman, J. S., *Electrochemical Systems*. 2nd edition ed. 1991: Prentice Hall,USA.

[149]. Wąsik, E., J. Bohdziewicz, and K. Ćwiklak, *Ion balance in NF-treated well water for drinking water production.* Desalination, 2005 :(1)186 .p. 81-87.

[150]. Colombani, J. and J. Bert, *Holographic interferometry study of the dissolution and diffusion of gypsum in water.* Geochimica et cosmochimica acta, 2007. 71(8): p. 1913-1920.

[151]. Bowen, W. R., A. W. Mohammad, and N. Hilal, *Characterisation of nanofiltration membranes for predictive purposes—use of salts, uncharged solutes and atomic force microscopy*. Journal of membrane science, 1997. 126(1): p. 91-105.

[152]. Ahmad, A. and B. Ooi, *Optimization of composite nanofiltration membrane through pH control: Application in $CuSO_4$ removal.* Separation and Purification Technology, 2006. 47(3): p. 162-172.

[153]. Bowen, R. and W. Mohammad, *Diafiltration by nanofiltration: prediction and optimization.* AIChE journal, 1998. 44(8): p. 1799-18.12

[154]. Bowen, W. and A. W. Mohammad, *Characterization and prediction of nanofiltration membrane performance—a general assessment.* Chemical Engineering Research and Design, 1998. 76(8): p. 885-893.

[155]. Bowen, W. R. and J. S. Welfoot, *Modelling the performance of membrane nanofiltration--critical assessment and model development.* Chemical engineering science, 2002. 57(7): p. 1121-1137.

[156]. Mohammad, A., Hilal, N., Al-Zoubi, H., and Darwish, N., *Prediction of permeate fluxes and rejections of highly concentrated salts in nanofiltration membranes.* Journal of membrane science, 2007. 289(1): p. 40-50.

[157]. Routh, J., Grossman, E. L., Murphy, E. M., and Benner, R., *Characterization and origin of dissolved organic carbon in Yegua ground water in Brazos County, Texas.* Ground Water, 2001. 39(5): p. 760-767.

[158]. Labbez, C., Fievet, P, Thomas, F., Szymczyk, A., Vidonne, A., Foissy, A., and Pagetti, P., *Evaluation of the "DSPM" model on a titania membrane: measurements of charged and uncharged solute retention, electrokinetic charge, pore size, and water permeability.* Journal of Colloid and Interface Science, 2003. 262(1): p. 200-211.

[159]. Dalwani, M., Benes, N.E., Bargeman, G., Stamatialis, D. and Wessling, M. *Effect of pH on the performance of polyamide/polyacrylonitrile based thin film composite membranes.* Journal of membrane science, 2011. 372 (1–2): p. 228-238.

[160]. Deen, W., *Hindered transport of large molecules in liquid-filled pores.* AIChE journal, 1987. 33(9): p. 1409-1425.

[161]. V. Silva; P. Prádanos, L.P., J. I. Calvo and A. Hernandez, *Relevance of hindrance factors and hydrodynamic pressure gradient in the monetisation of the transport of neutral solutes across nanofiltration membranes.* Chemical Engineering Journal, 2009. 149: p. 78–86.

[162]. Bowen, W. R. and H. Mukhtar, *Characterisation and prediction of separation performance of nanofiltration membranes.* Journal of membrane science, 1996. 112(2): p. 263-274.

[163]. Maiti, S. K., Lukka T. Y., Singh, S., Oberoi, H. S. and Agarwal, G. P., *Modeling of the separation of inhibitory components from pretreated rice straw hydrolysate by nanofiltration membranes.* Bioresource Technology, 2012. 114: p. 419-427.

[164]. Bowen, W. R. and J. S. Welfoot, *Predictive modelling of nanofiltration: membrane specification and process optimisation.* Desalination, 2002-1)147 . :(3p. 197-203.

[165]. Bowen, W. R., J. S. Welfoot, and P. M. Williams, *Linearized transport model for nanofiltration: development and assessment.* AIChE journal, 2002. 48(4): p. 760-773.

[166]. G. Birch, S. Parke, R. Siertsema, and J. M. Westwell, *Importance of molarvolumes and related parameters in sweet taste chemoreception.* Pure and Applied Chemistry, 1997. 69(4): p. 685–692.

[167]. Bandini, S. and D. Vezzani, *Nanofiltration modeling: the role of dielectric exclusion in membrane characterization.* Chemical engineering science, 2003. 58(15): p. 3303-3326.

[168]. P. Pivonka, D. Smith, and B. Gardiner, *Modelling of Donnan equilibrium in charge porous materials – a scale transition analysis*, in *VIII International Conference on Computations Plasticity* 2005: Barcelona.

[169]. Cuartas-Uribe, B., Vincent-Vela, M., Álvarez-Blanco, S., Alcaina-Miranda, M. and Soriano-Costa, E., *Nanofiltration of sweet whey and prediction of lactose retention as a function of permeate flux using the Kedem-Spiegler and Donnan steric Partioning models.* Separation and Purification Technology, 2007. 56(1): p. 38-46.

[170]. Koter ,S., *Determination of the parameters of the Spiegler–Kedem–Katchalsky model for nanofiltration of single electrolyte solutions.* Desalination, 2006. 198(1): p. 335-345.

[171]. Vezzani, D. and S. Bandini, *Donnan equilibrium and dielectric exclusion for characterization of nanofiltration membranes.* Desalination, 2002. 149(1-3): p. 477-483.

[172]. Richard Bowen, W. and A. Wahab Mohammad, *A theoretical basis for specifying nanofiltration membranes-Dye/salt/water streams.* Desalination, 1998. 117(1-3): p. 257-264.

[173]. Oatley, D. L., Cassey, B., Jones, P., and Richard Bowen, W., *Modelling the performance of membrane nanofiltration-recovery of a high-value product from a process waste stream.* Chemical engineering science, 2005. 60(7): p. 1953-1964.

[174]. Szymczyk, A. and P. Fievet, *Investigating transport properties of nanofiltration membranes by means of a steric, electric and dielectric exclusion model.* Journal of membrane science, 2005. 252(1): p. 77-88.

[175]. Dutournié, P., Limousy, L., Déon, S., and Bourseau, P., *Unsteady transport of divalent salt through a mineral membrane of ultrafiltration: Numerical estimation of physical parameters.* Desalination, 2011. 265(1-3): p. 184-189.

[176]. Gozálvez-Zafrilla, J. and A. Santafé-Moros, *Implementation of the DSPM model using a commercial finite element system.* Desalination, 2010. 250(2): p.844-840 .

[177]. Otero, J., Lena, G., Colina, J. M., Prádanos, P., Tejerina, F. and Hernandez, A., *Characterisation of nanofiltration membranes: Structural analysis by the DSPM model and microscopical techiques.* Journal of membrane science, 2006. 279(1): p. 410-417.

[178]. Santafé-Moros, A., J. Gozálvez-Zafrilla, and J. Lora-García, *Applicability of the DSPM with dielectric exclusion to a high rejection nanofiltration membrane in the separation of nitrate solutions.* Desalination, 2008. 221(1-3): p. 268-276.

[179]. Etter, D. M. and S. Elliott, *FORTRAN 77 with Numerical Methods ;Engineers and Scientist*. 1992: Benjamin-Cummings Publishing Co., Inc.

[180]. Vetterling, W. T., S. A. Teukolsky, and H. William, *Press, Numerical Recipes: Example Book (FORTRAN)*. 1992, Cambridge University Press, New York, NY, USA.

[181]. Geraldes, V. and A. M .Brites Alves, *Computer program for simulation of mass transport in nanofiltration membranes.* Journal of membrane science, 2008. 321(2): p. 172-182.

[182]. Press, W., Teukolsky, S., Vetterling, W., and Flannery, B., *Numerical recipes in Fortran 77: the art of scientific computing, vol. 1.* Fortran Numer. Recipes, 1992. 994.

[183]. Saltelli, A., T. H. Andres, and T. Homma, *Sensitivity analysis of model output: An investigation of new techniques.* Computational Statistics and Data Analysis, 1993. 15(2): p. 211-238.

[184]. Weirs, V. G., Kamm, J. R., Swiler, L. P., Tarantola, S., Ratto, M., Adams, B. M., R., William and Eldred, M., *Sensitivity analysis techniques applied to a system of hyperbolic conservation laws.* Reliability Engineering and System Safety, 2012. 107(0): p. 157-170.

[185]. Mohammad, W. A., L. Pei, and A. A. Kadhum, *Characterization and identification of rejection mechanisms in nanofiltration membranes using extended Nernst-Planck model.* Clean technologies and environmental policy, 2002. 4(3): p. 151-156.

[186]. Gozálvez-Zafrilla, J. M., B. Gómez-Martínez, and A. Santafé-Moros, *Evaluation of nanofiltration processes for brackish water treatment using the DSPM model.* Computer Aided Chemical Engineering, 2005. 20: p. 457-462.

APPENDICES

Appendix (1)

FORTRAN programme:

```
!            ********************************************************
!       *      This program used to assess the transport of ions in NF       *
!       *     membrane using classical four orders Rung-Kutta formula     *
!       *                    (with adjustable step size control)                *

!            ********************************************************
!                8888888888888888888888888888888888888888
!                888                      By                      888
!                888                                              888
!                888       Amer Naji Ahmed AL-Naemi               888
!                888                                              888
!                8888888888888888888888888888888888888888
!            ********************************************************

!                  ..... (Definitions & Units).....

!    cfeed: Ion feed concentration (mol/m^3).
!    cpermOld: Initial ion permeate concentration (mol/m^3).
!    cpermNew: Final ion permeate concentration (mol/m^3).
!    flux: Permeate volume flux (m^3/m^2.s).
!    val: Ion valance.
!    hind: Ion hindered diffusivity (m^2/s).
!    hidc: Ion hindered concentration (dimension less).
!    donnan: Donnan potential (V).
!    steric: Ion steric partitioning coefficient (dimension less).
!    abst: Absolute temperature (°K).
!    farcon: Faraday constant (C/mol).
!    unigas: Universal gas constant (J. mol^-1.K^-1).
!    1, 2: ions 1 and 2.
!    c1: concentration of ion 1 inside membrane (mol/m^3).
!    c2: concentration of ion 2 inside membrane (mol/m^3).
!    xx: x step size (independent variable).
!    x1: membrane active skin layer thickness at x=0 (micron).
!    x2: membrane equivalent active skin layer thickness at x = Delta x (micron).
!    N: Number of nods or number of steps NSTEP.
!    NMAX: Number of functions.
!    err: error ratio
!    vstart: starting value of c (based on Runge-Kutta code).
!    c (*): solution vector at x.
!    cout: output point at which the solution is desired.
!    Rejection1: Rejection (R %) of ion 1.
!    Rejection2: Rejection (R %) of ion 2.

!                  ..........
```

```
!                    ----------------------------------------


    IMPLICIT REAL (A-H, O-Z)
!
    DOUBLE PRECISION cfeed, cperm, flux
    DOUBLE PRECISION abst, farcon, unigas
    DOUBLE PRECISION val, hind, hidc
    DOUBLE PRECISION donnan, steric, Rej1, Rej2
!
    COMMON/path1/cfeed (10, 2), val (10, 2), hind (10, 2), hidc (10, 2)
    COMMON/path2/steric (10, 2), cperm (1000, 2)
    COMMON/path3/farcon, unigas, flux, nep, abst, node, donnan
    COMMON/path4/cpermOld (2), cpermNew (2)

    INTEGER NSTEP, NVAR
    PARAMETER (NVAR = 2, NSTEP = 300)
    INTEGER i, j
    REAL xx (1000), x1, x2, c (2, 1000), vstart (NVAR)
!
    COMMON /path/ xx, c
    EXTERNAL derivs

    OPEN (unit=10, file='Input1.dat', status='unknown')
    OPEN (unit=20, file='Output.dat', status='unknown')
!
!
    READ (10, *) nep, abst, farcon, unigas
    READ (10, *) flux

    i =1
    DO j = 1, 2
    READ (10, *) val (i, j), hind (i, j), hidc (i, j)
    READ (10, *) cfeed (i, j), donnan, steric (i, j)

    END DO
!
    WRITE (*, *) nep, abst, farcon, unigas
    WRITE (*, *) flux
    WRITE (*, *)

    i =1
    DO j = 1, 2
    WRITE (*, *) val (i, j), hind (i, j), hidc (i, j)
    WRITE (*, *) cfeed (i, j), donnan, steric (i, j)
    WRITE (*, *)

    END DO
!
```

```
!
!   Partitioning distribution at (feed-membrane interface):
!
      c (1, 1) = cfeed (1, 1)*steric (1, 1)
      c (1, 1) = c (1, 1)*EXP (- val (1, 1)*farcon*donnan/ (unigas*abst))
!
      c (2, 1) = cfeed (1, 2)*steric (1, 2)
      c (2, 1) = c (2, 1)*EXP (- val (1, 2)*farcon*donnan/ (unigas*abst))
!
!
!   Set a new definition inside the loop based on Runge-Kutta code

      vstart (1) = c (1, 1)
      vstart (2) = c (2, 1)
!
!   Set the initial membrane active skin layer thickness

      x1 = 0.0d0

!   Set the estimated equivalent membrane active skin layer thickness

      x2 = 8.14d-06

!
!
      CALL ADJUSTABLE (vstart, NVAR, x1, x2, NSTEP, derivs)
!
!
!   Estimate the percentage of rejection of each ion
!
!
      Rej1 = (1 - cpermNew (1)/ cfeed (1, 1))*100
      Rej2 = (1 - cpermNew (2)/ cfeed (1, 2))*100

!
!
```

```
!                    ----------------------------------------

!                              Results file

!                    ----------------------------------------
!

     i = 1
    WRITE (20, 10) i, xx (i), c (1, i), c (2, i)
    DO i = 2, NSTEP
      iz = i/30
      ii = 30*iz
      IF (i .EQ. ii) THEN
    WRITE (20, 10) i, xx (i), c (1, i), c (2, i)
    END IF
    END DO
 10   FORMAT (i6, 5(8x, e13.7))
    WRITE (20, *)
    WRITE (20, *)
    WRITE (20, *) cpermOld (1), cpermNew (1)
    WRITE (20, *) cpermOld (2), cpermNew (2)
    WRITE (20, *)
    WRITE (20, *)
    WRITE (20, *) ' Rejection (R %) 1 =', Rej1
    WRITE (20, *) ' Rejection (R %) 2 =', Rej2
!
!
    DO 11 i =1, 300
    PRINT *, i, xx (i), c (1, i), c (2, i)
 11   CONTINUE
     i = 300
    PRINT *
    PRINT *
    PRINT *, i, xx (i), c (1, i), c (2, i)
    PRINT *
    PRINT *
    PRINT *, cpermOld (1), cpermNew (1)
    PRINT *, cpermOld (2), cpermNew (2)

    END
!


!                    ----------------------------------------
```

```
!                    ------------------------------------------

      SUBROUTINE ADJUSTABLE (vstart, nvar, x1, x2, nstep, derivs)
!
      DOUBLE PRECISION cfeed, cperm, flux
      DOUBLE PRECISION abst, farcon, unigas
      DOUBLE PRECISION val, hind, hidc
      DOUBLE PRECISION donnan, steric, Rej1, Rej2
!
       COMMON/path1/cfeed (10, 2), val (10, 2), hind (10, 2), hidc (10, 2)
      COMMON/path2/steric (10, 2), cperm (1000, 2)
      COMMON/path3/farcon, unigas, flux, nep, abst, node, donnan
      COMMON/path4/cpermOld (2), cpermNew (2)
      INTEGER nstep, nvar, NMAX, NSTPMX
!
!     Set the maximum number of functions (NMAX)
!     Set the maximum number of values to be stored (NSTPMX)
!
      PARAMETER (NMAX = 2, NSTPMX = 1000)
      REAL x1, x2, vstart (nvar), xx (NSTPMX), c (NMAX, NSTPMX)
      EXTERNAL derivs
      COMMON /path/ xx, c
CU    USES rk4
      INTEGER i, k
      REAL h, x, dv (NMAX), v (NMAX)
!
150   CONTINUE
       DO 11   i = 1, nvar
        v (i) = vstart (i)
        c (i, 1) = v (i)
11      CONTINUE
      xx (1) = x1
      x = x1
      h = (x2 - x1)/ nstep
!     h: the step size value
      DO 13 k =1, nstep
      CALL derivs (x, v, dv)
      CALL rk4 (v, dv, nvar, x, h, v, derivs)
       x = x+h
       xx (k+1) = x
       DO 12   i = 1, nvar
        c (i, k+1) = v (i)
12    CONTINUE
      PRINT *, k, xx (k+1), c (1, k+1), c (2, k+1)
13    CONTINUE
!
```

```
!    Partitioning distribution at (membrane interface-permeate):

     cpermNew (1) = EXP (- val (1, 1)*farcon*donnan/ (unigas*abst))
     cpermNew (1) = c (1, 300)/ (steric (1, 1)*cpermNew (1))
!
     cpermNew (2) = EXP (- val (1, 2)*farcon*donnan/ (unigas*abst))
     cpermNew (2) = c (2, 300)/ (steric (1, 2)*cpermNew (2))

!    Permeate concentration change ratio

     ratio1 = ((cpermOld (1) – cpermNew (1))/ cpermOld (1))
     ratio2 = ((cpermOld (2) – cpermNew (2))/ cpermOld (2))
!
    err = 1.0d-03
!
     IF (ratio1 .le. err .and. ratio2 .le. err) GOTO 200
!
!    Using under relaxation technique
!
     relax = 0.8
!
     cpermNew (1) = relax*cpermOld (1) + (1- relax)*cpermNew (1)
     cpermNew (2) = relax*cpermOld (2) + (1- relax)*cpermNew (2)

!
     cpermOld (1) = cpermNew (1)
     cpermOld (2) = cpermNew (2)

!
     WRITE (*,*) cpermOld (1), cpermOld (2)
     WRITE (*,*) cpermNew (1), cpermNew (2)

!

     GOTO 150

200  CONTINUE

     RETURN

     END
!

!                              ------------------------------------------
```

```
!                    ------------------------------------------


      SUBROUTINE derivs (x, c, dcdx)
!
      REAL  : :  x, c (*), dcdx (*)

      DOUBLE PRECISION cfeed, cperm, flux
      DOUBLE PRECISION abst, farcon, unigas
      DOUBLE PRECISION val, hind, hidc
      DOUBLE PRECISION donnan, steric, Rej1, Rej2
!
      COMMON/path1/cfeed (10, 2), val (10, 2), hind (10, 2), hidc (10, 2)
      COMMON/path2/steric (10, 2), cperm (1000, 2)
      COMMON/path3/farcon, unigas, flux, nep, abst, node, donnan
      COMMON/path4/cpermOld (2), cpermNew (2)
!
!     The initial permeate concentration was assumed to be equal to the feed
!     concentration
!

      cpermOld (1) = cfeed (1, 1)*1.0d0
      cpermOld (2) = cfeed (1, 2)*1.0d0

!
!     The electrical potential gradient inside the membrane pores:
!

      fixed = (val (1, 1)*flux/ hind (1, 1))*(hidc (1, 1)*c (1) - cpermOld (1))
      fixed = fixed + (val (1, 2)*flux/ hind (1, 2))*(hidc (1, 2)*c (2) - cpermOld (2))
      fixed 1 = (farcon/ (unigas*abst))*(val (1, 1)**2*c (1) + val (1, 2)**2*c (2))
      fixed = fixed/ fixed 1

!
!     The ionic concentration gradient within the membrane pores:
!

      dcdx (1) = (flux/ hind (1, 1))*(hidc (1, 1)*c (1) - cpermOld (1))
      dcdx (1) = dcdx (1) - (val (1, 1)*c (1)*farcon/ (unigas*abst))*fixed
!
      dcdx (2) = (flux/ hind (1, 2))*(hidc (1, 2)*c (2) - cpermOld (2))
      dcdx (2) = dcdx (2) - (val (1, 2)*c (2)*farcon/ (unigas*abst))*fixed
!
      RETURN

      END
!
```

```
!                    ------------------------------------------

     SUBROUTINE rk4 (c, dcdx, n, x, h, cout, derivs)
!

     DOUBLE PRECISION cfeed, cperm, flux
     DOUBLE PRECISION abst, farcon, unigas
     DOUBLE PRECISION val, hind, hidc
     DOUBLE PRECISION donnan, steric, Rej1, Rej2
!
     COMMON/path1/cfeed (10, 2), val (10, 2), hind (10, 2), hidc (10, 2)
     COMMON/path2/steric (10, 2), cperm (1000, 2)
     COMMON/path3/farcon, unigas, flux, nep, abst, node, donnan
     COMMON/path4/cpermOld (2), cpermNew (2)
!
     INTEGER n, NMAX
     REAL h, x, dcdx (n), c (n), cout (n)
     EXTERNAL derivs
!
     PARAMETER (NMAX = 2)
     INTEGER i
     REAL h6, hh, xh, dcm (NMAX), dct (NMAX), ct (NMAX)
     hh = h*0.5
     h6 = h/6.
     xh = x+hh
     DO 11   i = 1, n
      ct (i) = c (i) + hh*dcdx (i)
11    CONTINUE
     CALL derivs (xh, ct, dct)
     Do 12   i =1, n
      ct (i) = c (i) + hh*dct (i)
12    CONTINUE
     CALL derivs (xh, ct, dcm)
     DO 13   i = 1, n
      ct (i) = c (i) + h*dcm (i)
      dcm (i) = dct (i) + dcm (i)
13    CONTINUE
     CALL derivs (x +h, ct, dct)
     Do 14   i = 1, n
      cout (i) = c (i) + h6*(dcdx (i) + dct (i) + 2.*dcm (i))
14    CONTINUE
     RETURN

     END
!
!                    ------------------------------------------
```

Appendix (2)

Thesis related activates:

- ***The first Iraqi Cultural Attaché conference for Engineering sciences for the period from 1-2 /10 /2011, University of London. (Oral presentation) for the paper entitled: (Zeta potential and surface charge density of ceramic Nano-Filtration membrane).***

- ***School of Chemical Engineering and Analytical Science post graduated Conference, 15 June 2012 – James Chadwick building (University of Manchester). (Oral presentation) for the paper entitled: (Rejection Behaviour of Calcium Sulphate in Ceramic TiO_2 Nanofiltration Membrane).***

- ***International Conference on Membranes in Drinking and Industrial Water Production, Leeuwarden, Netherlands, 10-12 September 2012. (Accepted oral presentation) for the paper entitled: (Rejection of $CaSO_4$ in tubular ceramic titanium dioxide Nanofiltration membrane).***

- ***Poster presented in the Postgraduate Student Conference (PGC), June 9th 2010. School of Chemical Engineering and Analytical Science (Reynolds Building - University of Manchester).***

- ***Poster presented in the Postgraduate Student Conference (PGC), June 29th 2011. School of Chemical Engineering and Analytical Science (MIB Building - University of Manchester).***